

ENGINEERED WATER REPELLENCY FOR INFILTRATION CONTROL IN COAL  
FLY ASH

by

Jenberu Lemu Feyyisa

A dissertation submitted to the faculty of  
The University of North Carolina at Charlotte  
in partial fulfillment of the requirements  
for the degree of Doctor of Philosophy in  
Infrastructure and Environmental Systems

Charlotte

2017

Approved by:

---

Dr. John L. Daniels

---

Dr. Vincent O. Ogunro

---

Dr. Miguel A. Pando

---

Dr. Wenwu Tang

---

Dr. Valery Z. Grdzlishvili

---

Dr. William B. Langley

©2017  
Jenberu Lemu Feyyisa  
ALL RIGHTS RESERVED

## I. ABSTRACT

JENBERU LEMU FEYYISA. Engineered water repellency for infiltration control in coal fly ash (Under the direction of Dr. JOHN DANIELS)

In 2014 approximately 47% of the 190 million short tons of coal combustion product (CCP) was recycled. As a construction material, coal fly ash (CFA) finds considerable use as a partial replacement for Portland cement, as structural fill, and as an additive for waste stabilization and environmental remediation (ACAA 2014). But still the larger portion is sent to disposal in ash impoundments or landfills. Recent regulations are accelerating the industry trend of dry ash handling and the closure of impoundments. In the case of ash that remains unencapsulated (e.g., in a structural fill, landfill, or dewatered/capped in place impoundment), concerns have been raised regarding the leaching of naturally occurring trace elements into groundwater. One mechanism to eliminate this concern is to treat ash so that it is water repellent, thereby preventing infiltration and leachate generation. Recent research has demonstrated promise, however little has been done regarding the relationship of governing parameters for water repellency, such as contact angle, infiltration pressure, grain size, and the mineralogical and chemical composition of fly ash. This study provides data and analysis to serve as a design basis for mitigating leachate generation through engineered water repellency. Engineering water repellency involves modifying the surface of CFA particles with organo-silane. The degree of water repellency is defined through contact angle (CA) and breakthrough pressure (BP) measurements. This study provides the first results of dynamic contact angle measurements for a modified coal fly ash (CFA) and compares the results with static contact angle measurements using three organo-silane (OS) chemicals. Five

types of CFA were tested using three different OS chemicals at different mix ratios (weight based). This dissertation reports on the pattern that each of the modified CFA exhibits as a function of treatment type and level as well as the unique relationship between steady state motion of the three-phase contact line and drop volume. The proposed dynamic approach reduces the standard error of apparent contact angle measurements from  $\pm 20^\circ$  or greater with conventional approaches to less than  $\pm 5^\circ$ . The reduction in error is attributed to improvements in experimental design that addresses substrate heterogeneity and roughness as well as drop size and motion. For each sample a minimum drop size at which the three-phase contact line motion reaches a stable motion has been identified. It was identified that for a certain combination of CFA and OS, there exists a threshold drop size that overcomes factors that otherwise render apparent CA measurements unreliable. The extent of water repellency varied considerably as a function of OS treated dosage, which ranged from 1:500 to 1:140 (OS: CFA, by weight). The CAs of all five unmodified CFAs were below  $90^\circ$  whereas modification results in values greater than  $135^\circ$  on average. This change in CA from hydrophilic ( $CA < 90^\circ$ ) to hydrophobic ( $CA > 90^\circ$ ) is indicative of water repellency, (no infiltration), by which leachate control is possible. Multiple breakthrough pressure (BP) experiments were conducted for different samples at different mix ratios to identify the performance of the modified surface to resist a positive water entry pressure. Results indicated that CFA can be modified and made sufficiently water resistant against infiltration using OS. Regression analysis between measured and calculated (from the Washburn equation) BP revealed that the calculated BP underestimates the measured one by a specific scale factor. The magnitude and pattern of the scale factor varies based on the type of CFA and OS used. It was found that when the CA of the modified CFA becomes

slightly greater than a threshold value, the relationship between CA and BP abruptly changes from linear to exponential. Based on these results; the Washburn equation should be adjusted for both a scale factor and the effect of pore CA. While the scale factor is related to changes in the surface energy of the material, the pore CA is related to the prevailing pressure of pore water, i.e., higher water entry pressure results in greater disparity. The proposed exponential relationship between measured apparent CA and BP is more robust and is consistent with the significance of pore (vs. apparent) contact angle as a function of surface energy. For example, at lower surface energy levels, the radius of water drop curvature in the pore space does not change much, and so pore CA approximates apparent CA as measured on flat surface. The relative abundance of chemicals and minerals in CFA and their corresponding sensitivity to OS modification has been investigated. In addition, surrogate indicators, such as the degree of alkalinity, amorphous content and reactivity are identified for each CFA. In terms of composition, a group of four variables were found to be most significant when using OS to modify CFA. Results showed that a semi log-transformed regressions model can effectively describe the relationship between water repellency and mineral composition (e.g., oxides, other minerals and their surrogates) in CFA. It has been found that the degree of water repellency of an OS treated CFA can be predicted using a limited number of minerals (only two) in CFA instead of the primary substrate (silica) that forms siloxane bonds with OS. Further, this study suggests that OS engenders water repellency with a variety of oxides. Class F fly ash is more easily rendered water repellent than Class C. When mixed with water, lime raises the pH of the solution, which in turn may adversely affect the bonding of OS molecules to Class C CFA. Results also indicate that the presence of magnesium oxide can partially improve OS bonding. In

summary; these data can be used by engineers to evaluate induced water repellency as an approach to increase ash use in applications where leachability is a concern.

## ACKNOWLEDGEMENTS

I would like to express my sincere gratitude and appreciation to my advisor, Dr. John Daniels for his insightful suggestions and professional guidance throughout the course of this study. I would also like to thank other member of my dissertation committee, Dr. Vincent Ogunro, Dr. Miguel Pando, Dr. Wenwu Tang, and Dr. Valery Grdzelishvili for their review and invaluable comments. Furthermore, I would like to extend special thanks to my wife Meseret Senbeta and my children, Kena and Ifaa for their support and encouragement which has made this endeavor a possibility.

The authors gratefully thank and acknowledge the financial support provided by the Environmental Research and Education Foundation (EREF). The views and conclusions contained herein are those of the writers and should not be interpreted as necessarily representing the official policies or endorsements, either expressed or implied, of the EREF.

## TABLE OF CONTENTS

LIST OF TABLES	xi
LIST OF FIGURES	xii
LIST OF ABBREVIATIONS	xvii
INTRODUCTION	1
LITERATURE REVIEW	4
CHAPTER 1: CONTACT ANGLE MEASUREMENT TECHNIQUE FOR A WATER REPELLENT COAL FLY ASH (CFA)	6
1.1 Abstract	6
1.2 Introduction	8
1.3 Theory	12
1.4 Materials and Procedures	16
1.4.1 Material and Equipment	16
1.4.2 Procedures	18
1.5 Results and Discussion	23
1.5.1 Static and Dynamic CA measurements	23
1.5.2 Dynamic CA measurement	29
1.5.2.1 Patterns of drops motion on the MCFA	30
1.5.2.2 Drop size and contact line motion	31
1.5.2.3 CA measurement and drop size	36
1.5.2.4 Kernel density distribution estimation	45
1.6 Summary and Conclusion	52
REFERENCES	55
CHAPTER 2: CAPILLARY BREAKTHROUGH PRESSURE MEASUREMENTS AND A MODIFIED WASHBURN EQUATION FOR ORGANO-SILANE TREATED COAL FLY ASH: CORRELATION BETWEEN CONTACT ANGLE AND BREAKTHROUGH PRESSURE	59
2.1 Abstract	59
2.2 Introduction	60
2.3 Methods	64



2.3.1 Materials and Equipment	64
2.3.2 Procedures	64
2.4 Results and Discussion	69
2.4.1 Relative performance of OS and CFA	69
2.4.2 BP measurements	70
2.4.2 Post BP imbibition	75
2.4.3 Pore size estimate	78
2.4.3.1 Grain size and packing density	78
2.4.3.2 Capillary pores size CFA-WCC	81
2.4.4 Model and prediction (Washburn equation)	83
2.4.5 Apparent and pore CA	85
2.4.6 Correlation between CA and BP	88
2.4.6.1 Exploratory data analysis	90
2.4.6.2 Identify underlying Influencing variable and conditioned plot	93
2.4.7 The Washburn equation for a positive water entry pressure	99
2.5 Conclusion	116
REFERENCES	119
CHAPTER 3: MINERAL AND CHEMICAL CONTROLS ON WATER	
REPELLENCY: A COMPARISON BETWEEN CLASS C AND F	
COAL FLY ASH	121
3.1 Abstract	121
3.2 Introduction	122
3.3 Materials and Methods	125
3.3.1 Materials	125
3.3.2 Methods	125
3.4 Results and Discussion	127
3.4.1 Minerals and Chemical Composition	127
3.4.2 Organo-silane Chemistry	131
3.4.3 Organo-silane and CFA	132
3.4.4 Variable Selection	132
3.4.5 Variable Selection and Modeling	134

3.4.6 Modeling and Verification	141
3.4.7 Discussion and conclusion	149
3.4.8 CaO and Hydrophobic Surface Formation	158
REFERENCES	164
OVERALL CONCLUSION: SUMMARY OF NEW KNOWLEDGE GAINED	173
1. CA Measurements	173
2. BP measurement and the Washburn equation	174
3. Wettability and CFA Compositions	175
APPENDIXES: ADDITIONAL FIGURES	
Rate of pressure: pre, during, and post BP corresponding to Figure 2.8 (chapter 2 BP versus time plot).	177

## LIST OF TABLES

TABLE 1.1. Images of drops released at different CFA grain coverage and CA measurements.	38
TABLE 1.2. Minimum recommended size of drops to measure accurate CA for different types of MCFA and OS across Different mix ratios. The recommended sizes of drops are based on repeatable measurement and statistical evaluation of relative velocity of contact line. Data not provided for CA less than $90^0$ .	48
TABLE 2 1. Estimated average packing density of different CFA samples	66
TABLE 2.2. Values of parameters in equations 3.5 and 3.6 for different modified CFA and OS, capillary (AEV) and Tetrahedral packing approach.	109
TABLE 3. 1. Summary of derivative composition of oxides for five types of CFA	131
TABLE 3.2 Summary of models' performance and their corresponding significant predictors to estimate BP	142

## LIST OF FIGURES

FIGURE 1.1. Contact angle measurement on hydrophobic (top) and hydrophilic (bottom) surface	11
FIGURE 1.2. Observed ( $\theta_A$ ) and Intrinsic ( $\theta_E$ ) CAs on a hypothetical rough surface.	14
FIGURE 1.3. a) CFA as received from different power stations and b) OS as Purchased	18
FIGURE 1.4. Model 260 standard Goniometer (A), and FlowTrac II (B)	19
FIGURE 1.5. Example picture of hanging (pendant) drop (a) and CA measurement for a stable drop (b)	20
FIGURE 1.6. Photo of expanding drop. Pulse application of droplets to facilitate stable contact line motion for dynamic CA measurement. Photos were taken at 13, 167, and 243 seconds after the initial drop (a) and subsequent droplets (b) and (c) were deposited, respectively	22
FIGURE 1.7. Pulse application of droplets to form stable contact line motion for dynamic CA measurement. Photo were taken at 13, 167, and 243 seconds after the initial drop (A) and subsequent droplets (B) and (C) were deposited, respectively.	22
FIGURE 1.8. Sample contact angle measurement using dynamic contact angle measurement approach. The static measurement represents the first measurement of contact angle for each case. Although droplets were deposited on same sample on a slide and the significant variation in initial contact angle measurement, all measurements eventually converge to an average $148^\circ$ , representing the actual contact angle measurement for the CFA treated with OS C-1 (1:125 (OS: CFA) mix ratio).	24
FIGURE 1.9. Sample contact angle measurements (three different measurements) arranged sequentially. All the three tests represent data of identical sample but with different initial droplet sizes. For larger initial drop volume (test 2) convergence to dynamic CA starts earlier, 50 seconds after the start of the experiment. But the final CA measurement for the three tests varied between $143^\circ$ and $144^\circ$ .	26
FIGURE 1.10. Statistical analysis for comparison of dynamic and static contact angle measurement for CFA Class F (utility C) modified with OS chemical (C-4) using different mix ratios. The error bars represent one standard deviation.	27

FIGURE 1.11. Statistical analysis for comparison of dynamic and static contact angle measurement for CFA Class F (utility C) modified with OS chemical (C-2) using different mix ratios. The error bars represent one standard deviation.	27
FIGURE 1.12. Statistical analysis for comparison of dynamic and static contact angle measurement for CFA Class F (utility C) modified with OS chemical (C-1) using different mix ratios. The error bars represent one standard deviation.	28
FIGURE 1.13. CA measurement using a dynamic measurement technique. For CFA Class F, C-1 chemical able to form higher CA measurement including smaller OS: CFA mix. After OS mix of 6 gm subsequent addition of chemicals does not change much CA measurements.	29
FIGURE 1.14. Different patterns of drop motion on the surfaces of the MCFA. The three-phase contact line; accelerates fast until the drop gets a certain volume (a), remains constant (b), and combination of both (c) while subsequent drops are released.	30
FIGURE 1.15. Contact line motion and shape of drops affecting CA measurement. First row shows different shapes of stable drop and second row is their corresponding response (expanding or retraction) after successive drop is released.	32
FIGURE 1.16. Example of degree of variation in CA measurements as a factor of drop volume for: CFA-3 treated using C-1 (a), CFA-2 treated using C-4 (b), and CFA-5 treated using C-2 (c) representing patterns: 1, 2, and 3 in Figure 2.4, respectively. Error bars represent one standard deviation.	37
FIGURE 1.17. CA measurements for different degree of grain size distribution	39
FIGURE 1.18. Plots of drops sizes at which acceleration reaches zero (velocity = 0.4 mm/sec.) for MCFA-1 mixed with OS: C-4 C-1, C-2 in columns 1,2, and 3 respectively. Rows represent mix ratio used in ascending order top down (2, 4, 6 and 8). Markers indicate repeated measurement for same sample.	40
FIGURE 1.19. Plots of drops sizes at which acceleration (velocity = 0.1 mm/sec.) reaches zero for MCFA-2 mixed with OS: C-1, C-2 and C-4 in columns 1,2, and 3 respectively. Rows represent mix ratio used in ascending order top down (2, 4, 6 and 8).	41
FIGURE 1.20. Plots of drops sizes at which acceleration reaches zero (velocity = 0.2 mm/sec.) for MCFA-5 mixed with OS: C-4, C-1 and C-2 in columns 1, 2, and 3 respectively. Rows represent mix ratio used in ascending	

order top down (2, 4, 6 and 8). Markers indicate tests.	42
FIGURE 1.21. Plots of drops sizes at which acceleration reaches zero for MCFA-3 mixed with OS: C-4, C-1 and C-2 in columns 1, 2, and 3 respectively. Rows represent mix ratio used in ascending order top down (2, 4, 6 and 8). Markers indicate tests.	43
FIGURE 1.22. Plots of drops sizes at which acceleration reaches zero for MCFA-6 mixed with OS: C-4, C-1 and C-2 in columns 1, 2, and 3 respectively. Rows represent the mix ratio used in ascending order top down (2, 4, 6 and 8). When drop volume is increased the contact line motion resembles pattern c but it's less hydrophobic property influences in such a way that higher variability of velocity observed for certain drop volume. Markers indicate tests.	44
FIGURE 1.23. Measured (left) and Kernel density distribution (right) contact line velocity to estimate the corresponding drop volume; a) CFA-3 treated using C1-8, b) CFA-5 treated using C1-8, and c) CFA-6 treated using C4-8	46
FIGURE 1.24. Dynamic CA measurements for different types of CFA mixed with three different types of OS chemicals after three-phase contact line is stabilized. First column for CFA (1-3) and second column for CFA (5 and 6)	50
FIGURE 1.25. Probability density distribution range of OS effectiveness to form hydrophobic surfaces. First column for CFA (1-3) and second column for CFA (5 and 6).	52
FIGURE 2.1. Material and equipment used for sample preparation and testing	65
FIGURE 2.2. Calculated (mass-volume) packing density of modified CFA samples	66
FIGURE 2.3. Testing materials and equipment's layout	67
FIGURE 2.4. Box plot for relative performance of; a) OS and b) CFA across all mix ratio. The box notches of CFA-1 and CFA-5 nearly overlap indicating the similarity of their median.	69
FIGURE 2.5. Pressure measurement and its rate of change to identify breakthrough pressure point	71
FIGURE 2. 6. Breakthrough pressure measurements at a breakthrough point for five CFA using three OS. First column for CFA 1, 2, and 3 and second column CFA 5 and 6, respectively.	72
FIGURE 2.7. Probability range of effectiveness of different CFA treated using OS products	74

FIGURE 2.8. Sample breakthrough pressure measurements for different CFA and OS at different mix ratio: a, b, c, d, e, and f for CFA1-C1, CFA2-C2, CFA3-C2, CFA3-C4, CFA5-C2, and CFA6-C1, respectively (CFA1-C1 represents sample coal fly ash number 1 treated using organo-silane number1)	77
FIGURE 2.9. Imbibition rate (explained through rate of change in pressure) inside modified CFA. In general, as dose of OS increases (except for CFA6-C1 with lowest BP) the rate of imbibition reduces. BP, Lines and Marks in legend represents range of initial breakthrough pressure, CFA and OS, respectively	79
FIGURE 2.10. Sample images of CFA grains (400x) used to count and measure grain size using Fluorescent Microscope BX51. Different background, grain distribution, and available software options were used to effectively disperse, count and measure	80
FIGURE 2.11. Sample CFA grain size distribution histogram	81
FIGURE 2.12. Soil (CFA) water characteristic curve for four CFA	82
FIGURE 2.13. Measured and calculated Breakthrough Pressure for a) CFA-1, b) CFA-2, c) CFA-3, and d) CFA-5 using measured pore size, cubic and tetrahedral packing approaches	86
FIGURE 2.14. Idealized sketch showing apparent and pore CA resulting due to the change in pore water radius	87
FIGURE 2.15. Measured CA and BP data for five CFA treated using three OS.	89
FIGURE 2.16. Plot of BP versus CA for five CFA treated using three OS	90
FIGURE 2.17. Linear regression models for different transformed scales	91
FIGURE 2.18. A linear regression diagnostic plot for all CFA and OS; a) ordinary linear regression, b) semi-log (BP) scale, c) semi-log (CA) scale, and d) log-log scale	92
FIGURE 2.19. Conditioned plot to identify the underlying influencing variables to model BP as a factor of CA	95
FIGURE 2.20. Ordinary Linear regression model for CA and BP grouped in type of CFA(black) and (CFA + OS); a) CFA-1, b) CFA-2, c) CFA-3, and d) CFA-5	96
FIGURE 2.21. A linear regression diagnostic plot for; a) CFA-1, b) CFA-2, c)	

CFA-3, and d) CFA-5.	97
FIGURE 2. 22. A linear regression diagnostic plot when grouped according to type of CFA and OS; a) CFA-1, b) CFA-2, c) CFA-3, and d) CFA-5	98
FIGURE 2.23. BP and CA liner modeling for CFA-1 treated using OS; C-1, C-2, and C-3 for a, b, and c in their order of arrangement. Figure d is an exponentially adjusted plot for a. BP for the three models were calculated using the capillary rise equation	101
FIGURE 2. 24. BP and CA liner modeling for CFA-2 treated using OS; C-1, C-2 and C-3 for a, b, and c their order of arrangement. BP for the three models were calculated using the capillary rise equation.	102
FIGURE 2.25. BP and CA liner modeling for CFA-3 treated using OS; C-1, C-2 and C-3 represented by a, b, and c respectively. Figures d and e represent an exponentially modified fitting models for a and c. BP for the three models were calculated using the capillary rise equation	104
FIGURE 2.26. BP and CA liner modeling for CFA-5 treated using OS; C-1, C-2 and C-4 represented by a, b, and c respectively. Figures d, e, and f represent an exponentially modified fitting models for a b, and c. BP for the three models were calculated using the capillary rise equation.	106
FIGURE 2.27. Measured and modeled Breakthrough Pressure for a) CFA-1, b) CFA-2, c) CFA-3, and d) CFA-5 using measured pore size and tetrahedral packing approaches.	108
FIGURE 2.28. a) Linear regression model and the corresponding b) residuals density distribution for measured BP versus calculated and modeled BP for CFA-1 and CFA-3	110
FIGURE 2.29. Linear regression model comparison between the two models for measured CA on flat surface and models predicted pore CA.	112
FIGURE 2.30. Linear regression between contact angle measured on flat surface and pore contact angle; a) CFA-1, b) CFA-2, c) CFA-3, and d) CFA-5	113
FIGURE 2.31. A detailed view and comparison between linear and exponential regression for contact angle measured on flat surface and pore contact angle for highly and super hydrophobic surfaces of modified CFA surface, CFA-3 treated using OS C1	114
FIGURE 2.32. A detailed view and comparison between; (a) linear and (b) exponential regression for contact angle measured on flat surface and pore contact angle for highly and super hydrophobic surfaces of MCFA surface,	



CFA-3 treated using OS C4.	115
FIGURE 2.33. Comparison between linear and exponential relationship between measured CA on flat surface and pore CA model for CFA-3	116
FIGURE 3.1. XRD and XRF analysis for; a) CFA-1, b) CFA-3, c) CFA2 and CFA 5, and d) CFA-6	129
FIGURE 3.2. Percentage composition of a) chemical and b) mineral composition for five CFA (total compositions account more than 90 and 98 percent, respectively).	131
FIGURE 3.3 Organo-functional silane bond formation with substrate through hydrolysis (F. de Buyl, Dow Corning)	132
FIGURE 3.4. Average breakthrough pressure measurements for different CFA using three OS products (chapter 2)	134
FIGURE 3.5. The relationship between derivative compositions and BP.	136
FIGURE 3.6. A log transformed measured and fitted BP; a) four groups, b) Class C CFA, and c) Class F CFA	139
FIGURE 3.7. Model diagnostic plot for; a) model 2, b) model 1, c) model 3, and d) model 4	140
FIGURE 3.8. Model diagnostic plot for the two types of CFA; a) Class C b) Class F	141
FIGURE 3.9. A normalized data showing mean and the corresponding z-score for oxides in CFA.	144
FIGURE 3.10. Cross validation residuals distribution for model 2 along with the two types of CFA, Class C and F	145
FIGURE 3.11. Cross validation residuals distribution for all major models	146
FIGURE 3.12. Plot of measured and predicted values for model 2; a) all types CFA, b) Class F CFA, and c) Class C CFA.	147
FIGURE 3.13. Plot of measured and predicted values for all models	148
FIGURE 3.14. Residual density plot for four models; a) predicted model and b) k-fold cross validated (fitted)	149
FIGURE 3.15. Comparison of model's accuracy using AIC values	149

FIGURE 3.16. The degree of water repellency (BP and CA) as a function of a) SiO <sub>2</sub> , b) Al <sub>2</sub> O <sub>3</sub> , and c) Fe <sub>2</sub> O <sub>3</sub> in CFA conditioned OS.	152
FIGURE 3.17. The degree of water repellency (BP and CA) as a function of SiO <sub>2</sub> conditioned by both Al <sub>2</sub> O <sub>3</sub> and Fe <sub>2</sub> O <sub>3</sub> .	154
FIGURE 3.18. The degree of water repellency (BP and CA) as a function of sum3conditioned by OS.	155
FIGURE 3.19. Correlation between BP and CA conditioned by SiO <sub>2</sub>	156
FIGURE 3.20. Correlation between BP and CA conditioned by Al <sub>2</sub> O <sub>3</sub>	157
FIGURE 3.21. Correlation between BP and CA conditioned by Fe <sub>2</sub> O <sub>3</sub>	157
FIGURE 3.22. The degree of water repellency (BP and CA) as a function of CaO conditioned by OS; column a) all CFA, b) all CFA without high MgO	160
FIGURE 3.23. The degree of water repellency (BP and CA) as a function of CaO conditioned by MgO	160
FIGURE 3.24. Comparison of water repellency of Class C and F CFA. CFA-6 (Class C) is the least to transform CFA surface to a water repellent one. However, same type, CFA-5 forms a sufficiently high water-resistant surface due to the presence of additional oxides, MgO	161
FIGURE 3.25. The degree of water repellency (BP and CA) as a function of group 1 model (Quartz + Gypsum) conditioned by OS	163
FIGURE 3.26. The degree of water repellency (BP and CA) as a function of group 4 model (Gypsum + Magnetite) conditioned by OS	164

## LIST OF ABBREVIATIONS

BP	breakthrough pressure
C-1	organo-silane product no 1
CA	contact angle
CCP	Coal Combustion Products
CFA	coal fly ash
cm	centimeter
dp	change in pressure
d <sub>sc</sub>	density, simple cubic packing approach
dt	change in time
d <sub>th</sub>	density, tetrahedral packing approach
kPa	kilo pascal
l	Liter
MCFA	modified coal fly ash
mm	millimeter
m	meter
mm <sup>3</sup>	cubic millimeter
nm	nanometer
μm	micrometer
OS	organo-silane
Mohm	Mega Ohm
Sec.	Second
θ <sub>a</sub>	Apparent contact
θ <sub>p</sub>	Pore contact angle



## INTRODUCTION

Coal-fired power currently accounts for 30% of electricity in the US and 40% worldwide. By 2040, coal is forecasted to represent 26% of electricity in the US and 30% worldwide. And if the use of coal ceased today, there would be more than ten billion tons of coal combustion residuals (CCR) across the globe, with much of it located in impoundments. Coal fly ash (CFA) is a component of CCR. While it is regarded as a useful construction material, it is also subject to leaching trace elements. For certain conditions and applications, such leaching can adversely impact groundwater quality. This concern prevents CFA from being fully utilized in structural fill and other unencapsulated applications. Efforts have been made to expand the beneficial re-use areas of CFA by transforming its surface to a water repellent one there by preventing leachate. For example (Daniels et al. 2009) presented an example on how to stabilize Class F CFA through laboratory experiment and demonstrated their results at a coal ash monofill site. Results from that study provided insights into potential applications of OS chemicals to reduce infiltration and subsequent leachate release from CFA.

In this study the theory and application of infiltration reduction/avoidance for modified CFA will be evaluated in detail through wettability theory and surface energy. First, we modify the surface of five types of CFA using three different organo-silane (OS) products. Second, based on the existing approach to measure surface energy, through contact angle measurement (CA), CA measurements will be evaluated for consistency and repeatability. This evaluation will guide the extent to which existing methods can be employed or whether new ones must be created to meet research needs. In addition, another parameter to estimate the degree of water repellency, breakthrough pressure will be

evaluated and correlated with CA measurements. Third, we investigate the relationship between BP and CA with physical parameters including grain size distribution, mineralogical composition of each fly ash (using XRF and XRD tests), components of OS hydrolysable molecules and covalent bond (between CFAs minerals and OSs). This investigation is intended to reveal fundamental and physical controls on the efficacy of engineered water repellency via surface modification with OS. The capillary rise equation for flow in porous media will be modified based on this research to facilitate a more accurate prediction of breakthrough pressure in OS modified CFA.

## OBJECTIVES AND RESEARCH QUESTIONS

This research has the following goals:

1. Transform the surface of different types of CFA using different OS from hydrophilic to hydrophobic.
2. Measure the degree of water repellency of the transformed CFA defined through CA and BP measurements. For CA measurement, a new and suitable measurement approach will be developed as there is no identified standard and procedure for the material. The new approach is used and evaluated with respect to the ability to provide repeatable measurements.
3. The relative performance of OS with different CFAs and vice versa will be evaluated and presented. Appropriate and economical application dose for a specific range of resistance to infiltration will be presented.

4. Mineralogical composition of each CFA and hydrolysable components of OS will be studied in detail as a basis for a model for estimating OS efficacy for a given CFA type.

Research questions:

1. Can CFA be made sufficiently a water repellent surface to avoid its leaching?
2. Can the surface energy of the MCFA be accessible and defined?
3. Can the capillary rise equation also be used for a positive water entry pressure?
4. What is the relationship between CA and BP for a MCFA?
5. What mineral, chemical, and their range of percentage composition influence the formation of a water repellent surface in CFA?

Motivation

Power production from coal is rapidly declining and shifting to other sources. However; even if this source of power production were to stop immediately, a significant volume (> two billion tons in the U.S. alone) of coal fly ash (CFA) has already accumulated. A concern for CFA destined for disposal or reuse is often the extent to which the material leaches various trace contaminants. As such, a motivating question is whether organo-silanes can be used to mitigate these concerns and allow CFA to be re-used in greater quantities in more applications as well as decreasing costs associated with effective disposal.

## LITERATURE REVIEW

A concern with the general management of CFA is the potential for leaching of trace elements (Feyyisa and Daniels 2016). Leachate from CFA contains concentrations of trace elements including (e.g., arsenic, barium, cadmium, chromium, mercury, lead) that may be in excess of applicable regulatory guidelines. Studies regarding chemical constituents of CFA and their corresponding field leachate can be found elsewhere (Daniels and Das 2006; EPRI 2005; EPRI and Department of Energy 2006; EPRI and Pacific Northwest Laboratories 1988; Thorneloe et al. 2010).

Daniels et al. (2009) and Daniels and Hourani (2009) conducted a field and laboratory based studies on how to improve coal ash and soil surfaces in order to create a hydrophobic (water repellent) surface. They used an OS chemical as a coupling agent and evaluated its impact on compaction, strength, swell and hydraulic properties of Class F CFA. They reported that OS modification increased strength, reduced swelling, and essentially eliminated infiltration capacity (Daniels and Hourani 2009). Their approach considers the treatment of CFA and soil in wet conditions that enhances infiltration reduction. Recent regulations are accelerating the industry trend of dry ash handling and the closure of impoundments. In circumstances where full control of leachate generation and seepage control are required (as in the case of CFA), the degree of repellency and resistance to a driving pressure is better defined when a material is tested in a dry state. The degree to which a given substrate will remain dry under certain conditions is related to wettability and surface energy theory. Wettability is the most important parameter for determining solid surface free energy (Baba et al. 2015) or the interaction of solid surface and liquid free surface energy (Erbil et al. 2003). Wettability and degree of water repellency



are defined through contact angle and break through pressure measurements. When no water molecules can infiltrate into a material under a given pressure head, it is considered non wettable or water repellent surface. Likewise, if a porous material allows water molecules to infiltrate between its grains, either under zero or certain induced pressure, it is considered wettable. Wetting is primarily related to: the physical chemistry, statistical physics, long range forces, and fluid dynamics (de Gennes 1985; Wenzel 1936); or the interfacial energy in solid-liquid-fluid system (Marmur 1998); and has influence on water movement in soils (Bachmann et al. 2000). However, the surface energy of materials is not easily quantified and can only be defined through CA measurement (Kwok and Neumann 1999). Literature has not been found, however, that quantifies the surface energy of CFA or OS MCFA. There is no fundamental understanding nor an engineering basis with which OS modification of CFA can be designed. This research is intended to provide both.

## CHAPTER 1

### CONTACT ANGLE MEASUREMENT TECHNIQUE FOR A WATER REPELLENT COAL FLY ASH (CFA)

#### 1.1 Abstract

A concern with the disposal, use, and general management of coal fly ash (CFA) is the potential for leaching of trace elements. Leachate from CFA can be reduced through transforming its wettable surface to a non-wettable one. This study provides data and analysis for an innovative method to mitigate leachate generation through engineered water repellency. Engineered water repellency involves modifying the surface of CFA particles with organo-silane. The extent to which the surface has been transformed to non-wettable is measured through apparent contact angle (CA) measurements. However, obtaining repeatable measurements of the apparent CA, particularly on rough and non-homogenous surfaces, is challenging. This study provides measurement data and compares static and dynamic contact angle measurements for a modified coal fly ash (CFA) using three organo-silane (OS) chemicals. Results indicate that OS has the ability to transform CFA from a hydrophilic material (contact angles less than  $90^0$ ) to one which is hydrophobic (contact angle greater than  $90^0$ ). Further analysis indicate that the extent of water repellency can be quantified more accurately with contact angle (CA) measurements determined by increasing a drop size until the three-phase contact line motion becomes approximately constant. For each sample a minimum drop size at which the three-phase contact line motion reaches a stable motion has been identified. This approach allows for CAs to be measured with an accuracy of  $\pm 5^\circ$ , as opposed to  $\pm 20^\circ$  or greater with conventional approaches. Five types of CFA were tested using three different OS chemicals at different

mix ratios (weight based). This chapter reports on the pattern that each of the modified CFA exhibits as a function of treatment type and level as well as the unique relationship between steady state motion of the three-phase contact line and drop volume. The extent of water repellency varied considerably as a function of OS treated dosage, which ranged from 1:500 to 1:140 (OS: CFA by weight). The CAs of all five unmodified CFAs were below  $90^\circ$  whereas the modified CFA resulted in average values of  $143^\circ$ ,  $135^\circ$ ,  $150^\circ$ ,  $158^\circ$ ,  $140^\circ$  for CFA-1, CFA-2, CFA-3, CFA-5 and CFA-6, respectively. This change in CA from hydrophilic ( $CA < 90^\circ$ ) to hydrophobic ( $CA > 90^\circ$ ) and super hydrophobic ( $CA > 150^\circ$ ) clearly indicates the property of highly water repellent material (no infiltration), as a result leachate control is possible. The data can be used by engineers to evaluate induced water repellency as an approach to increase ash use in applications where leachability is a concern.

Key words: CFA, CA, static CA, dynamic CA, contact line motion, drop size, steady state motion, OS

## 1.2 Introduction

In 2014 approximately 47% of the 190 million short tons of coal combustion product (CCP) was recycled in U.S.A. CCP includes boiler slag, flue gas desulfurization gypsum, bottom ash and coal fly ash (CFA). The primary reuse applications of CCP include concrete and concrete products, blended cement, and structural fill (ACAA, 2014). Details on these applications can be found elsewhere, for example for replacement of sand in concrete production (Singh and Siddique, 2013, 2014); for cement based composite (Chi and Huang, 2014; Wuet al., 2014); for adsorption application (Wang et al., 2008); for PVC composite (van der et al., 2014); for pile stabilization methods (Pei., 2015); and for soil amelioration and agricultural use (Basu et al., 2009; Jala and Goyal, 2006). However, despite these efforts to increase re-use, the majority of CCP continues to be landfilled. Concerns for leaching have prevented CFA from being fully utilized in structural fill and other unencapsulated applications.

Leaching of trace elements is also the primary environmental concern associated with CFA at its disposal sites, whether in impoundments or dry ash monofills. Leachate from coal fly ash (CFA) contains concentrations of trace elements (e.g., boron, sulfate, total dissolved solids) that may be in excess of applicable regulatory guidelines. Studies regarding chemical constituents of CFA and their corresponding field leachate can be found elsewhere ( Daniels and Das, 2006; EPRI, 2005; EPRI and Department of Energy, 2006; EPRI and Pacific Northwest Laboratories, 1988; Thorneloe, Kosson , Sanchez , Garrabrant , and Helms, 2010).

Recent state and federal regulations have been implemented in response to failure of CFA impoundments are in favor of the industrial management trend towards dry ash

handling and have prompted the closure of existing CFA impoundments (EPA, 2015; General Assembly, 2014). One alternative mechanism to eliminate or reduce concerns related to CFA leaching is to treat the ash to make it water repellent (hydrophobic), thereby preventing infiltration and leachate generation, as recommended in the U.S. EPA's proposed rule (US EPA, 2010).

Danielset al. (2009) and Daniels and Hourani (2009) conducted field and laboratory based studies on how to improve coal ash and soil in order to create a hydrophobic (water repellent) surface. They used an organo-silane (OS) chemical as a coupling agent and evaluated its impact on compaction, strength, swell and hydraulic properties of Class F CFA. They reported that OS modification increased strength, reduced swelling, and essentially eliminated infiltration capacity (Daniels and Hourani, 2009). Results from these studies have provided clear insights and encourage the application of OS chemicals to change the surface properties of CFA. However, their work did not describe surface modification in terms of the degree of wettability and surface energy. The extent to which solid surfaces are modified and become water repellent are better explained through wettability. To that end, Keatts (2014) used a static sessile drop approach and manually measured contact angle (CA) at the solid liquid interface for the modified Class F CFA using varying concentration of OS.

While preventing infiltration is the main objective of OS treatment, it must be related to repeatable measurements of CA for use in routine characterization, design, and construction. The extent to which solid surfaces are modified and become sufficiently water repellent can be explained through wettability.

Wettability defines the degree of wetting when a solid surface is in contact with liquid and is a function of the relative surface energy of the solid and liquid (Yuan and Lee, 2013). Wettability has been described as the most important parameter for determining solid surfaces free energy (Baba et al., 2015), and defining the interaction of solid surface and liquid free surface energy (Erbil., 2003). Wetting is primarily related to: the physical chemistry, statistical physics, long range forces, and fluid dynamics (de Gennes, 1985; Wenzel, 1936); or the interfacial energy of the system in solid, liquid and fluid system (Marmur, 1998); and has influence on water movement in soils (Bachmann et al., 2000). However, the surface energy of materials is not easily accessible and can only be defined through CA measurement (Kwok and Neumann, 1999). Conventionally defined, the CA is the angle measured at the liquid-solid-gas interface, as shown in Figure 1.1. According to (Yuan and Lee, 2013) the interface where these three-phases co-exist is known as the three-phase contact line Figure 1.1. Such CA measurements are sensitive to experimental conditions. For instance Kwok and Neumann (1999) explained that minor vibrations can cause advancing CAs to decrease, resulting in errors of several degrees. Furthermore, as pointed out by Amirfazli and Neumann (2004) measurement of CAs on rough and non-homogeneous surfaces is challenging and as such substrate-specific techniques must often be developed.

The simplest and often most appropriate method to estimate surface energy is through CA measurement (Kwok and Neumann, 1999). Accurate CA measurement requires extreme experimental care. Even very minor vibrations can cause advancing CA to decrease, resulting in errors of several degrees (Kwok and Neumann, 1999). Amirfazli and Neumann (2004) suggested CA phenomena are more complex than practitioners

typically realize, resulting in misleading data and conclusions (Kwok and Neumann 1999). As many discussed, (de Gennes, 1985; Heib et al., 2015; Kwok and Neumann, 1999; Marmur, 1998; Schmitt et al., 2014; Wenzel, 1936) contact angle measurements obtained using Young's equation are not suitable for rough and non-homogenous surfaces. The surface modified CFA is neither smooth nor homogenous. If roughness is a factor, then contact angle measurements defined exclusively with Young's equation are meaningless (Kwok and Neumann, 1999).

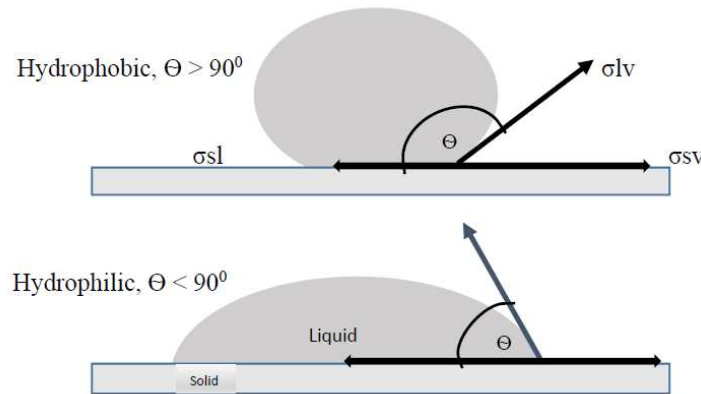


Figure 1.1. Contact angle measurement on hydrophobic (top) and hydrophilic (bottom) surface

(With permission from ASCE. This material may be downloaded for personal use only. Any other use requires prior permission of the American Society of Civil Engineers.)

This paper provides a summary of relevant theory as needed to provide context for the experimental data.

This study reports on a new approach to measure CA and data for measurement of CAs for different types of CFA modified with OS chemicals. We outline: 1) CA measurement technique for CFA; 2) the dependency of CA measurement on drop size; 3)

the requirement for achieving steady state motion of the three-phase contact line before a reliable CA measurement can be made; 4) the minimum size of drops required to measure accurate CA for different CFA surfaces and OS:CFA mix ratios, i.e., the size of the advancing drop at which item 3 above occurred; 5) data for five different types of CFA surfaces using three different OS chemicals; and 6) a summary of the relative performance of each of the CFA with the selected OS chemicals.

### 1.3 Theory

The study of wetting in terms of CAs was first reported by Young in the early 19<sup>th</sup> century (Kwok and Neumann, 1999; Marmur, 1998). Yet the acquisition of accurate CA measurements remains the subject of many investigations (Beatty and Smith, 2010; Imeson et al., 1992). On smooth and ideal surfaces, the mechanical equilibrium of a liquid drop applied on a solid surface under the interfacial tensions  $\sigma_{lv}$  (liquid-vapor),  $\sigma_{sv}$  (solid-vapor) and  $\sigma_{sl}$  (solid-liquid) interfaces control the geometry of a liquid drop and the resulting CA. The horizontal equilibrium of the drop is often expressed in terms of Young's equation (Kwok and Neumann, 1999) as follows:

$$\sigma_{lv} \cos(\theta) = \sigma_{sv} - \sigma_{sl} \quad 1.1$$

However; in practice, since most solid surfaces are far from being smooth and homogeneous. Because of the difficulty in measuring accurate CA on rough and non-homogenous surfaces, several studies including (Cassie, 1948; de Gennes, 1985; Duncan et al., 1995; Lichao., 2007; Kwok and Neumann, 1999; Marmur, 1997, 1998; Rotenberg et



al., 1983; Wenzel, 1936) have modified Young's equation for rough and heterogeneous surfaces.

Wenzel (1936) and Cassie (1948) have modified Young's equation to measure contact angles on a rough and heterogeneous surface, respectively. For example, to prevent erroneous contact angle values, Wenzel related an apparent contact angle ( $\theta_A$ ) to the intrinsic contact angle ( $\theta$ ) through a roughness term ( $r$ ), as indicated in Equation 1.2.

$$\cos(\theta_A) = r \cos(\theta) \quad 1.2$$

Where  $\sigma_{lv}$ ,  $\sigma_{sv}$ , and  $\sigma_{sl}$  are the interfacial tensions defined above and  $\theta$  is the contact angle as defined in Figure 1.1.

According to the Wenzel (1936) theory roughness can have an influence on the spreading of a drop of liquid in either way, i.e., it can be either increased or decreased. In terms of capturing heterogeneity, Cassie (1948) related the observed CA ( $\theta_A$ ) to the relative fraction of different chemicals ( $f_1$  and  $f_2$ ) Equation 1.3 having separate intrinsic CAs ( $\theta_1$  and  $\theta_2$ ) (Bachmann et al., 2000).

$$\cos(\theta_A) = f_1 \cos(\theta_1) + f_2 \cos(\theta_2) \quad 1.3$$

However; none of these studies described the role of drop size over a rough and non-homogeneous surface. Even if the effect of roughness and non-homogeneity have been understood to affect CA measurement, the trend to measure CA of many drops (same or different size) separately and then averaging remains a universal approach. Recent studies such as (Heib et al., 2015) called such type of measurement as a static wetting. They argue

that such type of measurements cannot represent CA measurement on rough surfaces. In fact, such types of CA measurement, simply dropping a liquid on rough and non-homogeneous surfaces and measuring the tangent line (CA) have shown significant surface energy variations.

In addition to well documented difficulties in making repeatable CA measurements for heterogeneous materials, the above theories have been challenged by several researchers e.g., see (Lichao et al., 2007; Kwok and Neumann, 1999; Song et al., 2015).

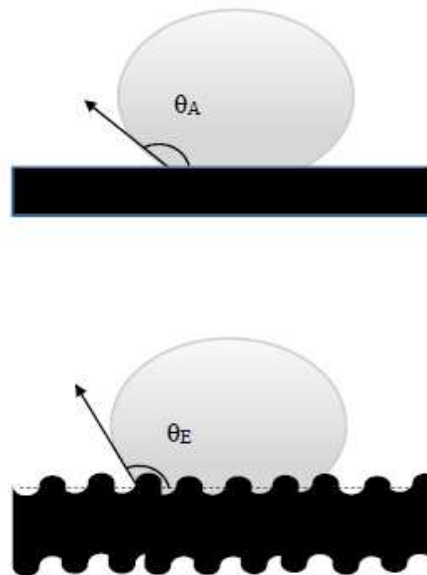


Figure 1.2. Observed ( $\theta_A$ ) and Intrinsic ( $\theta_E$ ) CAs on a hypothetical rough surface

(With permission from ASCE. This material may be downloaded for personal use only. Any other use requires prior permission of the American Society of Civil Engineers.)

Kwok and Neumann (1999) suggested the need to include other influencing factors in the measurement and interpretation of CAs on solid surfaces. Accordingly, they modified the preceding equations and cast the CA measurement as a function of accessible

and non-accessible quantities as shown in Equation 1.4 to identify these factors (Río and Neumann, 1997).

$$\sigma_{lv} - \sigma_{sl} = g(\sigma_{lv}, \sigma_{sv}, \text{dipole} - \text{dipole}, \text{hydrogen bonding}) \quad 1.4$$

Where  $g$  represents an unknown functional relation.

In order to consider the accessible and non-accessible factors that influence experimental CA measurements, Kwok and Neumann (1999) employed a dynamic CA measurement technique such that the initial sessile drop volume is increased and the drop radius along the three-phase contact line expands. The overall shape of the drop is measured with time and referred to as the Axisymmetric Drop Shape Analysis-Profile (ADSA-P) method. First, they supplied an initial sessile drop of about 3.0 mm in diameter. Then, they increased the drop volume from 50 mm<sup>3</sup> to 70 mm<sup>3</sup> after stopping drop supply when contact radius reaches about 4.1 mm. Through this experimental study, they found that CAs rise linearly with increase in contact line radius, and then stabilize and become nearly constant after contact radius reaches about 5.0 mm. As a result, they were able to establish a systematic relationship between line tension and the cosine of the CA; see also Hefer et al., (2006). While it was clear in terms of the need to use dynamic methods, Kwok and Neumann's work does not provide a basis for specifying a recommended drop size and the expected variations of drop size for varying solid surfaces. Furthermore, the physical basis for why repeatable measurements are made possible when the contact line radius reaches a given threshold (i.e., 5.0 mm) is not clear. Kwok and Neumann (1999) argue that the increase in drop volume is only useful to avoid the influence of line tension, the free

energy per unit length or tensile force of the contact line tension at contact line. However; more recent experimental data (Gao et al., 2007) show that the contact area of a liquid drop (or drop size) on solid surfaces is less important in determining wettability than contact lines. The latter show that CA behavior is determined only by the interaction of liquid and solid at the three-phase contact line (Lichao et al., 2007).

The present study, combines the efforts of previous researchers. Specifically, we propose that both drop size (e.g., Kwok and Neumann 1999) and an advancing three-phase contact line motion (e.g., Song et al. 2015) are needed to accurately reflect the physical phenomena which are responsible for repeatable CA measurements in CFA treated monolayers

## 1.4 Materials and methods

### *1.4.1 Material and Equipment*

Five types of CFA: Class F Utility A (CFA-1), Class F Utility B (CFA-2), Class F Utility C (CFA-3), Class C Utility B (CFA-5) and Lignite Coal Utility B (CFA-6) were collected from local utilities in the eastern U.S, Figure 1.3(a). Six aqueous phase organo-silane chemicals Figure 1.3(b) were received from DOW Corning (referred to herein as C-1, C-2 and C-3), Zydex Industries (C-4 and C-5) and L&Q International (C-6), but only three (C-1, C-2 and C-4) were selected at the initial screening based on their performance such that samples of MCFA treated using a specific OS but unable to yield sufficient water repellency were not considered for further study. Deionized water (approximate resistance = 16 MOhm) is used for mixing and liquid droplet. The basic hardware components for Axisymmetric Drop Shape Analysis-profile (ADSA-P) Model 260 Standard

Goniometer/Tensiometer set consists of camera, leveling stage, micro syringe fixture, back light, the advanced 3-axis stage with fine and coarse vertical adjustment and modular leveling stage and a PC as shown in Figure 1.4(a). It has the ability to capture time series data, with a resolution of  $0.01^\circ$  and accuracy of  $\pm 0.10^\circ$ , over user-defined intervals providing a unique opportunity to collect a large number of measurements. Details on ADSA-P may be found elsewhere (Cheng et al., 1990; Río and Neumann, 1997; Rotenberg et al., 1983). Pressure-volume controller by Geo Comp (FlowTrac II) Figure 1.4(b) was used and fitted with a Goniometer to pump and pour droplets of a required sizes at a required rate.



a)

Figure 1.3. a) CFA as received from different power stations and b) OS as purchased



b)

Figure 1.3. continued

#### *1.4.2 Procedures*

Different CFA and OS chemicals mix ratios by weight ranging from 2 to 8 g/kg (OS/CFA by weight) (range of OS effectiveness after preliminary analysis) were considered. First the required amounts of CFA, OS chemical, and DI water (40 percent by weight of CFA to ensure complete mixing and distribution of OS) were measured. Then the measured OS chemical was mixed with DI water using laboratory specimen cups and shaken for 3- 5 minutes. Next the OS-DI water mixture was again mixed with CFA, a fraction of both at a time to form a better and more evenly distributed mix. The sample was mixed manually for 3-5 minutes continuously until a visually homogeneous mixture was achieved (Feyyisa and Daniels, 2016). Finally, samples were oven dried between 60<sup>0</sup> and 158 <sup>0</sup>F for 24 – 72 hours depending on the type of CCP used (recommendations based on whether samples contained minerals which would be changed by higher temperatures, e.g., hydrated gypsum). Before preparing the samples for testing the dry samples were checked

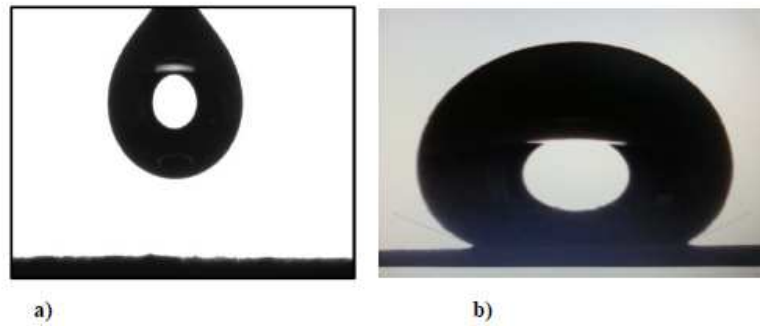
for any change in net weight (weight loss has to account only for the DI water used for appropriate distribution of OS across CFA grains).



Figure 1. 4. Model 260 standard Goniometer (A), and FlowTrac II (B)

To prepare a planar monolayer of CFA, samples were first crushed with a mortar and pestle to pass through a No. 200 sieve (for CFA-5 and CFA-6) to remove any agglomerations. The processed ash was applied to one side of double sided tape (3M Part # 112L) which had been affixed to a glass slide (GSC International Part # 4-13051). The slide was then tapped repeatedly to remove any loose particles. This process of applying and pressing the ash was repeated to ensure full coverage of the tape and to form a consistent “mono-layer” of particles. While ensuring the full coverage, MCFAs were grouped in to two categories to measure repeatable CAs. The first group (CFA-1, CFA-2 (higher mix ratio), and CFA-3) are samples which require a small quantity (as little as able to change the color of the tape) to spread but without the presence of loose particle. Whereas; the other group (CFA-2 (lower mix ratio), CFA-5, and CFA-6) require a thicker visible layer to be formed on the tape. In both cases, however, full coverage and adherence are important than degree of compactness since the shape of the drop is a function of the

surface energy at liquid-solid-gas interface. During this layering step, close attention was given to forming a planar monolayer, otherwise highly variable results were obtained ( $\pm 30^\circ$ ). Once the slide was prepared, it was positioned on the goniometer apparatus which has a leveled sample holding table, a backlighting source (fiber optic illuminator), and a supporting arm.



a) Hanging (pendant) drop

b) stable drop

Figure 1. 5. Example picture of a) hanging (pendant) drop and b) CA measurement for a stable drop

(With permission from ASCE. This material may be downloaded for personal use only. Any other use requires prior permission of the American Society of Civil Engineers.)

Then using the Precision Combo Calibration Device (model no. 100-27-31-C) the physical reference distance between the sample and camera (U1 Series SuperSpeed Digital Camera 100 fps) was set so that the profile measurements were accurate in both x and y axes.

The dispensing needle had an opening with a diameter of 0.635 mm. The tip of the needle was carefully lowered to between 3-5 mm above the slide. The height of the needle tip was adjusted to allow sufficient space for the expanding drop while adding subsequent droplets as shown in Figure 1.5 and Figure 1.6. The CA was measured using the sessile



drop technique (Bachmann et al., 2000), but in this case the size of the drop was increased (pulse application) with time, dynamic approach. This technique consists of applying initial drop of water to the modified CFA surface and then subsequent droplets to same initial drop Figure 1.6 while measuring the angle formed at the intersection of the modified CFA and drop surfaces. Using the ADSA software, provided with the Goniometer-260, time series images were captured over 1 second (pre-specified) intervals, a total of 250 images and recordings were collected for each test. The FlowTrac-II was used to inject drops on to the slide, through its in-built high precision micro stepper motor that moves a piston in a water-filled cylinder, via a modified outlet extension. Droplets were regulated semi-manually (for timing) at a rate of 0.00095 l/sec., to control the size and timing of each drop (Feyyisa and Daniels, 2016). As part of this study, a new testing protocol has been developed for the CA measurement of CFA; drop volume is allowed to expand over a relatively larger area Figure 1.6 and Figure 1.7 through the releasing of successive droplets over an interval of 40 to 60 seconds (depending on an initial drop size and degree of hydrophobicity of the sample) until steady state motion of the three-phase contact line is maintained. Before maintaining a steady state motion, all CA measurements vary considerably following the release of subsequent drops. Once the drop volume reaches certain size, varying for different MCFA, contact line motion nearly reaches a steady state motion and is no longer affected by subsequent droplets. Once the three-phase contact line maintains this state of motion, CA measurements converge and remain stable.

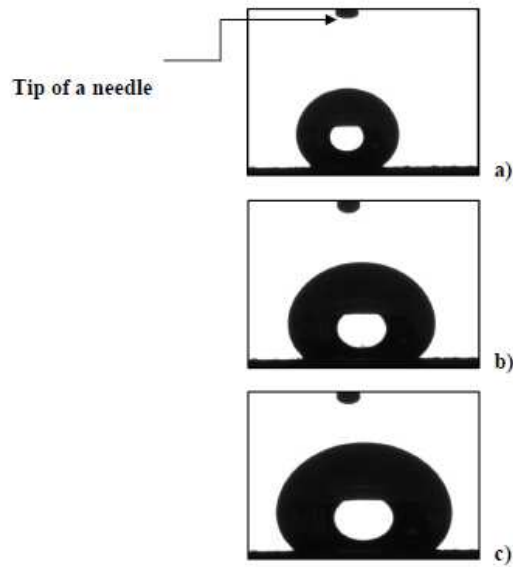


Figure 1. 6. Image of expanding drop. Pulse application of droplets to facilitate stable contact line motion for dynamic CA measurement. Image were taken at 13, 167, and 243 seconds after the initial drop (a) and subsequent droplets (b) and (c) were deposited, respectively.

(With permission from ASCE. This material may be downloaded for personal use only. Any other use requires prior permission of the American Society of Civil Engineers.)

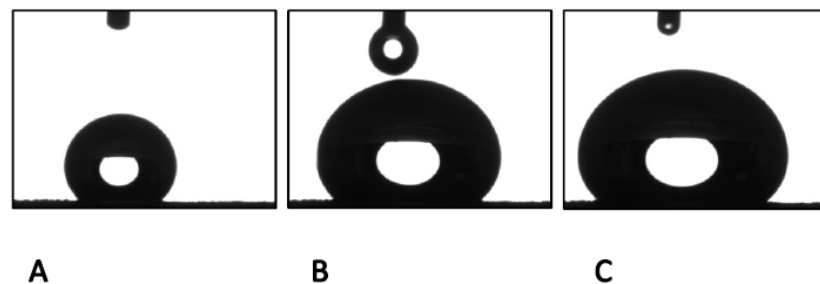


Figure 1.7. Pulse application of droplets to form stable contact line motion for dynamic CA measurement. Image were taken at 13, 167, and 243 seconds after the initial drop (A) and subsequent droplets (B) and (C) were deposited, respectively.

## 1.5 Results and discussion

### *1.5.1 Static and dynamic CA measurements*

Figure 1.8 shows example of dynamic CA measurement approach for four identical (OS: CFA mix) samples. The figure represents CA measurement for CFA treated using C-1 OS product (8 gm/kg mix). Varying initial drop sizes (10.41, 12.72, 16.43, and 23.41 mm<sup>3</sup>, Figure 1.8 (A, B, C and D, respectively)) were deposited, using a dynamic sessile drop approach, at different locations on the slide. The initial resulting CA values varied between 135° and 154°, a nearly 20° variations. As the drop volume is increased, the measured CA values increase Figure 1. a, decrease Figure 1. c, and/or oscillate Figure 1. b in its approach to a stable value. However, once a threshold volume is reached, the final measurements converge at approximately 148°, and this value taken as being more accurate and reflective of accommodating factors such as roughness, heterogeneity, chemical effects such as hydrogen bonding and dipole interaction. Similar improvements have been observed for all other OS chemicals across different mix ratios. This variable (e.g., increasing) approach to a stable CA value has also been reported by (Kwok and Neumann, 1999) (but discarded for oscillating and decreasing trends). Figure 1.9 provides another way to evaluate this behavior. It shows a continuous plot of three separate tests with C-2. Each test consists of 250 individual measurement.

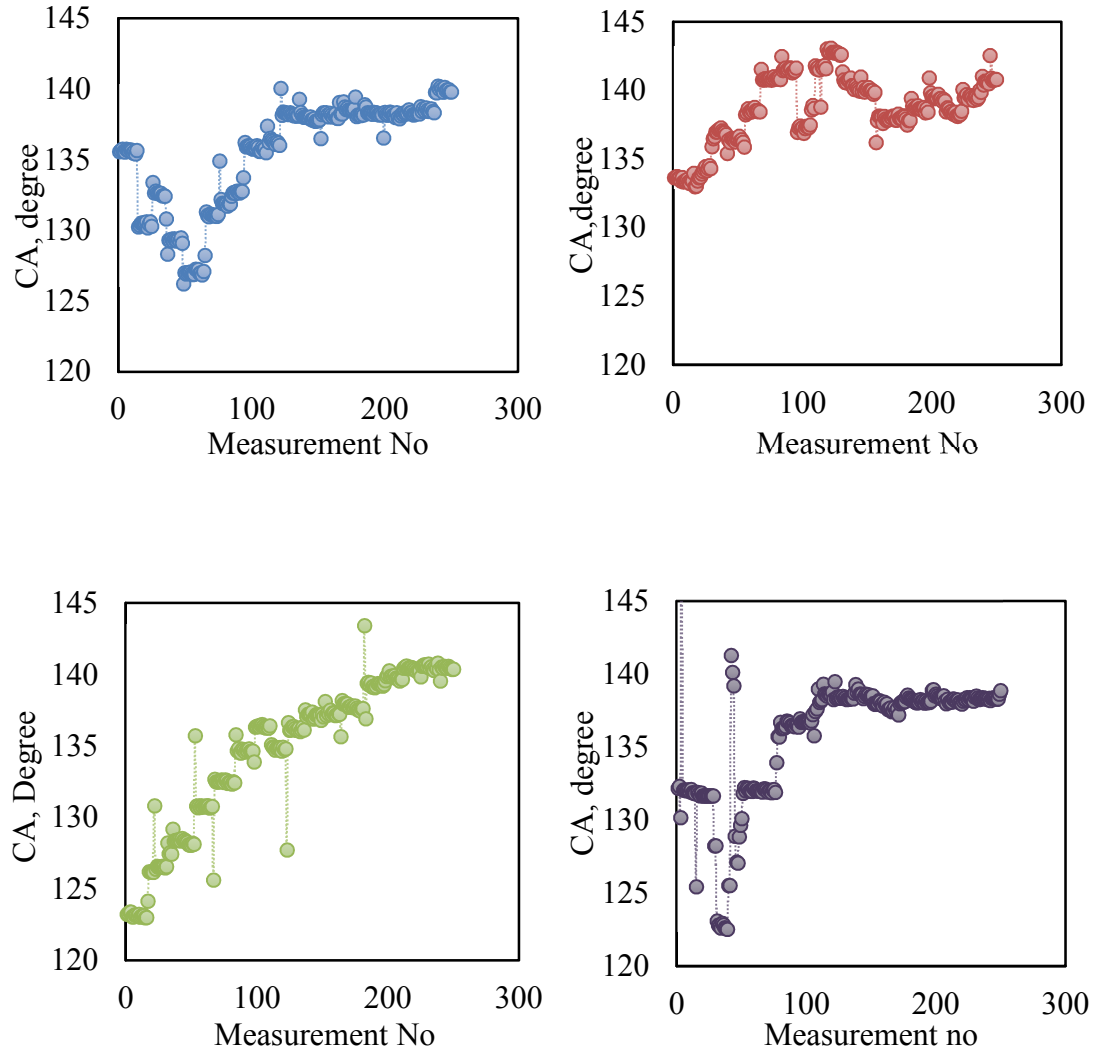


Figure 1. 8. Sample contact angle measurement using dynamic contact angle measurement approach. The static measurement represents the first measurement of contact angle for each case. Although droplets were deposited on same sample on a slide and the significant variation in initial contact angle measurement, all measurements eventually converge to an average  $148^\circ$ , representing the actual contact angle measurement for the CFA treated with OS C-1 (1:125 (OS: CFA) mix ratio).

The CA of a given drop evolves as discussed above: decreasing, increasing, oscillating or combinations of all as the volume increases. Initial drop sizes are different ( $27.06$ ,  $32.40$ , and  $12.41 \text{ mm}^3$ , respectively according to their sequence) while subsequent increments are at equal rate, i.e.,  $0.0009 \text{ L/s}$ . As depicted in Figure 1.9, despite increases in

drop volume and differences in droplet size at the end of each experiment (72.83, 64.72, and 41.12 mm<sup>3</sup>, respectively according to their sequence), contact angle measurements remain nearly constant after certain drop volume and measurement number. This is a clear demonstration for the requirement of a threshold drop size to measure accurate CA. As observed in the figure, initial CA varies from 131<sup>0</sup> to 140<sup>0</sup> while the final variability for the three tests is between 143<sup>0</sup> and 144<sup>0</sup>. The individual path to stability is attributed to surface roughness, heterogeneity of CFA, and the relative distribution of OS on the CFA. As a result, the sudden expansion or contraction, slip/stick according to (Kwok and Neumann, 1999) and, pinning/de-pinning according to (Bertola and Wang, 2015) of contact line (the line where the three-phases: liquid, solid and air intersect) motion are also overcome once the threshold size of the drop is maintained. This steady motion of the three-phase contact line provides repeatable CA measurement.

The use of dynamic measurements (at steady state motion of contact line) and existence of a threshold volume was found to apply to all mix ratios and chemicals. This manifests as reduced variation in dynamic measurements as compared to static measurements as shown in Figures 1.8 and 1.9.

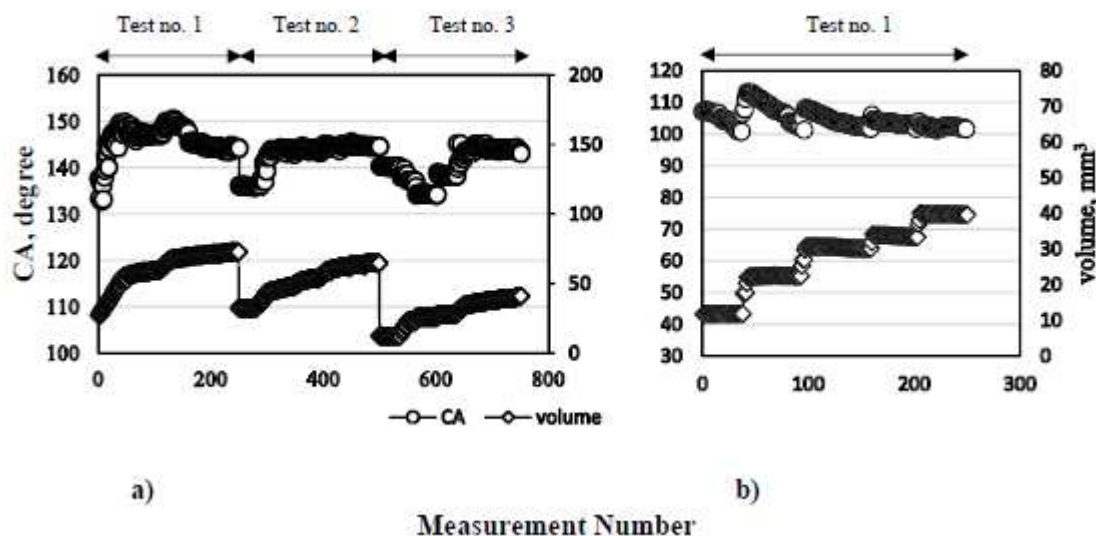


Figure 1. 9. Sample contact angle measurements (three different measurements) arranged sequentially. a) All the three tests represent data of identical sample but with different initial droplet sizes. For larger initial drop volume (test 2) convergence to dynamic CA starts earlier, 50 seconds after the start of the experiment. But the final CA measurement for the three tests varied between  $143^{\circ}$  and  $144^{\circ}$ . While b) shows a convergence of CA just before application of a drop.

(With permission from ASCE. This material may be downloaded for personal use only. Any other use requires prior permission of the American Society of Civil Engineers.)

In most cases, a higher variation in measurement occurs with less OS treatment (i.e., lower OS: CFA treatment ratios). With increasing treatment and hydrophobicity, the consistency increases. This is attributed to the OS effectively occupying more binding sites on CFA surfaces, reducing the surface energy and rendering it more uniform (and hydrophobic). In addition to greater variability, static measurements of CA tend to be lower for a given mix ratio. For example, as shown in Figure 1.10 to Figure 1.12, the CA of an OS mix of 10g/kg is  $136^{\circ}$  (static) while the same mix has a CA of  $148^{\circ}$  (dynamic), a statistically significant increase of  $12^{\circ}$ .

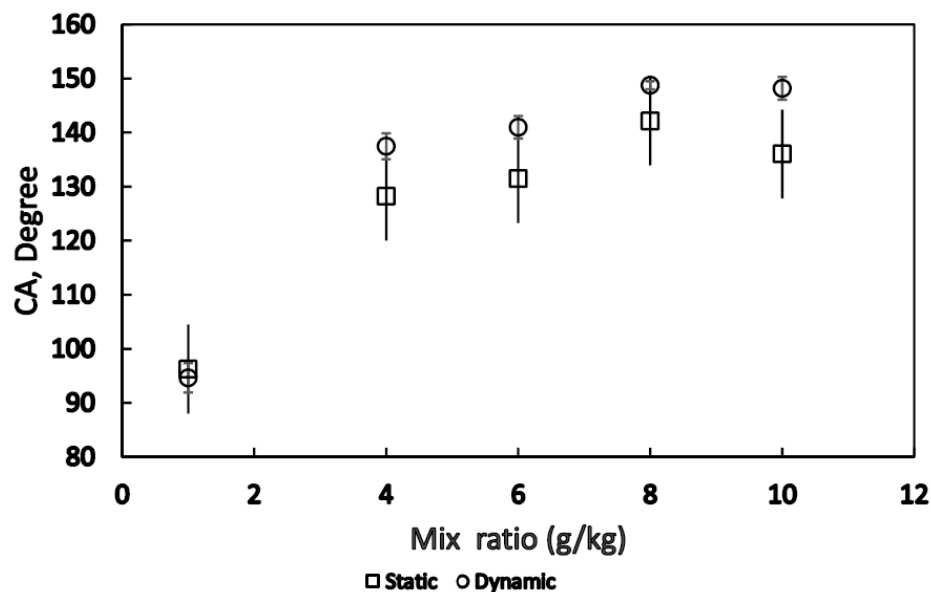


Figure 1. 10. Statistical analysis for comparison of dynamic and static contact angle measurement for CFA Class F (utility C) modified with OS chemical (C-4) using different mix ratios. The error bars represent one standard deviation.

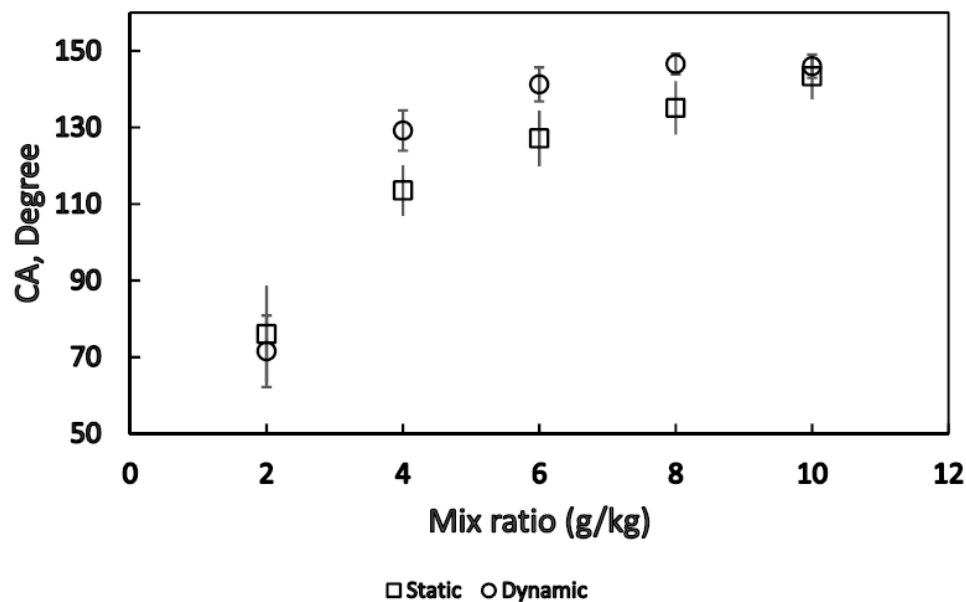


Figure 1.11. Statistical analysis for comparison of dynamic and static contact angle measurement for CFA Class F (utility C) modified with OS chemical (C-2) using different mix ratios. The error bars represent one standard deviation.

Different chemicals have shown different performance to change the surface energy of CFA, as shown in Figure 1:10 to Figure 1:12 . Factors that influence the performance of each chemical was not the intention of this study. However, based upon a given chemical's observed ability to increase the measured CA, mix designs can be developed. For example; while C-1 chemical requires as little as 2g/kg (OS: CFA) to produce contact angle of about  $140^{\circ}$ , it requires at least three times as much of the C-2 and C-4 chemicals to achieve the same water repellency.

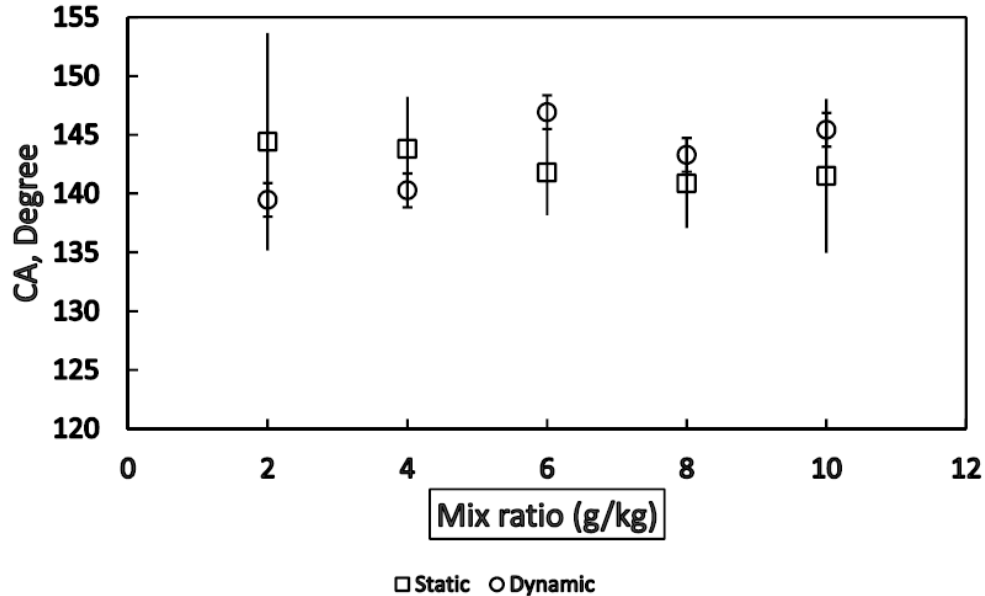


Figure 1.12. Statistical analysis for comparison of dynamic and static contact angle measurement for CFA Class F (utility C) modified with OS chemical (C-1) using different mix ratios. The error bars represent one standard deviation.

It has to be noted that beyond mix ratio of 6 g/kg (OS: CFA) the degree of change in hydrophobicity is negligible. This information, coupled with insight regarding the required level of water repellency for a given particle size, level of compaction and



temperature (Jordan et al., 2015), provides a basis for designing for water repellency, e.g., to limit infiltration and/or to prevent leachate generation.

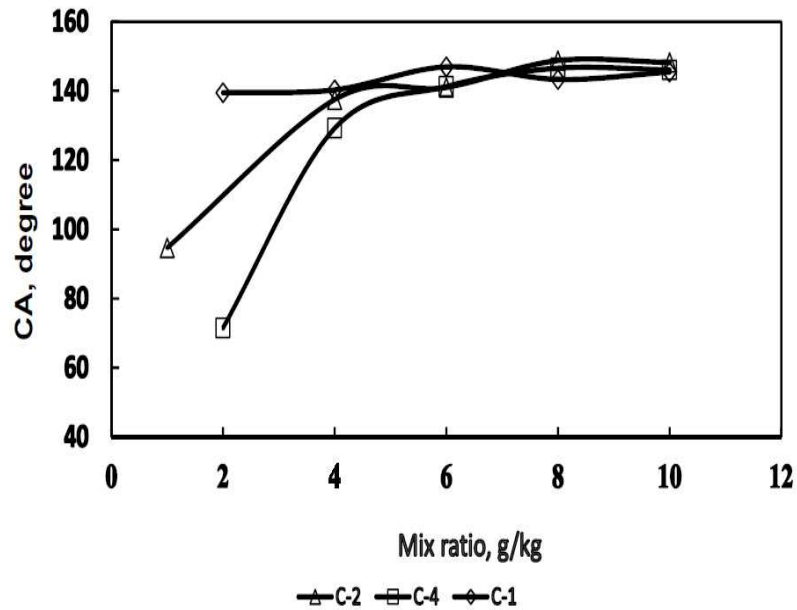


Figure 1. 13. CA measurement using a dynamic measurement technique. For CFA Class F, C-1 chemical able to form higher CA measurement including smaller OS: CFA mix. After OS mix of 6 gm subsequent addition of chemicals does not change much CA measurements.

(Figures 1:10 to 1:13 With permission from ASCE. This material may be downloaded for personal use only. Any other use requires prior permission of the American Society of Civil Engineers.)

### 1.5.2 Dynamic contact angle measurement

As concluded in section 1.5.1, accurate/repeatable measurement of CA on the MCFA surface is only achieved when a dynamic CA measurement technique is used. The technique was adopted through increasing drop size over the surface until the surface roughness and other factors in Equation (4) that influence CA measurements are minimized. The results show that DI water drops follow certain patterns on the MCFA

surfaces until it maintains a steady state motion, from which accurate CA measurements can be determined. The observed patterns and steady state motion characteristics are described in the following subsections.

*1.5.2.1 Patterns of drops motion on the MCFA:* In general, three main patterns were observed, as shown in Figure 1.14: a reduced acceleration (a), constant (zero) acceleration (b), and mixed type (highly variable and followed by reduced) acceleration (c), have been observed. The type of patterns observed are related more to the type of CFA than the chemicals and showed consistent phenomenon across all mix ratio tested.

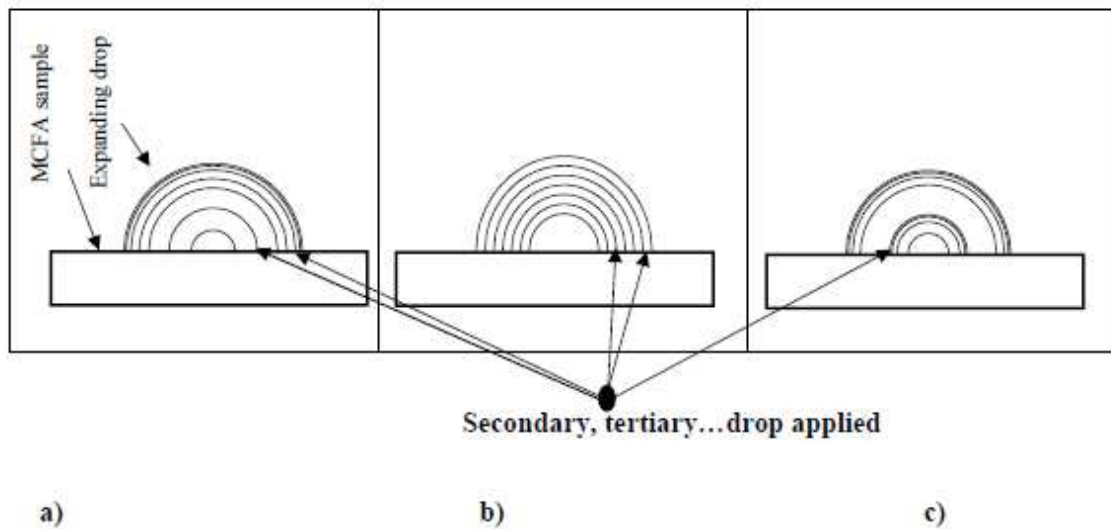


Figure 1.14. Different patterns of drop motion on the surfaces of the MCFA. The three-phase contact line; accelerates fast until the drop gets a certain volume (a), remains constant (b), and combination of both (c) while subsequent drops are released.

(With permission from ASCE. This material may be downloaded for personal use only. Any other use requires prior permission of the American Society of Civil Engineers.)

However, surfaces forming CA approximately less than  $110^\circ$  show the tendency of mixed type acceleration for all CFA and OS mix samples. Type (a) shows reduced acceleration motion in which the three-phase contact line advances less with increasing volume. Type (b) shows a constant acceleration type of a motion in which the contact line advances at a constant rate with increasing volume. The third type (c) shows mixed types (a and b) of motion.

While not observed, there is a fourth type of motion reported by (Bertola and Wang, 2015). In this case, there is a sudden expansion (positive velocity or accelerated motion), followed by a recoil (negative velocity or deaccelerated motion) of three-phase contact line motion Figure 1.15. Contraction (negative velocity) occurs when a drop endeavors to minimize surface energy while perturbed by the kinetic energy of a falling drop (approximately from 2-4 mm). This retraction time has been reported to be very short for a pure liquid on rough surface; within 40 and 50 micro-second (Rein, 1993) and (Bertola and Wang, 2015), respectively. To avoid inaccuracies in CA measurement from these phenomenon, the initial drop was allowed for up to 30 seconds to maintain stability before starting measurements. Furthermore, in order to avoid external influences such as kinetic motion of the subsequent droplets on measurements, data related to such extreme positive and negative conditions were not directly considered in data interpretation because such behavior result in inaccurate CA measurements.

*1.5.2.2 Drop size and contact line motion:* Contrary to the observations made by Li (1996) and (Belibelet al., 2016) regarding the non-dependence of CA measurement on drop volume, our study on MCFA found that different initial drop volumes resulted in varying

CA measurements. Theoretically, despite the sizes of drops, the surface energy of the MCFA (for a particular OS: CFA mix used) must be equal as long as the liquid used for a drop is same, as energy must be constant (de Gennes, 1985). That means despite the size of drops the surface energy of both the liquid and the solid surface does not vary. If the surface energy of both phases is constant and kept under constant third phase (gas), the mechanical equilibrium and subsequently the CA between these phases remains constant. In reality, surface roughness and heterogeneity of MCFA particles have a significant effect that manifests as a function of drop sizes. As pendant drops impinge upon the surface there is an unpinning of the three-phase contact line from its existing location and sudden movement to a new location.

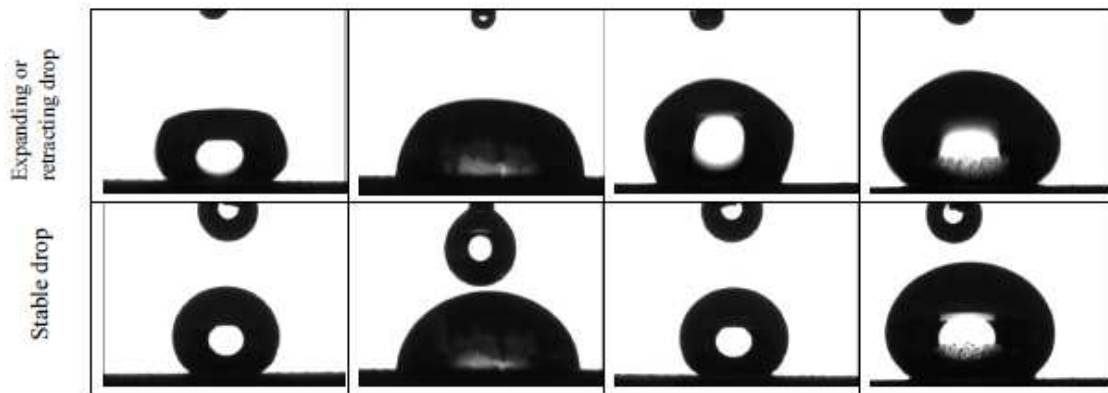


Figure 1.15. Contact line motion and shape of drops affecting CA measurement. Second row shows different shapes of stable drop and the firsts row is their corresponding response (expanding or retraction) after successive drop is released.

(With permission from ASCE. This material may be downloaded for personal use only. Any other use requires prior permission of the American Society of Civil Engineers.)

This phenomenon is known as stick/slip (Kwok and Neumann, 1999) or pinning and unpinning (Bertola and Wang, 2015). It has been determined that this sudden change

in position of the contact line (particularly for smaller/initial drop), as influenced by surface roughness, introduces variability into CA measurements. To suppress the influence of roughness (Nickelsen et al., 2015) and heterogeneity for accurate CA measurements, many studies have designed different approaches and techniques, for example a relationship shown in Equation (4) through including “accessible” and “non-accessible” factors. The determination of these accessible and non-accessible factors can be considered only through suitable experimental techniques and procedures during measurement (Kwok and Neumann, 1999). Some studies (Kwok and Neumann, 1999; Marmur, 2006) have proposed that the increase in drop size suppresses factors influencing CA measurements. Others for example Koc and Bulut (2014) and Santner et al. (2012) try to suppress this effect through polishing the solid surfaces. In particular, Kwok and Neumann (1999) used the application of low rate dynamic CA experiment (to increase drop size) and identified that after drop reaches a contact line diameter of 4.8 mm CA measurement does not change significantly. However, this explicit dimension of a drop does is clearly a function of the substrate under consideration. For MCFA in this study, it has been determined that different samples of the MCFA have different dimensions when the three-phase contact line motion is stabilized.

In this experimental study, different patterns of the three-phase contact line motion have been identified for five MCFA surfaces (MCFA-1, MCFA-2, and MCFA-3 follow patterns of Figure 1.14(a), MCFA-5 follows pattern in Figure 1.14(b), and MCFA-2 and MCFA-6 follow pattern in Figure 1.14(c). Moreover, the threshold drop size required for repeatable CA measurements was found to vary as well. As shown in the figure, three separate tests were conducted at different times but with identical mix ratios Figure 1.9(a). Three different initial drop sizes were deposited on the MCFA, after which a CA

measurement was made once per second for 250 seconds. Despite the initial trend of CA variation (increasing, decreasing, or both) all the three measurements converge to 144, 143, and 144 degrees, according to their arrangements tests 1, 2, and 3. This suggests once the drop reaches a threshold size (depending on the type of CFA and OS) further increase in the drop volume does not affect CA measurement because stable motion of the contact line is maintained. Figure 1.9(b) shows CA measurements for CFA-2 and the different behavior exhibited as the three-phase contact line motion becomes stable. As shown in the Figure, CA measurements are affected significantly when initial subsequent drops are added. However as drop size increases beyond the threshold level and the subsequent contact line expands a further release of drops do not affect CA measurements. This repeatable measurement of CA again results from stable motion of the contact line. Furthermore, while nearly equal volume of droplets was supplied their individual effect on CA measurements asymptotically diminishes. For example, in Figure 1.9(b), CA measurements converge to 100.82, 101.31, 101.73, 101.69, and 101.56 degrees. Such behavior is consistent with a conclusion that static CA measurements effectively represent lower energy surfaces, as in the case of the modified CFA-2 (smaller mix) and CFA-6. That said, a minimum amount of time is required before the contact line motion is stable.

Once this convergence and stability of contact line motion has been maintained, further increases in drop volume do not significantly affect the trend. It is at this point that the CA measurement is repeatable. The values which correspond to this stability are shown in Table 1.1. Each plot represents data collected from 2000 to 2500 measurements having variable initial drop sizes but identical CFA and OS mix ratios. The figure reveals that CA measurements vary up to  $20^\circ$  during the initial stages of the measurement, consistent with

previous reports, e.g., 5- 20 degrees in Goodet al., (1979) as well as Feyyisa and Daniels, (2016), and followed by either a rising, falling or both towards its stable state based on the OS: CFA mix used (higher mix relatively shows less CA measurement variability). As the drop size is further increased, the discrepancy of successive measurements of CA is reduced until it stabilizes between  $2^0$  and  $5^0$ . This range is consistent with recommendations by Duncan et al. (1995) that any method should detect a CA variation of 1- 5 degrees over 1-5 mm change in contact radius.

Certain initial drop volume limitations were identified for certain MCFA types. For example, for super hydrophobic surfaces (i.e. surfaces with a CA greater than  $150^0$ ) such as modified CFA-5, CA measurements could not be made with drops less than approximately  $25 \text{ mm}^3$ . Smaller drops are too unstable for a measurement to be made. This can be attributed to the pressure difference between the internal and external surfaces of a drop as small droplets experience disproportionately high internal pressure on super hydrophobic surfaces. The change in pressure is a function of surface tension and drop diameter.

As shown in Figure 1.9(a) test no.2, while initial larger drops tend to approximate the dynamic CA faster, slowly smaller drops also assume nearly equal measurement. According to Marmur (1998) when the internal energy of the solid-liquid-fluid interface reached a minimum, stability is maintained. In a different study Marmur (2006) related this drop stability with drop size such that larger drop sizes are able to provide more accurate CA measurements than smaller ones. The influence of drop size on CA measurement accuracy has also been discussed in various ways: drops require a certain energy level to advance on rough and heterogeneous surfaces (Johnson and Dettre, 1964), therefore larger

drop sizes are able to overcome many of the factors influencing CA measurements such as, surface roughness and heterogeneity (Kwok and Neumann, 1999). Size alone does not address CA measurement inaccuracy, as de Gennes (1985) concluded that the slip/stick effects will remain. As such, it is the method proposed herein that can address both stick-slip and surface roughness.

As shown in Figure 1.16 a steady motion of the drop results when the three-phase or triple line according to (de Gennes, 1985) is pinned or transformed to a new location at a constant speed, and CA measurements converge to values fluctuating within a range less than  $5^{\circ}$ . Furthermore, the rate at which this steady state motion occurs is highly depend on both the type of CFA and the performance of OS chemicals. The other advantage of using this proposed experimental technique is that CA hysteresis, defined as the difference in measurement of left and right angle, is reconciled. In this study CA hysteresis went from up to  $15^{\circ}$  at the beginning to less than  $2^{\circ}$ . Any measurement of CA that does not consider the stability and motion of a drop (the three-phase contact line velocity) can leads to significant measurement error.

*1.5.2.3 CA measurement and drop size:* As the foregoing illustrates, repeatable CA measurements are possible only when contact line motion is at steady state. Steady state motion of the drop is achieved when drop size, depending on the type of CFA, reaches a threshold size. By using this technique, the variation in CA angle measurements was significantly reduced, between  $0^{\circ}$  -  $5^{\circ}$  over change in contact line from 2 to  $> 3$ mm, depending upon the type of chemical and mix ratio on one hand and type of ash used on the other. This reduction in variability is consistent with the assumption that a solid surface



has a constant surface energy. Plots of the three-phase contact line velocity versus drop size have been shown in Figure 1.18 to Figure 1.22.

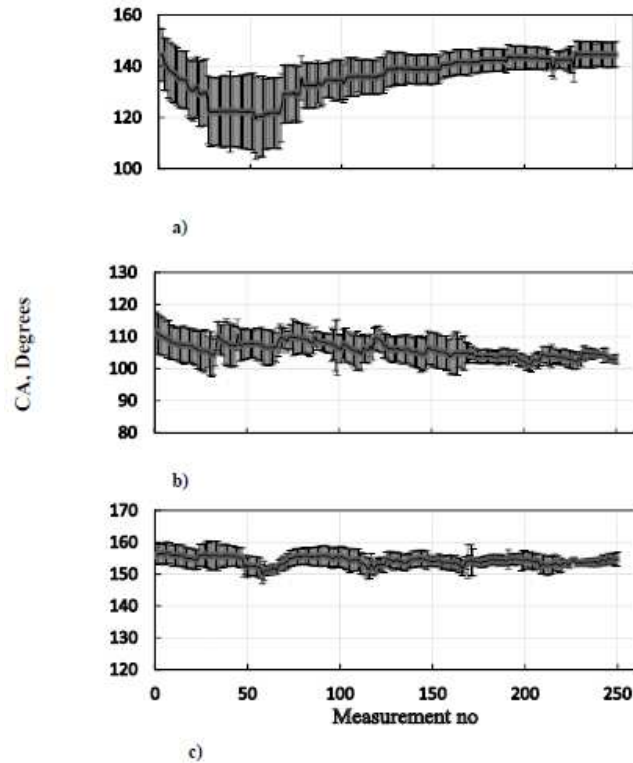



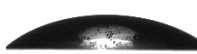



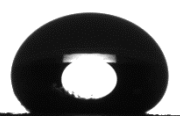

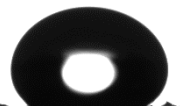
Figure 1.16. Example of degree of variation in CA measurements as a factor of drop volume for: CFA-3 treated using C-1 (a), CFA-2 treated using C-4 (b), and CFA-5 treated using C-2 (c) representing patterns: 1, 2, and 3 in Figure 2.4, respectively. Error bars represent one standard deviation.

(With permission from ASCE. This material may be downloaded for personal use only. Any other use requires prior permission of the American Society of Civil Engineers.)

The velocity of a drop is measured by calculating the time required for the three-phase contact line to move or expand while supplying subsequent drops. The drop size corresponding to zero acceleration is that which allows for repeatable CA measurements. The actual measurements of CA for the five CFA modified using three OS are shown in Figure 1.24. The relative performance of OS across dose used have been shown in the

Figure. Once the threshold size of a drop is maintained, repeatable CA measurement is possible independent of the amount and density of grains (layering) where a drop is released. The term “density” is used informally as it was not measured in terms of mass per unit volume on the glass plates. However, varying densities were prepared and evaluated as shown in Figure 1.17 for CFA-3. The table is representative of behavior for CFA1-3, however, it was observed that CFA-5 and CFA-6 requires at least a “high” density to ensure repeatable measurements. “High” in this context means that the glass plate cannot be visible and must be completely obscured by the ash particles Table 1.1. As the shown in the table, and CA measurements do not vary from the degree of coverage or quantity of grains over which the drop is released.

Table 1.1. Images of drops released at different CFA grain coverage and CA measurements.

	Plan view of drops and CFA grain arrangement on the tape	Description	Drop image through Goniometer during CA measurement	Average range of CA measurement
1		No density		$0^{\circ} - 90^{\circ}$
2		Low density		$141.6^{\circ} - 143.2^{\circ}$
3		High density		$139.4^{\circ} - 143.1^{\circ}$
4		Very high density		$140.1^{\circ} - 144.7^{\circ}$

In some cases, this is achieved almost immediately as in the case of MCFA-5 which requires a larger initial drop size due to its super-hydrophobic ( $CA > 140^\circ$ ) surface.

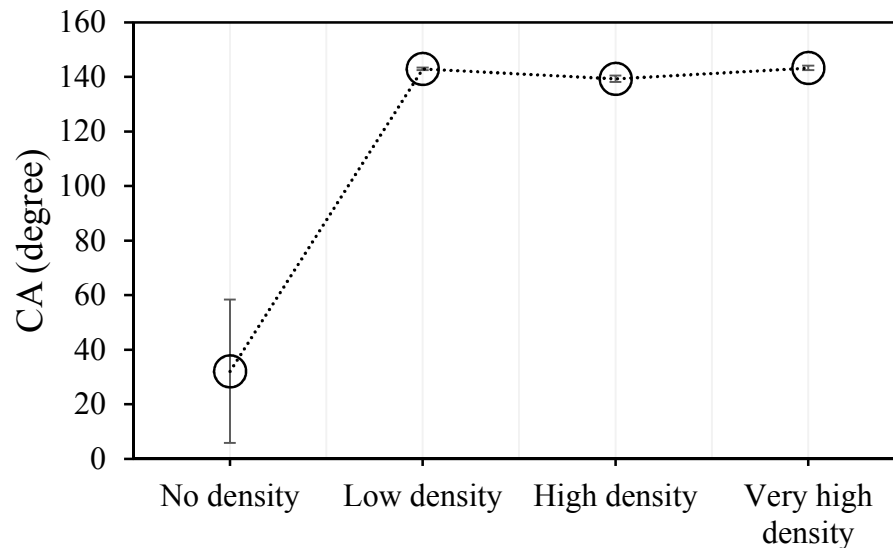


Figure 1.17. CA measurements for different degree of grain size distribution

The following Figures 1.18 – 1.22 illustrate different velocity of the three-phase contact line motion towards stability. In most cases while drop size increased velocity does not change significantly. This is the case in which MCFA-5 forms a higher CA and requires a relatively larger drop size to rest on the sample. Minor fluctuations in velocity is due to external factors (such as ambient air circulation and laboratory/structural vibrations).

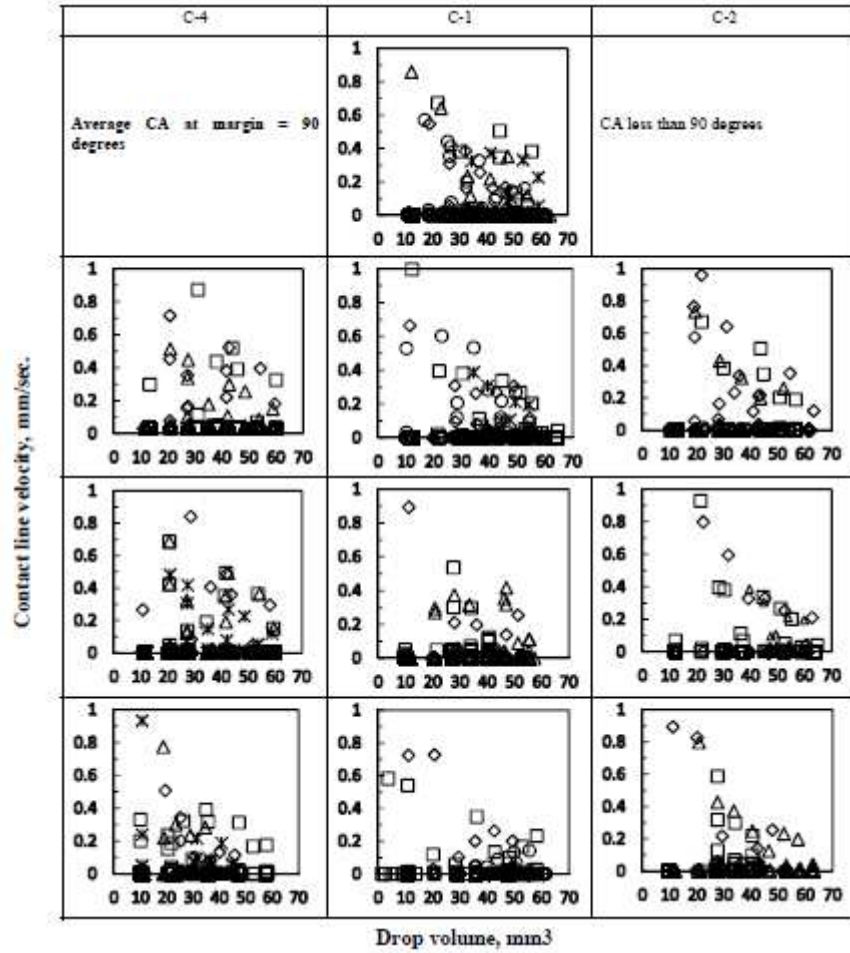


Figure 1.18. Plots of drops sizes at which acceleration reaches zero (velocity = 0.4 mm/sec.) for MCFA-1 mixed with OS: C-4 C-1, C-2 in columns 1,2, and 3 respectively. Rows represent mix ratio used in ascending order top down (2, 4, 6 and 8). Markers indicate repeated measurement for same sample.

(With permission from ASCE. This material may be downloaded for personal use only. Any other use requires prior permission of the American Society of Civil Engineers.)

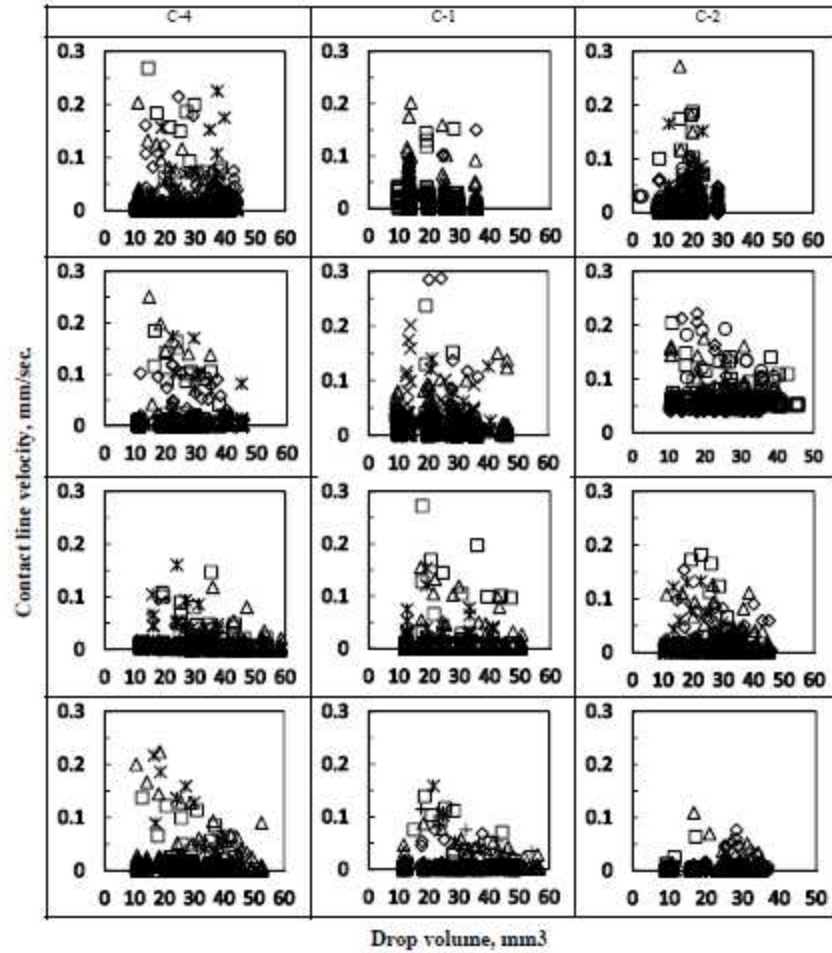


Figure 1.19. Plots of drops sizes at which acceleration (velocity = 0.1 mm/sec.) reaches zero for MCFA-2 mixed with OS: C-1, C-2 and C-4 in columns 1,2, and 3 respectively. Rows represent mix ratio used in ascending order top down (2, 4, 6 and 8).

(With permission from ASCE. This material may be downloaded for personal use only. Any other use requires prior permission of the American Society of Civil Engineers.)

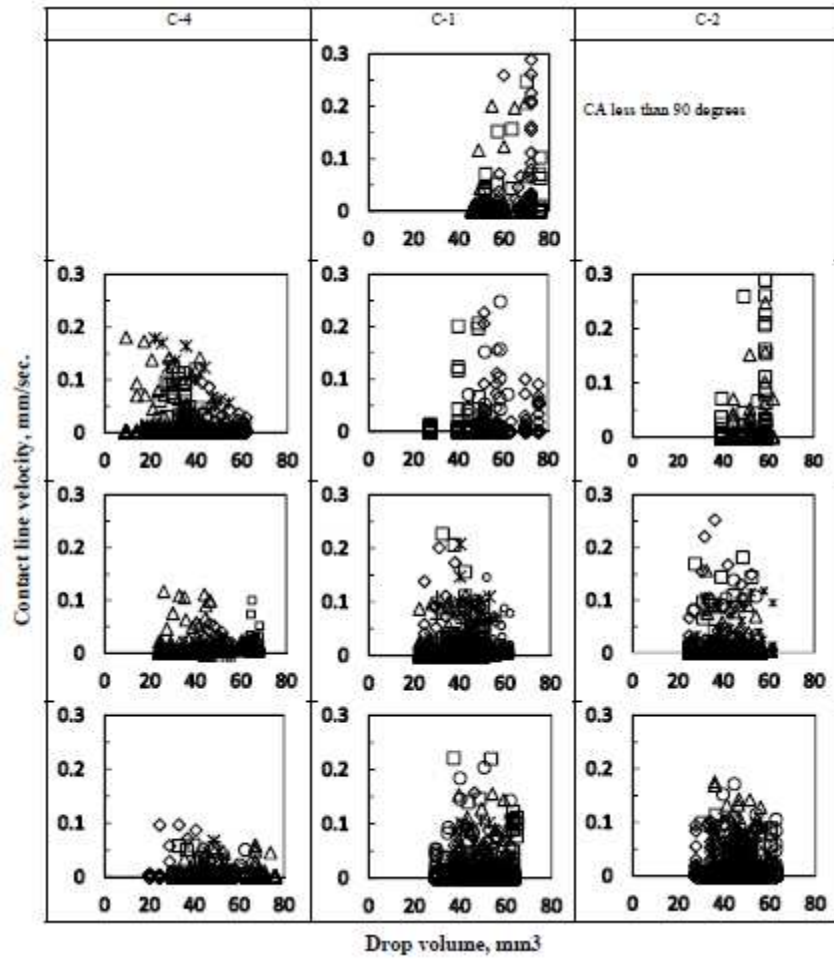


Figure 1.20. Plots of drops sizes at which acceleration reaches zero (velocity = 0.2 mm/sec.) for MCFA-5 mixed with OS: C-4, C-1 and C-2 in columns 1, 2, and 3 respectively. Rows represent mix ratio used in ascending order top down (2, 4, 6 and 8). Markers indicate tests.

(With permission from ASCE. This material may be downloaded for personal use only. Any other use requires prior permission of the American Society of Civil Engineers.)

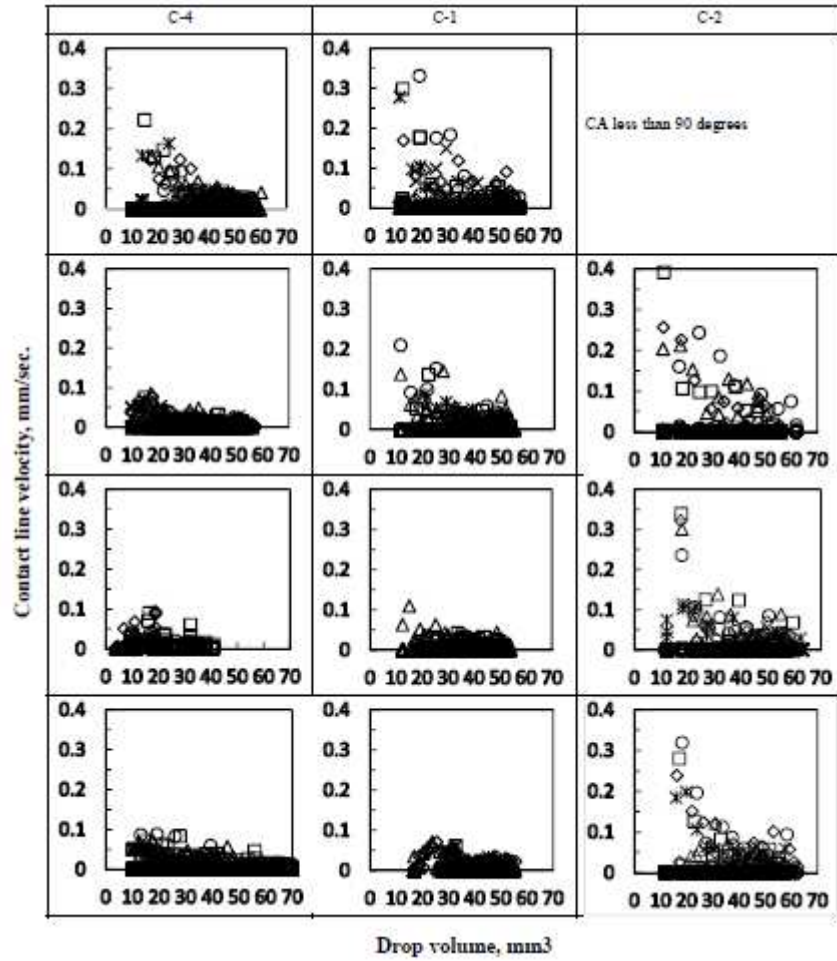


Figure 1.21. Plots of drops sizes at which acceleration reaches zero for MCFA-3 mixed with OS: C-4, C-1 and C-2 in columns 1, 2, and 3 respectively. Rows represent mix ratio used in ascending order top down (2, 4, 6 and 8). Markers indicate tests.

(With permission from ASCE. This material may be downloaded for personal use only. Any other use requires prior permission of the American Society of Civil Engineers.)

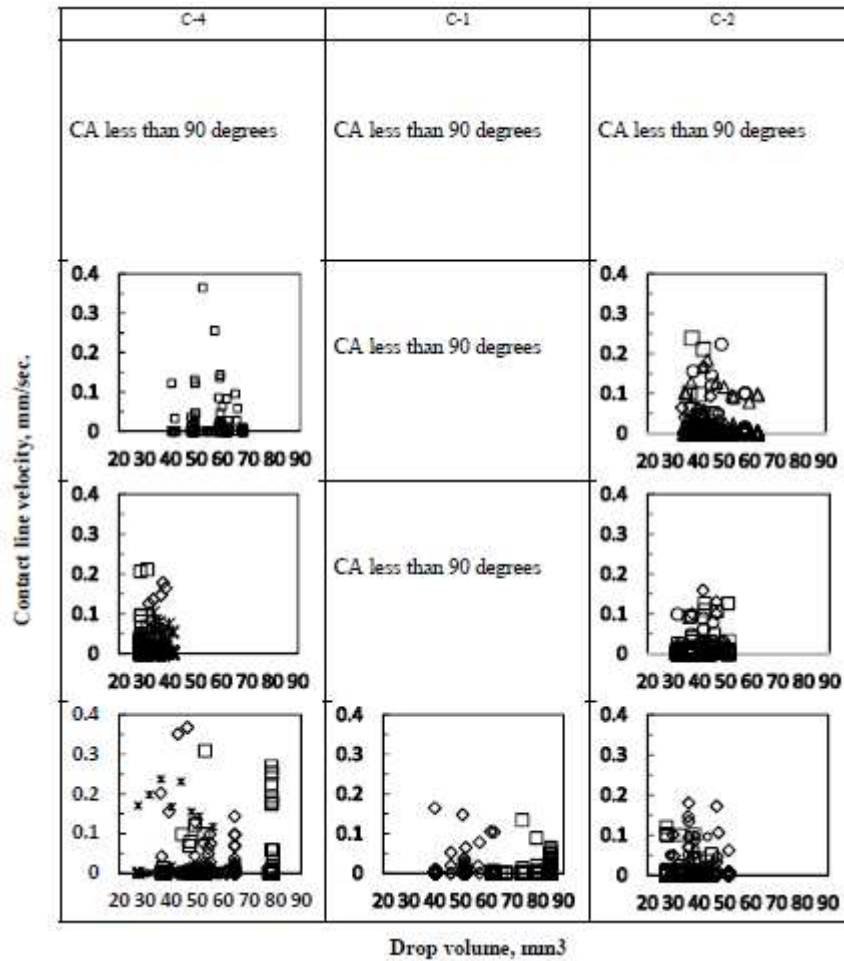


Figure 1.22. Plots of drops sizes at which acceleration reaches zero for MCFA-6 mixed with OS: C-4, C-1 and C-2 in columns 1, 2, and 3 respectively. Rows represent the mix ratio used in ascending order top down (2, 4, 6 and 8). When drop volume is increased the contact line motion resembles pattern c but it's less hydrophobic property influences in such a way that higher variability of velocity observed for certain drop volume. Markers indicate tests.

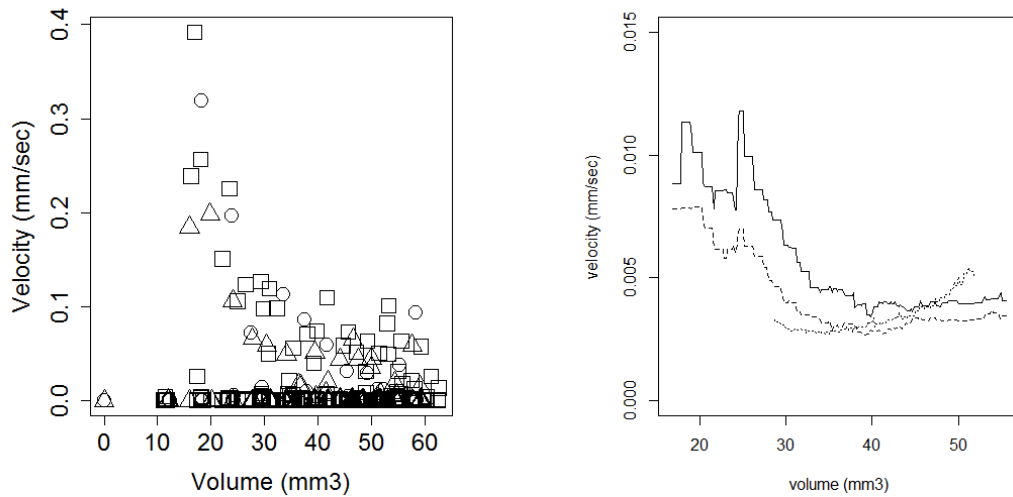
(With permission from ASCE. This material may be downloaded for personal use only. Any other use requires prior permission of the American Society of Civil Engineers.)



1.5.2.4 *Kernel density distribution estimation*: To deduce the actual velocity of a drop where the three-phase contact line motion becomes nearly constant is subjective Figure 1.18 to Figure 1.22. Kernel density distribution Equation (1.5) was used to identify the patten and estimate the size of a drop where three-phase contact line motion becomes constant. This type of approach does not assume any underlying distribution, non-parametric. It depends on the data at each datum. Figure 1.23 shows sample contact line motion and its corresponding kernel density distribution estimate.

$$f(x) = \frac{1}{nh} \sum_{i=1}^n k\left[\frac{(x-x_i)}{h}\right] \quad 1.5$$

Where n = number of variables, k=kernel (normal distribution), h= band width, xi= mean, and x =variable.



a)

Figure 1.23. Calculated (left) and Kernel density distribution (right) contact line velocity to estimate the corresponding drop volume; a) CFA-3 treated using C1-8, b) CFA-5 treated using C1-8, and c) CFA-6 treated using C4-8

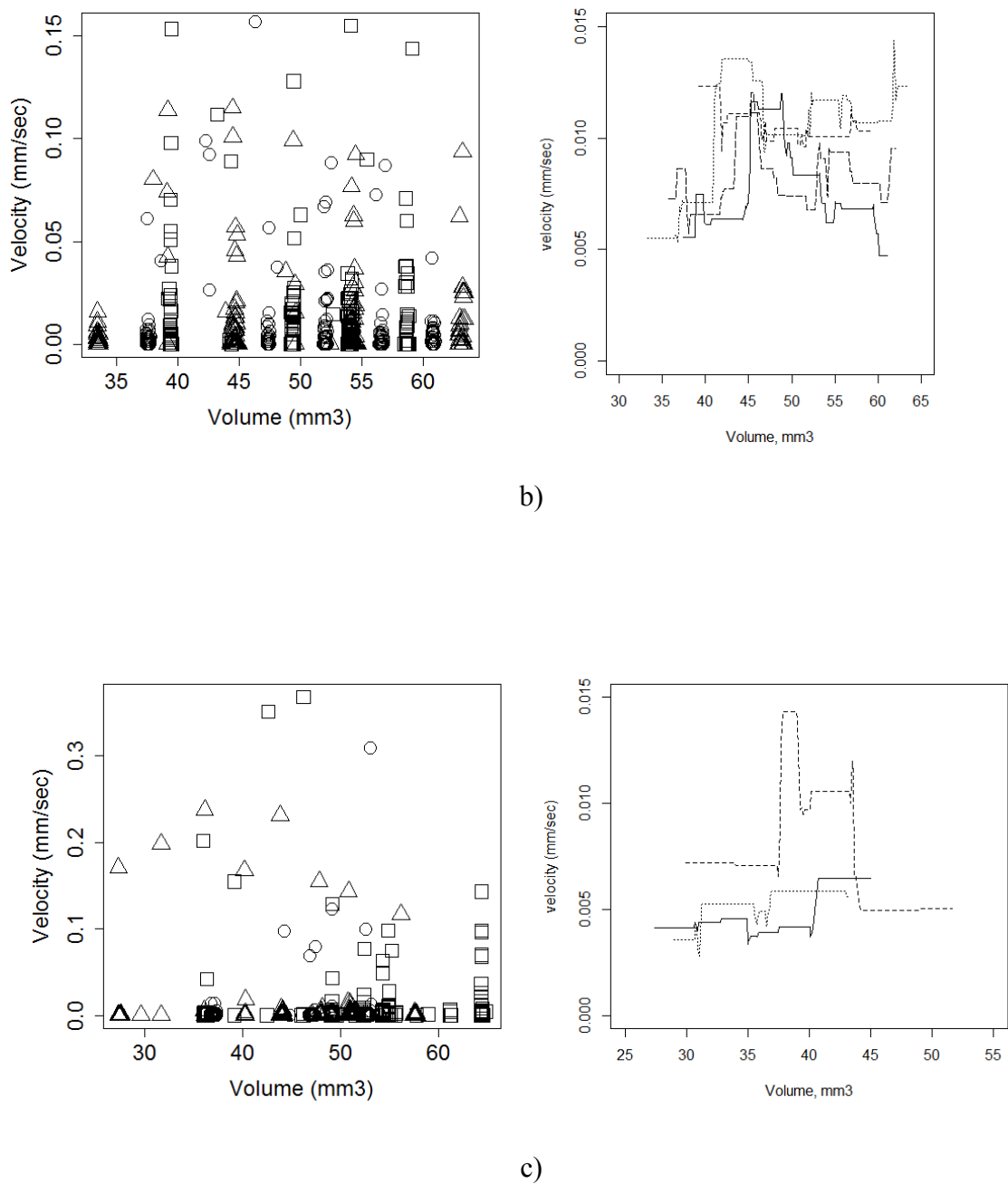


Figure 1.23. continued

To recommend an appropriate minimum size of a drop required to measure CA accurately (in conjunction to Kernel distribution), a statistical analysis has been conducted

for the change in the standard deviation of velocity of the three-phase contact line motion after every droplet. The test begins by considering the initial drop volume (considering all data) and continues forward to the point where subsequent drops were released. For example, while calculating the change in velocity after releasing the second drop, velocity data of the initial drop is not considered. Based on this statistical analysis, Table 1. 2 provides a recommendation for minimum drop size for CA measurement for the samples tested.

Table 1. 2. Minimum recommended size of drops to measure accurate CA for different types of MCFA and OS across different mix ratios. The recommended sizes of drops are based on repeatable measurement and statistical evaluation of relative velocity of contact line. Data not provided for CA less than 90<sup>0</sup>, where applicable.

			Drop size, mm <sup>3</sup>		Standard deviation		
MCFA	OS	OS-CFA (g/kg)	Initial	Minimum recommended	Initial	After stable motion maintained	Percent improved
	C-1	2	11	47	0.05871	0.03698	37.02
		4	10	43	0.06337	0.03474	45.17
		6	10	39	0.06869	0.04200	38.86
		8	9	33	0.04550	0.03559	21.78
	C-2	2	0	0			
CFA-1		4	10	44	0.06071	0.03636	40.11
		6	12	37	0.08239	0.04326	47.49
		8	9	33	0.05582	0.03820	31.56
	C-4	2	9	44	0.03097	0.01634	47.25
		4	15	44	0.02179	0.00462	78.80
		6	10	43	0.07433	0.05143	30.81
		8	10	35	0.06432	0.01708	73.45
	C-1	2	9	34	0.02103	0.02092	0.50
		4	12	27	0.02779	0.02204	20.69
		6	12	30	0.01531	0.01315	14.10
		8	10	30	0.01708	0.00998	41.60
	C-2	2	11	>40	0.02419	0.01990	17.74
CFA-2		4	11	35	0.01533	0.00892	41.78

		6	15	32	0.01954	0.01178	39.70
		8	10	32	0.01738	0.00821	52.77
	C-4	2	9	35	0.01858	0.01331	28.37
		4	10	35			
		6	10	35	0.02179	0.00462	78.80
		8	13	24	0.00998	0.00679	32.02
	C-1	2	11	40	0.02716	0.00609	77.59
		4	10	38	0.02021	0.00800	60.42
		6	11	28	0.01533	0.00892	41.78
		8	9	25	0.01217	0.00743	38.96
	C-2	2	11	48			
CFA-3		4	9	41	0.02413	0.01109	54.04
		6	10	28	0.01533	0.00892	41.78
		8	10	20	0.02088	0.01295	38.00
	C-4	2	9	35	0.01063	0.00221	79.25
		4	9	33	0.06135	0.00646	89.48
		6	12	30	0.02034	0.00545	73.22
		8	10	25	0.00993	0.00941	5.18
	C-1	2	50	75	0.02366	0.02607	-10.20
		4	37	62	0.02263	0.02507	-10.80
		6	27	53	0.02225	0.01901	14.55
		8	39	53	0.02419	0.01914	20.87
	C-2	2	28	72			
CFA-5		4	25	60	0.02436	0.02609	-7.08
		6	25	51	0.02336	0.02509	-7.08
		8	35	55	0.02690	0.02921	-8.59
	C-4	2					
		4	25	44	0.02198	0.02341	-6.48
		6	19	50	0.02523	0.01365	45.90
		8	33	70	0.00808	0.00768	4.96
	C-1	2	0	0			
		4	0	0			
		6	0	0			
		8	0	62	0.01837	0.01305	28.96
	C-2	2	0	0			
		4	34	53	0.02534	0.01959	22.67
		6	31	50	0.01750	0.02645	-51.13
		8	29	51	0.02402	0.00238	90.08
	C-4	2					
		4		65	0.03505	0.01256	64.17
		6		37	0.02218	0.01350	39.11
		8		53	0.04582	0.06512	-42.13

(With permission from ASCE. This material may be downloaded for personal use only. Any other use requires prior permission of the American Society of Civil Engineers.)

In the case of MCFA-5, virtually any drop size will yield an accurate CA measurement and only a smaller improvement is observed as the drop volume is increased. Of all materials, MCFA 6 was the most unique. While further study is required, this difference in behavior is ostensibly related to the material composition, i.e., lignite coal ash which is different than any other material, i.e., having less silica by weight and therefore less bonding with OS chemicals.

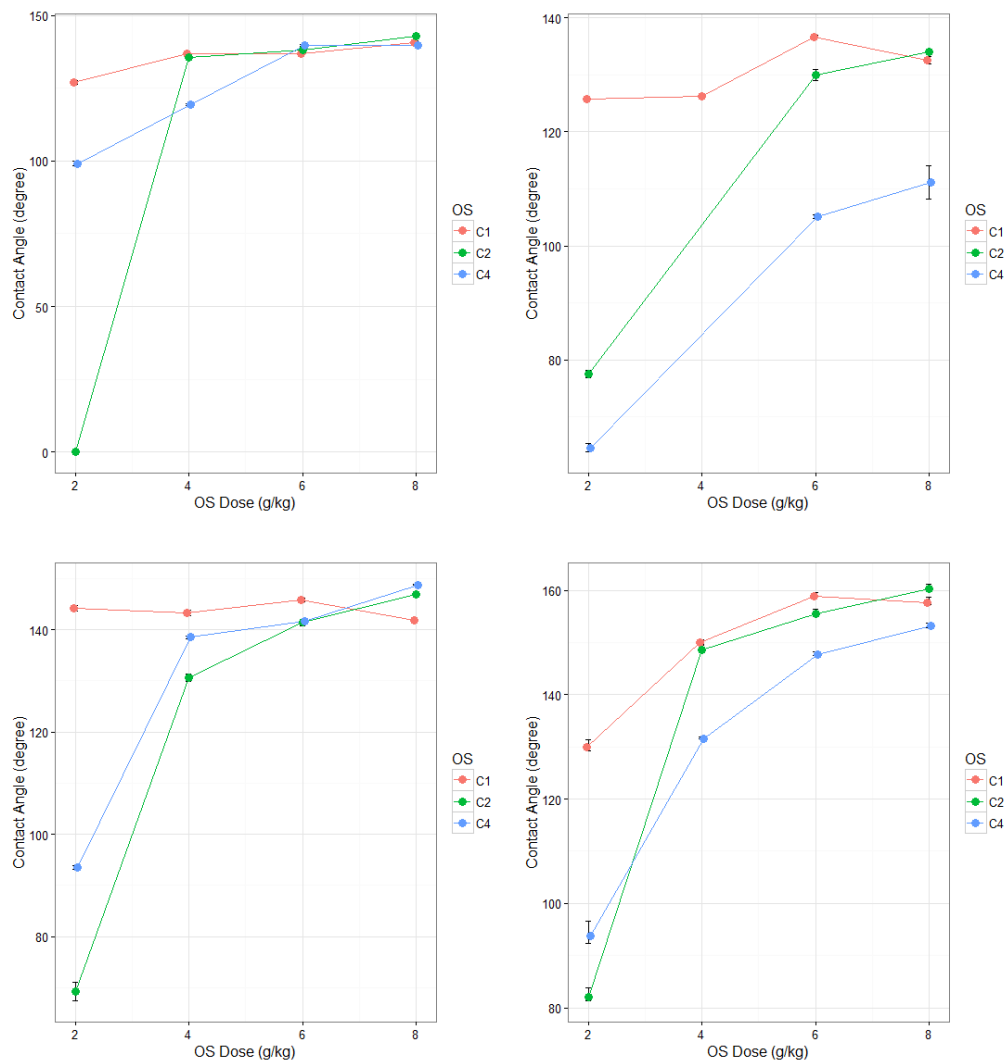


Figure 1.24. Dynamic CA measurements for different types of CFA mixed with three different types of OS chemicals after three-phase contact line is stabilized. First column for CFA (1-3) and second column for CFA (5 and 6)

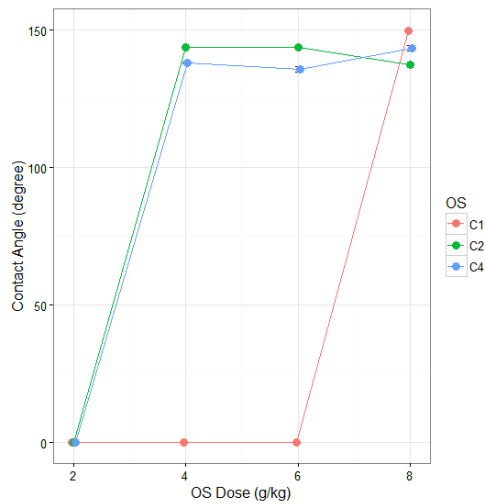


Figure 1.24. continued

(With permission from ASCE. This material may be downloaded for personal use only. Any other use requires prior permission of the American Society of Civil Engineers.)

Figure 1.25 depicts the probability density distribution of OS in terms of its ability to increase the CA and render a surface hydrophobic. It shows the probability range an OS chemical able to form a water repellent character regardless of the ratio OS: CFA mix used. Generally, OS product C-1 results in greater water repellency as defined by a CA that has the smallest standard deviation except for CFA-6. The performance of OS when used to treat CFA-6 showed a larger disparity particularly C-1.

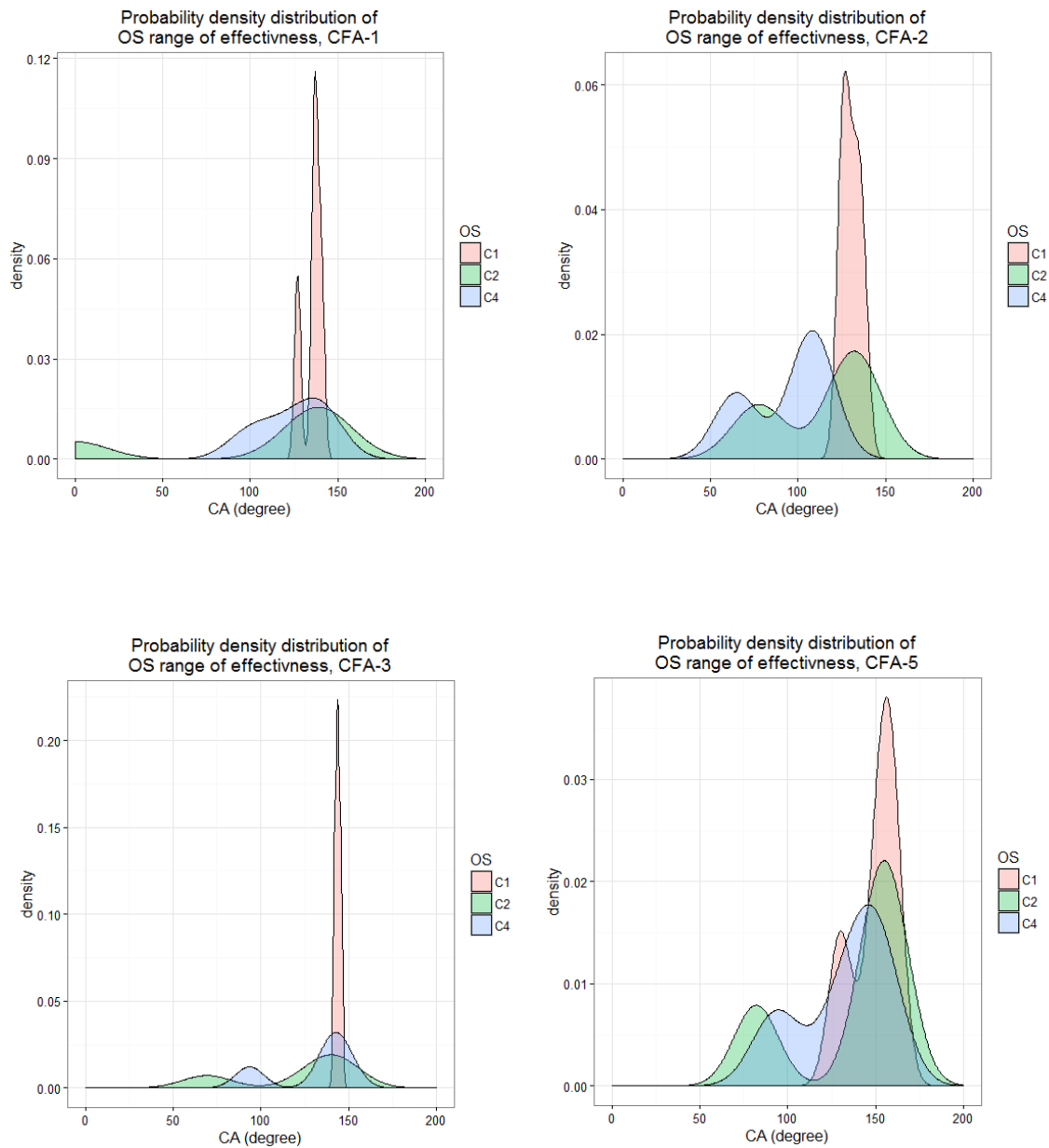


Figure 1.25. Probability density distribution range of OS effectiveness to form hydrophobic surfaces. First column for CFA (1-3) and second column for CFA (5 and 6).

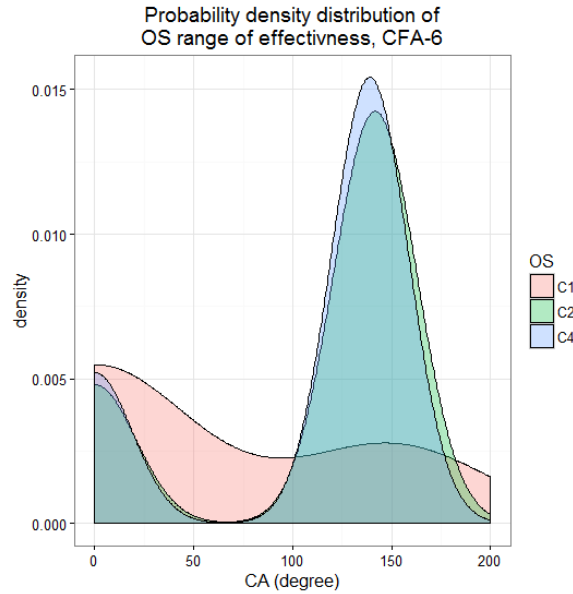


Figure 1.25. continued

(With permission from ASCE. This material may be downloaded for personal use only. Any other use requires prior permission of the American Society of Civil Engineers.)

## 1.6 Summary and Conclusion

This study reports on the modification CFA from hydrophilic ( $CA < 90^\circ$ ) to hydrophobic material ( $CA > 90^\circ$ ). CA values should be measured with a dynamic, rather than static approach. In particular, a new approach (based on dynamic contact angle technique- ADSA) is suitable and reliable to measure contact angle of the modified CFA. While conventional static measurement techniques to measure CA for modified CFA have showed significant variability (up to  $20^\circ$ ) for identical samples, variability is reduced by an order of magnitude ( $2^\circ$ - $5^\circ$ ) for the dynamic technique. In addition to greater variability, static measurements of CA tend to be lower for a given mix ratio. The proposed dynamic technique involves the continuous addition of the wetting fluid until a threshold volume has been reached, beyond which the CA value remains constant. This behavior applied to all chemicals investigated. In general, use of a larger initial droplet size leads to a stable



final CA value more quickly. Also, with increasing hydrophobicity, the consistency of CA values increases. This is attributed to the OS effectively occupying more binding sites on CFA surfaces.

OS can be used to transform coal fly ash (CFA) from a wettable material to one that is water repellent. The extent to which water repellency has been engendered is typically quantified with CA measurements. This study provides supporting data for an innovative approach to measure CAs of CFA that was modified to increase its water repellency using OS chemicals, i.e., MCFA. The results herein indicate that a dynamic, advancing method of CA measurement increases the accuracy for MCFA. Specifically, a drop size is allowed to expand over the sample until the three-phase contact line motion becomes constant in order to provide repeatable measurements. As a result, for each sample a threshold drop size at which the three-phase contact line motion reaches a stable motion has been identified. This new method provides a more accurate and repeatable method for determining CA on rough and heterogeneous surfaces, in particular MCFAs. It also addresses the pattern that each of the MCFA exhibits as a function of treatment as well as the unique relationship between steady state motion of the three-phase contact line and drop volume. The technique described allows for CAs to be measured within an accuracy of  $5^\circ$ , as opposed to  $20^\circ$  or greater with conventional approaches. The new technique is also expected to work effectively for similar porous materials such as fine-grained soils, but requires further study. In sum this study indicates the possibility of transforming CFA surfaces from fully wettable surface (hydrophilic,  $CA = 0^\circ$  for untreated CFA) to non-wettable (hydrophobic, CA up to  $162^\circ$ ) suggesting the possible elimination of leachate from

CFA. Such a possibility could increase the extent and diversity of CFA beneficial use and applications.

## REFERENCES

- ACAA, 2014. "Coal Combustion Product (CCP) Production and Use Survey Report"  
<https://www.acaa-usa.org/Portals/9/Files/PDFs/2013ReportFINAL.pdf> (Nov. 14, 2015)
- Amirfazli, A., and Neumann, A. W. (2004). "Status of the three-phase line tension: a review." *Advances in Colloid and Interface Science*, 110(3), 121-141.
- Baba, E. M., Cansoy, C. E., and Zayim, E. O. (2015). "Optical and wettability properties of polymers with varying surface energies." *Applied Surface Science*, 350, 115-120.
- Bachmann, J., Ellies, A., and Hartge, K. H. (2000). "Development and application of a new sessile drop contact angle method to assess soil water repellency." *Journal of Hydrology*, 231–232(0), 66-75.
- Basu, M., Pande, M., Bhadoria, P. B. S., and Mahapatra, S. C. (2009). "Potential fly-ash utilization in agriculture: A global review." *Progress in Natural Science*, 19(10), 1173-1186.
- Beatty, S. M., and Smith, J. E. (2010). "Fractional wettability and contact angle dynamics in burned water repellent soils." *Journal of Hydrology*, 391(1–2), 97-108.
- Belibel, R., Avramoglou, T., Garcia, A., Barbaud, C., and Mora, L. (2016). "Effect of chemical heterogeneity of biodegradable polymers on surface energy: A static contact angle analysis of polyester model films." *Materials Science and Engineering: C*, 59, 998-1006.
- Bertola, V., and Wang, M. (2015). "Dynamic contact angle of dilute polymer solution drops impacting on a hydrophobic surface." *Colloids and Surfaces A: Physicochemical and Engineering Aspects*, 481, 600-608.
- Cassie, A. B. D. (1948). "Contact angles." *Discussions of the Faraday Society*, 3(0), 11-16.
- Cheng, P., Li, D., Boruvka, L., Rotenberg, Y., and Neumann, A. W. (1990). "Automation of axisymmetric drop shape analysis for measurements of interfacial tensions and contact angles." *Colloids and Surfaces*, 43(2), 151-167.
- Chi, M., and Huang, R. (2014). "Effect of circulating fluidized bed combustion ash on the properties of roller compacted concrete." *Cement and Concrete Composites*, 45, 148-156.
- Daniels, J. L., and Hourani, M. (2009). "Soil Improvement with Organo-Silane." *Advances in Ground Improvement*, American Society of Civil Engineers, 217-224.
- Daniels, J. L., Hourani, M. S., and Harper, L. S. (2009). "Organo-silane chemistry: A water repellent technology for coal ash and soils." *World of Coal Ash (WOCA)* Lexington, KY, USA.
- Daniels, L. J., and Das, P. G. (2006). "Leaching Behavior of Lime–Fly Ash Mixtures." *Environmental Engineering Science*, 23.
- de Gennes, P. G. (1985). "Wetting: statics and dynamics." *Reviews of Modern Physics*, 57(3), 827-863.

- Duncan, D., Li, D., Gaydos, J., and Neumann, A. W. (1995). "Correlation of Line Tension and Solid-Liquid Interfacial Tension from the Measurement of Drop Size Dependence of Contact Angles." *Journal of Colloid and Interface Science*, 169(2), 256-261.
- EPA, U. S (2010). "Hazardous and Solid Waste Management System; Identification and Listing of Special Wastes; Disposal of Coal Combustion Residuals From Electric Utilities." *Federal Register* 75(161). EPA, U. S (2015). "<Hazardous and Solid Waste Management System; Disposal of Coal Combustion Residuals From Electric Utilities; Final Rule>." *Federal Register* / Vol. 80,(No. 74).
- EPRI (2005). "Chemical Constituents in Coal Combustion Product Leachate: Boron." Department of Environmental Health Sciences, University of California Los Angeles, CA 90095-1772.
- EPRI, and Department of Energy, U. S. (2006). "Characterization of Field Leachates at Coal Combustion Product Management Sites: Arsenic, Selenium, Chromium, and Mercury Speciation." PA: 2006. 1012578.
- EPRI, and Pacific Northwest Laboratories, R. W. (1988). "Leachate chemistry at the Montour Fly Ash test cell." EPRI, Montour, 104.
- Erbil, H. Y., Demirel, A. L., Avcı, Y., and Mert, O. (2003). "Transformation of a Simple Plastic into a Superhydrophobic Surface." *Science*, 299(5611), 1377-1380.
- Feyyisa, J., and Daniels, J. (2016). "A Dynamic Contact Angle Measurement Technique for Water-Repellent Coal Fly Ash (CFA)." *Geo-Chicago 2016*, American Society of Civil Engineers, 925-938.
- Gao, L., and McCarthy, T. J. (2007). "How Wenzel and Cassie Were Wrong." *Langmuir*, 23(7), 3762-3765.
- General Assembly, N. C. (2014). "<SENATE BILL 729>." session 2013.
- Good, R. E., Good, N. F., and Andresen, J. W. (1979). "16 - The Pine Barren Plains." Pine Barrens, R. T. T. Forman, ed., Academic Press, 283-295.
- Hefer, A. W., Bhasin, A., and Little, D. N. (2006). "Bitumen Surface Energy Characterization Using a Contact Angle Approach." *Journal of Materials in Civil Engineering*, 18(6), 759-767.
- Heib, F., Hempelmann, R., Munief, W. M., Ingebrandt, S., Fug, F., Possart, W., Groß, K., and Schmitt, M. (2015). "High-precision drop shape analysis (HPDSA) of quasistatic contact angles on silanized silicon wafers with different surface topographies during inclining-plate measurements: Influence of the surface roughness on the contact line dynamics." *Applied Surface Science*, 342(0), 11-25.
- Imeson, A. C., Verstraten, J. M., van Mulligen, E. J., and Sevink, J. (1992). "The effects of fire and water repellency on infiltration and runoff under Mediterranean Class Forest." *CATENA*, 19(3-4), 345-361.
- Jala, S., and Goyal, D. (2006). "Fly ash as a soil ameliorant for improving crop production—a review." *Bioresource Technology*, 97(9), 1136-1147.
- Johnson, R. E., and Dettre, R. H. (1964). "Contact Angle Hysteresis. III. Study of an Idealized Heterogeneous Surface." *The Journal of Physical Chemistry*, 68(7), 1744-1750.

- Keatts, M. I. (2014). "Geotechnical controls on organo-silane modification of soils and coal combustion fly ash." 1585353 M.S., The University of North Carolina at Charlotte.
- Koc, M., and Bulut, R. (2014). "Assessment of a Sessile Drop Device and a New Testing Approach Measuring Contact Angles on Aggregates and Asphalt Binders." *Journal of Materials in Civil Engineering*, 26(3), 391-398.
- Kwok, D. Y., and Neumann, A. W. (1999). "Contact angle measurement and contact angle interpretation." *Advances in Colloid and Interface Science*, 81(3), 167-249.
- Li, D. (1996). "Drop size dependence of contact angles and line tensions of solid-liquid systems." *Colloids and Surfaces A: Physicochemical and Engineering Aspects*, 116(1-2), 1-23.
- Marmur, A. (1997). "Line Tension and the Intrinsic Contact Angle in Solid-Liquid-Fluid Systems." *Journal of Colloid and Interface Science*, 186(2), 462-466.
- Marmur, A. (1998). "Line tension effect on contact angles: Axisymmetric and cylindrical systems with rough or heterogeneous solid surfaces." *Colloids and Surfaces A: Physicochemical and Engineering Aspects*, 136(1-2), 81-88.
- Marmur, A. (2006). "Soft contact: measurement and interpretation of contact angles." *Soft Matter*, 2(1), 12-17.
- Nickelsen, S., Moghadam, A. D., Ferguson, J. B., and Rohatgi, P. (2015). "Modeling and experimental study of oil/water contact angle on biomimetic micro-parallel-patterned self-cleaning surfaces of selected alloys used in water industry." *Applied Surface Science*, 353, 781-787.
- Pei, X., Zhang, F., Wu, W., and Liang, S. (2015). "Physicochemical and index properties of loess stabilized with lime and fly ash piles." *Applied Clay Science*, 114, 77-84.
- Rein, M. (1993). "Phenomena of liquid drop impact on solid and liquid surfaces." *Fluid Dynamics Research*, 12(2), 61.
- Río, O. I. d., and Neumann, A. W. (1997). "Axisymmetric Drop Shape Analysis: Computational Methods for the Measurement of Interfacial Properties from the Shape and Dimensions of Pendant and Sessile Drops." *Journal of Colloid and Interface Science*, 196(2), 136-147.
- Rotenberg, Y., Boruvka, L., and Neumann, A. W. (1983). "Determination of surface tension and contact angle from the shapes of axisymmetric fluid interfaces." *Journal of Colloid and Interface Science*, 93(1), 169-183.
- Santner, G., Freytag, B., Juhart, J., Baumgartner, E., Schmied, F., and Teichert, C. (2012). "Adhesive Power of Ultra High Performance Concrete from a Thermodynamic Point of View." *Journal of Materials in Civil Engineering*, 24(8), 1050-1058.
- Schmitt, M., Hempelmann, R., Ingebrandt, S., Munief, W., Durneata, D., Groß, K., and Heib, F. (2014). "Statistical approach for contact angle determination on inclining surfaces: "slow-moving" analyses of non-axisymmetric drops on a flat silanized silicon wafer." *International Journal of Adhesion and Adhesives*, 55, 123-131.
- Singh, M., and Siddique, R. (2013). "Effect of coal bottom ash as partial replacement of sand on properties of concrete." *Resources, Conservation and Recycling*, 72, 20-32.
- Singh, M., and Siddique, R. (2014). "Strength properties and micro-structural properties of concrete containing coal bottom ash as partial replacement of fine aggregate." *Construction and Building Materials*, 50, 246-256.

- Song, D., Song, B., Hu, H., Du, X., and Ma, Z. (2015). "Contact angle and impinging process of droplets on partially grooved hydrophobic surfaces." *Applied Thermal Engineering*, 85, 356-364.
- van der Merwe, E. M., Mathebula, C. L., and Prinsloo, L. C. (2014). "Characterization of the surface and physical properties of South African coal fly ash modified by sodium lauryl sulphate (SLS) for applications in PVC composites." *Powder Technology*, 266, 70-78.
- Thorneloe, A. S., Kosson, S. D., Sanchez, F., Garrabrant, C. A. n. a., and Helms, G. (2010). "Evaluating the Fate of Metals in Air Pollution Control Residues from Coal-Fired Power Plants." *Environ. Sci. Technol.*, 44, 7351-7356.
- Wang, S., Ma, Q., and Zhu, Z. H. (2008). "Characteristics of coal fly ash and adsorption application." *Fuel*, 87(15-16), 3469-3473.
- Wenzel, R. N. (1936). "Reststance of solid surfaces to wetting by water." *Ind. Eng. Chem*, 28(8), 988-994.
- Wu, T., Chi, M., and Huang, R. (2014). "Characteristics of CFBC fly ash and properties of cement-based composites with CFBC fly ash and coal-fired fly ash." *Construction and Building Materials*, 66, 172-180.
- Yuan, Y., and Lee, T. R. (2013). "Contact Angle and Wetting Properties." 51, 3-34.

## CHAPTER 2

### A CAPILLARY BREAKTHROUGH PRESSURE MEASUREMENTS AND A MODIFIED WASHBURN EQUATION FOR ORGANO-SILANE TREATED COAL FLY ASH: CORRELATION BETWEEN CA AND BP

#### 2.1 Abstract

One method to minimize contaminant leaching from coal fly ash (CFA) involves modifying its surface to become water repellent. Five CFA types have been modified using three organo-silane (OS) products at different mix ratios. Multiple breakthrough pressure (BP) experiments were conducted for different samples at different mix ratios to identify the performance of the modified particle surfaces to resist a positive water entry pressure. Results indicated that CFA can be modified and made sufficiently water resistant (up to 10 m pressure head) against infiltration by using OS products. Once the breakthrough pressure is exceeded, subsequent infiltration depends less upon pore size and more upon type of OS, type of CFA and mix ratio. Such a resistance can prevent infiltration of water into CFA, thereby eliminating leachate generation. The Washburn equation was applied to predict the BP of the modified CFA. The Washburn equation requires an estimate of the pore radius and three approaches were used to for this purpose. BP estimates using pore diameters derived from the soil water characteristic curve (air entry value) and from an assumption of tetrahedral packing were reasonably close to experimental values than a cubic packing. It has been identified that for a modified CFA using OS products the Washburn equation should be adjusted by two variables, one to account for linear changes in surface energy, and another to account for exponential changes from apparent to pore contact angle (CA). The apparent CA measured on a flat surface and the prevailing CA that manifests between individual pores of a compacted matrix of particles pore CA is related linearly up to

approximately  $140^\circ$ , beyond which the relationship is better explained using exponential function. The relationship between the two water repellency parameters was established using exploratory data analysis technique. It was shown that CA and BP are better related when evaluated based on the type of OS and CFA used. Accordingly, both parameters are related linearly but not proportionally for all types of CFA and OS. However, best fitting of CA and BP model was observed when modeling is conducted based on the underlying parameters; CFA and type of OS used. Further the degree to which the applied pressure affects the pore contact angle depends on the type of OS (e.g., alkyl chain), dosage and CFA.

Key words: Breakthrough Pressure, Contact Angle, Coal Fly Ash, Organo-Silane, pore size, pore contact angle, dose

## 2.2 Introduction

Motivation for this work derives in part from an interest in reducing the contaminant leaching from coal fly ash (CFA), thereby increasing opportunities for beneficial use as well as minimizing potential groundwater impacts during disposal. One method to reduce aqueous leaching of contaminants from any porous medium into the prevailing pore fluid is to prevent water entry through engineered water repellency. The extent of water repellency may be defined by capillary breakthrough pressure (BP), which represents the pressure required to drive a non-wetting liquid in to porous media. Hildenbrand et al., (2002) defined capillary BP as the excess pressure required to drive a non-wetting phase and displace a wetting phase as a continuous flow throughout the pore space. Other authors have referred to BP by different names depending on the area of



practice, including penetration of a liquid (Washburn, 1921) in liquid dynamics; entry value or non-wetting fluid bubbling (Wanget al., 2000) in hydraulics of repellency; sealing capacity (Gaoet al., 2014; Heathet al., 2012; Li et al., 2005; Liuet al., 2014; Rezaeyanet al., 2015) in oil and gas exploration; water resistance (Bartellet al., 1948) in textile industry; breakthrough pressure (Fink and Myers, 1969) in silicone modified soils for water harvesting. Water resistance or BP of a porous material depends on the interfacial tension formed between the two phases, wetting and non-wetting, at their interfaces. Capillary breakthrough pressure, P is expressed as (Washburn, 1921);

$$P = - \frac{2 \sigma \cos(\theta)}{r} \quad 2.1$$

Where  $\sigma$  is the interfacial tension between wetting and non-wetting phase;  $\theta$  is the contact angle formed between a liquid/gas and pore material; and  $r$  is the equivalent pore radius.

The terms wetting and non-wetting are system dependent. (Wang et al., 2000). For hydrophilic soils and industrial byproducts, water is the wetting fluid and air is the non-wetting fluid. When soils and industrial byproducts are rendered hydrophobic, air becomes the wetting fluid and water becomes the non-wetting fluid. When a CFA surface is modified using OS, it is rendered water repellent (hydrophobic) and becomes able to resist water entry in to its pore space (Feyyisa and Daniels, 2016; Feyyisaet al., 2017). The degree of resistance to water entry varies depending on the interfacial tension formed between the modified CFA and water. Such changes in interfacial tension through changing the OS-CFA mix ratio are documented in Feyyisa et al., (2017). In addition to measuring interfacial tension between modified CFA and water (i.e., contact angle (CA) measurements), the

physical resistance of the modified surface to infiltration is quantified through BP measurements. In addition to measuring interfacial tension between modified CFA and water, the physical resistance of the modified surface to infiltration is scaled through BP measurements. Since Washburn (1921) formulated Equation (2.1) to relate pore size with BP of porous materials this approach remains popular and is used in many fields to determine the degree of resistance to infiltration, despite some shortcomings under certain specific cases (Dimitrovet al., 2007; Heath et al., 2012; Jooset al., 1990; Martic et al., 2002; O'Loughlinet al., 2013). To determine pore radius in the classical equation mercury intrusion method is widely used, e.g., ASTM D4404-10. Through this approach mercury (non-wetting) is forced (pressure) through a porous medium from which a representative/maximum pore diameter is calculated.

Under certain circumstances however, recent studies have shown that the physical effect of pore size is less controlling. For example, Heath et al. (2012) identified that the presence of organic materials in pore space significantly change the role of pore size in Equation (2.1). Others have acknowledged limitations in the Washburn equation, and especially with respect to pore diameter and have proposed alternative relationships (Dimet al., 2016; Kloubek, 1981; Rigby and Edler, 2002). According to their theory, the shape that a meniscus form (pore contact angle) is governed by the magnitude of the pore size at higher intrusion pressure. Similarly; Liet al., (2014) have recognized limitations in conventional relationships between contact angle and pore diameter. The authors distinguish a pore contact angle measured in glass capillary tubes from contact angles measured on flat plates. Using the same glass in both cases, Li et al. (2014) obtained different results for contact angle depending on whether the measurement was made in a

capillary tube instead of on a flat plate, a finding that is not supported by Young's equation which presumes no effect by substrate geometry. The authors experimentally observed that the value of the pore contact angle approaches that of the flat plate contact angle when the pore diameter is sufficiently large. Kloubek (1981) formulated an empirical relationship between the variation in product  $\sigma \cos(\theta)$  and  $r$  as an alternative solution to the Washburn equation. This relationship was subsequently used by others including Rigby and Edler (2002) and Rigby et al., (2004). In the case of OS-modified CFA, we also hypothesize that the classical Washburn equation requires a modification, particularly the value of the independently measured  $\cos(\theta)$  reflected through pore size, to use for the modified CFA using OS.

Additionally; contact angle and breakthrough pressure measurements both measure the degree to what the surface of a material is changed to resist water entry in to pores. However; the relationship between these two parameters for hydrophobic surfaces is not clear. The relationship formulated by Washburn equation is based on a hydrophilic surface. But many used the equation for hydrophobic surfaces without the need to check its applicability when the surface of the porous material is changed. This study analyzes the relationship between CA and BP and identifies variables that influence the relationship between them.

The purpose of this study is to: 1) modify different types of CFA surfaces in order to render a water repellent character, 2) measure BP for the modified surface using different OS dosage and identify the relative performance of OS-CFA mixtures, 3) evaluate the patterns of post breakthrough imbibition based on dosage, 4) identify a relationship between BP and calculated pore size in equation (2.1) to estimate pore contact angle for

the CFA treated using OS, 5) use to evaluate the applicability of the Washburn equation for the modified CFA, and 6) establish the correlation between CA and BP when a positive water entry pressure is used.

## 2.3 Methods

### 2.3.1 *Materials and Equipment*

Five types of CFA- Class F Utility A (CFA-1), Class F Utility B (CFA-2), Class F Utility C (CFA-3), Class C Utility B (CFA-5) and Lignite Coal Utility B (CFA-6) - were collected from local utilities in the eastern U.S. Three aqueous phase OS chemicals were received from DOW Corning and Zydex Industries. Two laboratory pressure cells were modified; the inner wall was fixed permanently with circular hollowed rigid holder. The holder serves: 1) to hold the porous stone, and 2) prevents leakage between the cell wall and porous stone. A pressure flow controller by Geo Comp FlowTrac II (the Source; Figure 1.4(b)) was used and connected to the pressure cell (the sample holder) and a computer via a transducer to supply DI water (resistance  $> 16 \text{ MOhm-cm}$ ) under pressure. Porous Stones (P/N HM-4184.70) 70mm and filter paper 100 mm diameter were used. Two transducers from Omega Engineering, Inc. (PX409-030GUSBH and PX209-015G5V) were connected between the source and cell to the computer.

### 2.3.2 *Procedures*

The mixing procedure and ratio of OS: CFA (by weight) used in Feyyisa et al. (2017) to form a dry modified CFA surface were used for this study. After the sample was oven dried between  $60^{\circ}$  and  $158^{\circ}\text{F}$  for 24 – 72 hours (Feyyisa et al., 2017; Wang et al.,

2000) it was crushed using a mortar and pestle to pass through a No. 200 sieve. Before pouring and packing the sample in to a cell, a plastic pipe spacer 7.6 cm in diameter was cut to 10 cm height (to direct and allow a stable motion and even spread of DI water just below the sample) and was placed vertically into a cell. A porous stone was covered with filter paper using tape and mounted on the rigid holder that was permanently fixed to the interior wall of the cell. The porous stone-filter paper unit perimeter was wrapped with thread sealant tape to facilitate further leakage control between the unit and cell. The sample was then poured in to the cell and gently packed using laboratory spatula. From mass density relationship, the approximated average density of the sample was estimated and tabulated, Table 2.1. The results are also presented graphically in Figure 2.2.

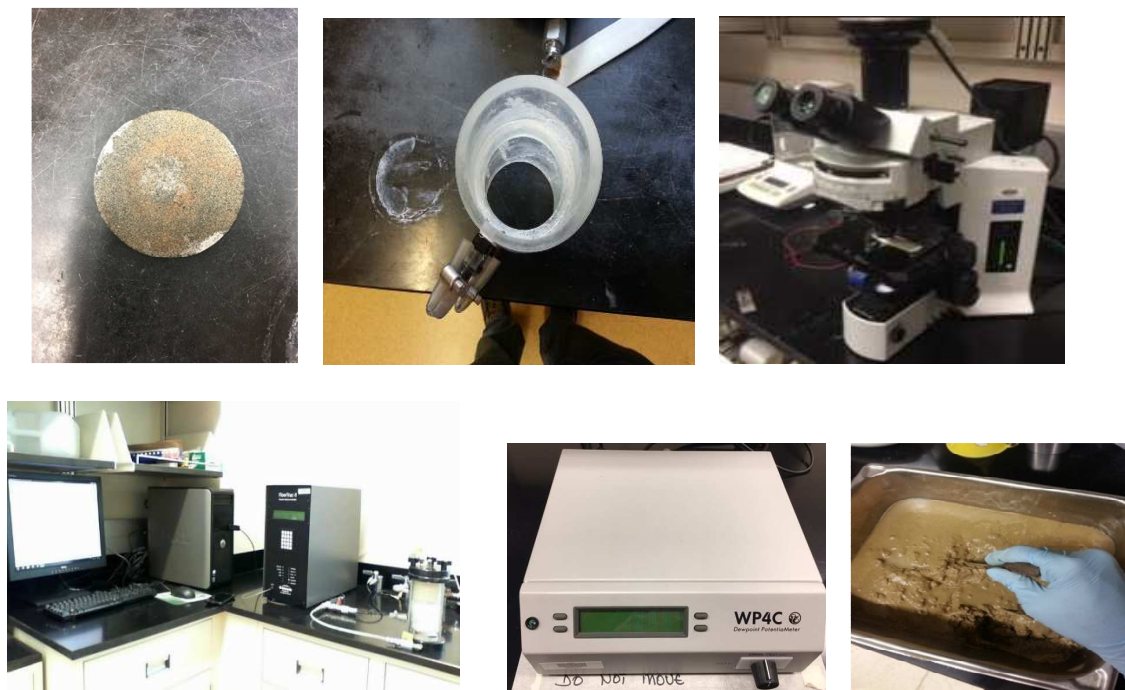


Figure 2. 1. Material and equipment used for sample preparation and testing

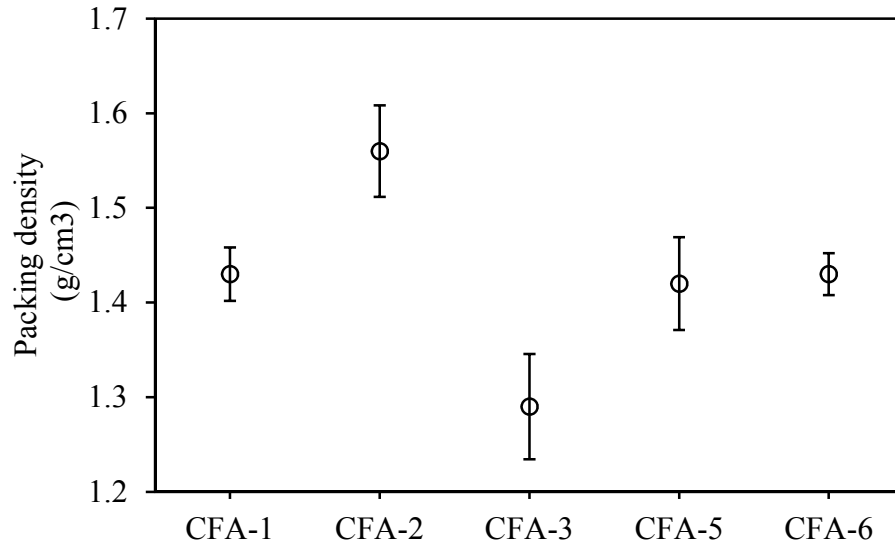


Figure 2.2. Calculated (mass-volume) packing density of modified CFA samples

Once the sample was filled to the 7 cm depth, porous stone was moved in between the sample and top cover of a pressure cell to facilitate equal pressure distribution to the sample while tightening the cell. Full tightening of the cell, however, was carried out during and after air entrapped between grain particles of the modified CFA sample had been removed. This removal procedure was administered during the initial stage of pressure application.

Table 2. 1. Estimated average packing density of different CFA samples

CFA	CFA-1	CFA-2	CFA-3	CFA-5	CFA-6
Packing density (g/cm <sup>3</sup> )	1.43	1.56	1.29	1.42	1.43
Standard deviations	0.028	0.048	0.056	0.049	0.022

Prior to connecting the cell to the pressure source, the bottom space of the cell was filled with water up to the surface of porous stone. The general layout is shown in Figure 2.3.

The bottom part of the cell unit was then connected to a DI water tap and the space between the inlet of the cell and the porous stone was carefully and slowly filled to remove the entrapped air through the top cover. Care was taken not to remove the fine particles of the sample with the air.

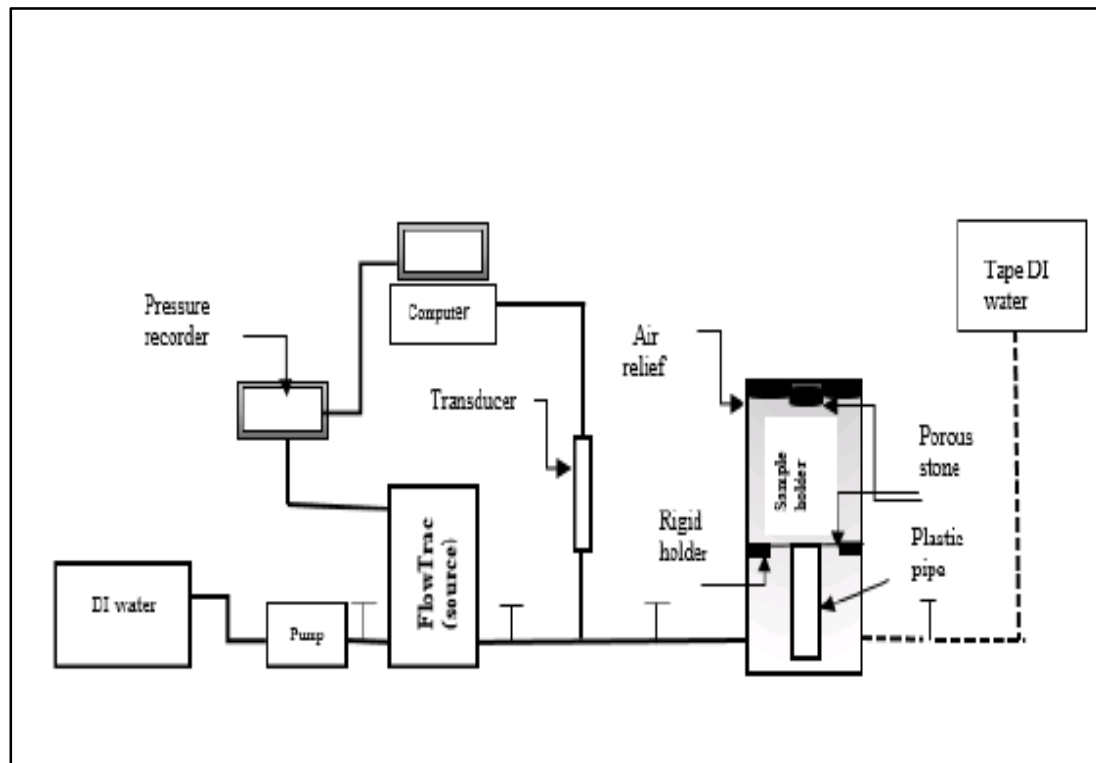


Figure 2. 3. Testing materials and equipment's layout

The cell was then connected to the source and transducer using a tube. Before that the source pumped (from external storage) and emptied multiple times until visible bubbles of air in the tube disappeared from the inlet tube. Likewise, the front discharging tube was also cleared of air by applying pressure and waiting until multiple drops released to open air and no visible bubbles of air are found in the tube before connecting to the cell. The

source was then turned on and a pressurized flow begun discharging to the cell. Water level and pressure records rose steadily until water reached the sample just above the porous stone. Pressure was increased at a rate of 3.4 kPa/sec. and readings were taken every second. This value was adapted as a compromise between the desire to reach BP point in a manageable time for higher resistant samples and to attain a clear breakthrough point for less resistance samples. Once the rising water saturated the porous stone and reached the modified CFA, resistance developed and a sudden rise in slope of pressure-time graph was observed. At this point the applied rate of pressure increase and become a variable function of the sample and the FlowTrac device. That means the mass moved in (expressed in terms of pressure) is increased with time and built as increase in pressure inside until it breaks and starts infiltrating, conservation of mass and energy. The degree of rise in slope of pressure-time plot varied based on the degree of resistance encountered such that a sharp rise resulted for super hydrophobic surfaces. The test was stopped and all readings discarded whenever any type of leakage (either in the tube or joints) was observed as this significantly affects reading. The test was also restarted whenever visible bubbles of water were observed through the top cover of the cell before maximum resistance of the sample had been reached. Such situations occasionally happened due to poor tightening of the top cover and thread sealant tap. Once the maximum resistance of the sample was reached and imbibition begun, the source was allowed to run at a pre-defined incremental rate until the water reached the top of the sample, the source was emptied, or sufficient data had been recorded before stopping. The cell was then disconnected, emptied, cleaned and dried for the next test.



## 2.4 Results and Discussions

### 2.4.1 Relative performance of OS and CFA

In this study a total of 260 BP experiments, with a minimum of 4 tests per sample were conducted, providing sufficient replication (Hildenbrand et al., 2002). BP results were found to vary accordingly to the type and dosage of OS as well as the type of CFA. Of the three OS types C-1 exhibited superior performance to C-2 and C-4 Figure 2.4. The latter two show similar performance both in terms of their averages and ranges of variability as captured by the overlap of box plot notches (the median value). In addition C-1 exhibited considerable dispersion across five different CFAs (variation resulting from type of CFA and/or mix ratio) compared to C-2 and C-4. C-2 and C-4.

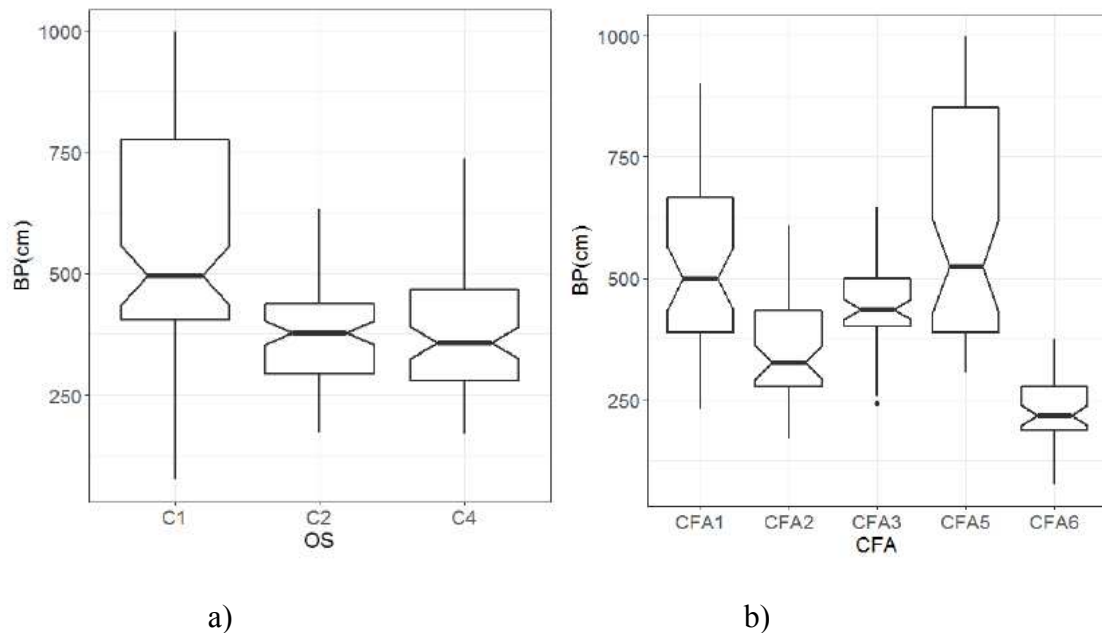


Figure 2. 4. Box plot for relative performance of; a) OS and b) CFA across all mix ratio. The box notches of CFA-1 and CFA-5 nearly overlap indicating the similarity of their median.

The performance of the five types of CFA's are shown in Figure 2. 4(b). CFA-5 maintained the highest BP values, followed by CFA-1, CFA-3, CFA-2, and CFA-6 in that order. The low BP values obtained with CFA-6 is likely due to its higher calcium (oxides) content which affects the hydrolysis and reactivity of minerals in CFA-OS reaction. The reaction details may be found elsewhere (de Buyl, 2004; Thierry Materne, 2012). CFA-5 shows highest dispersion in BP whereas CFA-6 shows the smallest dispersion.

#### *2.4.2 Breakthrough Pressure measurements*

An equal rate of increase in pressure (3.4 kPa/second; 35 cm H<sub>2</sub>O/second) was adopted for testing. During the initial phase of the test, a plot of pressure vs time remains linear, see also Fink and Myers (1969) and Carrillo et al., (1999) until the rising water reached the sample. After this point the graph begins to rise and becomes sharper towards a breakthrough point Figure 2. 5. As depicted in the example figure the point at which a breakthrough occurs and infiltration begins is determined from pressure vs time graph as the highest inflection point of the graph. Some of the actual measurements for pressure versus time and its corresponding slope are shown in Figure 2.8. BP measurement across different CFA, OS, and dosage used are shown in Figure 2.7.

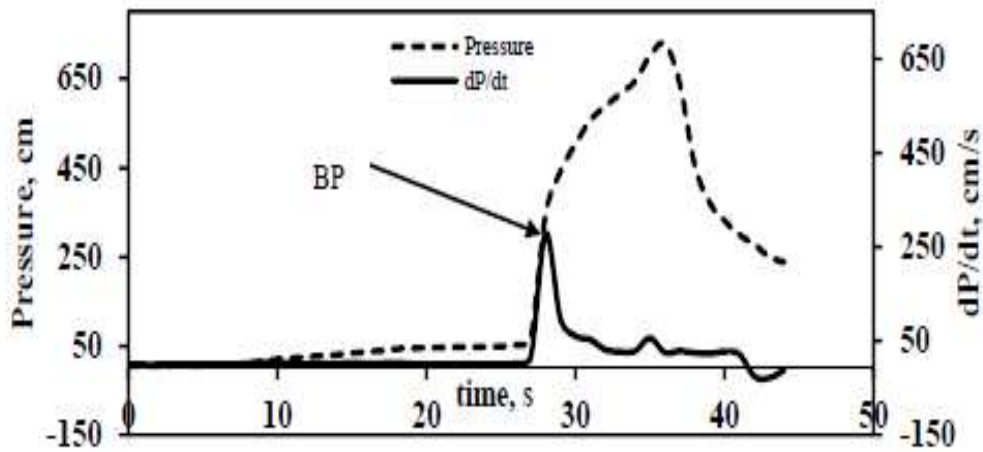


Figure 2. 5. Pressure measurement and its rate of change to identify breakthrough pressure point

Beyond the inflection point the slope of the graph either levels off (Carrillo et al., 1999; Fink and Myers, 1969), follows a certain pattern until the test is stopped and declines sharply, or reaches the maximum capacity of the transducer after which it levels off. The overall pressure versus time relationship solely depends on the degree of water repellency formed. Using this approach BP measurements were conducted for the five CFAs treated using the three types of OS (C-1, C-2, and C-4). The results indicate that both CFA-1 and CFA-5 when treated using C-1 exhibit greater repellency compared to others. The least water repellency for a given dosage was obtained with CFA-6.

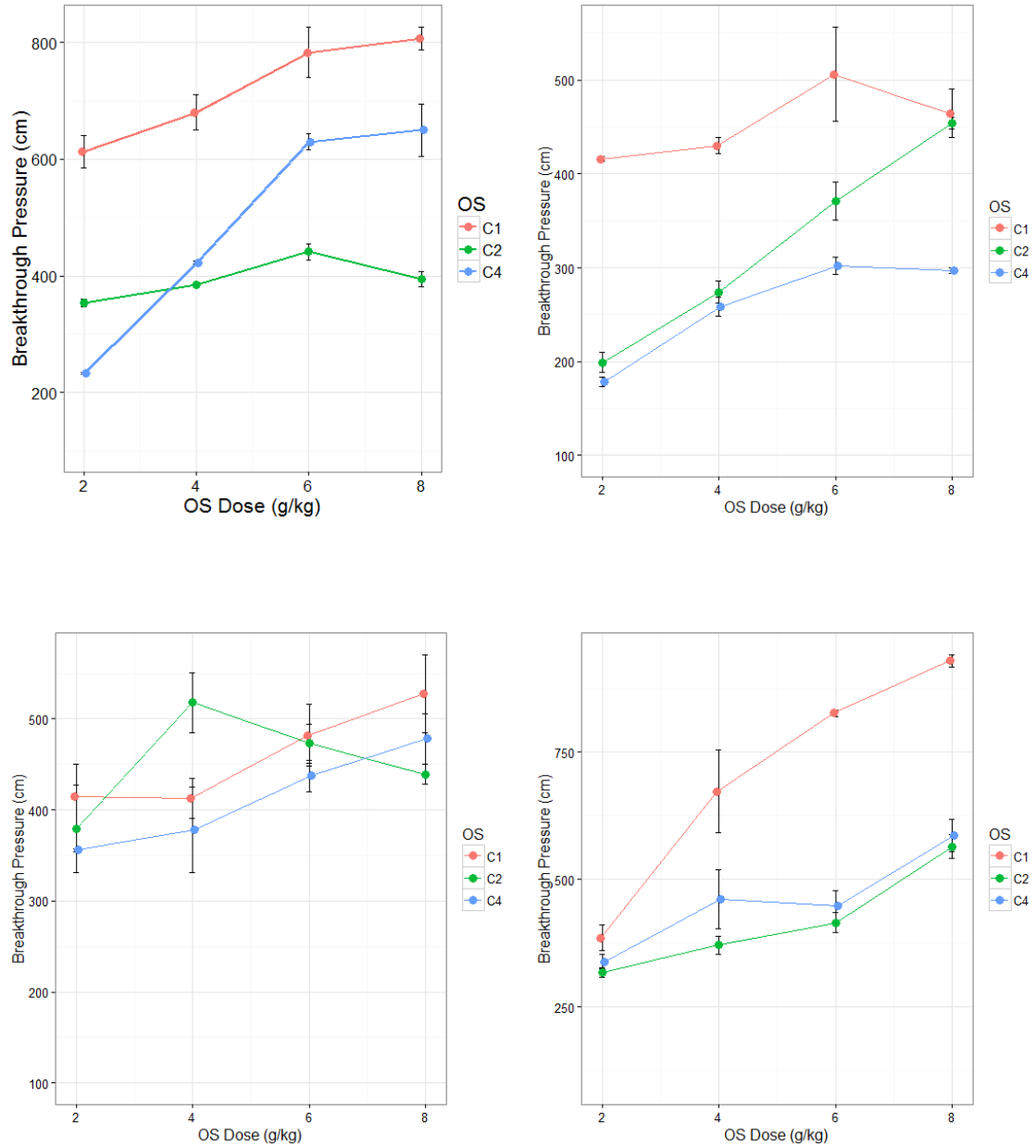


Figure 2. 6. Breakthrough pressure measurements at a breakthrough point for five CFA using three OS. First column for CFA 1, 2, and 3 and second column CFA 5 and 6, respectively.

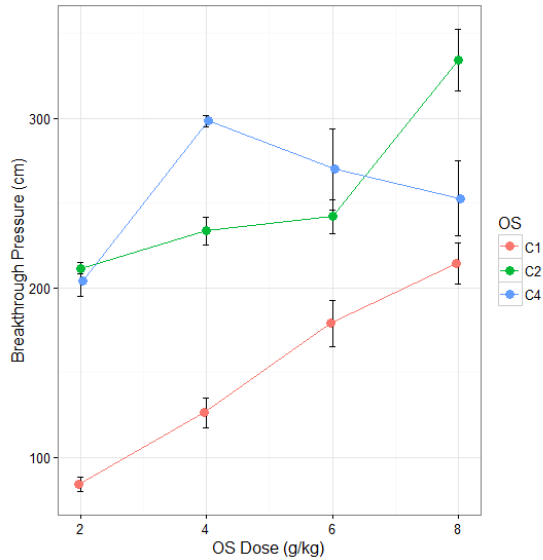


Figure 2. 6. continued

For comparison, the minimum BP observed for CFA-1 treated using C-1 was over 600 cm. whereas, the highest resistance observed for CFA-6 was below 400 cm. The probability range of effectiveness of CFA with OS is shown in Figure 2. 7. This difference is likely due to the difference in the chemical and mineralogical compositions of the CFA and OS which impact the formation of a covalent bond (Danielset al., 2009). The effect of mineralogical and chemical composition on the formation of a bond is discussed in chapter 3. The maximum dosage of OS beyond which any increase in rate either results in no change or a decline in surface energy varies considerably across OS and CFA; see also Feyyisa et al., (2017). Increasing the dosage does not necessarily increase the BP, as eventually there is a point of diminishing return. For example, when CFA-1 is treated using C-1, an increase in the mix ratio by 300 percent raises BP by only 31 percent.

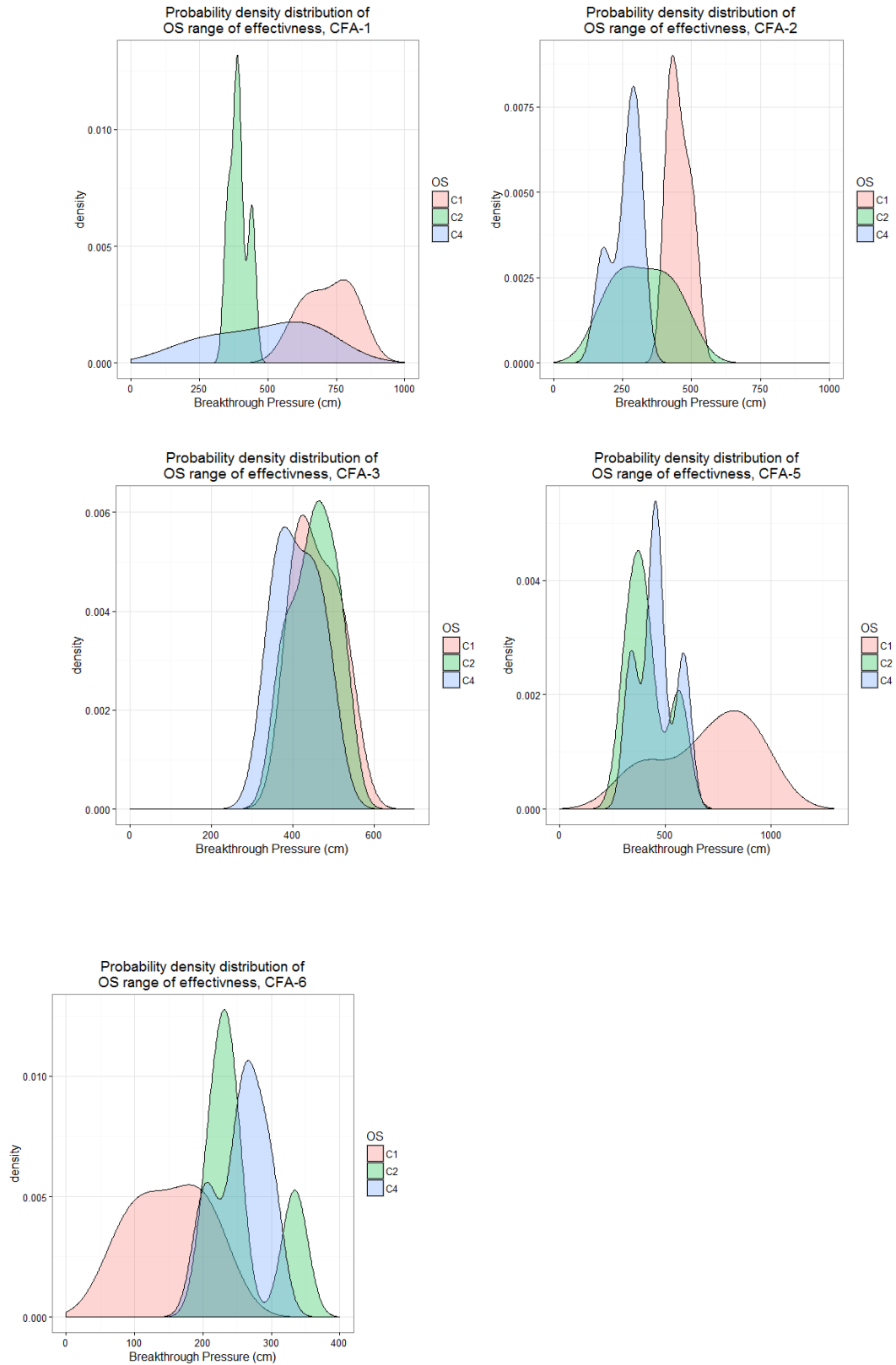


Figure 2. 7. Probability range of effectiveness of different CFA treated using OS products

#### 2.4.2 Post breakthrough imbibition

Once resistance to flow is overcome and infiltration through the modified CFA pores is initiated, the source continues to supply DI water at a pre-defined rate of pressure rise until it is stopped, flow reaches the top surface, or the source runs out of water. The rate of change in pressure during imbibition is directly related to the rate of flow into the pore space; the micro stepper motor delivers corresponding volume of water to meet the required pressure (3.4 kPa/second; 35 cm H<sub>2</sub>O/second). This rate of change in pressure (slope of pressure-time curve) with respect to time is calculated and plotted against time. Figure 2. 8 shows sample patterns based on different OS and mix ratios for a given CFA. To maintain the user defined time based change in pressure the motor controls a piston which moves through a water filled cylinder (Geocomp, 2017). Thus, a continuous increment of pressure (built inside) guarantees the ability to drive pressurized water (increases the rate of increase in pressure) and breaks the sample layer by layer, which makes imbibition through the pore space possible.

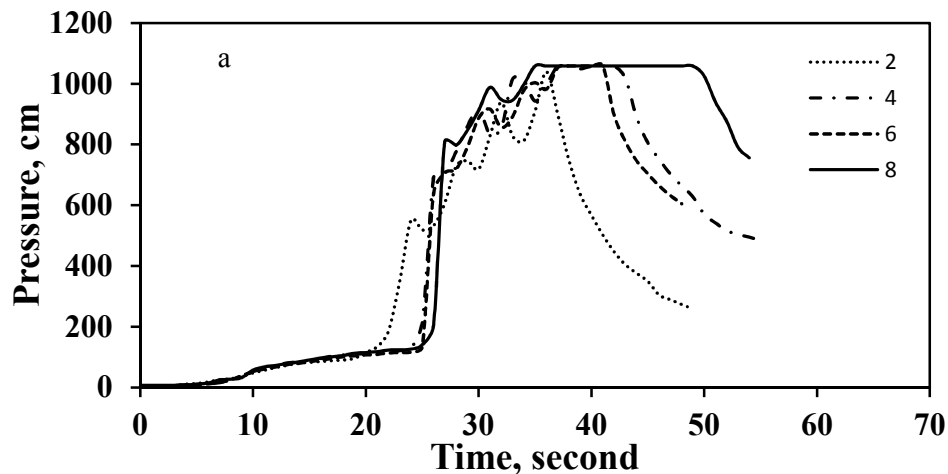


Figure 2. 8. Sample breakthrough pressure measurements for different CFA and OS at different mix ratio: a, b, c, d, e, and f for CFA1-C1, CFA2-C2, CFA3-C2, CFA3-C4, CFA5-C2, and CFA6-C1, respectively (CFA1-C1 represents sample coal fly ash number 1 treated using organo-silane number1)

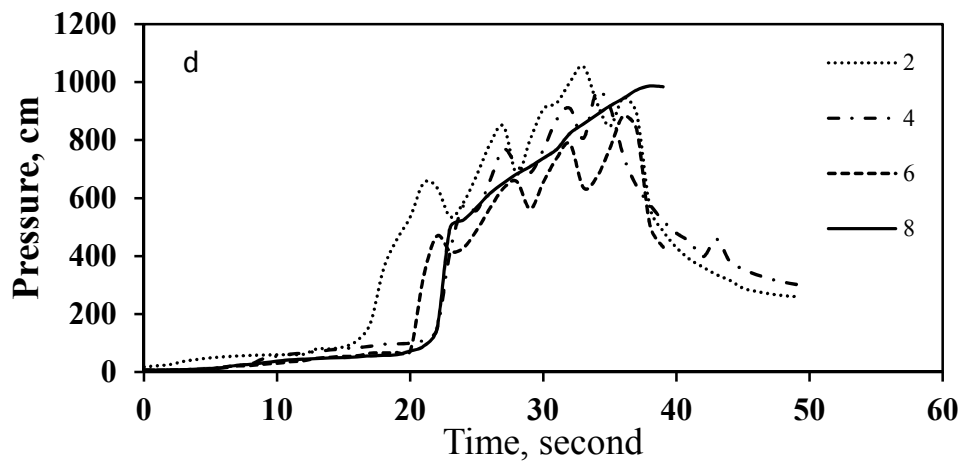
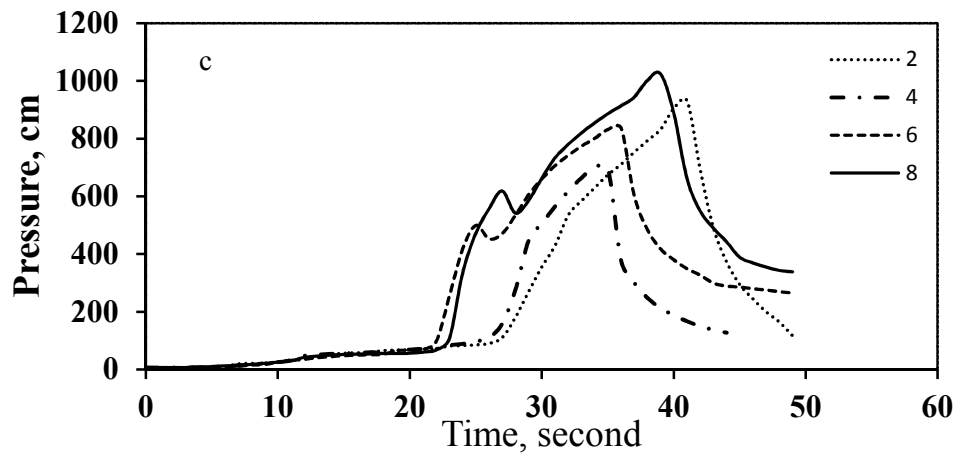
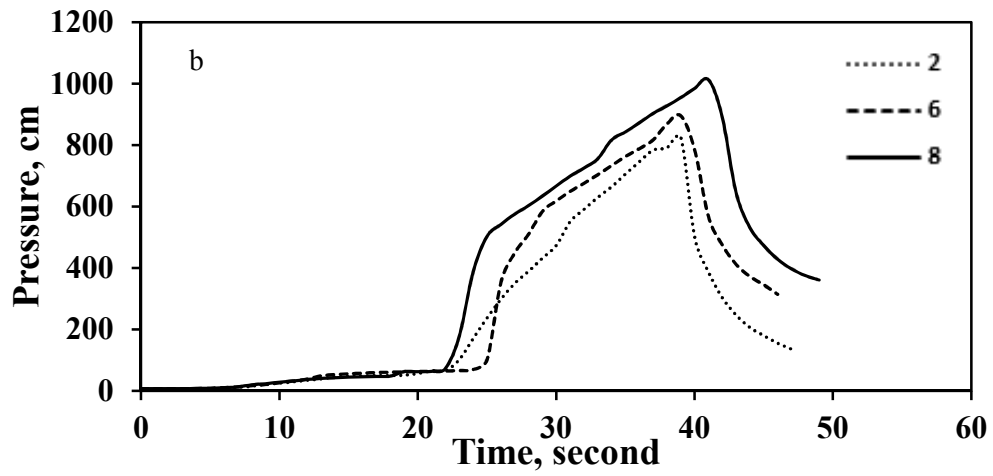


Figure 2. 8. continued



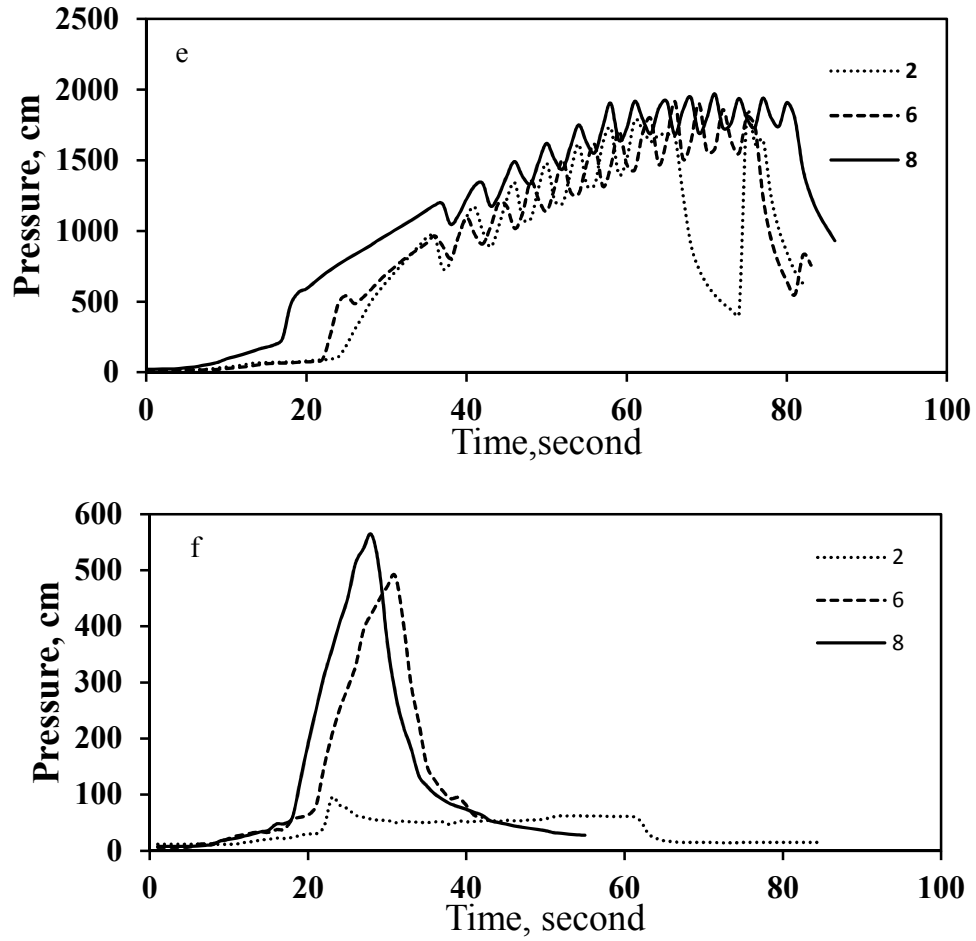


Figure 2. 8. continued

Consequently, the quantity and rate of water supplied by the motor depends on the demand to meet the incremental pressure. This demand is governed by the degree of resistance encountered from the sample (the built-in pressure forces the motor steeper to coup up with the demand). Thus, this self-adjustment of the source controls the cycle and extent of its motor steps movement and is reflected on the BP vs time graph such that the amplitude of the figure is related to the oscillation steps of the motor to meet the demand. For lower BP once, infiltration into pores is initiated, the pre-determined incremental pressure rate becomes lower to keep the pace requiring more discharge. The discharge

required to meet this higher infiltration rate was regulated through longer-range oscillation of the source motor steps. On the other hand, for higher BP samples higher resistance is encountered across each distance/layer and affects infiltration rate causing quite slow imbibition Figure A-1 (Appendixes). Hence the pre-defined pressure rate becomes higher as a result steeper's motor short-range oscillation. It was noted that, even if measurement was difficult, the depth of imbibition after a BP for lower resistance samples such as CFA-2 treated using C-2 (at 2 g/kg mix ratio) and higher resistance samples such as CFA-1 using C-1 (at 8 g/kg mix ratio) was estimated as 30 mm and less than 1.5 mm, respectively. In summary, the rate of imbibition (explained through change in pressure) depends on the mix ratio used; generally higher mix ratios result in forming higher resistance and thus less rate of imbibition.

#### *2.4.3 Pore size estimate*

*2.4.3.1 Grain size and packing density:* As discussed above, even if similar grain size distribution (samples pass No 200 sieve, 0.074 mm) and packing approach were used it is required to measure individual CFA particles size for a better estimate of pore size. A fluorescent microscope (OLYMPUS BX51, STREM) was used to measure the average grain size, which in turn, was used to estimate pore size. It also provides insight into particle morphology. Figure 2. 10 shows a microscopic image of the particles and their grain size distribution. A large quantity of

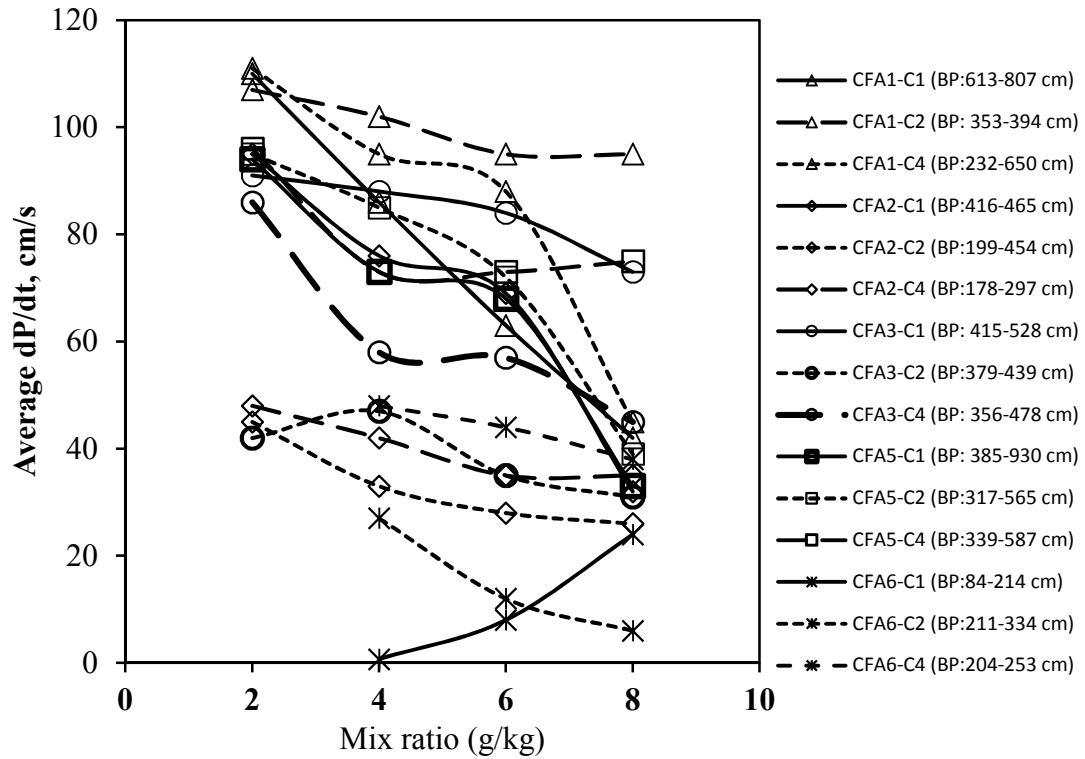


Figure 2.9. Imbibition rate (explained through rate of change in pressure) inside modified CFA. In general, as dose of OS increases (except for CFA6-C1 with lowest BP) the rate of imbibition reduces. BP, Lines and Marks in legend represents range of initial breakthrough pressure, CFA and OS, respectively.

particles falls in the range between 0-10  $\mu\text{m}$  for all types of CFA. The mean radius of grain is 29  $\mu\text{m}$ , 22  $\mu\text{m}$ , 17  $\mu\text{m}$ , and 30  $\mu\text{m}$  for CFA-1, CFA-2, CFA-3, and CFA-5, respectively. In order to have similar packing density a laboratory spatula was used and from mass-volume relationship density of packing was calculated. Based on this approach the average packing density in Table 2.1 was used.

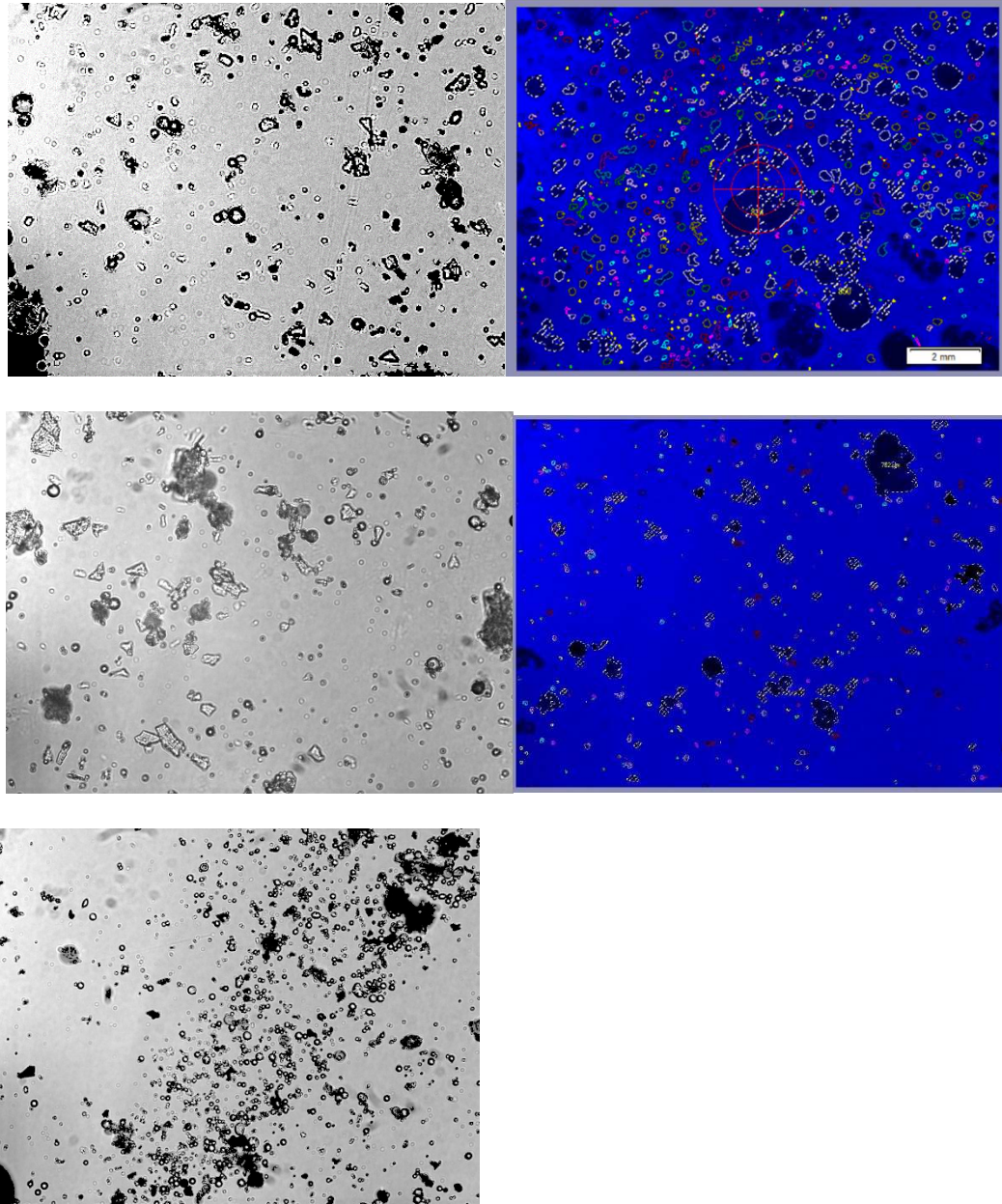
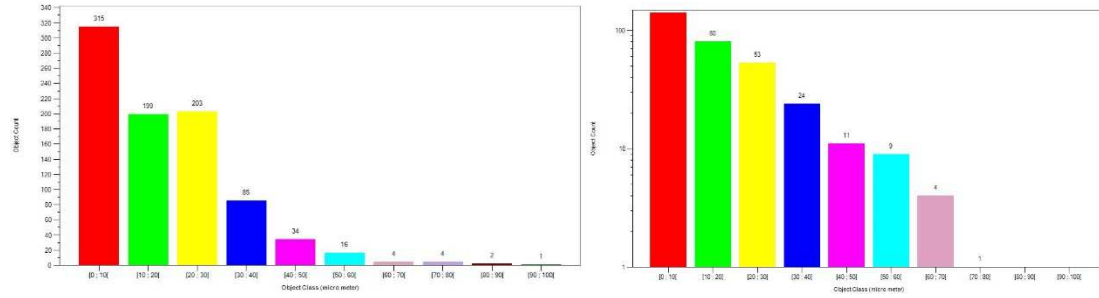
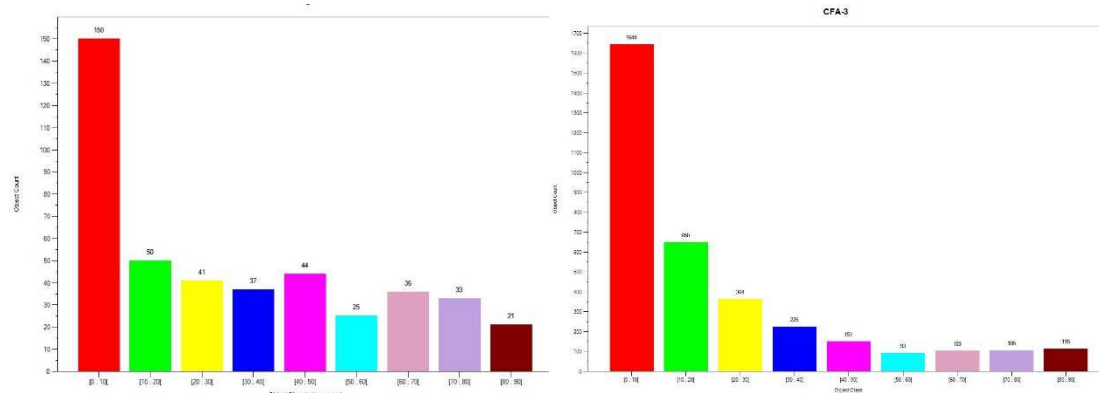


Figure 2. 10. Sample images of CFA grains (400x) used to count and measure grain size using Fluorescent Microscope OLYMPUS BX51. Different background, grain distribution, and available software options were used to effectively disperse, count and measure



### CFA-3



### CFA 1

Figure 2.11. Sample CFA grain size distribution histogram

**2.4.3.2 Capillary Pores size (CFA-WCC):** In addition to measuring particle size, air entry value (AEV) of samples was also estimated based on soil water characteristic curve (SWCC), in this case (CFA water characteristic curve (CFA-WCC)). The CFA-WCC was developed from a dew-point hygrometer (Decagon Device WP4). Four fine grained (pass No 200 sieve, 0.074 mm) CFA; CFA-1, CFA-2, CFA3, and CFA5) samples were prepared. Using a standard sample preparation approach and a laboratory procedure the samples were molded in to a WP4 cap so that an approximated density of packing was maintained. To

calculate volumetric water content and pore size of the samples a procedure and approach described in (Lu and Likos, 2004) was followed.

The fitting model for measured and calculated volumetric water content and total suction was estimated using van Genuchten equation,

$$Se = \frac{\theta - \theta_r}{\theta_s - \theta_r} = \left( \frac{1}{1 + (\alpha\phi)^n} \right)^m \quad 2.2$$

$$K\phi = Ks(Se)^{0.5} [1 - (1 - (Se)^{1/m})^m]^2$$

$S_e$  = Effective saturation  
 $K_u$  = Unsaturated hydraulic conductivity  
 $K_s$  = Saturated hydraulic conductivity  
 $\alpha$ ,  $m$  and  $n$  = fitting parameters correlating pore size, rate of desorption, and residual water content, respectively

Using the CFA-water CC shown in Figure 2.12 total suction head was determined for the corresponding AEV. It should be noted that the osmotic pressure for all samples were assumed negligible.

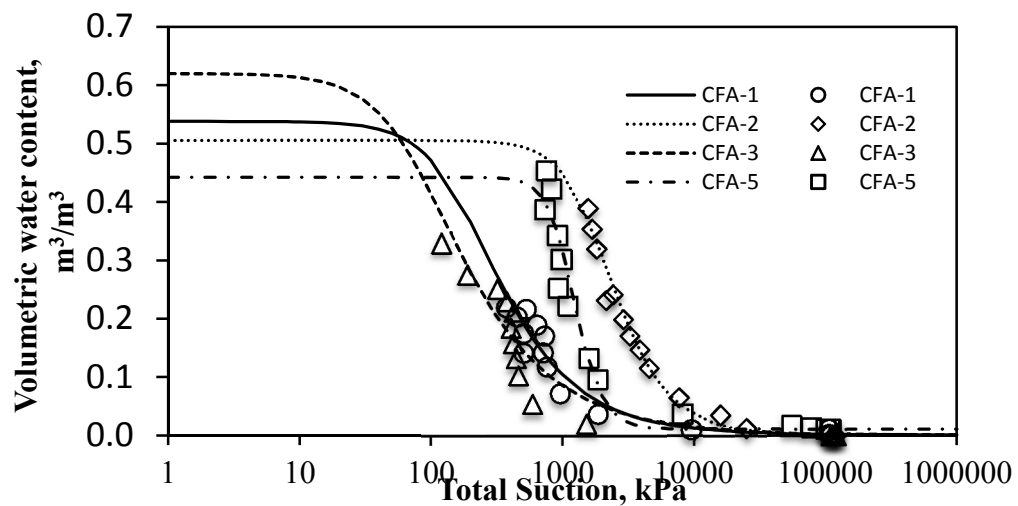


Figure 2.12. Soil (CFA) water characteristic curve for four CFA

#### 2.4.4 Model and prediction (Washburn equation)

The main challenge to apply the Washburn (capillary rise) equation (2.1) was to determine the surrogate pore size of each CFA sample. Using the measurements of particles size and total suction head three different approaches were used. From the SWCC (CFA-WCC)) and calculated total suction the Washburn equation was used to calculate the pore size. In equation (2.1), CA for the untreated CFA and the surface tension of water at 22<sup>0</sup>C were estimated and used as zero and 70.25mN/m, respectively. The second and third approach are related to measuring the particles size so that a simple cubic and tetrahedral packing approaches were used to estimate pore size. To estimate the pore size the relationship between particles diameter and pore size based on packing approach and particles shape discussed in Lu and Likos (2004) was applied. Accordingly; the pore size of samples based on particles diameter for simple cubic( $d_{sc}$ ) and tetrahedral ( $d_{th}$ ) packing were applied Equations 3.2 and 3.3, respectively

$$d_{sc} = 0.45 * d \quad 2.3$$

$$d_{th} = 0.15 * d \quad 2.4$$

An average value of  $d$  (particles diameter as measured using the fluorescent microscope) was used to estimate pore size. For the case of positive entry pressure in hydrophobic system (such as mercury intrusion), the larger pore size governs initial entry. In this study instead of larger particles an average value was used for three main reasons. First ash is typically characterized by a uniform gradation. This gradation was made even more uniform by sieving all samples through a No 200 sieve. As such the actual distribution of pore is expected to be narrow. The second one was that while performing the test, once

the resistance of the sample was exceeded and infiltration in to pores occurred gradual moistening of samples around the circumference of the glass holder went at equal rate around the circumference (visual observation). This phenomenon continues until wetting the all sample was completed or testing terminated. In other words, there is no finger type infiltration/imbibition observed throughout the testing procedure. The absence of such a phenomenon suggests; either there is no significant difference in pore space or due to the magnitude of a positive entry pressure infiltration path does not matter once the resistance of the sample is overcome. The final argument is based on Figure 2.11. As shown in the bar charts the quantity of larger particles in all the samples are insignificant to influence the pattern of infiltration with higher water entry pressure. For example, while larger particle radius is about 0.4 percent and about 4 percent, the smallest is 38 percent and 32 percent for CFA-1 and CFA-3, respectively.

Based on this approach, Equations 2.1, 2.2, and 2.3 were applied where required and the pore size of the samples were estimated as; 0.002149 mm, 0.0002878 mm, 0.003598 mm, and 0.00028783 mm for CFA-1, CFA-2, CFA-3, and CFA-5 in their order. However; using the calculated pore radius for CFA-2 and CFA-5 resulted in an inconceivably large estimated BP, i.e., by one order of magnitude. While not measured, it is possible that the osmotic pressure was greater for these samples, and as noted above, osmotic pressure was neglected. Measurement error may also be another reason. Hence, for both CFAs (CFA-2 and CFA-5) pore size estimate was conducted using only both simple cubic and tetrahedral packing approach. Plots of measured and calculated BP are shown in Figure 2.13. As shown in the Figure there exists a scaling between the measured and calculated (using the capillary equation) BP values. The Washburn equation was



derived based on a negative pressure (capillary suction head) in which water rises by capillary action. This study deals with a hydrophobic surface where a positive entry pressure forces water in to pores of finely grained (pass the No 200 mm sieve) modified CFA.

However, the theory of capillary rise equation should also work for a hydrophobic surface except in this case, infiltration or unsaturated flow is initiated by a positive entry pressure. However, for such a specific cases adjustment to the equation is required. For example; according to the works of many (Carrillo et al., 1999; Dim et al., 2016; Kloubek, 1981; Li et al., 2013; Li et al., 2014; Rigby et al., 2004; Rigby and Edler, 2002) when a positive pressure is applied to force a liquid in to porous media, there is a change of two parameters, namely  $\sigma$  and  $\cos(\theta)$  in Equation (1). However, when a wetting liquid such as water (instead of mercury) is used to test a chemically modified and non-homogenous porous materials such as the modified CFA using OS the  $\sigma \cos(\theta)$  factor may not be the only change. For example, Li et al. (2014) found that the chemical structure of a liquid, i.e., the existence of hydrophilic and hydrophobic alkyl chains changes in the pore contact angle.

#### *2.4.5 Apparent and pore contact angle*

Pore CA is different from apparent CA (CA measured on a flat surface). When a positive pressure is applied to a liquid to initiate infiltration in porous media the liquid in the pore space deformed Figure 2.14 as a result its radius of curvature at the is reduced (Rigby et al., 2004; Li et al., 2013). Water entry is a function of both pore size and surface energy.

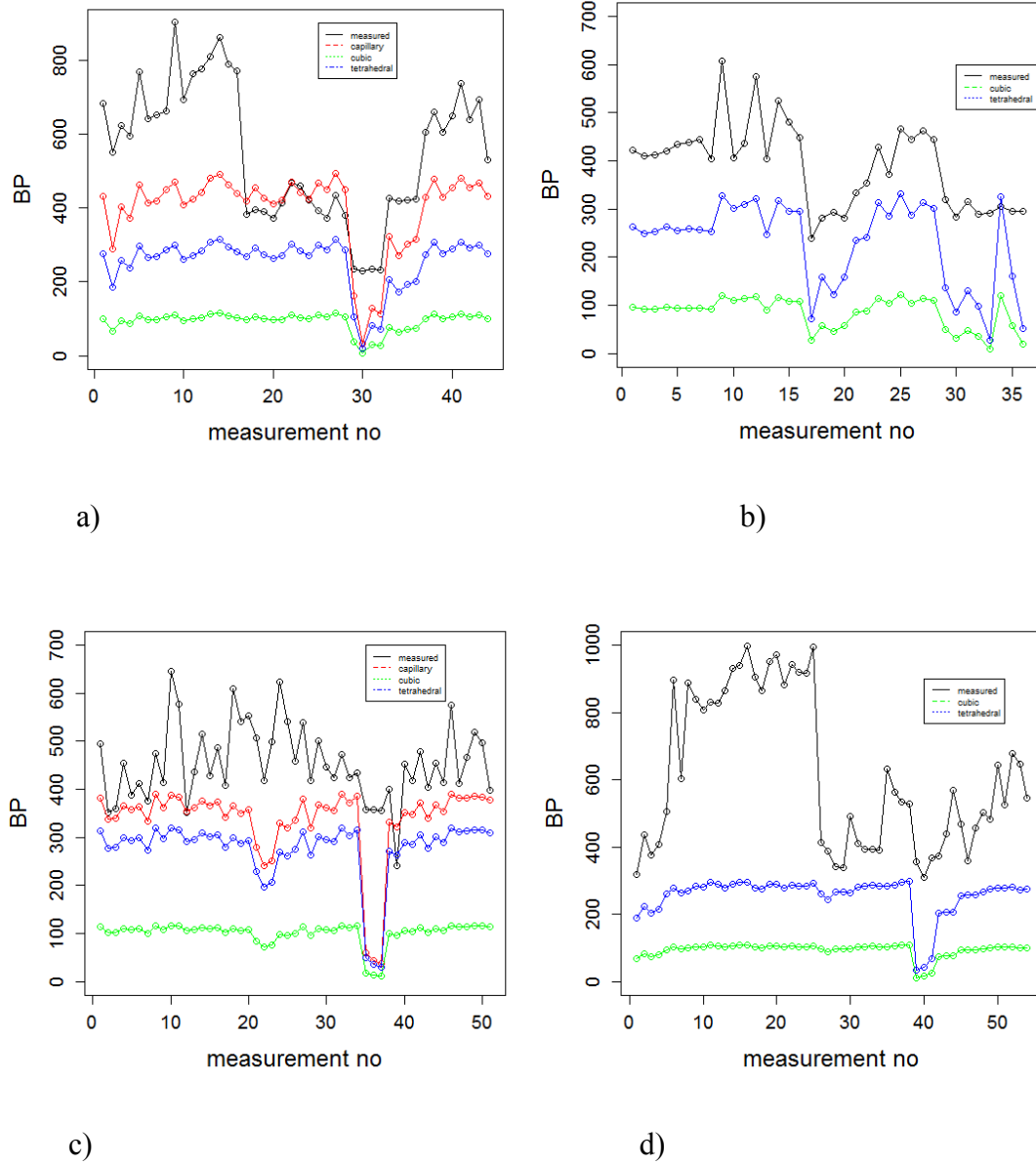


Figure 2.13. Measured and calculated Breakthrough Pressure for a) CFA-1, b) CFA-2, c) CFA-3, and d) CFA-5 using measured pore size, cubic and tetrahedral packing approaches.

Henry (1948) distinguishes between water resistance and water repellency, noting that water repellency is a function is a function of the surface energy, i.e., as inferred from

contact angle measurements. Water resistance is a function water repellency and the pore diameter, i.e., the pore diameter must be small.

As depicted in Figure 2. 8, and Figure 2.9 identical CFA have different BP and rates of infiltration based on the treatment type and dosage applied besides having equal pore size. The role of pore size in the Washburn equation is well established. The value of the contact angle measured on a flat surface is different that which manifests within pores. This difference increases with increasing pressure, especially beyond some threshold value.

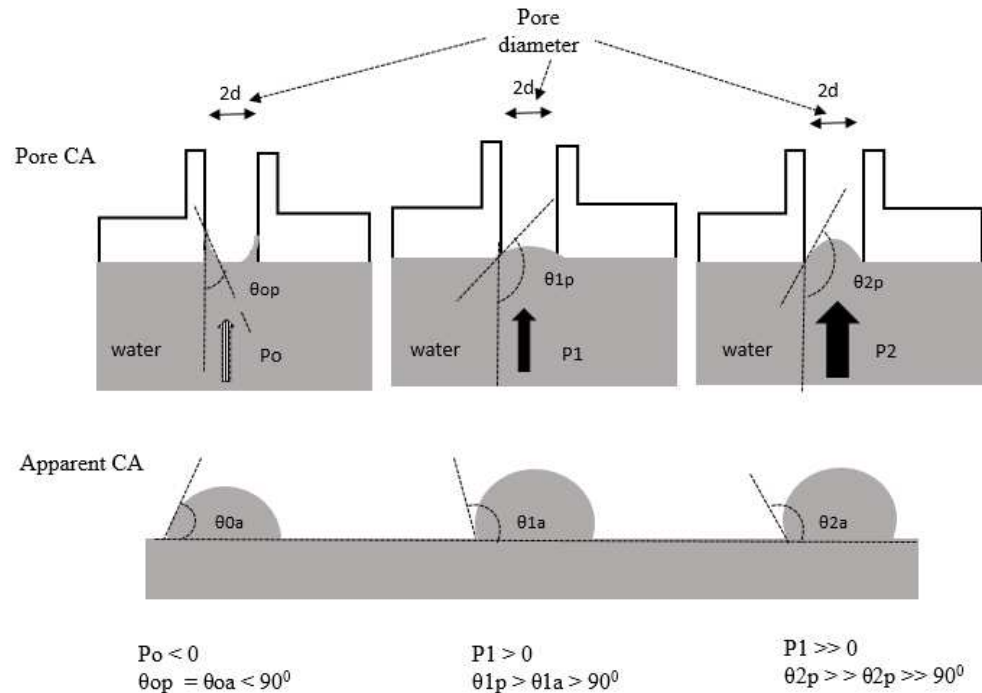


Figure 2.14. Idealized sketch showing apparent and pore CA resulting due to the change in pore water radius

Many studies including (Carrillo et al., 1999; Rigby and Edler, 2002; Rigby et al., 2004; and Li et al., 2013 ) have recognized this distinction. As such when using a CA

measured on flat surface for estimates of BP via the Washburn equation, it should be corrected.

However; pore CA is not easily accessible and quantifiable variable. Moreover, it is not the purpose of this study to measure the magnitude of pore CA. In addition, since pore CA is formed from a resistance encountered (surface energy), its magnitude should be a function of the magnitude of BP. On the other hand, BP is also a function of CFA (that includes the type and quantity of oxides, minerals, and their relative abundance) and OS (type, mix ratio, and alkyl chains).

#### *2.4.6 Correlation between CA and BP*

Measured data for CA in chapter one was used for analysis. Plots of BP versus CA with their corresponding CFA is shown in Figure 2.15 and Figure 2.16. For further analysis data screening was conducted. Accordingly; measurement of CA less than  $90^0$  were removed from the list with their corresponding BP.

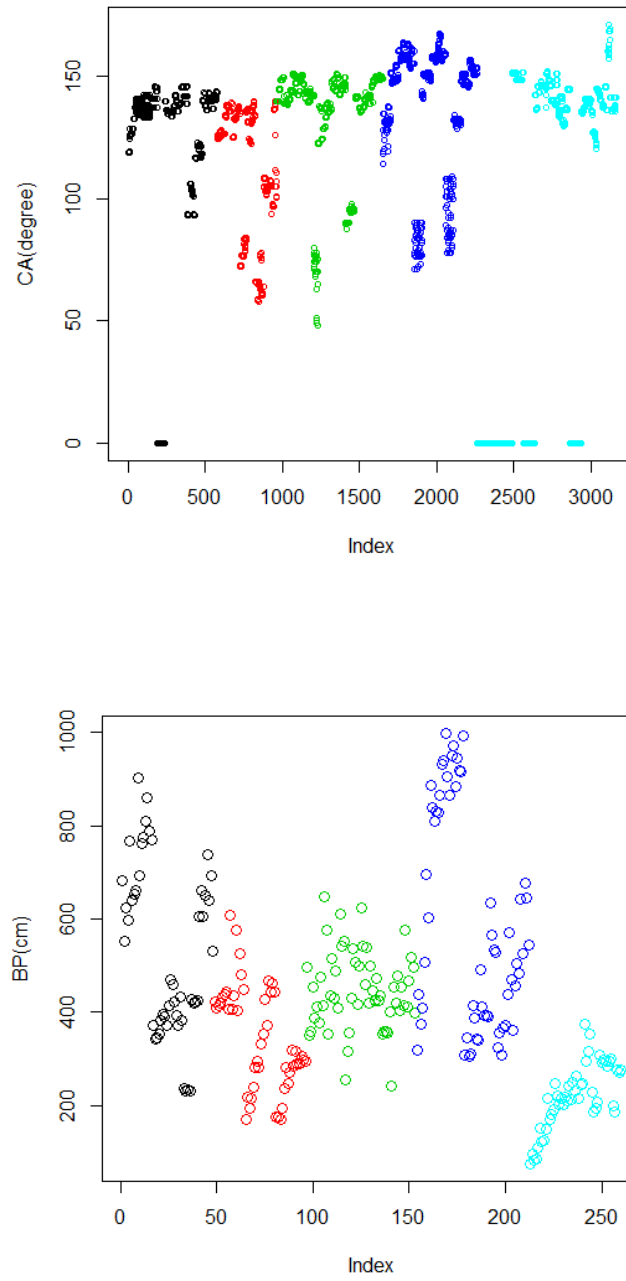


Figure 2. 15. Measured CA and BP data for five CFA treated using three OS.



Figure 2.16. Plot of BP versus CA for five CFA treated using three OS

*2.4.6.1 Exploratory data analysis:* To establish a relationship between the two water repellent parameters a normal and different transformed scales were used Figure 2.17. First an ordinary linear regression for all the measurements despite the difference in type of CFA, OS, and dose was conducted. Using this approach, a small  $R^2 = 0.2854$  has been observed. Further a diagnostic plot showed that residuals of CA followed a certain pattern at larger BP Figure 2.18(a). Further a significant discrepancy in the quantiles (Q-Q plot) is observed. Next another approach; a semi-log transformed (alternatively for BP and

CA), and log-log transformed analysis were conducted. Results from the three regression models showed a slightly higher R-squared (except one), 0.2516, 0.3352, and 0.3044 for semi-log (BP), semi-log (CA), and log-log Figure 2.17, respectively. For the same reason in ordinary linear regression model, these models do not fit well Figure 2.18 (b, c, and d).

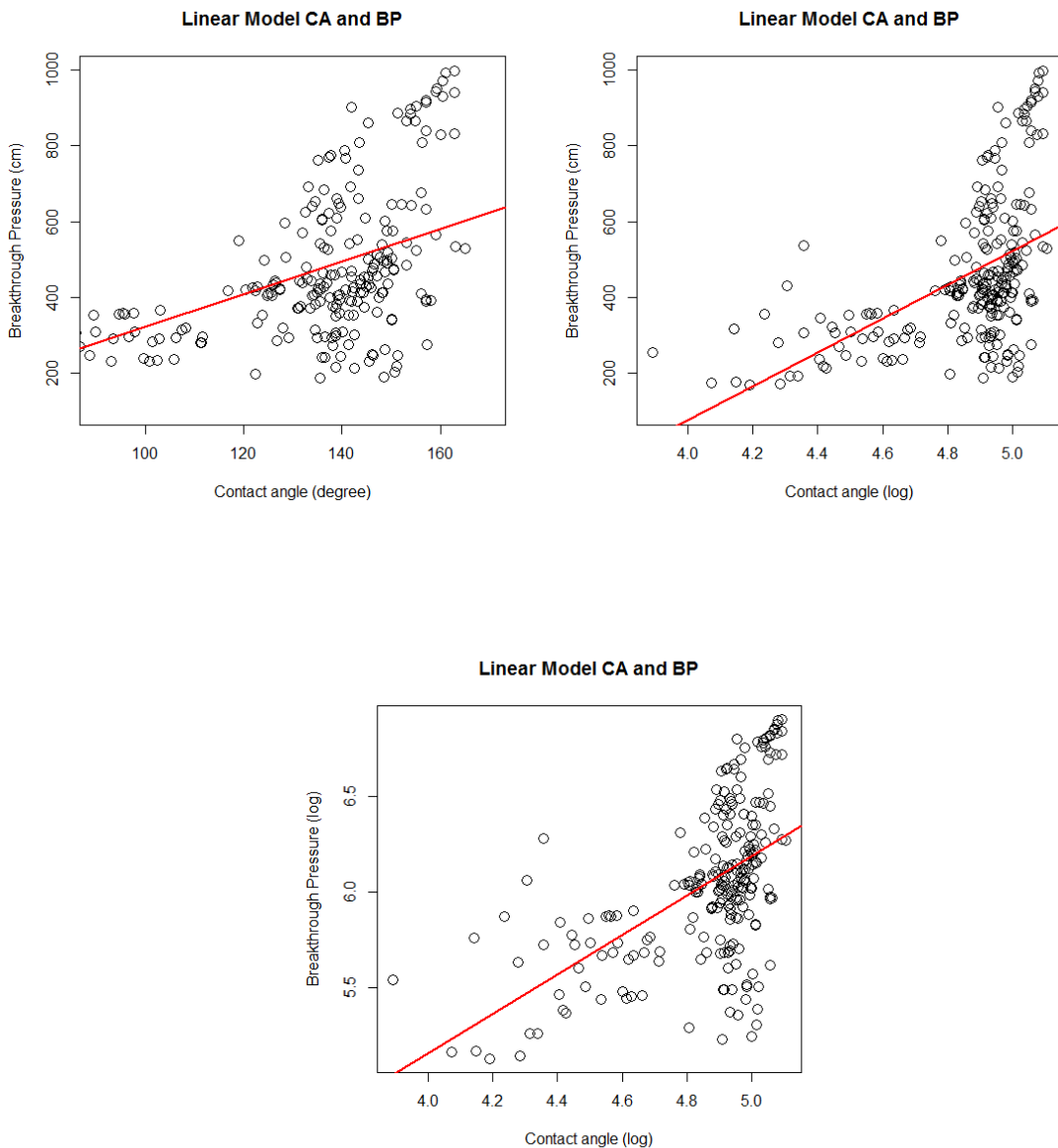


Figure 2.17. Linear regression models for different transformed scales

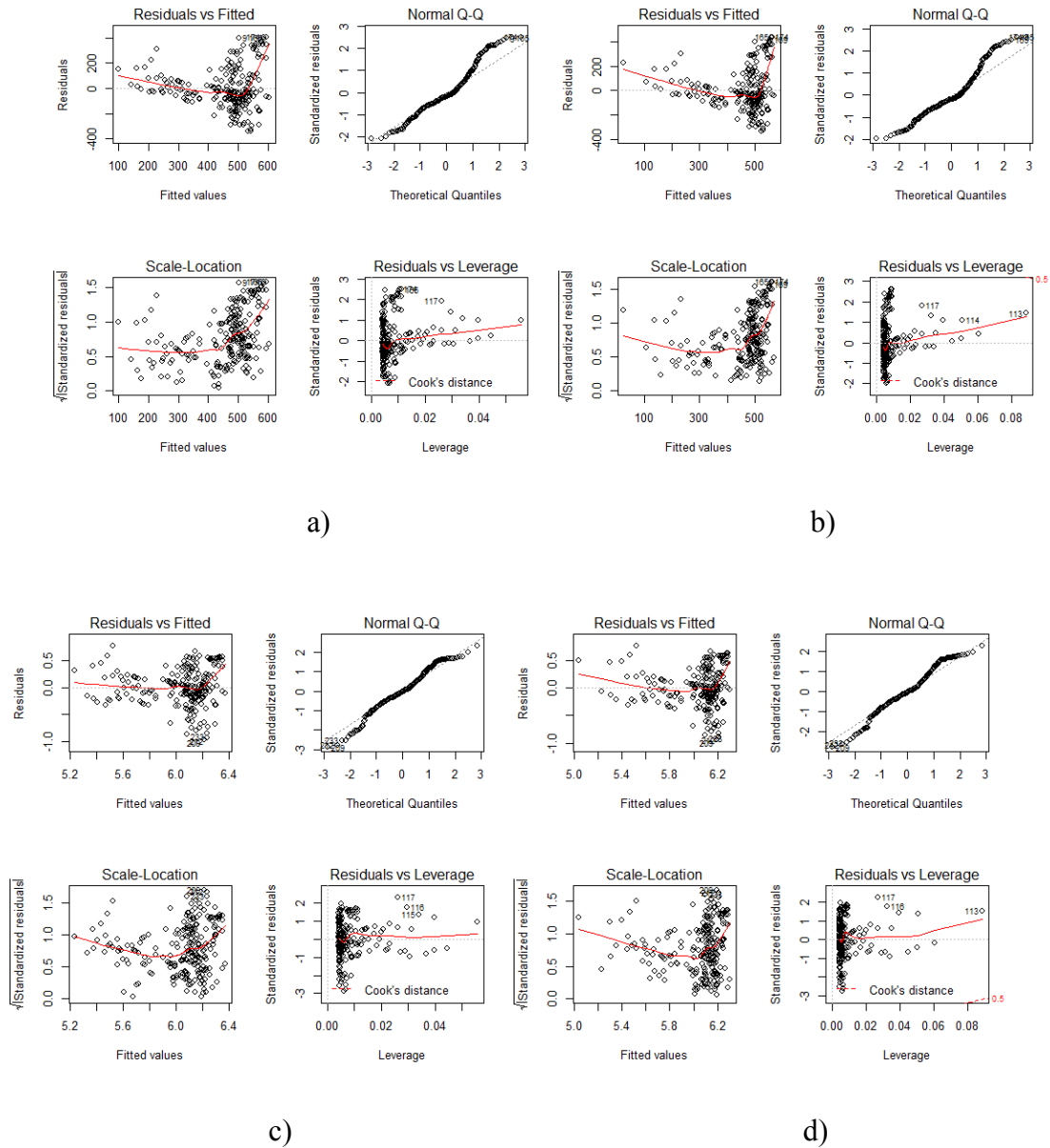


Figure 2.18. A linear regression diagnostic plot for all CFA and OS; a) ordinary linear regression, b) semi-log (BP) scale, c) semi-log (CA) scale, and d) log-log scale

But a clear insight into the residuals pattern of all the four models shows that at larger BP, CA follows a certain unique pattern.



*2.4.6.2 Identify underlying Influencing variable and conditioned plot:* Using all the factors together such that the type of CFA, OS, and the applied mix ratio to predict BP based on CA measurement only did not provided a good fitting model despite change in scale. This suggest that there exists an underlying additional variable to influence the relationship. Hence, to identify and use the underlying variable in the model was required. Due to this a conditional plot in which a linear regression between BP and CA are partially evaluated (conditioned) based on type of CFA, OS and mix ratio used Figure 2.19. As shown in the Figure, a regression based on the type of CFA and OS shows a variability than dose. This suggests the relationship between CA and BP is more explained by the type of CFA and OS used. Based on this analysis that based on separate CFA was conducted Figure 2.20 (black lines). Results showed that, an average R-squared, 0.4136, an improvement from previous models, was observed. A further look at the diagnostic plot using CFA shows that the residuals plot does not follow similar pattern as the previous models. Even if there are some unique patterns that the residuals plot of the regression model follows Figure 2.21; first, the patterns are not similar, and second the magnitude of the residuals are reduced from its corresponding ordinary linear regression when CFA are considered together. The absence of a similar pattern shows that the variability is a function of the individual CFA, OS, and dosage.

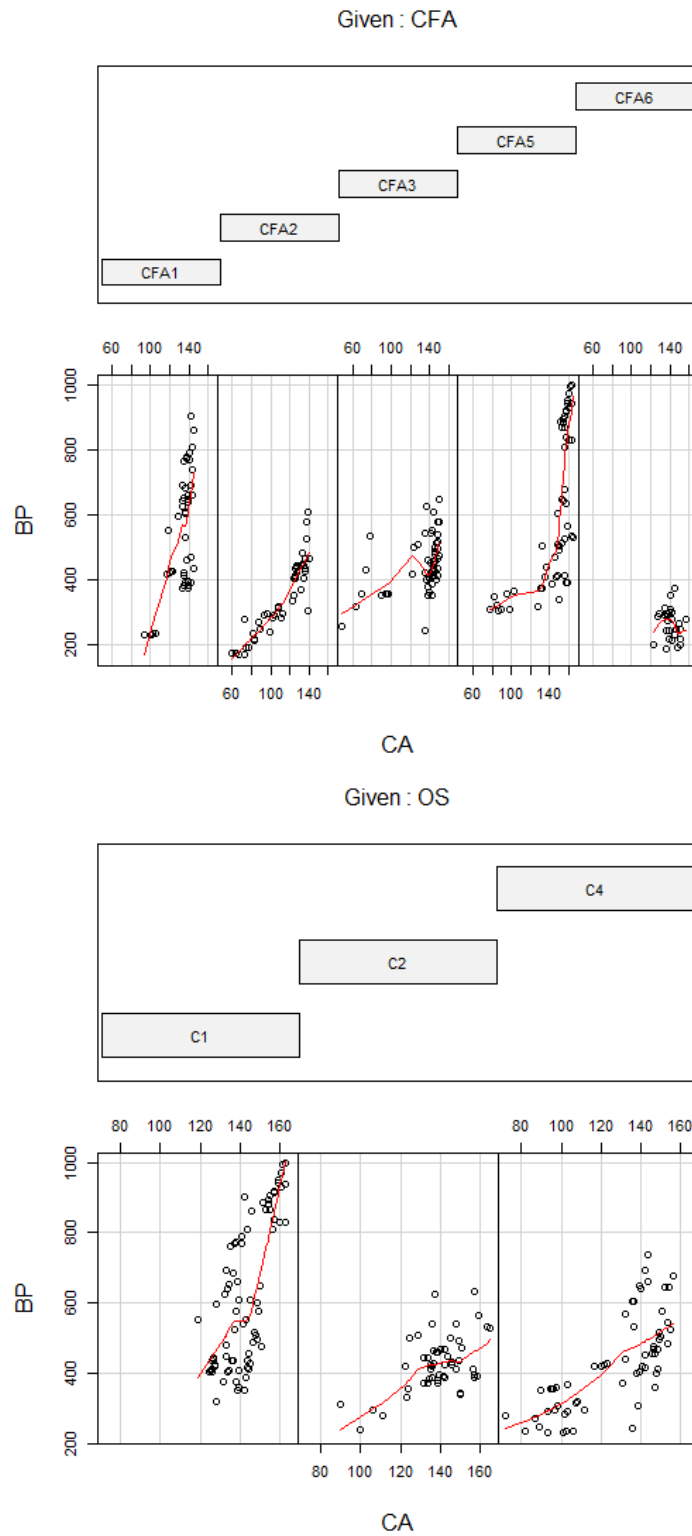


Figure 2.19. Conditioned plot to identify the underlying influencing variables to model BP as a factor of CA

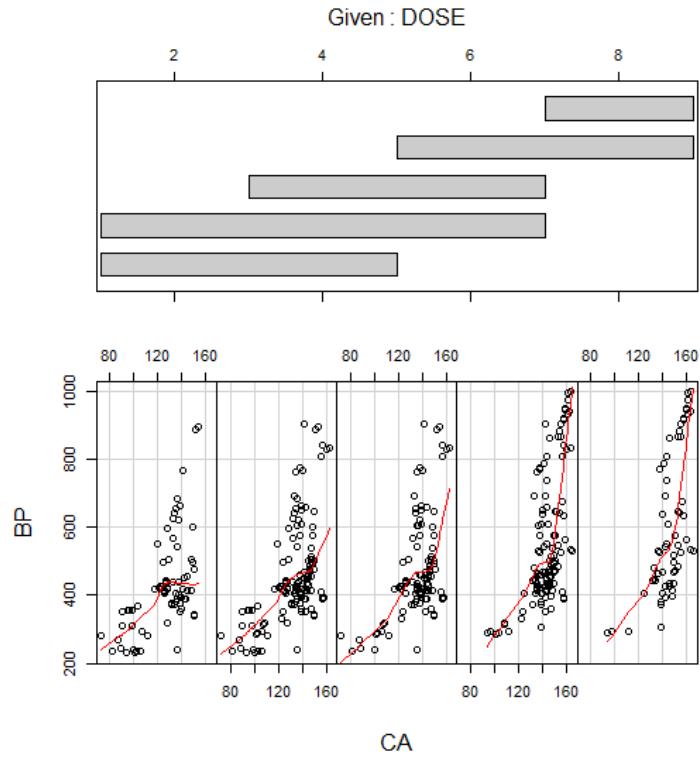
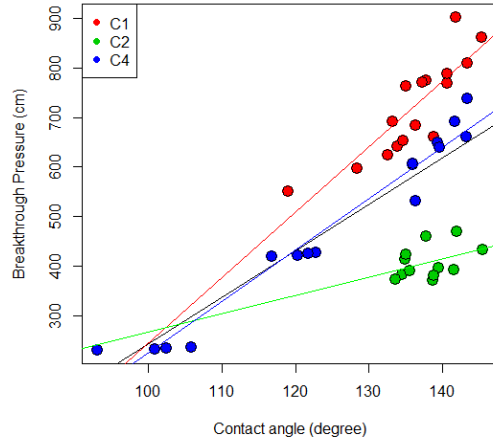
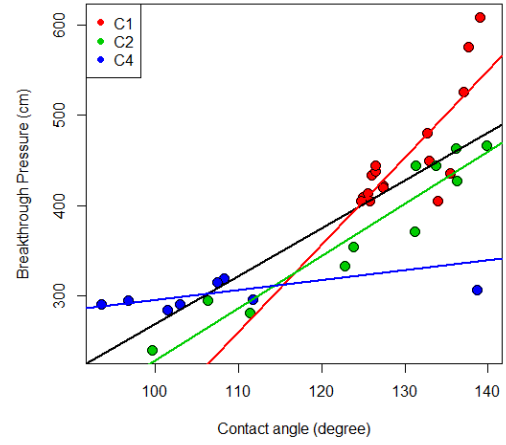


Figure 2.19. continued

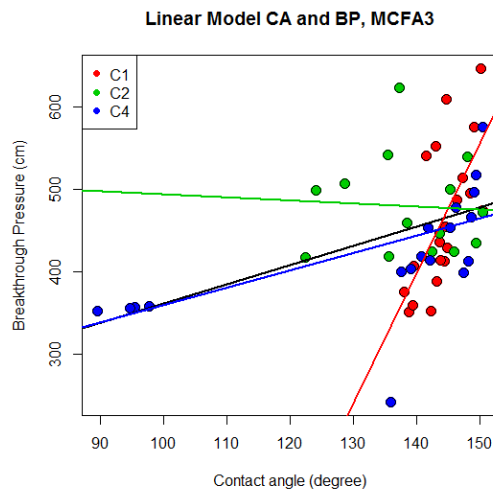
Finally modeling using measurement of CA versus BP by including all types of CFA and OS was conducted Figure 2.20 (colored lines). The corresponding diagnostic plot is depicted in Figure 2.22. This approach improves model fitness, average R-square = 0.777. This model shows a better fit when compared to the analysis conducted for CFA alone. Residuals variability and Q-Q plot also improved and accepted as better fit.



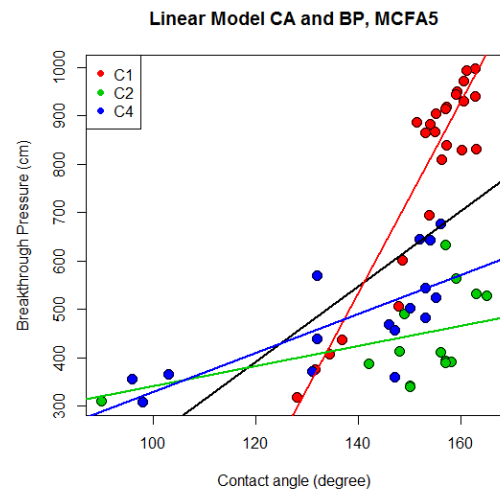
a)



b)



c)



d)

Figure 2.20. Ordinary Linear regression model for CA and BP grouped in type of CFA(black) and (CFA + OS); a) CFA-1, b) CFA-2, c) CFA-3, and d) CFA-5

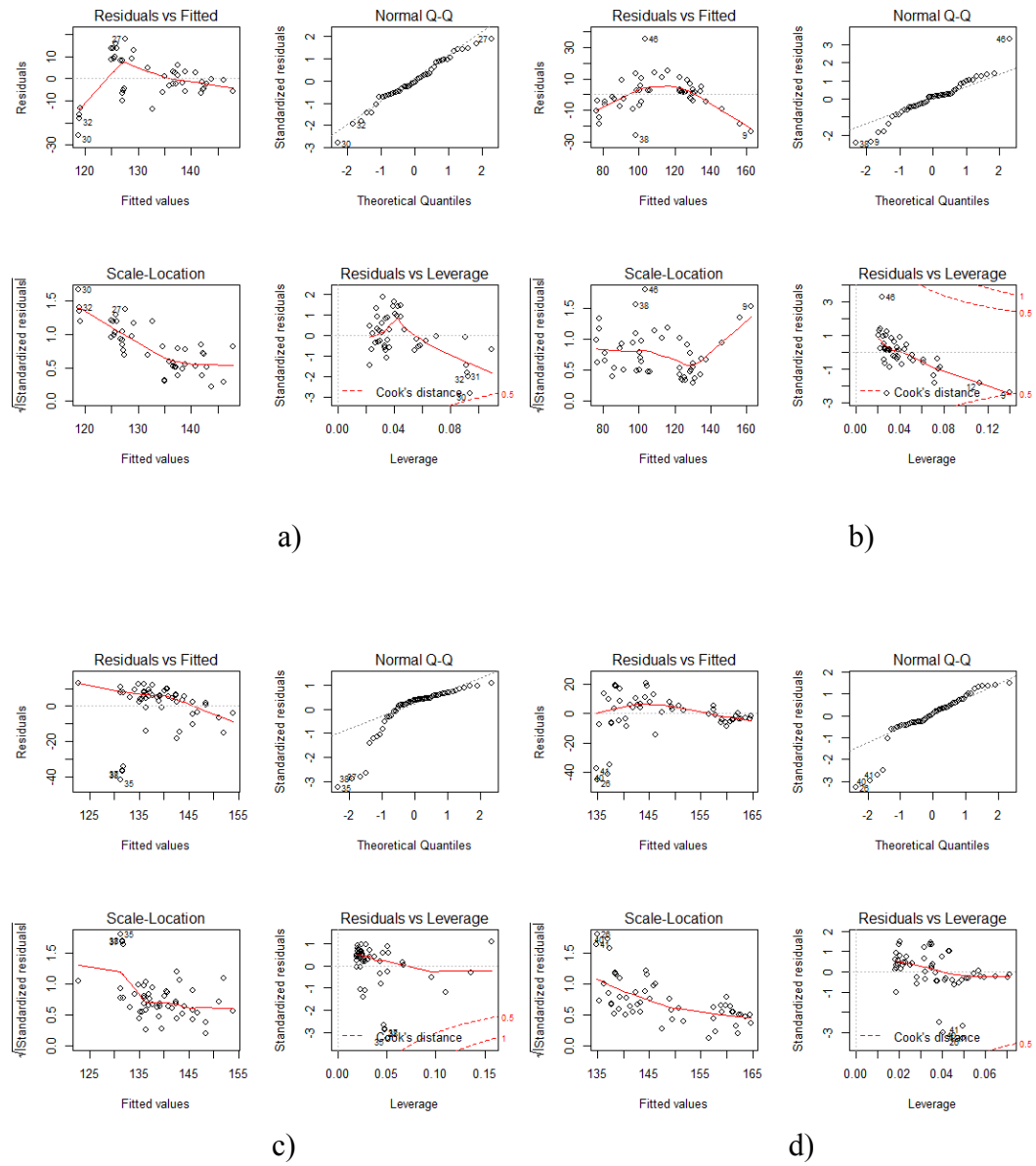


Figure 2.21. A linear regression diagnostic plot for; a) CFA-1, b) CFA-2, c) CFA-3, and d) CFA-5.

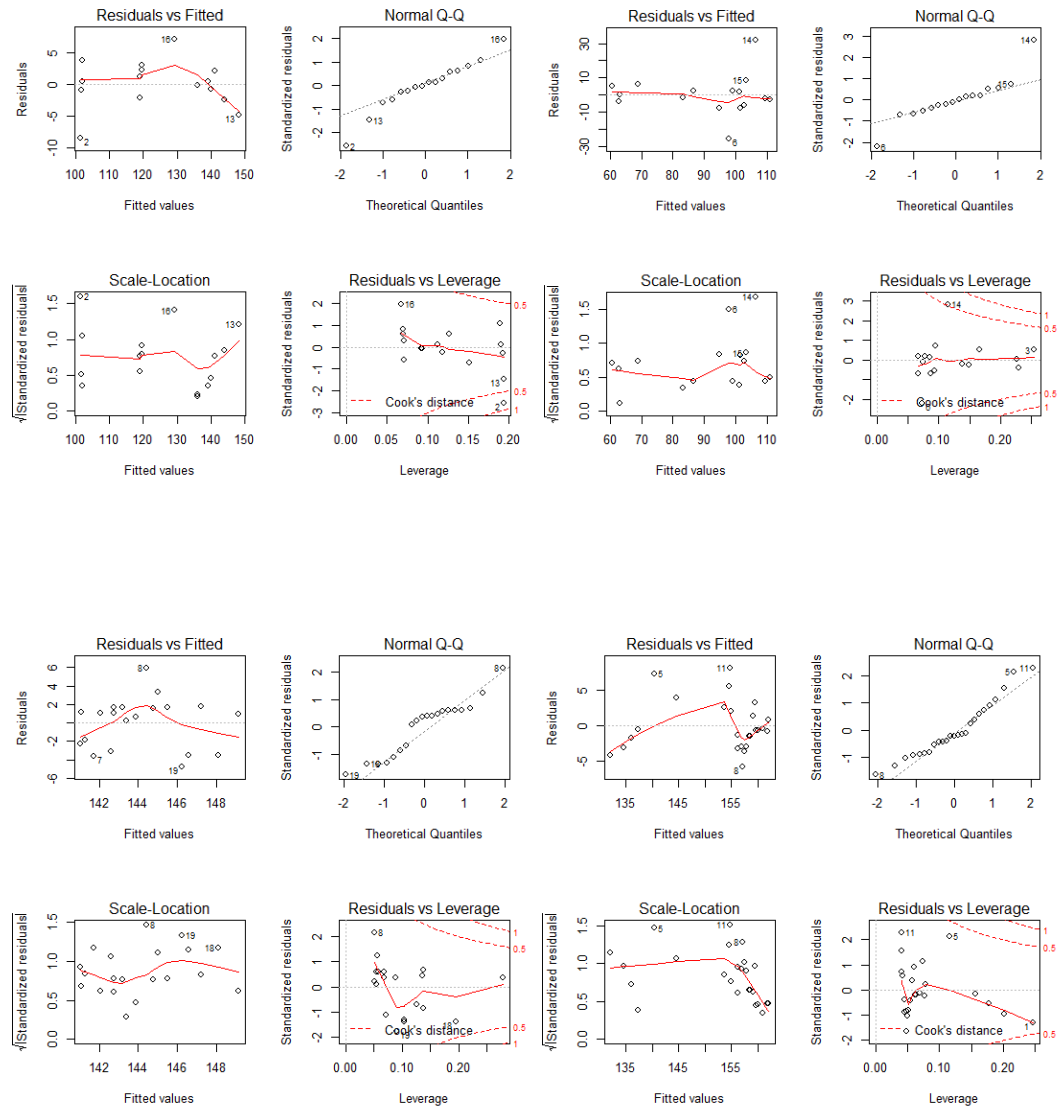


Figure 2. 22. A linear regression diagnostic plot when grouped according to type of CFA and OS; a) CFA-1, b) CFA-2, c) CFA-3, and d) CFA-5.

As shown in Figure 2.19 the relationship between CA and BP were evaluated using three conditioning parameters; type of CFA, OS and Dose applied. CA versus BP varies based on the type of CFA and OS. However; the relationship is not affected by dosage applied across CFA and OS used, the respond for it is consistent. This concludes that the

relationship between CA-BP is better explained using the underlying parameters the type of CFA and OS used, not dosage applied.

#### *2.4.7 The Washburn equation for a positive water entry pressure*

As shown in Figure 2.13 there exists a scale factor between the measured and calculated BP using the Washburn equation results from change in CA, from flat surface CA to pore CA. Hence, to use Washburn equation for the modified CFA the equation should be corrected for change in CA from measurement on flat surface to pore CA.

To estimate the scale factor (to account for the difference flat surface and pore CA), a linear relationship between measured CA versus measured and estimated BP was observed in Figure 2.13 and Figure 2.23 to Figure 2.26. As depicted in the Figures while the degree of hydrophobicity increases the divergence (scale factor) between measured and modeled BP increases. These Figures (Figures 2.23 to Figure 2.26) also provide a backward forecast which indicates that this divergence is reduced and in some cases becomes negligible as the contact angle is reduced. This results from the fact that at a boundary between hydrophilic and hydrophobic surfaces ( $CA = 90^0$ ) the effect of treatment is diminished and all lines should assume a similar value since all are packed with same density. The point where the backward forecasted graphs met affects the type of relationship between the water repellent parameters. For example, CFA-3 treated using C-1 and C-4 in Figure 2.25 (a and c), and CFA-5 treated using C-1 and C-2 Figure 2.26 (a and b) their backward forecast shows lines met at CA more than  $90^0$ . This indicates a different physical mechanism under high pressure and requires different fitting model. Following this shortcoming, an exponential relationship has been developed for this

particular case. Their corresponding Figures are shown in Figure 2.25 (d and e) and Figure 2.26 (d and e), respectively. The backward linear forecast of the corresponding figures shows plots converge and intercept or approach each other near the boundary between hydrophilic and hydrophobic surfaces. As a result, measured BP and CA data of a single CFA was divided based on type of OS used Figure 2.21. It was concluded that when the CA of the modified CFA becomes slightly greater than  $140^{\circ}$  (the characteristic of a highly hydrophobic and super hydrophobic ( $CA > 150^{\circ}$ ) surfaces), the relationship between CA and BP abruptly changes from a linear relationship to an exponential one. The exponential relationship between measured CA and BP provides a better fit and is consistent with the expectation that the distinction between surface and pore CA is only significant at higher pressures. At lower pressure (e.g., low levels of water repellency), the curvature of water within pores is not changed significantly and the pore CA approximates CA as measured on flat surface. In some cases, for example as depicted in Figure 2.25(c), Figure 2.26 (b), the samples form CA of more than  $140^{\circ}$  and yet little change occurs under pressure. Much appears to depend on the specific OS and CFA types involved.



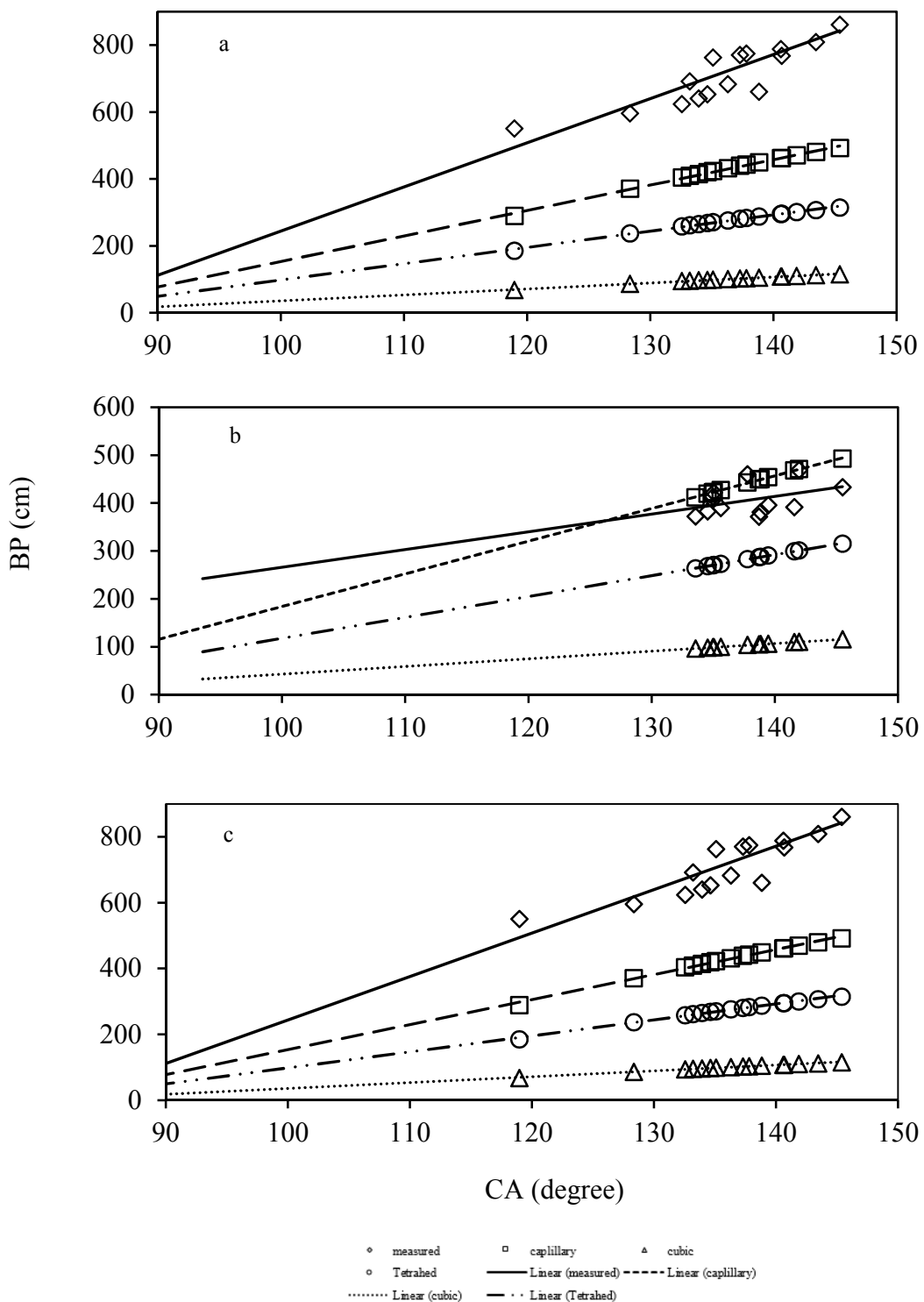


Figure 2.23. BP and CA liner modeling for CFA-1 treated using OS; C-1, C-2, and C-3 for a, b, and c in their order of arrangement. Figure d is an exponentially adjusted plot for a. BP for the three models were calculated using the capillary rise equation.

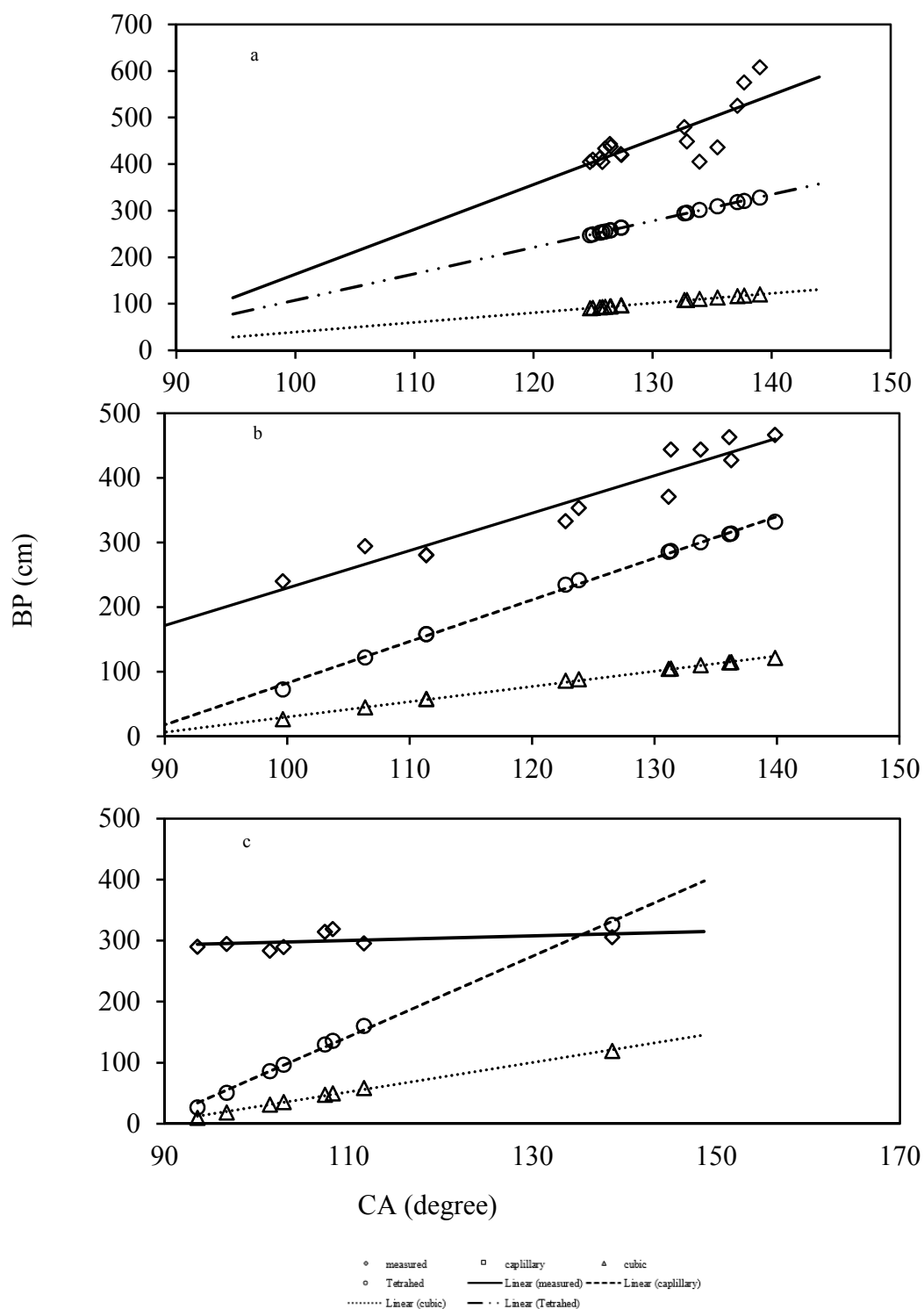


Figure 2. 24. BP and CA liner modeling for CFA-2 treated using OS; C-1, C-2 and C-3 for a, b, and c their order of arrangement. BP for the three models were calculated using the capillary rise equation.

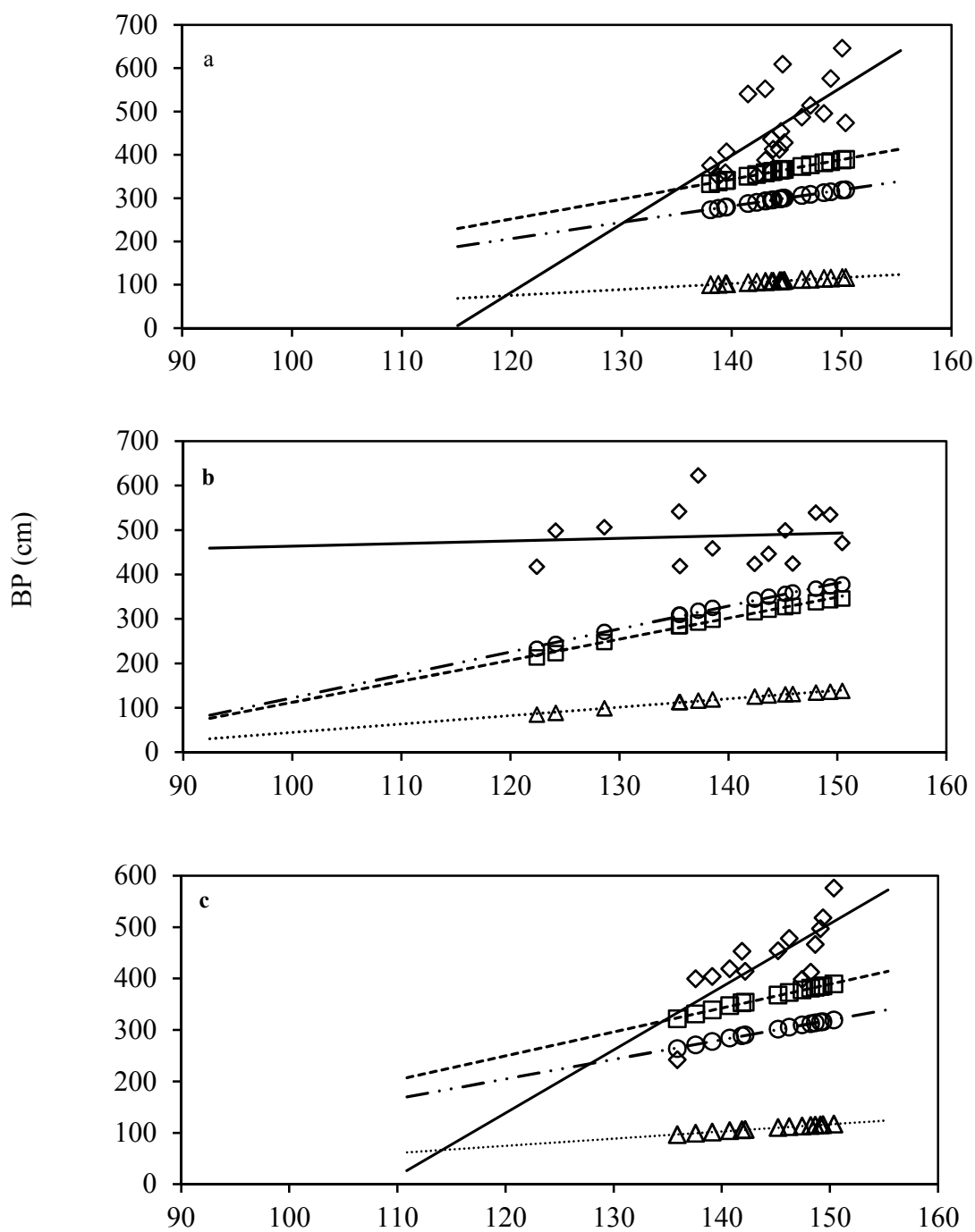


Figure 2.25. BP and CA liner modeling for CFA-3 treated using OS; C-1, C-2 and C-3 represented by a, b, and c respectively. Figures d and e represent an exponentially modified fitting models for a and c. BP for the three models were calculated using the capillary rise equation

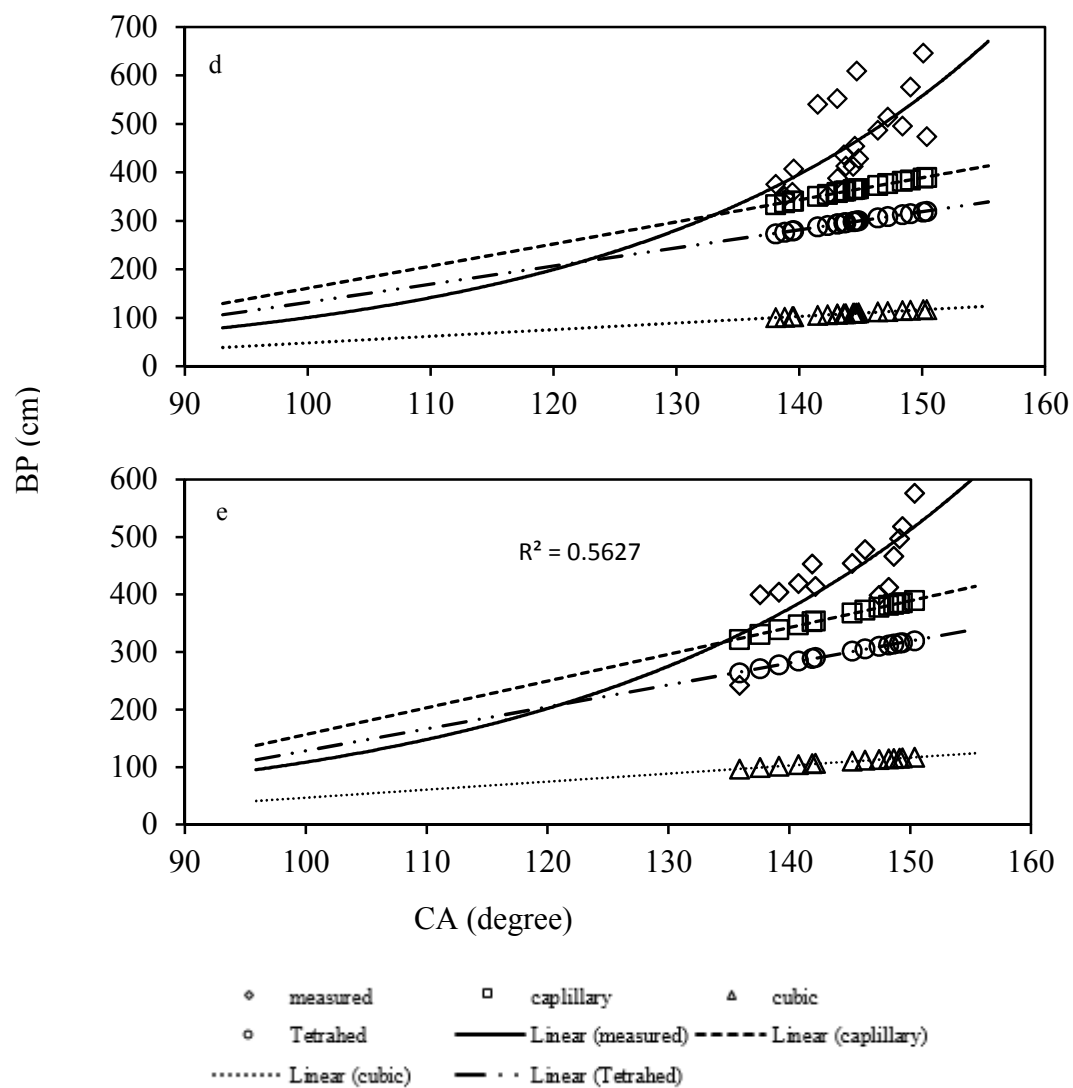
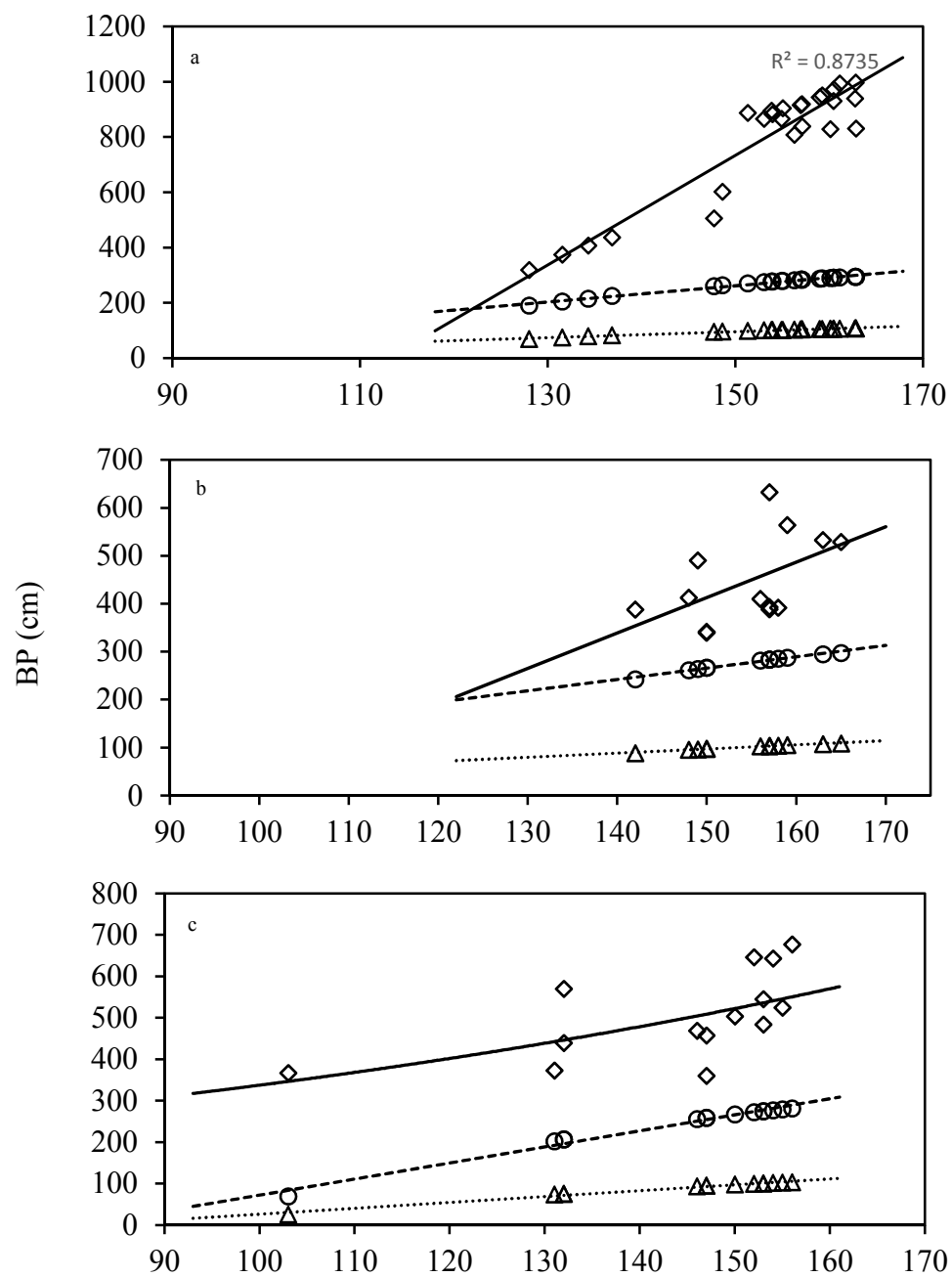


Figure 2.25. continued



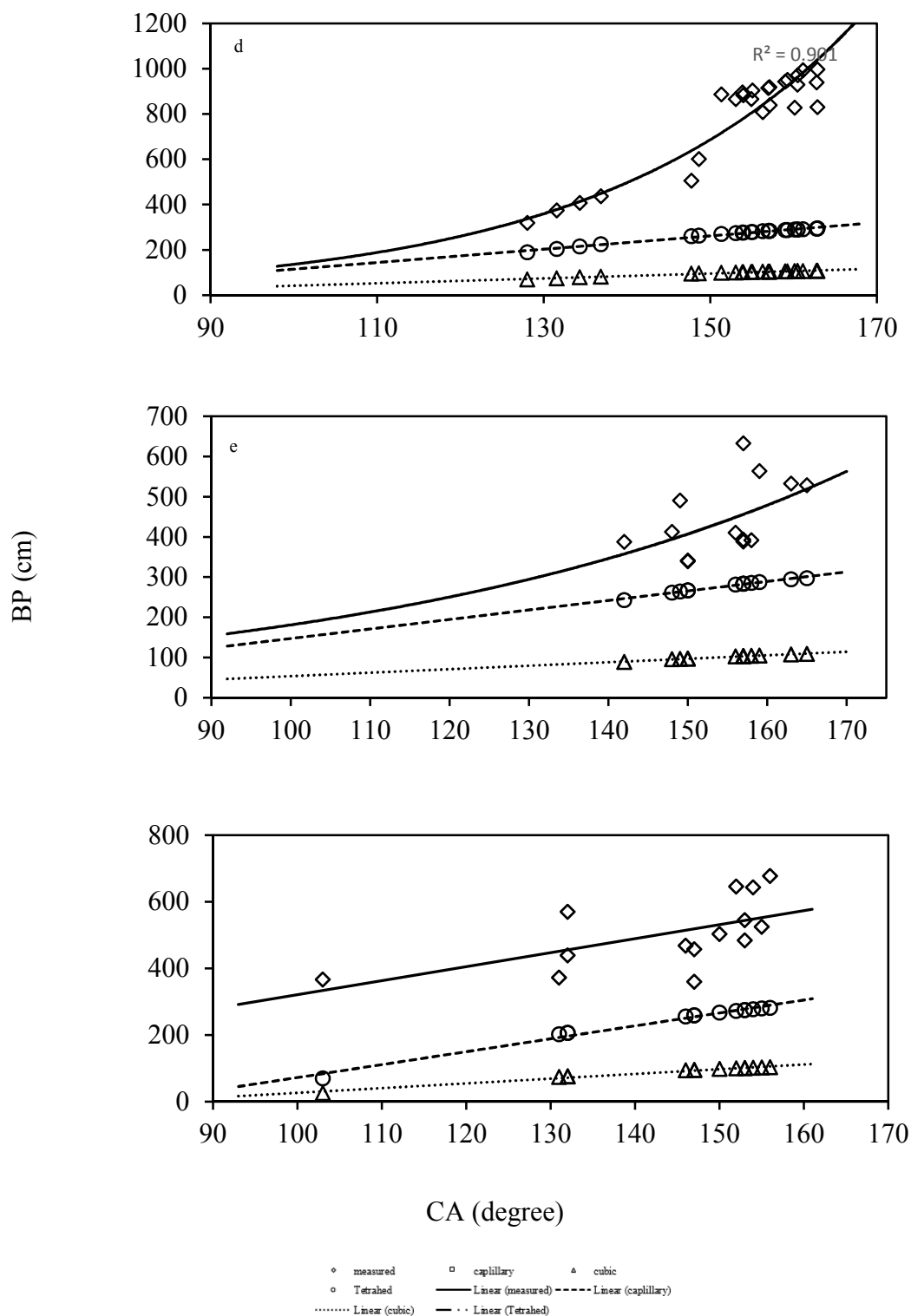


Figure 2.26. BP and CA liner modeling for CFA-5 treated using OS; C-1, C-2 and C-4 represented by a, b, and c respectively. Figures d, e, and f represent an exponentially modified fitting models for a b, and c. BP for the three models were calculated using the capillary rise equation.

The performance of each model was also evaluated from this relationship. The simple cubic packing approach not only under estimate BP values, but also all the calculated values fall below 150 cm. As a result, this approach was not considered for further evaluation and modeling. A scale factor was calculated and proposed for correction to the Washburn equation. The scale factor considers the two cases; for samples that form CA up to highly hydrophobic (CA >140°) linear relationship was used (Equation 2.5) but beyond that an exponential relationship was used (Equation 2.6). The general form of the adjusted Washburn equation is explained in two forms; linear scale and exponential scale. Values of coefficients in the modified equation are explained in table 2.2 for different CFA and OS. The relevant model is shown in Figure 2.27.

$$P = \frac{2 \sigma \cos(\theta)}{r} + A(\theta) + B \quad 2.5$$

$$P = \frac{2 \sigma \cos(\theta)}{r} + m e^{n(\theta)} - k \quad 2.6$$

All the units of length are in terms of cm.

The physical meaning of these equation is as follows;

When CA is less than about 140° a linear scale factor can be used to adjust the equation based on measured CA on flat surface Equation 2.5. Whereas as the CA increases, that means an increase in BP to infiltrate the water in to pore space, pore water radius changes Figure 2.14 as a result rapid change in pore CA. Due to this change in relationship to

exponential one Equation 2.6. Using the fitted value and coefficients in Table 2.2, a

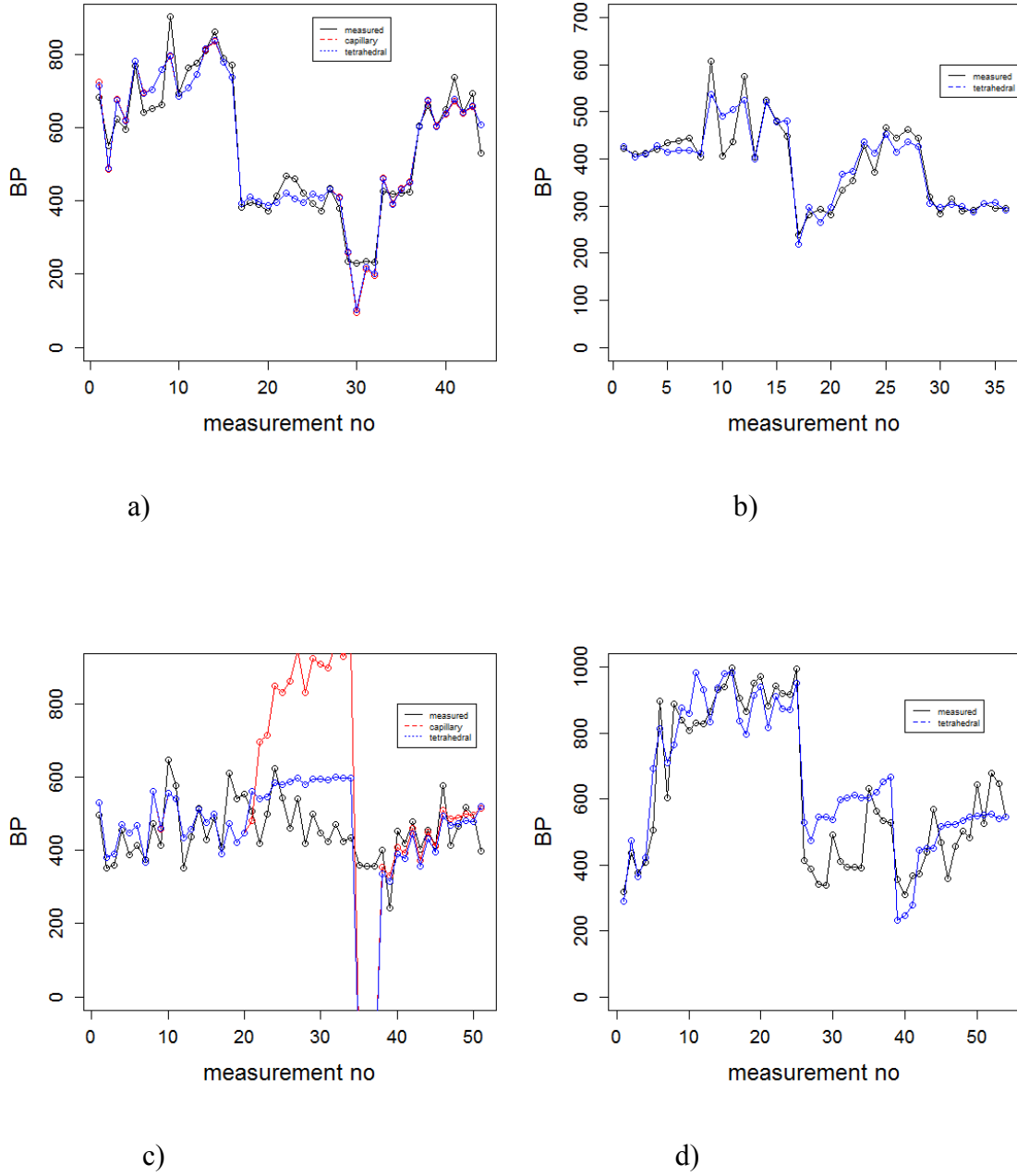


Figure 2.27. Measured and modeled Breakthrough Pressure for a) CFA-1, b) CFA-2, c) CFA-3, and d) CFA-5 using measured pore size and tetrahedral packing approaches.



Table 2. 2. Values of parameters in equations 3.5 and 3.6 for different modified CFA and OS, capillary (AEV) and Tetrahedral packing approach.

OS	Tetrahedral											
	CFA-1			CFA-2			CFA3			CFA-5		
	A	B		A	B		A	B		A	B	
C-1	8.337	-688.06		3.955	-340.42		12.01	-156.39		16.885	-206.69	
C-2	-0.669	214.61		-0.65	211.91		-4.583	799.31		5.902	-605.99	
C-4	5.717	-449.48		-6.219	841.8		8.465	-11.53		1.232	84.64	
	Capillary											
C-1	5.596	-469.4					11.187	-151.22		4.561(θ)-294.77		
C-2	-3.128	393.92					-4.155	766.68				
C-4	2.62	-181.88					7.628	-1027		4.650 (θ)-308.12		

comparison plot of residual distribution with models generated from pore size estimate is shown in Figure 2.28. As shown in the Figure, the fitted model improved the estimated values.

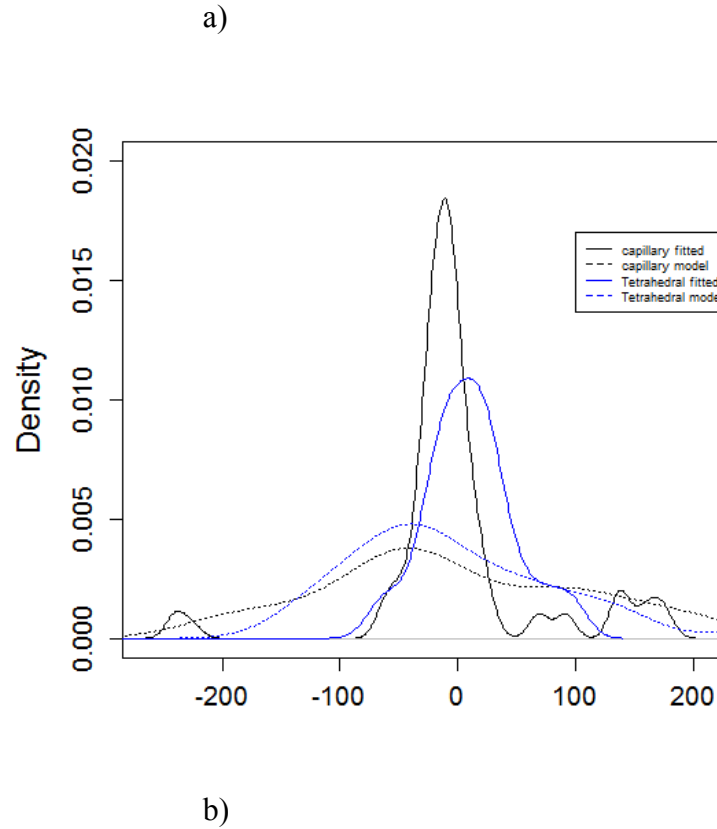


Figure 2.28. a) Linear regression model and the corresponding b) residuals density distribution for measured BP versus calculated and modeled BP for CFA-1 and CFA-3

To verify the fitness of the models, capillary (AEV) and tetrahedral packing, a general (for all CFA and OS) linear regression model for measured and estimated CA (pore CA) was shown Figure 2.29. As depicted in the Figure the pore size estimate using AEV approach fits better,  $R^2 = 0.7257$  against 0.6173 for Tetrahedral. Best fit of the models, however; observed when the evaluation considers the effect of both type of CFA and OS Figure 2.30, average  $R^2$  for all greater than 0.98. However; as discussed above and shown in Figure 2.22 and Figure 2.23 to Figure 2.26, BP is related to CA exponentially when all the measured CAs falls in the range of highly and super

hydrophobic surface ( $>140^\circ$ ). Accordingly, for CFA-3 the exponential relationship is applied and shown in Figure 2.31 and Figure 2.33. As depicted in the Figures, the exponential model not only fits the measured data better it also correctly reflects the expected change in behavior at the line of demarcation between hydrophilic and hydrophobic systems (i.e.,  $CA = 90^\circ$ ). Figure 2.33 shows a residual density distribution comparison between the linear and exponential pore CA model. As shown in the Figure, the exponential relationship between CA on flat surface and pore CA shows a better fit.

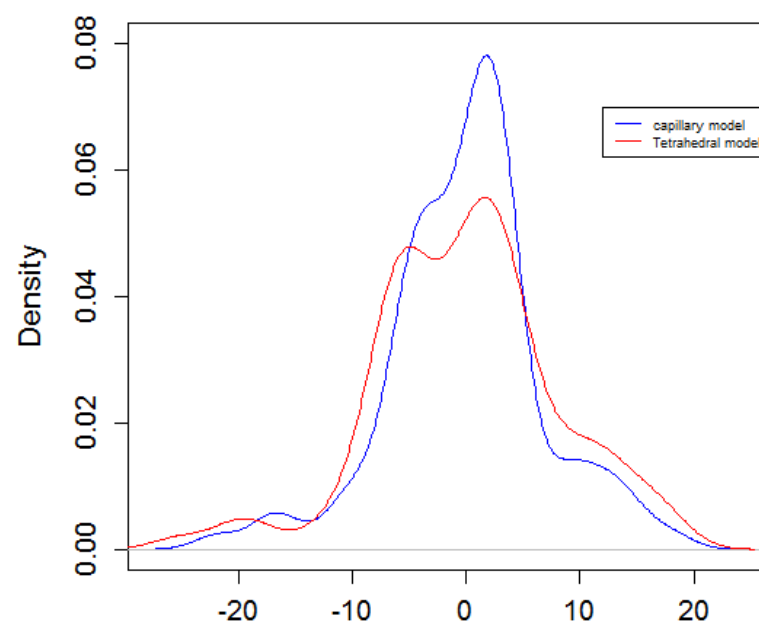
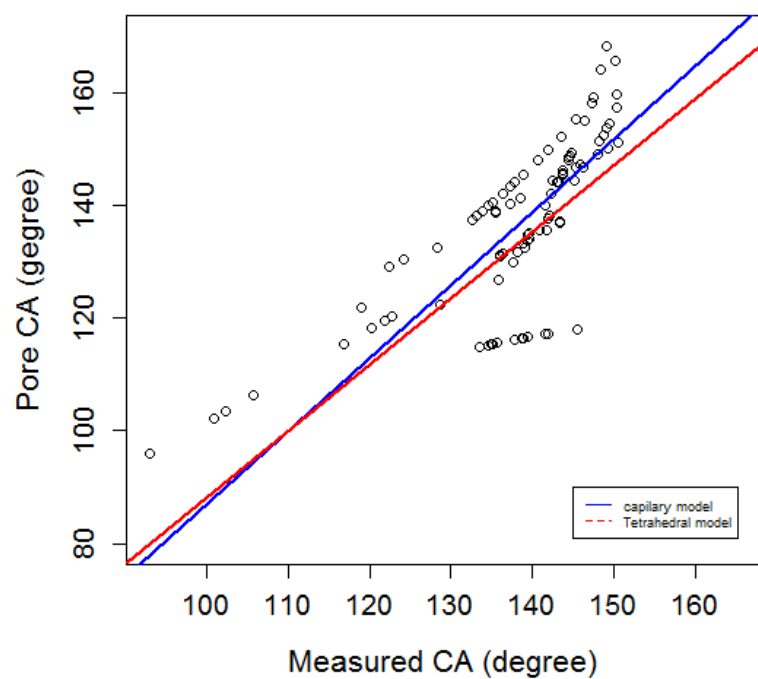


Figure 2.29. Linear regression model comparison between the two models for measured CA on flat surface and models predicted pore CA.

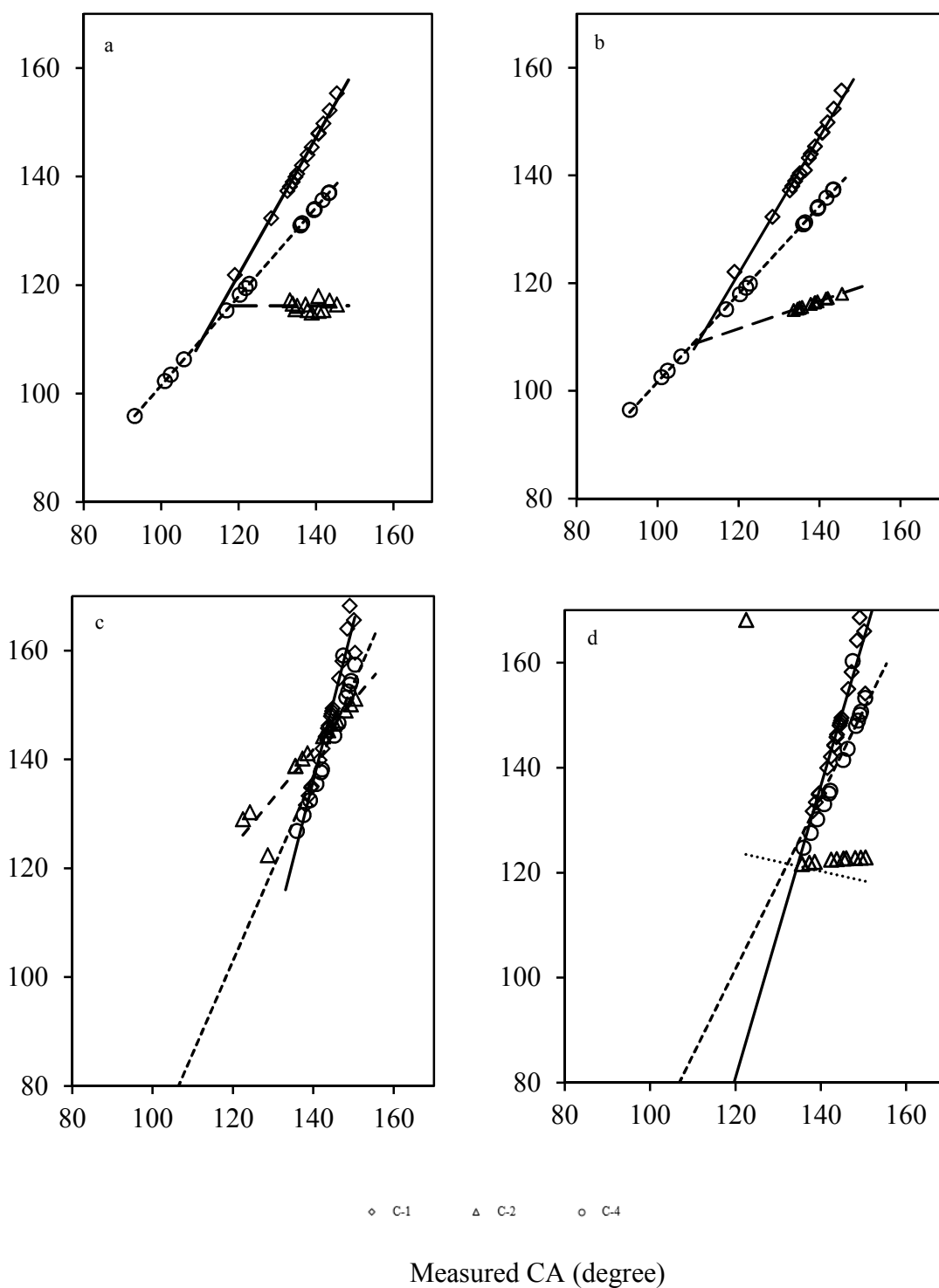


Figure 2.30. Linear regression between contact angle measured on flat surface and pore contact angle; a) CFA-1, b) CFA-2, c) CFA-3, and d) CFA-5.

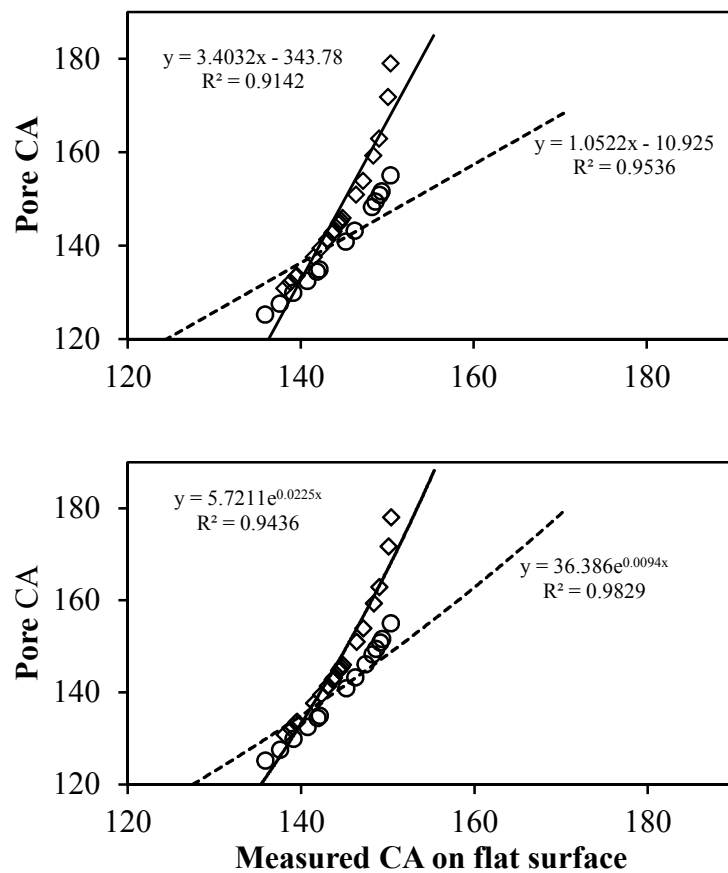


Figure 2.31. A detailed view and comparison between linear and exponential regression for contact angle measured on flat surface and pore contact angle for highly and super hydrophobic surfaces of modified CFA surface, CFA-3 treated using OS C1

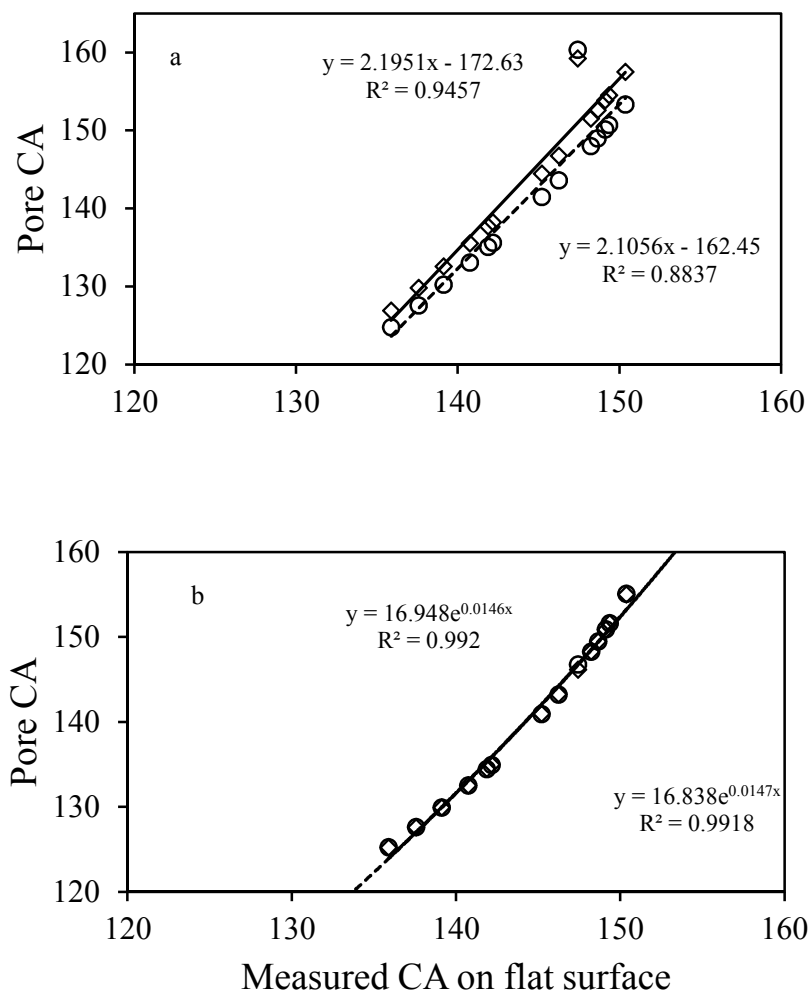


Figure 2.32. A detailed view and comparison between; (a) linear and (b) exponential regression for contact angle measured on flat surface and pore contact angle for highly and super hydrophobic surfaces of MCFA surface, CFA-3 treated using OS C4.

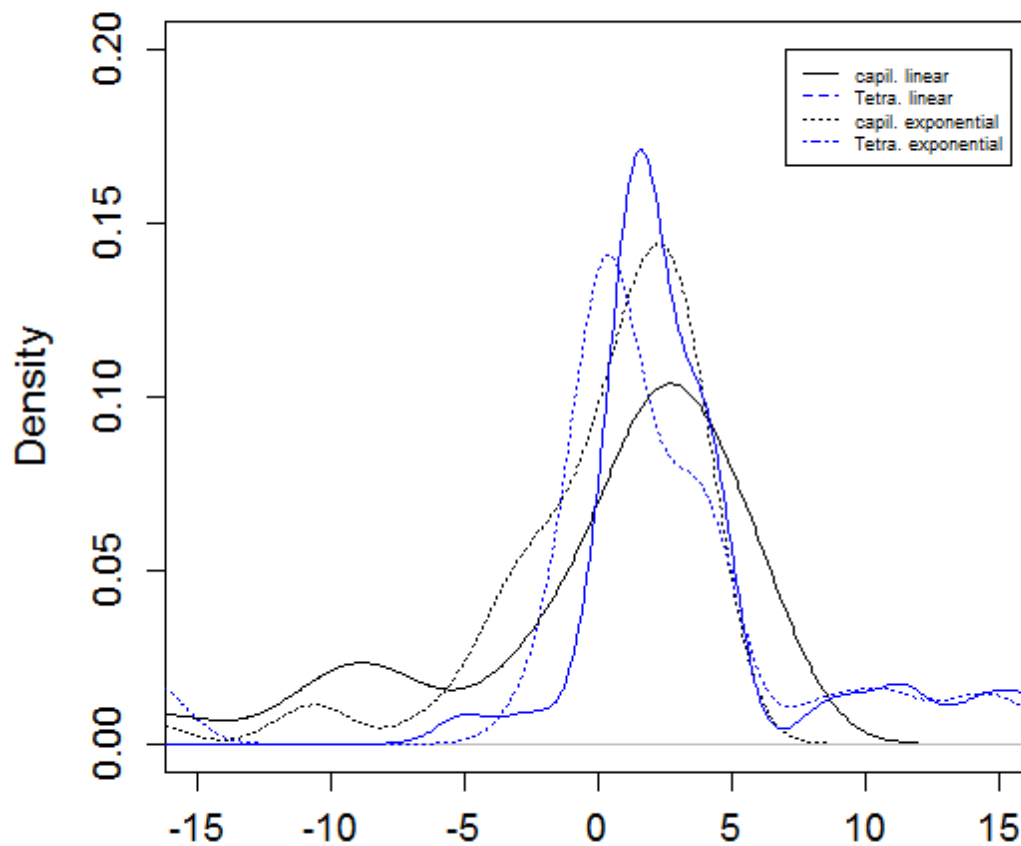


Figure 2.33. Comparison between linear and exponential relationship between measured CA on flat surface and pore CA model for CFA-3

## 2.5 Conclusions

This study has demonstrated that the surface of CFA can be modified and made sufficiently water repellent using OS products. The degree to which the surface can be made water repellent and able to withstand a positive water entry pressure was identified through breakthrough pressure measurements. Accordingly; using this innovative approach a resistance to infiltration up to 10 m (e.g., using CFA-5 treated using C-1) of



water head has been achieved. Such a resistance can prevent infiltration of water in to pore space there by preventing leaching of CFA. Further, the performance of five CFA when treated using three OS across different mix ratios has been presented. In general, up to a certain threshold (mostly 8 g/kg), a linear relationship has been observed between mix ratio and BP after which the relationship is either remains constant or declines.

This study has identified that for CFA modified using OS the rate of imbibition after overcoming the maximum resistance to flow is influenced significantly by the OS dosage and its effect on surface energy. A linear regression between measured BP and CA and calculated BP showed that the calculated BP under estimates BP to a certain scale factor. The physical meaning of the scale factor is related to the change and magnitude of surface energy as a result application of a positive entry pressure. This conclusion encompasses the change in  $\sigma \cos(\theta)$  in the Washburn equation. The magnitude and pattern of the scale factor varies based on the type of CFA and OS. The two main parameters of water repellency, CA and BP were correlated to find the type of their relationship for the modified CFA surface. In general, there is a positive correlation between CA and BP. However; CA and BP of the modified CFA are better related when categorized based on type of CFA and OS. But the OS dosage used for treatment does not alter the relationship. It has been found that when CA is slightly more than  $140^\circ$  the scale of the relationship between CA and BP changes abruptly and becomes exponential. It is believed that; while the chemical and mineral compositions in each CFA are main parameters for the type of CFA, the percent of reactive minerals, alkyl chains, and hydrolysable groups characterize OSs. The capillary rise equation was applied to predict BP of the modified CFA. Three approaches were used to estimate the pore size of the samples. It has been shown that the

pore size estimate using CFA-WCC and Tetrahedral packing approaches better predicted BP when used in the capillary rise (Washburn) equation. Hence for a modified CFA using OS products the Washburn equation should be modified in two factors, a linear and an exponential, due to the change of measured CA to pore CA. It was found that when the CA of the modified CFA becomes slightly greater than  $140^{\circ}$  (the characteristic of a highly hydrophobic and super hydrophobic ( $CA > 150^{\circ}$ ) surfaces), the relationship between CA and BP abruptly changes from a linear relationship to an exponential one, presumably due to a high deformation as a result a smaller pore water radius. The exponential relationship between measured CA and BP not only fits the measured data better it also correctly reflects the expected change in behavior at the line of demarcation between hydrophilic and hydrophobic systems (i.e.,  $CA = 90^{\circ}$ ). At lower surface energy since much energy is not required to force water in to pore space the radius of water molecule in the pore space does not change much, as a result pore CA approximates CA as measured on flat surface. Further the degree to which the applied pressure affects the pore contact angle depends on the type of OS, dose applied, hydrophilic and hydrophobic alkyl chains.

## REFERENCES

- Bartell, F. E., Purcell, W. R., and Dodd, C. G. (1948). "The measurement of the effective pore size and of the water-repellency of tightly woven textiles." *Discussions of the Faraday Society*, 3(0), 257-264.
- Carrillo, M. L. K., Letey, J., and Yates, S. R. (1999). "<Measurement of Initial Soil-Water Contact Angle of Water Repellent Soils>." *Soil Science Society of America Proceedings*, 63(3), 433-466.
- Daniels, J. L., Mehta, P., Vaden, M., Sweem, D., Mason, D. M., Zavareh, M., and Ogunro, V. (2009). "Nano-scale Organo-silane applications in geotechnical and geoenvironmental engineering." *International Journal of Terraspace Science and Engineering*, 1(1), 19-27.
- Dim, P. E., Fletcher, R. S., and Rigby, S. P. (2016). "Improving the accuracy of catalyst pore size distributions from mercury porosimetry using mercury thermoporometry." *Chemical Engineering Science*, 140, 291-298.
- Dimitrov, D. I., Milchev, A., and Binder, K. (2007). "Capillary Rise in Nanopores: Molecular Dynamics Evidence for the Lucas-Washburn Equation." *Physical Review Letters*, 99(5), 054501.
- F. de Buyl (2004). "<Organo-Functional Silanes,PDF.pdf>." *Silicones in Industrial Applications, in Inorganic Polymers*, Nova Science Publishers.
- Feyyisa, J., and Daniels, J. (2016). "A Dynamic Contact Angle Measurement Technique for Water-Repellent Coal Fly Ash (CFA)." *Geo-Chicago 2016, American Society of Civil Engineers*, 925-938.
- Feyyisa, J. L., Daniels, J. L., and Pando, M. A. (2017). "Contact Angle Measurements for Use in Specifying Organosilane-Modified Coal Combustion Fly Ash." *Journal of Materials in Civil Engineering*, 29(9).
- Fink, D. H., and Myers, L. E. (1969). "<Synthetic hydrophobic soils for harvesting precipitation >."
- Gao, S., Wei, N., Li, X., Wang, Y., and Wang, Q. (2014). "Cap Rock CO<sub>2</sub> Breakthrough Pressure Measurement Apparatus and Application in Shenhua CCS Project." *Energy Procedia*, 63, 4766-4772.
- Geocomp, C. (2017). "FlowTrac-II Volume Pressure Controller." <[http://www.geocomp.com/Products/Lab\\_Systems\\_FlowTrac2](http://www.geocomp.com/Products/Lab_Systems_FlowTrac2)>. (2/13/2017).
- Heath, J. E., Dewers, T. A., McPherson, B. J. O. L., Nemer, M. B., and Kotula, P. G. (2012). "Pore-lining phases and capillary breakthrough pressure of mudstone caprocks: Sealing efficiency of geologic CO<sub>2</sub> storage sites." *International Journal of Greenhouse Gas Control*, 11, 204-220.
- Hildenbrand, A., Schlomer, S., and Krooss, B. M. (2002). "Gas breakthrough experiments on fine-grained sedimentary rocks." *Geofluids*, 2, 3-23.
- Joos, P., Van Remoortere, P., and Bracke, M. (1990). "The kinetics of wetting in a capillary." *Journal of Colloid and Interface Science*, 136(1), 189-197.
- Kloubek, J. (1981). "Hysteresis in porosimetry." *Powder Technology*, 29(1), 63-73.
- Li, S., Dong, M., Li, Z., Huang, S., Qing, H., and Nickel, E. (2005). "Gas breakthrough pressure for hydrocarbon reservoir seal rocks: implications for the security of long-term CO<sub>2</sub> storage in the Weyburn field." *Geofluids*, 5(4), 326-334.

- Li, X., Fan, X., Askounis, A., Wu, K., Sefiane, K., and Koutsos, V. (2013). "An experimental study on dynamic pore wettability." *Chemical Engineering Science*, 104, 988-997.
- Li, X., Fan, X., and Brandani, S. (2014). "Difference in pore contact angle and the contact angle measured on a flat surface and in an open space." *Chemical Engineering Science*, 117, 137-145.
- Liu, J. F., Davy, C. A., Talandier, J., and Skoczylas, F. (2014). "Effect of gas pressure on the sealing efficiency of compacted bentonite–sand plugs." *Journal of Contaminant Hydrology*, 170, 10-27.
- Lu, N and Likos, W., (2004). "Unsaturated soil mechanics." John Wiley and Sons, Inc., New Jersey.
- Martic, G., Gentner, F., Seveno, D., Coulon, D., De Coninck, J., and Blake, T. D. (2002). "A Molecular Dynamics Simulation of Capillary Imbibition." *Langmuir*, 18(21), 7971-7976.
- O'Loughlin, M., Wilk, K., Priest, C., Ralston, J., and Popescu, M. N. (2013). "Capillary rise dynamics of aqueous glycerol solutions in glass capillaries: A critical examination of the Washburn equation." *Journal of Colloid and Interface Science*, 411, 257-264.
- P. Rigby, S., S. Fletcher, R., and N. Riley, S. (2004). "Characterisation of porous solids using integrated nitrogen sorption and mercury porosimetry." *Chemical Engineering Science*, 59(1), 41-51.
- Rezaeyan, A., Tabatabaei-Nejad, S. A., Khodapanah, E., and Kamari, M. (2015). "A laboratory study on capillary sealing efficiency of Iranian shale and anhydrite caprocks." *Marine and Petroleum Geology*, 66, Part 4, 817-828.
- Rigby, S. P., and Edler, K. J. (2002). "The Influence of Mercury Contact Angle, Surface Tension, and Retraction Mechanism on the Interpretation of Mercury Porosimetry Data." *Journal of Colloid and Interface Science*, 250(1), 175-190.
- Thierry Materne, F. d. B., Gerald L. Witucki (2012 ). "<Organosilane Technology in Coating Applications: Review and Perspectives >." Dow Corning Corporation. , P.O. Box 994, Midland, MI 48640 USA
- Wang, Z., Wu, L., and Wu, Q. J. (2000). "Water-entry value as an alternative indicator of soil water-repellency and wettability." *Journal of Hydrology*, 231–232, 76-83.
- Washburn, E. W. (1921). "The Dynamics of Capillary Flow." *Physical Review*, 17(3), 273-283.
- Washburn, E. W. (1921). "Note on a Method of Determining the Distribution of Pore Sizes in a Porous Material." *Proceedings of the National Academy of Sciences of the United States of America*, 7(4), 115-116.

## CHAPTER 3

### MINERAL AND CHEMICAL CONTROLS ON WATER REPELLENCY OF CFA: A COMPARISON BETWEEN CLASS C AND F COAL FLY ASH

#### 3.1 Abstract

One method to minimize contaminant leaching from coal fly ash (CFA) involves modifying its surface to become water repellent. Five types of CFA; CFA-1, CFA-2, CFA-3, CFA-5 and CFA-6 have been modified using three organo-silane (OS) products at different mix ratios. Multiple breakthrough pressure (BP) experiments were conducted for different samples at different mix ratios to identify the performance of the modified surface to resist a positive water entry pressure (chapter 3). The contribution of oxides and mineral in CFA were analyzed without considering OS effects. Results showed that a semi log-transformed regressions models can effectively establish the relationship between water entry resistance (BP) and the composition of chemicals, minerals, composition of derivatives, and all variables. Out of the four models, BP has been better predicted using two minerals in CFA (gypsum and magnetite) followed by the all variables model (quartz and gypsum). The main oxide composition in CFA ( $\text{SiO}_2$ ,  $\text{Al}_2\text{O}_3$ ,  $\text{CaO}$ , and  $\text{Fe}_2\text{O}_3$ ) are oxides that influence its response to OS modification. In the field of water repellency these oxides, particularly  $\text{SiO}_2$  are significant. However, it was identified that  $\text{SiO}_2$ , besides its abundance and defining reactivity with OS not the best indicator of potential water repellency for a given OS modification, small z-value. Difference in prediction is dictated by other components.

In addition, it has been identified that if the pozzolanic state of the modified CFA is between 61 and 84 percent, a higher water repellent surface is formed, 61 percent being the

highest. Above this threshold, it follows a reduced response. Similarly; the range at which the percent of major minerals and oxides are effective to transform CFA to a water repellent surface has been identified and presented. In general terms, Class C CFA surface cannot be transformed sufficiently to a water repellent character when treated using OS products due to high CaO content. CaO when mixed with water, it rises the concentration of alkali in the solution. Even if this dissociation and formation of high alkali concentration is used to transform CFA to a usable material for other applications, this process may undermine the formation of covalent bonds between OS and CFA. However, results show that if the amount of MgO in Class C CFA exceeds 2 percent, then this behavior is mitigated.

Key words: Oxides, minerals water repellence, coal fly ash, organo-silane

### 3.2 Introduction

Coal fly ash (CFA) is a waste by product evolved from coal power plants. The management and disposal of CFA is one of the areas where much attention has been given due to the concern of its leachate generation. Regulations are accelerating towards its beneficial re-use by transforming CFA in to a usable property. The transformation of CFA using different additives is one of the area of focus for the opportunity to reuse and stabilization as a result leachate generation and volume of CFA sent to landfills is reduced. For instance geopolymers combined with CFA for stabilization (Bankowskiet al., 2004), geopolymers combined with CFA for construction and building materials (Bökeet al., 2015), red mud combined with CFA to promote alkali activated high compressive strength material (Chooet al., 2016), alkali solutions combined with CFA to produce zeolites

(Murayama et al., 2002; Poole et al., 2000; Querol et al., 2002), Bromide combined with CFA to increase mercury adsorption of CFA sorbent (Zhang et al., 2017), alkali (NaOH and  $\text{Ca}(\text{OH})_2$ ) and combined with CFA to extract Alumina (Bai et al., 2010; Li et al., 2014), and acid ( $\text{H}_2\text{SO}_4$ ) combined with CFA to extract Alumina (Bai et al., 2011). A review of compounds used to transform CFA to usable materials is documented elsewhere in (Blissett and Rowson, 2012).

The transformation using different agents of CFA to a usable material for a specific purpose is related to the mineralogical composition of CFA and at the same time its interaction with the transforming agent. The relative abundance of oxides and minerals in CFA determines the type of a reactions which may occur upon mixing with additives. This in turn, influences the desired opportunity for appropriate re-use or disposal. Boycheva et al.,(2013) discussed the chemical composition of CFA dictates its success for use in different applications. Many studies are underway to expand the beneficial reuse of CFA. Motivation for this work derives in part from an interest in reducing the contaminant leaching from coal fly ash (CFA), thereby increasing opportunities for beneficial use as well as minimizing potential groundwater impacts (Feyyisa, 2012) during disposal. One method to reduce aqueous leaching of contaminants from any porous medium into the prevailing pore fluid is to prevent water entry through engineered water repellency. The extent of water repellency may be defined by capillary breakthrough pressure (BP), which represents the pressure required to drive a non-wetting liquid in to porous media (Chapter 2). Daniels et al. (2009), Feyyisa and Daniels (2016), Feyyisa et al. (2017) demonstrated a significant effort and showed the possibility that different types of CFA can be transformed to water repellant material using OS. Notwithstanding these references, the performance

regarding water repellency of different CFA when combined with OS products remains unclear. The prospect of chemical and mineralogical composition with the efficacy of OS modification is of great significance in the areas of leachate containment in CFA.

One of the most reactive components in CFA is CaO. When present in sufficient quantities, the lime can react with water to form pozzolanic reactions, which in turn gives rise to an increase in strength. When CaO is mixed with water two important processes take place; the rise in pH of the solution and the breakdown of covalent bonds. The pH value of the solution rises due to the dissociation property of CaO and  $\text{Ca(OH)}_2$  as a result releases high  $\text{OH}^-$  (Wu et al., 2014). Subsequently, the formation of high  $\text{OH}^-$  ions in the solution according to Wu et al. (2014) and Bankowski et al. (2004) results in the breakdown of bonds, for example, Si-O-Si, Si-O-Al. In another study Poggemann et al., (2003) discussed that CaO as a classical modifier used to break the Si-O bond. Due to this and other unique properties; such as Cementitious character, calcium rich CFA can serve in a variety of structural applications. Park et al., (2016) identified the presence of CaO in larger proportion increases the compressive strength of CFA. In addition, with high CaO content CFA may easily be converted to zeolite, and/or used as an absorbent, or stabilizer. However; the effect of CaO to transfer CFA to water repellent surface using OS is not clear. Hence to identify the types of CFA (Class C and F) and its oxides and mineral compositions that influence the formation of water repellency requires investigation.

The objective of this study are to 1) Correlate water repellency (through CA and BP) with oxides, minerals and the compositions of derivative to identify most significant variable/s. It also investigates the range at which the percentage compositions of variables/group of variables are more effective to form water repellent CFA surface. 2)



Investigates and present the performance against water repellency of the two major types of CFA (Class C and F) when mixed with OS products. The performance of the modified surface are related with oxides and minerals to identify most significant variables and the range of its/their effectiveness.

### 3.3 Methods

#### *3.3.1 Materials and Equipment*

Five types of CFA (Class C and F) were collected from local utilities in the eastern and south-eastern U.S. Three aqueous phase OS chemicals were received from DOW Corning and Zydex Industries. Two laboratory pressure cells were modified; the inner wall was fixed permanently with circular hollowed rigid holder. The holder serves: 1) to hold the porous stone, and 2) prevents leakage between the cell wall and porous stone. A pressure flow controller by Geo Comp FlowTrac II Figure 1. connected to the pressure cell (the sample holder) and a computer via a transducer to supply DI water (resistance > 16 MOhm-cm) under pressure. Porous Stones (P/N HM-4184.70) 70mm and filter paper 100 mm diameter were used. A transducer from Omega Engineering, Inc. (PX409-030GUSBH) was connected between the source and cell to the computer.

#### *3.3.2 Procedures*

The mixing procedure and ratio of OS: CFA (by weight) used in Feyyisa et al. (2017) to form a dry modified CFA surface were used for this study. After the sample was oven dried between 60<sup>0</sup> and 158 <sup>0</sup>F for 24 – 72 hours (Feyyisa et al., 2017; Z. Wang et al., 2000) it was crushed using a mortar and pestle to pass through a No. 200 sieve. Before

pouring and packing the sample in to a cell, a plastic pipe spacer 7.6 cm in diameter was cut to 10 cm height (to direct and allow a stable motion and even spread of DI water just below the sample) and was placed vertically into a cell. A porous stone was covered with filter paper using tape and mounted on the rigid holder that was permanently fixed to the interior wall of the cell. The porous stone-filter paper unit perimeter was wrapped with thread sealant tape to facilitate further leakage control between the unit and cell. The sample was then poured in to the cell and gently packed using laboratory spatula. Once the sample was filled to the 7 cm depth, porous stone was moved in between the sample and top cover of a pressure cell to facilitate equal pressure distribution to the sample while tightening the cell. Full tightening of the cell, however, was carried out during and after air entrapped between grain particles of the modified CFA sample had been removed. This removal procedure was administered during the initial stage of pressure application. Prior to connecting the cell to the pressure source, the bottom space of the cell was filled with water up to the surface of porous stone. The bottom part of the cell unit was then connected to a DI water tap and the space between the inlet of the cell and the porous stone was carefully and slowly filled to remove the entrapped air through the top cover. Care was taken not to remove the fine particles of the sample with the air.

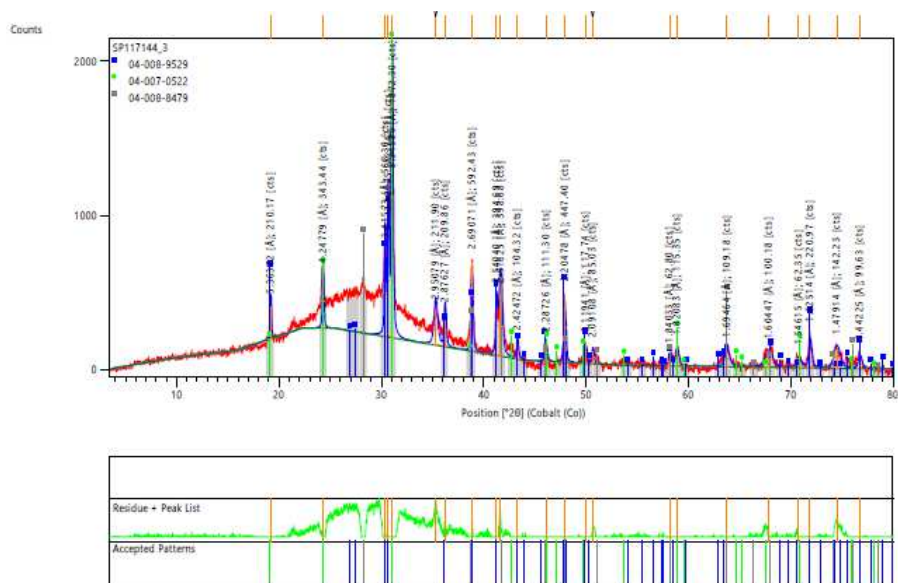
The cell was then connected to the source and transducer using a tube. Before that the source pumped (from external storage) and emptied multiple times until visible bubbles of air in the tube disappeared from the inlet tube. Likewise, the front discharging tube was also cleared of air by applying pressure and waiting until multiple drops released to open air and no visible bubbles of air are found in the tube before connecting to the cell. The source was then turned on and a pressurized flow begun discharging to the cell. Water level

and pressure records rose steadily until water reached the sample just above the porous stone. Pressure was increased at a rate of 3.4 kPa/second; 35 cm H<sub>2</sub>O/second and readings were taken every second. This value was adapted as a compromise between the desire to reach BP point in a manageable time for higher resistant samples and to attain a clear breakthrough point for less resistance samples. Once the rising water saturated the porous stone and faced off the modified CFA, resistance developed and a sudden rise in slope of pressure-time graph was observed. The point at which a breakthrough pressure happens and imbibition begins is calculated from the slope of pressure time curve, the maximum point of inflection of the curve.

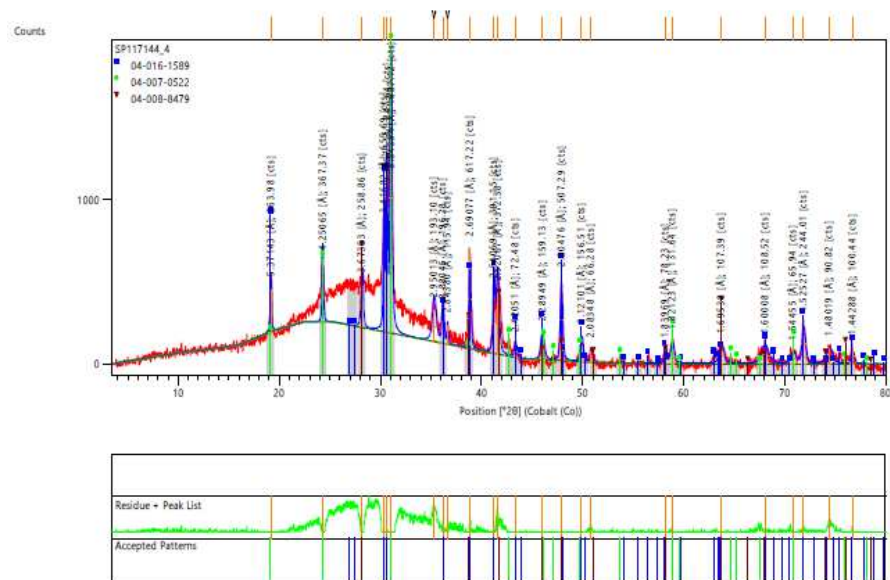
### 3.4 Results and discussion

#### *3.4.1 Minerals, oxides, and their derivative compositions*

The American Society for Testing and Materials (ASTM) specification No.C618-84 grouped CFA in to two main classes based on its chemical compositions, Class C and F CFA. Accordingly, if CFA has a total sum of Al<sub>2</sub>O<sub>3</sub>, Fe<sub>2</sub>O<sub>3</sub>, and SiO<sub>2</sub> (sum3) greater than 50 % but less than 70 % defined as Class C; if sum3 is greater 70 % Class F. Summary of XRF and XRD (American ASSAY laboratories) and for comparison the percentage by weight of summary of previous work are shown in Figure 3.1. As shown in the Figure chemical composition of data used in current analysis Figure 3.2 (a and b) fall in the average value of the previous works Figure 3.2(c). In addition to grouping in to types, amorphous phase alkalinity and non-crystalline percent has been calculated. Accordingly; summary sum3 along with amorphous phase alkalinity of five CFAs are summarized in Table 3.1.

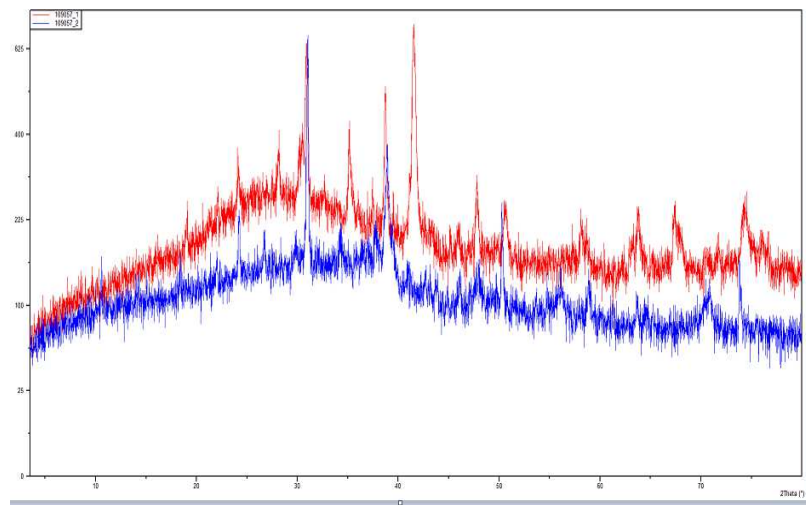


a)

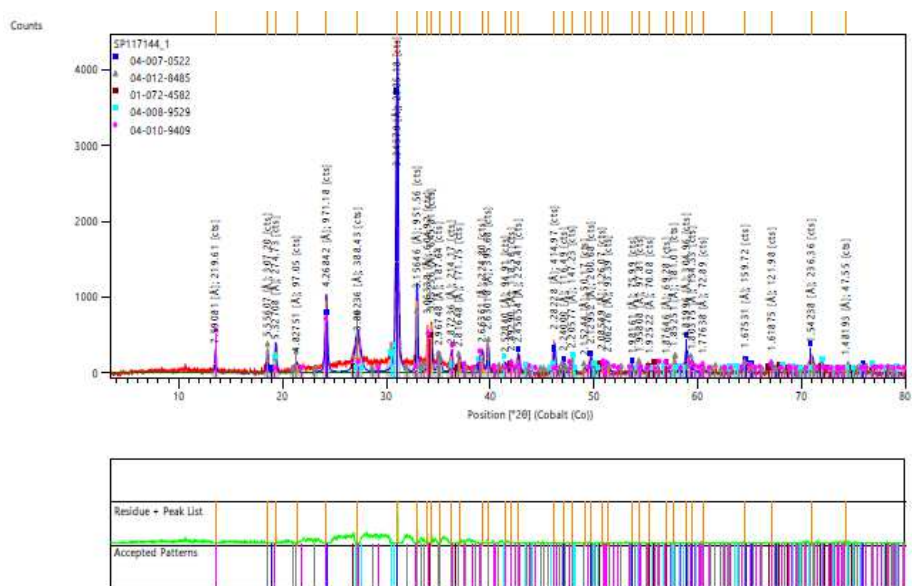


b)

Figure.3.1 XRD and XRF analysis for; a) CFA-1, b) CFA-3, c) CFA2 and CFA 5, and d) CFA-6



c)



d)

Figure.3.1 continued

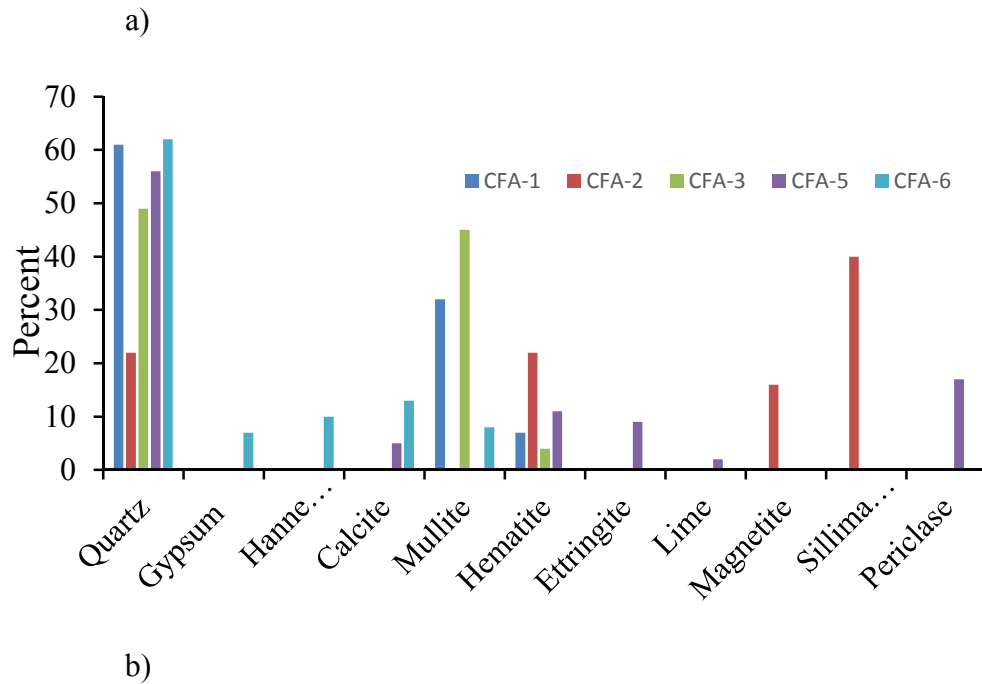
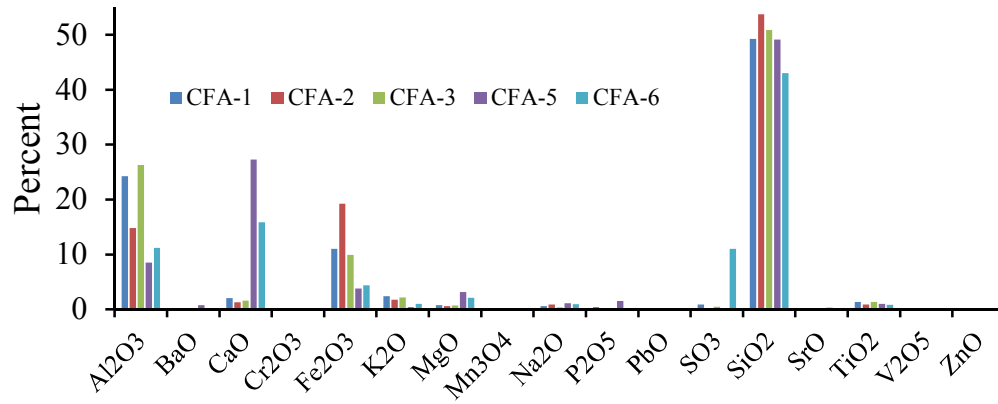
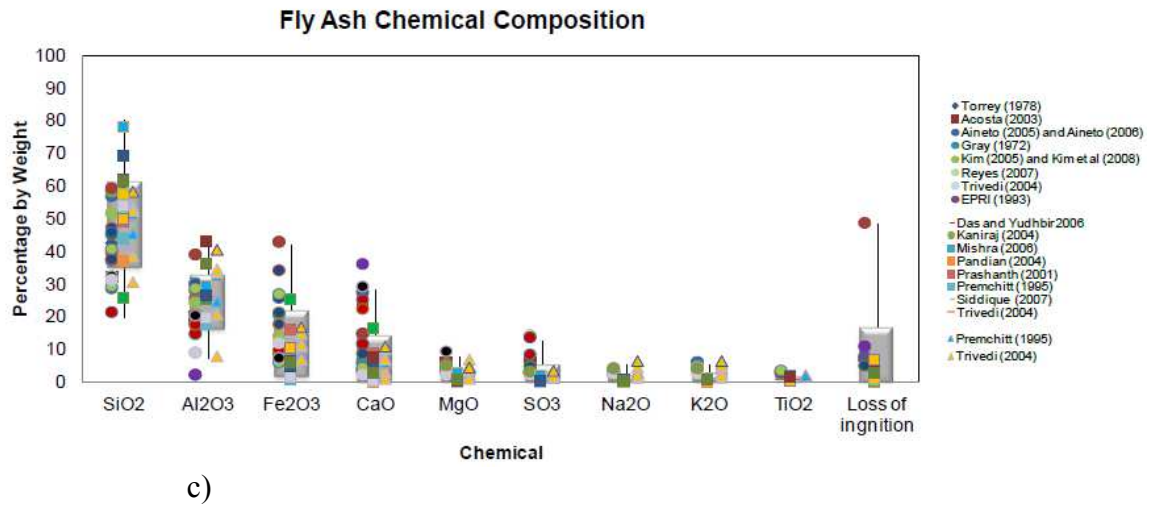


Figure 3.2 Percentage composition of a) chemical and b) mineral composition for five CFA (total compositions account more than 90 and 98 percent, respectively).



Adopted from EPRI (Technical Report, 2012), Geotechnical Properties of Fly Ash and Potential for Static Liquefaction Volume 1 – Summary and Conclusions

Figure 3.2 continued

As per the ASTM standard of classification; CFA 1, CFA 2, and CFA-3 are typed as F, whereas CFA-5 and CFA-6 are grouped in Class C.

Table 3. 1. Summary of derivative composition of oxides for five types of CFA

Variables	CFA-1	CFA-2	CFA-3	CFA-5	CFA-6
Sum3*	84.48	87.81	87.11	61.45	58.62
Alkalinity**	0.5494	0.3102	0.5617	0.7924	0.6760

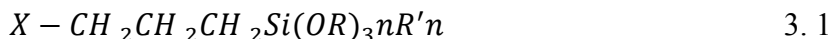
\*sum (SiO<sub>2</sub>, Al<sub>2</sub>O<sub>3</sub>, and Fe<sub>2</sub>O<sub>3</sub>)

\*\* (Al<sub>2</sub>O<sub>3</sub>+CaO+MgO)/SiO<sub>2</sub>

### 3.4.2. Organo-silane chemistry

A silane that contains at least one silicon carbon bond is known as OS (Dow coming). Organo-functional silanes are molecules carrying two different reactive groups

on their silicon atom Figure 3.3 as a result they can react and couple with very different materials (e.g., inorganic surfaces and organic resins via covalent (Dow corning). Organo-functional silanes have the following typical molecular structure:



where  $n = 0, 1, 2$

As shown in the equation OS contain two different types of reactive groups namely; the hydrolysable group (OR) and the organo functional group (X). The hydrolysable group Si-OR hydrolyzes readily with water forming silanol (Si-OH) and condense with metal hydroxyl groups and forms a very stable siloxane via covalent a bond, Si-O-M; where (M = Si, Al, Fe, etc.)Figure 3.3. This allows surface treatment, coupling and assembling of very dissimilar surfaces chemically ((Dow corning).

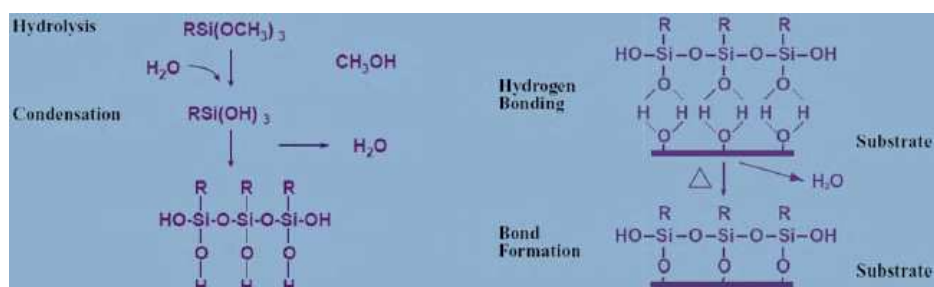


Figure 3.3 Organo-functional silane bond formation with substrate through hydrolysis (F.de Buyl, Dow Corning)

### 3.4.3. OS and CFA (substrate)

As discussed in the above section, OS hydrolyzed in water and form a permanent bond with substrates. In our case CFA becomes a substrate and when mixed with OS using



DI water. The hydrolysable group of OS dissociates and form a covalent bond with metals in the substrate (CFA). The preference to form a covalent bond of metals in CFA depends solely on the reactivity of the constituents. For example, the reactivity of substrate materials and silane effectiveness can be arranged from poor to excellent as; gypsum ( $\text{CaSO}_4$ ) – inorganic oxides (e.g.  $\text{Fe}_2\text{O}_3$ ) – alumino-silicate – Quartz – Silica. Details regarding the reactivity of metallic elements and minerals can be found elsewhere in (Arkles et al., 2014). As such, the presence of high quartz, silica and alumino-silicate in CFA is indicative of high potential for surface transformation via OS treatment. On the other hand, a large amount of gypsum in CFA reflects reduced opportunity to form a water repellent surface. Similarly, the performance of different OS is characterized by the percentage of its active ingredient, linker length, and the type of alkane chains. For example; while OS C-1 has an active ingredient of more than 52 percent, OS C-2 has only 40 percent of its total emulsion.

#### *3.4.4 Variables selection for modeling*

To relate BP (Figure 3.4) with the constituents of CFA only, OS was not included in the list of variables. Instead additional variables called derivatives were added as one group of variables. These derivatives, as the name implies, derived from constituents of CFA such that the percentage of their combinations and ratios can affect the behavior and reactivity of CFA when mixed with other materials. For example, the total sum of ( $\text{SiO}_2$ ,  $\text{Al}_2\text{O}_3$ , and  $\text{Fe}_2\text{O}_3$ ), Alkalinity (Moon et al., 2016) in CFA were considered as additional variables to investigate their effects for different applications. Similarly, these two derivative constituents together were used in this study as one group of variables to correlate with BP.

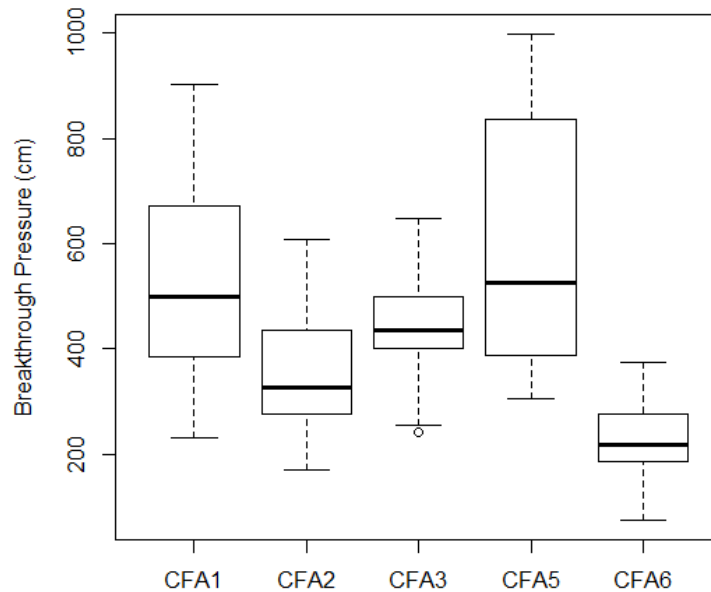


Figure 3.4 Average breakthrough pressure measurements for different CFA using three OS products (chapter 3)

### 3.4.5 Variable selection and modeling

The effect (positive or negative) of individual chemical (oxides) and mineral constituent in CFA to form a water repellent surface when mixed with OS were evaluated. This evaluation is based on their relative abundance as determined using XRD and XRF analysis Figure 3.1. Four groups of variables (predictors) were selected. The first and second group (models 1 and 2) are based on the mineral and chemical composition Figure 3.1(b) and Figure 3.1(a), respectively. The third group considers the effect of derivative composition from XRD and XRF analysis; such that amorphous phase alkalinity and pozzolanic state in CFA (model 3). According to Moon et al. (2016) high alkalinity causes high solubility as a result favors more reaction to take place. The total pozzolanic state, (the total sum of  $\text{Al}_2\text{O}_3$ ,  $\text{SiO}_2$ ,  $\text{Fe}_2\text{O}_3$  (sum3)) are oxides which form a primary bond with

OS to form a water repellent surface. The fourth group considers all the above groups together as an independent variable (model 4). This grouping approach helps to precisely identify the effect of individual variables (model 1, model 2, and model 4) and their combined effect (model 3 and model 4) to affect the water repellent parameters. In the evaluation, however, OS and its mix ratio were deliberately removed from being considered as one of the independent variables. These models help to facilitate and limit comparison among the chemicals/oxides, minerals, and their derivative. In other words, the analysis was based on identifying the sensitivity of BP with a unit change (standardized deviation) to the composition of individual chemical, mineral, and derivatives in CFA. The analysis does not show the state and affinity to form a covalent bond between the trace elements/chemicals in CFA and OS. It rather shows the sensitivity of water repellency to a unit change in the content of variables. Both pozzolanic and alkalinity are linearly related with BP due to their solubility (Moon, 2016) as a result it facilitates the formation of bond with OS, Figure 3.5.

In general, when evaluating the performance of CFA with their oxides content to form a water repellent surface using OS, the presence in higher proportion of  $\text{Al}_2\text{O}_3$ ,  $\text{Fe}_2\text{O}_3$ , and  $\text{SiO}_2$  and low proportion of  $\text{CaO}$  and  $\text{MgO}$  in Class F CFA favor the formation of larger BP. But for Class C CFA a mixed response has been observed; CFA-5 showed a linear relationship but CFA-6 related with BP inversely. Further CFA with a higher  $\text{CaO}$  proportion able to form the highest BP when treated with OS. But being second in  $\text{CaO}$  percent content, CFA-6 has the least to form water entry resistant surface. BP related linearly with alkalinity across all CFA.

Different exploratory data analysis approaches a linear regressions approach, ordinary linear regression, generalized least square regression were applied to correlate BP with the groups of variables. In addition to the four main groups, group 1 was extended further to identify most significant variables to model BP based on the two main types of CFA, Class C and Class F. Accordingly; a best fitting model for four groups of variable and additional two (for types of CFA) are shown in Figure 3.6. Summary of groups with their corresponding model and variables are shown in Table 3. 2.

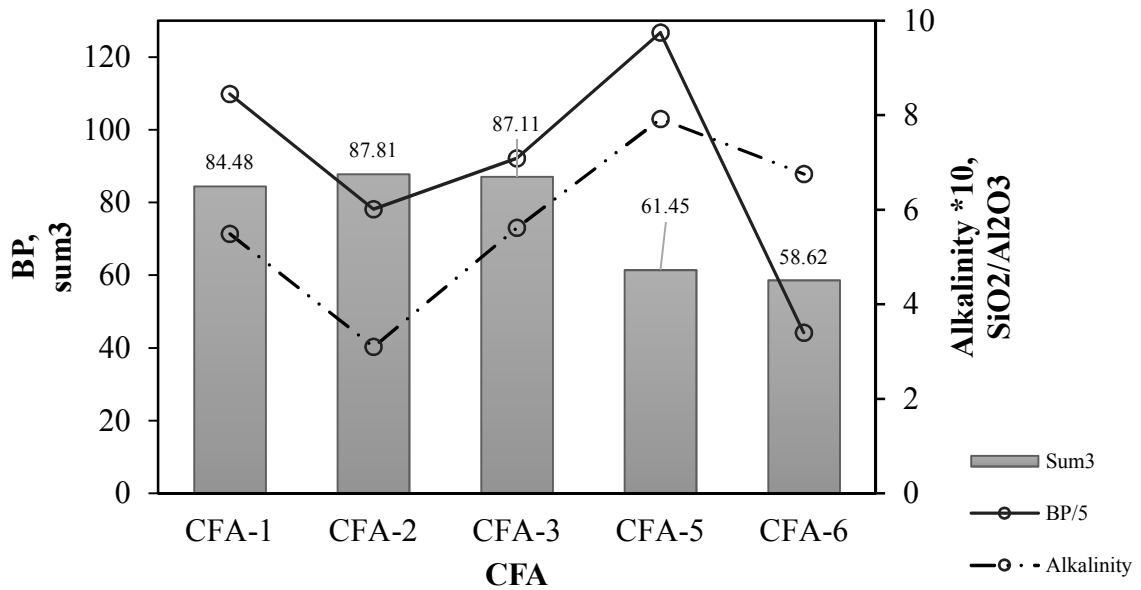
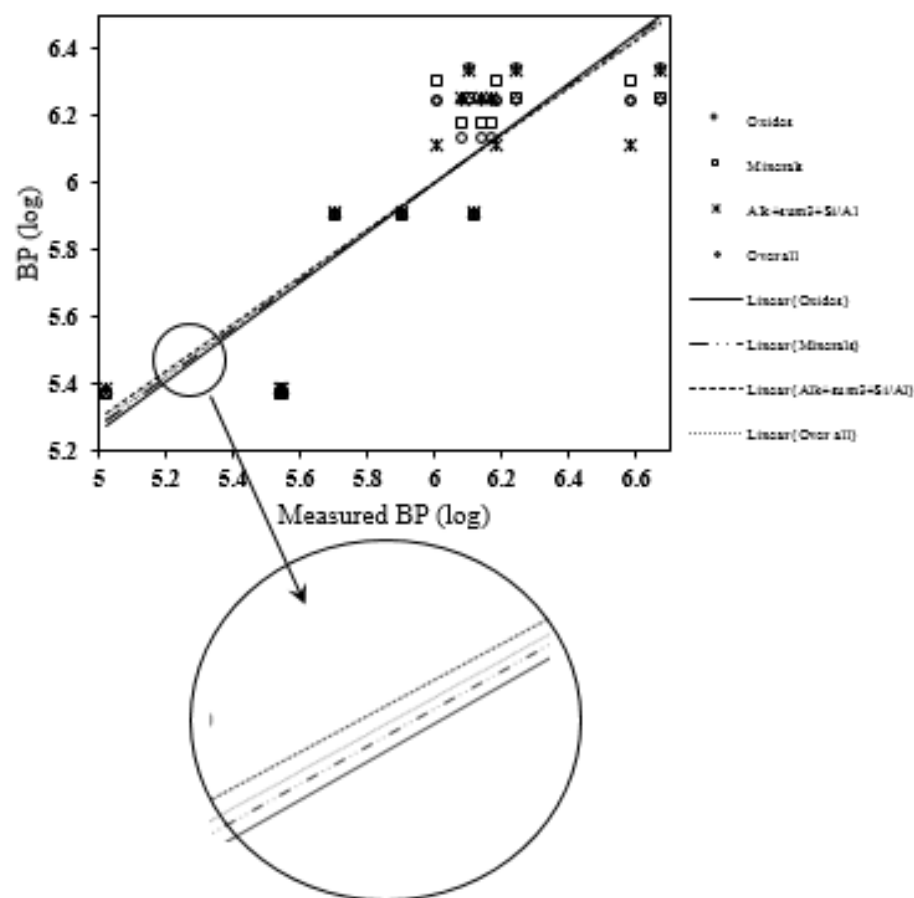


Figure 3. 5. The relationship between derivative compositions and BP.

Results show that 4 chemicals ( $\text{Al}_2\text{O}_3$ ,  $\text{CaO}$ ,  $\text{Fe}_2\text{O}_3$ , and  $\text{K}_2\text{O}$ ) of group one variables are identified as most significant oxides to affect BP. Whereas, only 2 minerals (quartz and gypsum) were selected as best predictors from group 1. The significance level of the hybrid composition showed that both the two together, instead of individual have significant effect

on the model. Model 4 (group four variables) includes all variables in groups 1, 2, and 3 together, 27 variables. Results show that using only two variables, Gypsum and Magnetite, (out of the twenty-seven variables) BP can be best estimated, R-squared about 0.72. In general, all the four main models and additional two for the type of CFA able to predict BP (R-squared between 0.7 and 0.8), except for Class F CFA, R-squared = 0.4149 Figure 3.6(c). This accuracy is considered good, because BP is a factor of both these variables, OS type, and dosage applied. As discussed above OS effect is not included in the analysis but its significance to affect BP prediction is unequivocal. For example; the performance to predict BP separately for Class F CFA is poor due to the comparative composition of variables. Out of all variables, only  $K_2O$  emerges as significant variable while using exploratory data analysis, even if its prediction accuracy is still low. This results from the comparative composition of variables in Class F CFA, all Class F possess nearly equal and similar composition of oxides, particularly CFA-1 and CFA-3. However; when OS is included in the variables, the model predicts satisfactorily along with  $K_2O$ , R-squared = 0.7469 (an improvement of more than 0.3.) Hence, to accept the performance of models without considering OS in the list of variables is rational. On the other hand, the two Class C CFA are composed of oxides that vary significantly Figure 3. 1. As a result, the prediction of BP using either  $CaO$ ,  $Al_2O_3$ ,  $Fe_2O_3$ ,  $Mn_3O_4$ ,  $SO_3$ ,  $MgO$  and  $K_2O$  without OS showed better fit, R-squared approximated to 0.8 but higher p-value.



a)

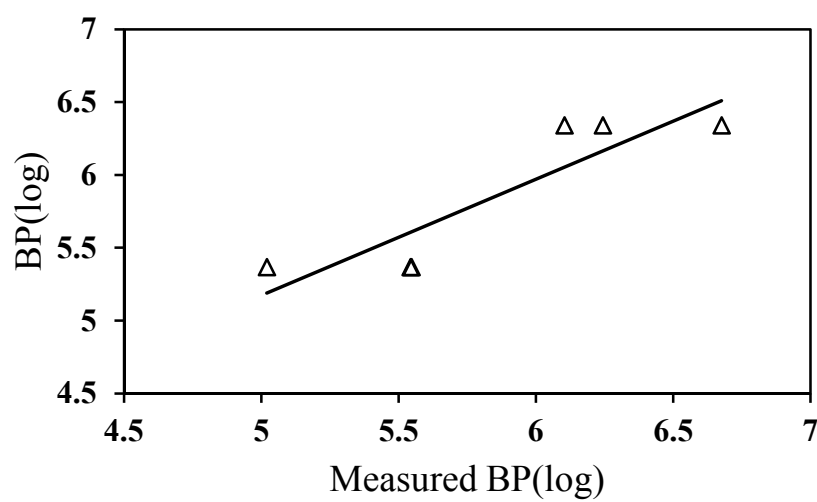
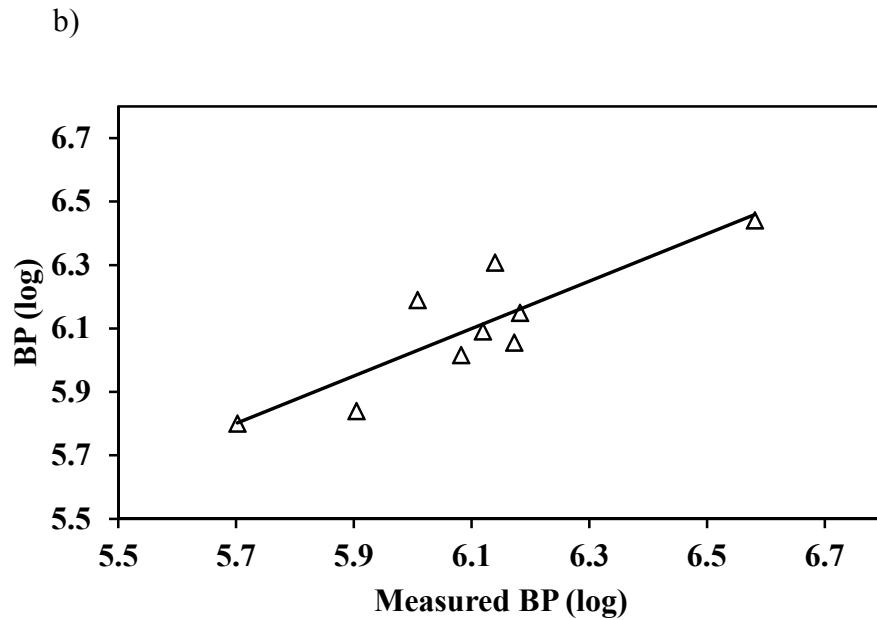


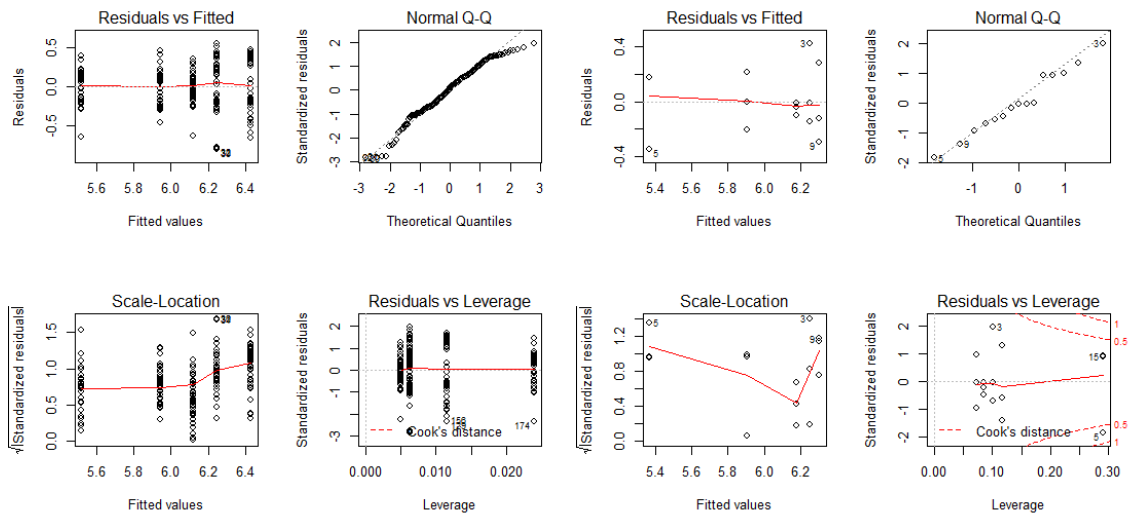
Figure 3.6. A log transformed measured and fitted BP; a) four groups, b) Class C CFA, and c) Class F CFA



c)

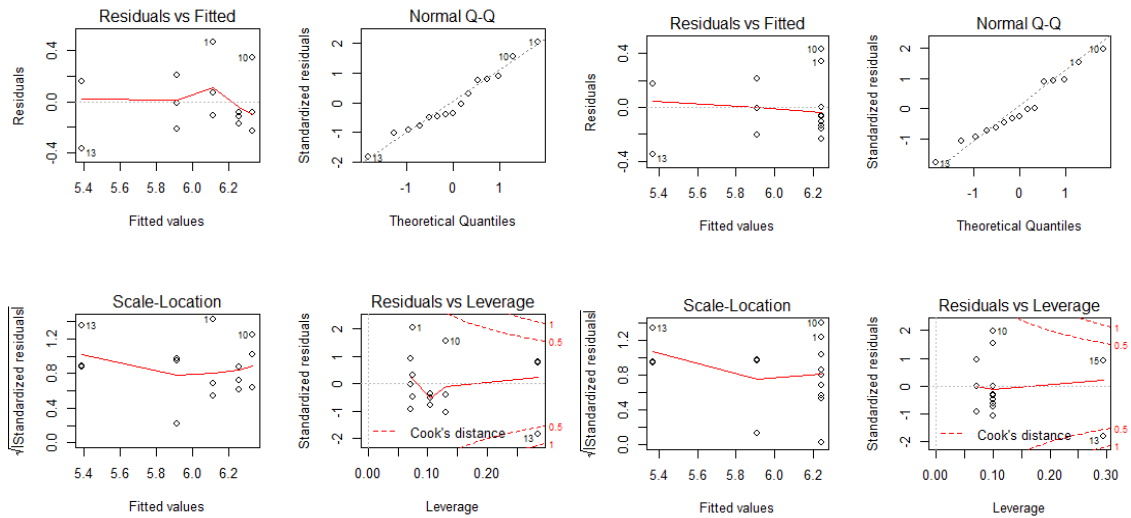
Figure 3.6. continued

A diagnostics plot for the models is shown in Figure 3. 7 and Figure 3. 8. As shown in Figure 3. 7, the distribution of residuals has no pattern except for model 3, which shows towards higher values of BP. The quartile plot also shows a better fit to the line except for model 2. The effect of outliers on the model shows that; for model 2 there is no data that influence the model but one or two data become beyond cook's distance for the rest of the models. Regarding the plot for the type of CFA, Figure 3. 8 Class C is considered a good fit but for Class F residual plot follows certain pattern at different levels of BP.



a)

b)



c)

d)

Figure 3. 7. Model diagnostic plot for; a) model 2, b) model 1, c) model 3, and d) model 4



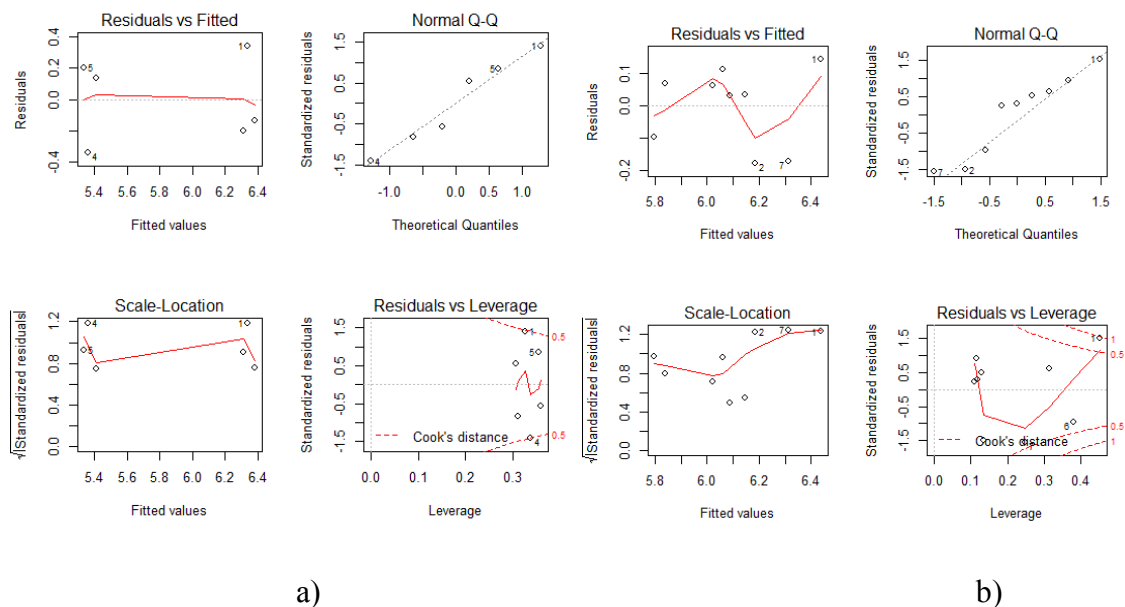


Figure 3. 8 Model diagnostic plot for the two types of CFA; a) Class C b) Class F

### 3.4.6 Model Verification and validation

Best fitting models were selected for four groups and additional two for the main types of ash, C and F. As shown in the model major oxides and minerals in CFA are not significant in the models Table 3.2. Rather other rare oxides and minerals seem more significant. For example; Silicon oxides are known to form a water repellent surface when mixed with OS products.

Table 3. 2 Summary of models' performance and their corresponding significant predictors to estimate BP

No	Parameter to model	Model		Predictors		No of variables	P-value
		Linear model (log transformed), R2	Generalized Linear model AIC	Oxides and minerals	Model equation		
1	Model 2	0.744	6.1661	Al2O3+ CaO+ Al2O3+K2O	log(BP) = Al2O3 + CaO + Fe2O3 + K2O	15	0.005186
2	Model 2 (Class C)	0.7967	6.1661	CaO	log(BP)= 4.023 + 0.08499*CaO	15	0.2849
		0.7967	6.1661	Al2O3	log(BP) = 12.49 - 1.619*Fe2O3	15	
		0.7967	6.1661	Fe2O3	log(BP) = 9.433 - 0.364*Al2O3	15	
		0.7967	6.1661	Mn3O4	log(BP) = 6.584 - 24.285*Mn3O4	15	
		0.7967	6.1661	SO3	log(BP) = 6.341 - 0.088*SO3	15	
		0.7967	6.1661	MgO	log(BP) = 3.516 + 0.891*MgO	15	
		0.7967	6.1661	K2O	log(BP) = 7.049-1.646*K2O	15	
3	Model 2 (Class F)	0.4149		Only K2O/SO3	log(BP) = 4.933+ 0.555*K2O	15	0.06115
	Model 2 (Class F - OS)	0.7469		with K2O/SO3 +OS	log(BP)= 5.114+ 0.555*K2O -0.252*C2 -0.291*C4	15	0.0594
4	Model 1	0.7287	3.7638	Quartz + Gypsum	log(BP) = 5.681+ 0.01*Quartz -0.135*Gypsum	10	0.000399
5	Model 3	0.6998	7.766	Alkalinity+sum3	log(BP) = -13.950+ 4.063*sum3 +0.213*Si/Al	3	0.003253
6	Model 4 (1+4+5)	0.7167	4.4141	Gypsum + Magnetite	log(BP) = 2.921*Alk = 6.24311 - 0.125*Gypsum - 0.021*Magnetite	28	0.000517

However, due to its comparable presence in all CFAs (varies only between 43 and 53 percent) it did not explain observed differences in BP. This phenomenon has been verified through data normalization. A normalized data provides two important variables, the center and z-score, to compare the relative significance among variables. Centering

finds the mean of the variable; whereas the z-score as shown in Equation 3.2 shows the values of a normalized variable with mean zero and a standard deviation of one. As a result, all the variables were compared on similar base.

$$Z_i = \frac{x - \mu}{\sigma} \quad 3.2$$

As shown in Table 3.2 the most significant variables for model 1 are; CaO, Al<sub>2</sub>O<sub>3</sub>, Fe<sub>2</sub>O<sub>3</sub>, K<sub>2</sub>O, R-Squared greater than 0.7. As depicted in Figure 3. 9 the three oxides have the highest z-score values compared to the remaining ones. As depicted in the Figure SiO<sub>2</sub> is the highest (mean) oxides in CFA. In addition, this oxide is known in the field of water repellency as the main transforming agent. However; due to its lower z-value (compared to other four oxides Figure 3. 9) is not significant enough to model BP. Hence it is identified that SiO<sub>2</sub>, notwithstanding its abundance and leading role to transform surfaces to a water repellent one, it does not support to predict the magnitude of water repellency of an OS modified CFA surface.

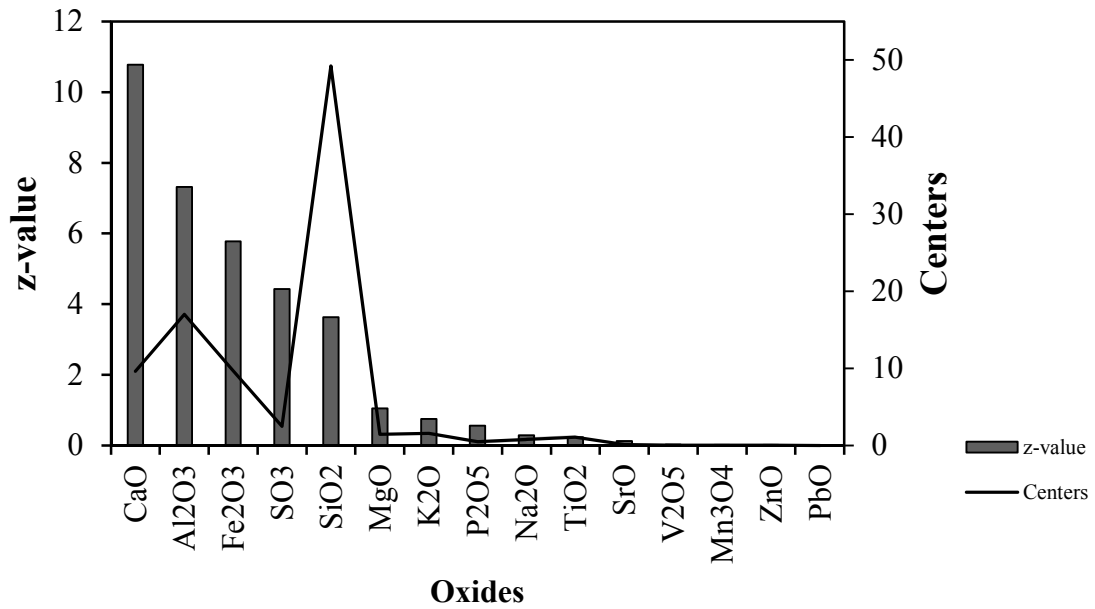


Figure 3. 9. A normalized data showing mean and the corresponding z-score for oxides in CFA.

The predictive performance of the models was assess using the k-fold cross validation approach. The k-fold cross validation algorithm is used to assesses the predictive performance of the model beyond the available data and uncertainties. A k-mean cross validation divides available data in to k equal values. It predicts data in such a way that, the first group of data k<sub>1</sub> is withheld while the others (k-1) are used to predict. The cycle continues and finally all the predicted k<sub>s</sub> are calculated. The predicted values then compared with the model results for fitness Figure 3.10 and Figure 3.11.

Accordingly; the total number of available data for each model were divided randomly in to three to five groups of equal sizes (k-fold). For each test one group is withheld for validation when k-1 group were used for training.

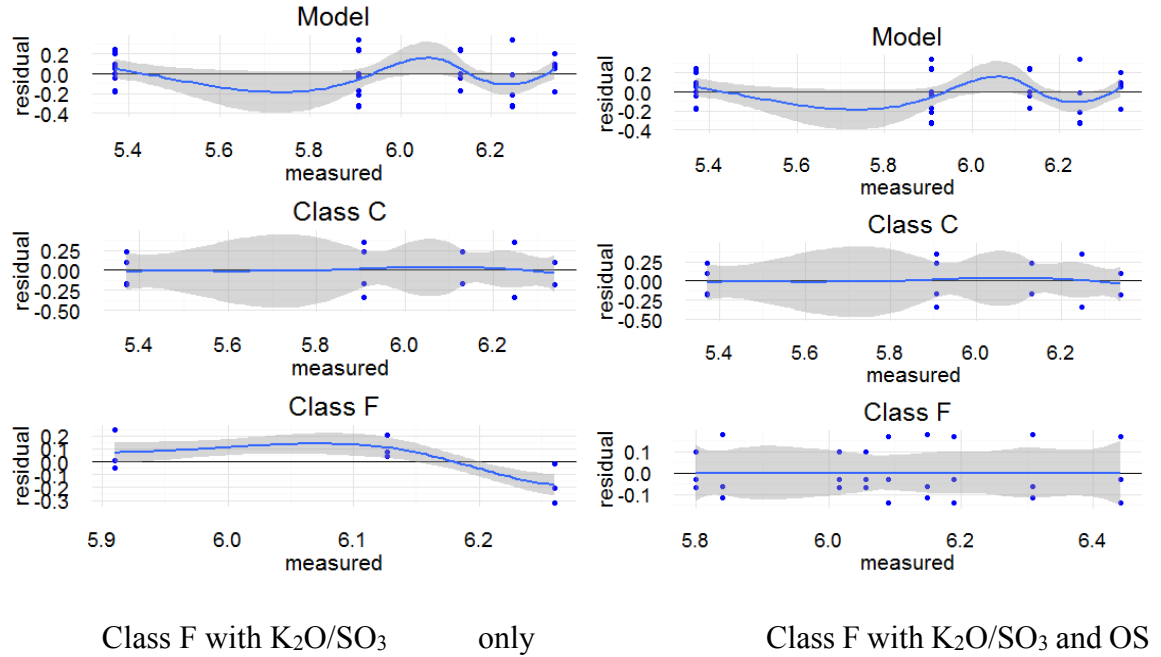


Figure 3. 10. Cross validation residuals distribution for model 2 along with the two types of CFA, Class C and F

For model 2 first all the CFAs were modeled despite their types. Second CFAs were divided and modeled according to their types, Class C and Class F Figure 3.6. As depicted in the Figure Table 3.2,  $K_2O$  or  $SO_3$  are considered as a significant variable. However; due to the poor distribution of residuals OS is used alongside with oxide and improves fitness. This shows that the prediction capacity of significant variables in Class F CFA is poor ( $R$ -squared = 0.4149 Table 3.2). As a result, OS (variable) should complement oxide to improve the prediction performance ( $R$ -squared = 0.7469).

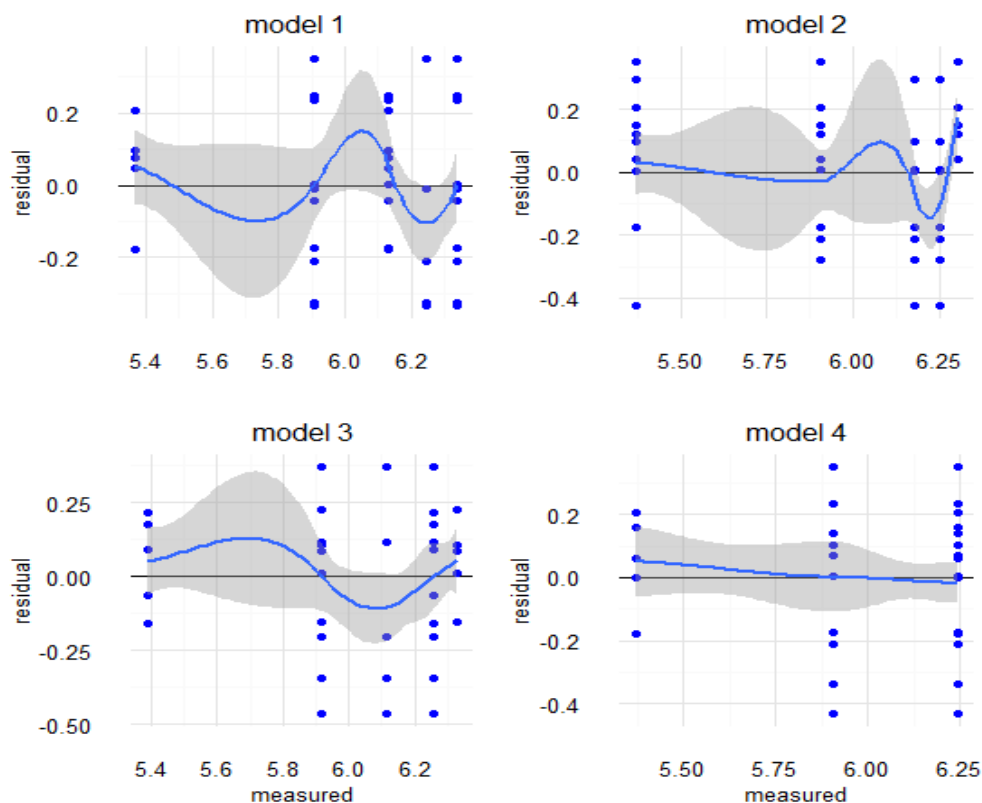
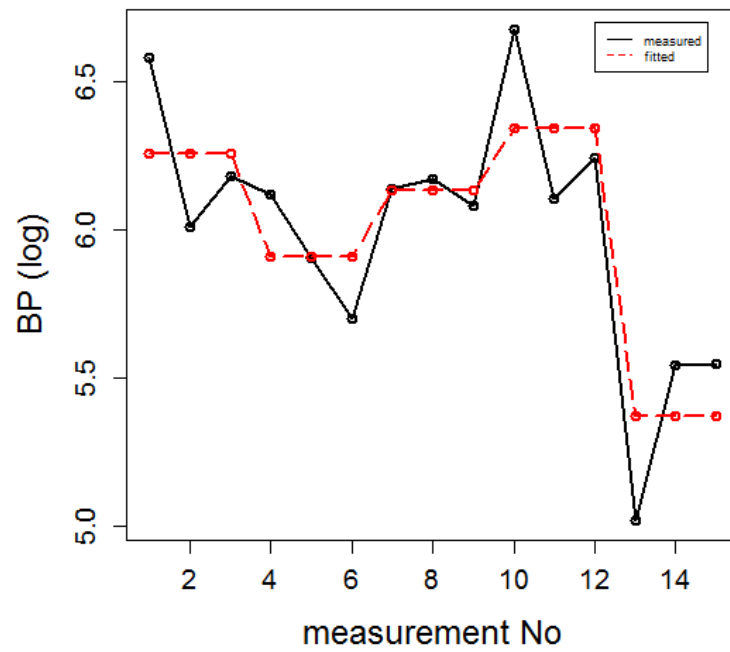
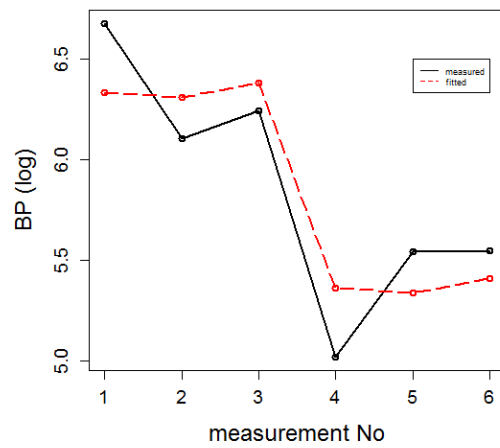


Figure 3. 11. Cross validation residuals distribution for all major models

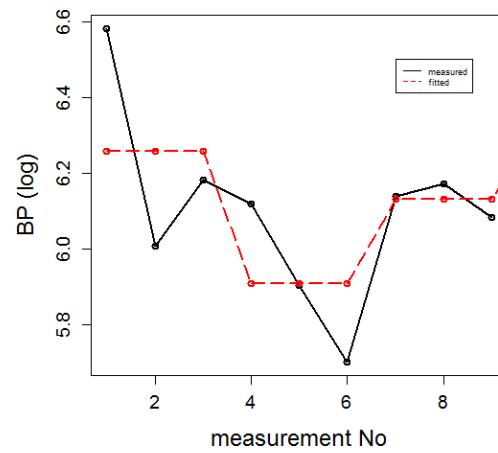
Figure 3.12 and Figure 3.13 depicted comparison plots of measured and fitted value of log (BP). Out of the four models, model 1 achieves a better fit and approximates the range of measured values. Prediction accuracy of the model and k-fold cross validation is shown in Figure 3.6, Figure 3.10, and Figure 3.11. As shown in the Figure all models achieve a reasonable fit. However; the relative quality of models prediction was evaluated based on their AIC value Figure 3.15. Accordingly; model 1 (mineral composition) has the lowest AIC value followed by model 4 (combination of all) and model 2 (oxides composition), in their order. Hence, it has been found that using two minerals, quartz and gypsum of model 1 or gypsum and magnetite of model 4, the magnitude of water entry resistance of CFA when treated using OS product can be predicted.



a)



b)



c)

Figure 3. 12. Plot of measured and predicted values for model 2; a) all types CFA, b) type F CFA, and c) Class C CFA.

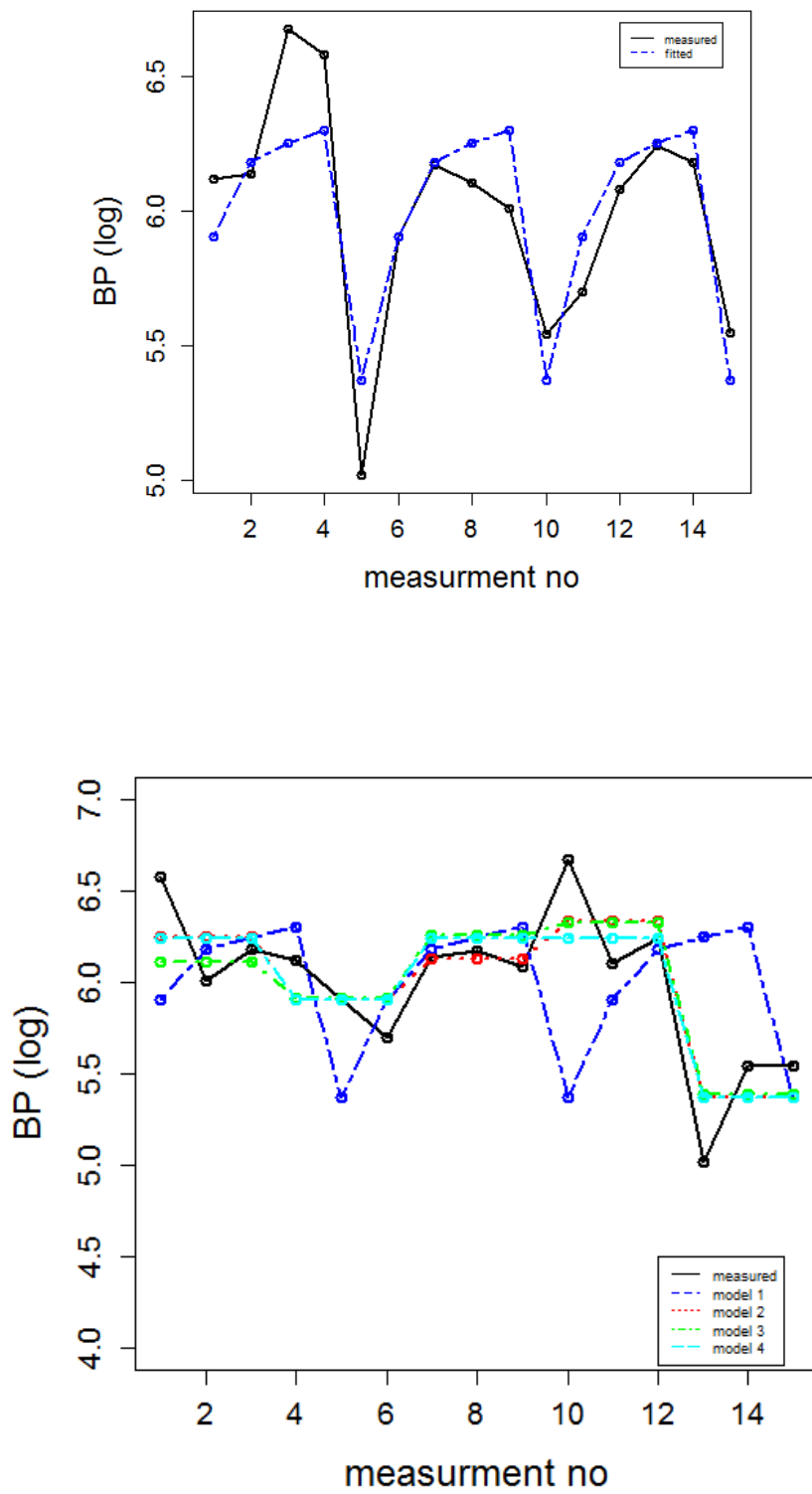


Figure 3. 13. Plot of measured and predicted values for all models



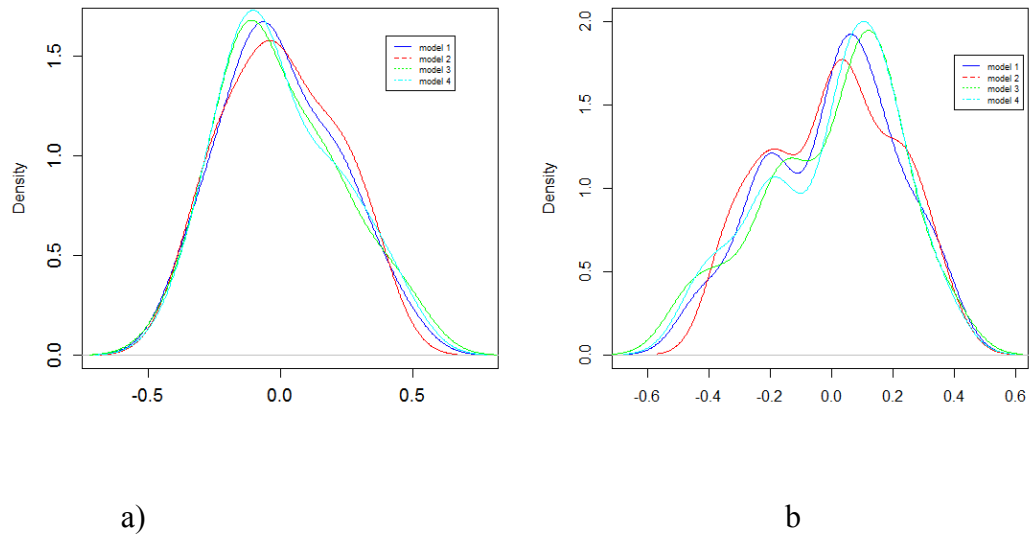


Figure 3. 14. Residual density plot for four models; a) predicted model and b) k-fold cross validated (fitted)

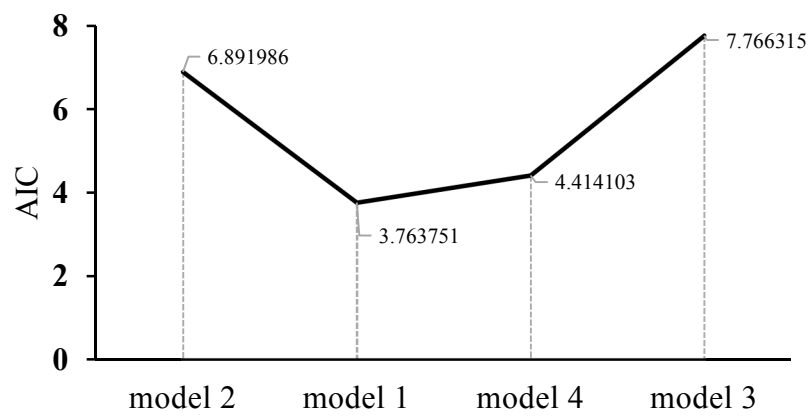


Figure 3. 15. Comparison of model's quality using AIC values

### *3.4.7 Discussion and conclusion*

The correlation between combined oxides, minerals, and their derivative in OS treated CFA and water repellency has been conducted. In order to evaluate the effect of one oxide on the other to form a high water repellent surface a co-plot regression was used. As depicted in Figure 3. 16 there is a strong relationship between water repellency and percentage of  $\text{SiO}_2$  in CFA for the three OS products. When compared, the relationship is stronger with OS C-1. However; for  $\text{Al}_2\text{O}_3$  and  $\text{Fe}_2\text{O}_3$  the relationship between water repellency and the oxides follows a reduced pattern. This suggests that to transform the surface of CFA to sufficiently high water repellent surface the percentage of  $\text{Al}_2\text{O}_3$  and  $\text{Fe}_2\text{O}_3$  should be as small as possible, all the three panels BP follows a decline patter beyond a certain range. For example, as shown in the Figure the total percent of  $\text{SiO}_2$ ,  $\text{Al}_2\text{O}_3$ , and  $\text{Fe}_2\text{O}_3$  in CFA should not be more than about 49, 10, and 5 percent to form a sufficiently water repellent surface, respectively. Further; percentage combination of these oxides is also evaluated conditioned by each other. For example; the relationship between water repellency and  $\text{SiO}_2$  was evaluated for a given rang of  $\text{Al}_2\text{O}_3$  and  $\text{Fe}_2\text{O}_3$  in CFA. As depicted in Figure 3. 17 there is a strong relationship between water repellency and  $\text{SiO}_2$  for a lower range of  $\text{Al}_2\text{O}_3$  and  $\text{Fe}_2\text{O}_3$ . At higher level of  $\text{Al}_2\text{O}_3$  and  $\text{Fe}_2\text{O}_3$  water repellency of the modified surface follows a decreasing pattern. For both water repellency parameters, the highest percentage at which  $\text{SiO}_2$  correlated strongly with water repellency is 49. The range at which  $\text{Al}_2\text{O}_3$  and  $\text{Fe}_2\text{O}_3$  should be limited to obtain s strong correlation between water repellent surface and  $\text{SiO}_2$  is shown in Figure 3. 17. Separately, the effect of  $\text{SiO}_2$  on the correlation between CA and BP was evaluated. Figure 3.19 depicted the correlation between both water repellency parameters conditioned by  $\text{SiO}_2$ . Additionally, when  $\text{SiO}_2$

exceeds the above threshold the relationship between CA and BP is affected. Similarly, even if not clear as  $\text{SiO}_2$ , the correlation between CA and BP when conditioned by  $\text{Al}_2\text{O}_3$  and  $\text{Fe}_2\text{O}_3$  shows changes when their percentage composition increases, even if not very consistent Figure 3.20 and Figure 3.21.

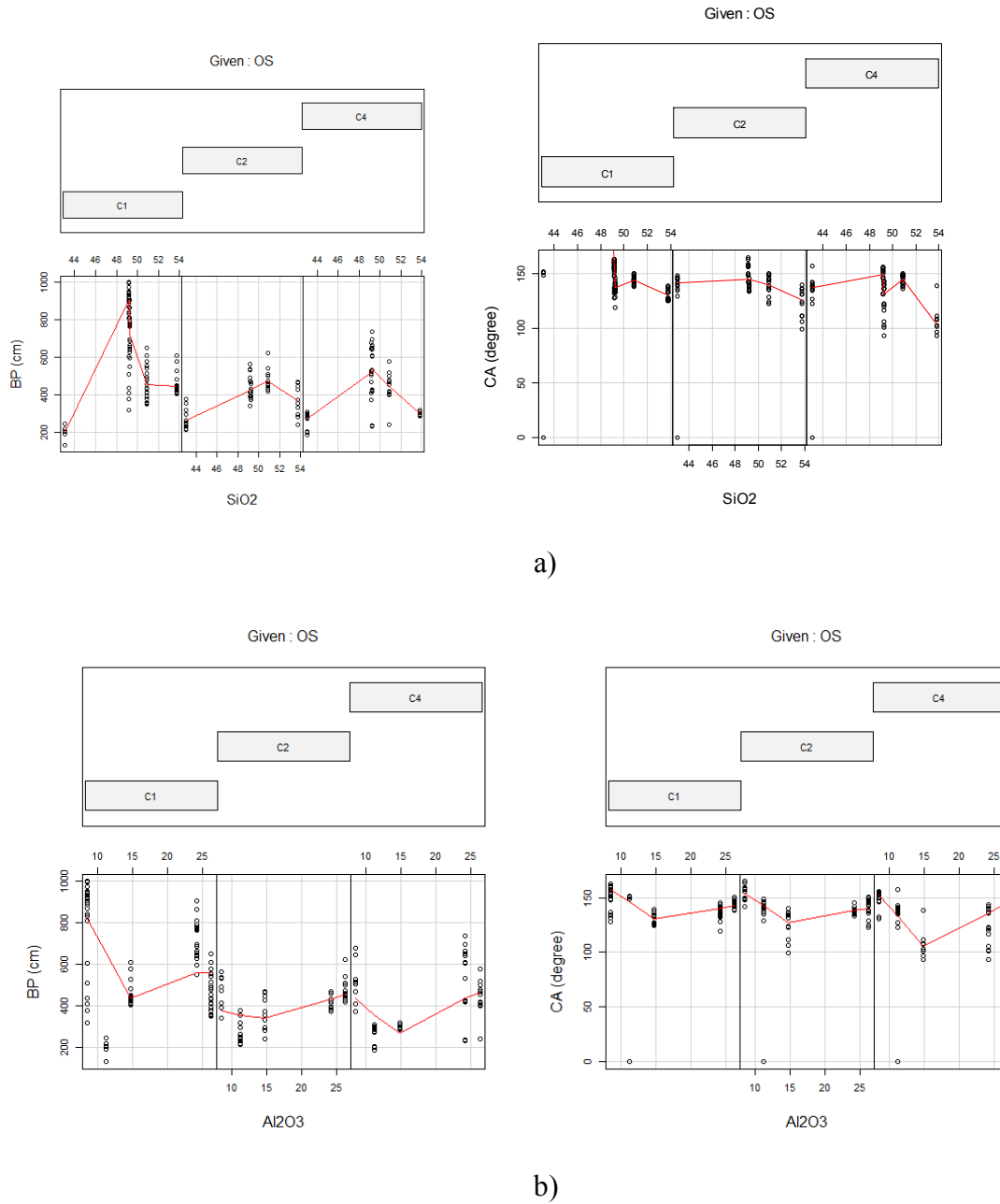
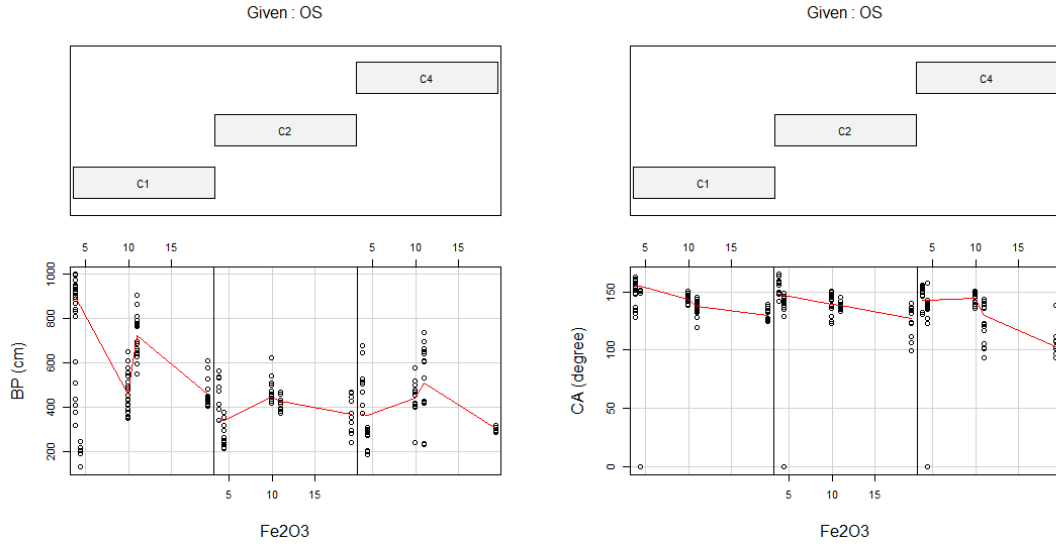


Figure 3. 16. The degree of water repellency (BP and CA) as a function of a)  $\text{SiO}_2$ , b)  $\text{Al}_2\text{O}_3$ , and c)  $\text{Fe}_2\text{O}_3$  in CFA conditioned OS.



c)

Figure 3. 16. continued

Further as discussed in the above sections and shown in Figure 3. 18 the total sum of the three main oxides (sum3) in CFA affects the performance of water repellency when treated using OS. As shown in the Figure the relationship between BP and sum declines for OS C-1, improves for OS C-2, and Stronger for OS C-4. However; with CA it follows a slightly declining pattern for the three panels of OS. However; in general the relationship is strong at a lower sum3, 61 percent. Further; the maximum range where significant reduction for BP is observed when sum3 is about 84 percent.

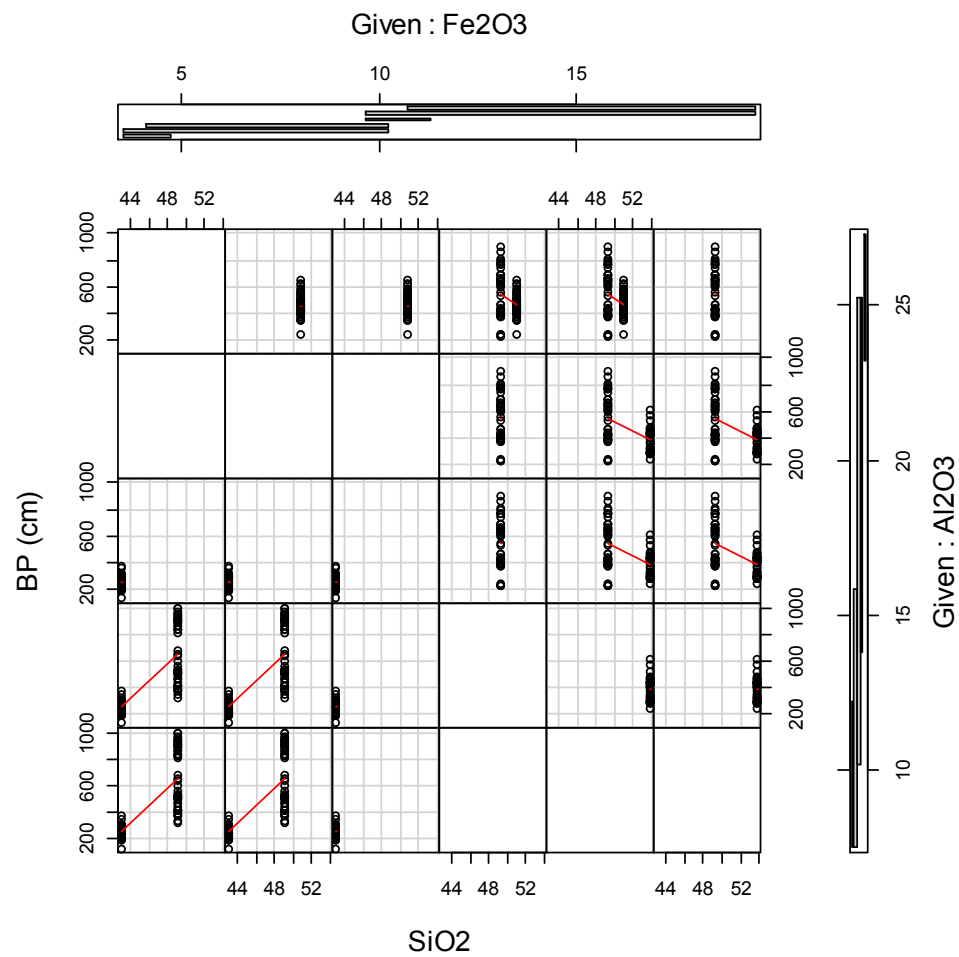


Figure 3. 17. The degree of water repellency (BP and CA) as a function of  $\text{SiO}_2$  conditioned by both  $\text{Al}_2\text{O}_3$  and  $\text{Fe}_2\text{O}_3$ , simultaneously.

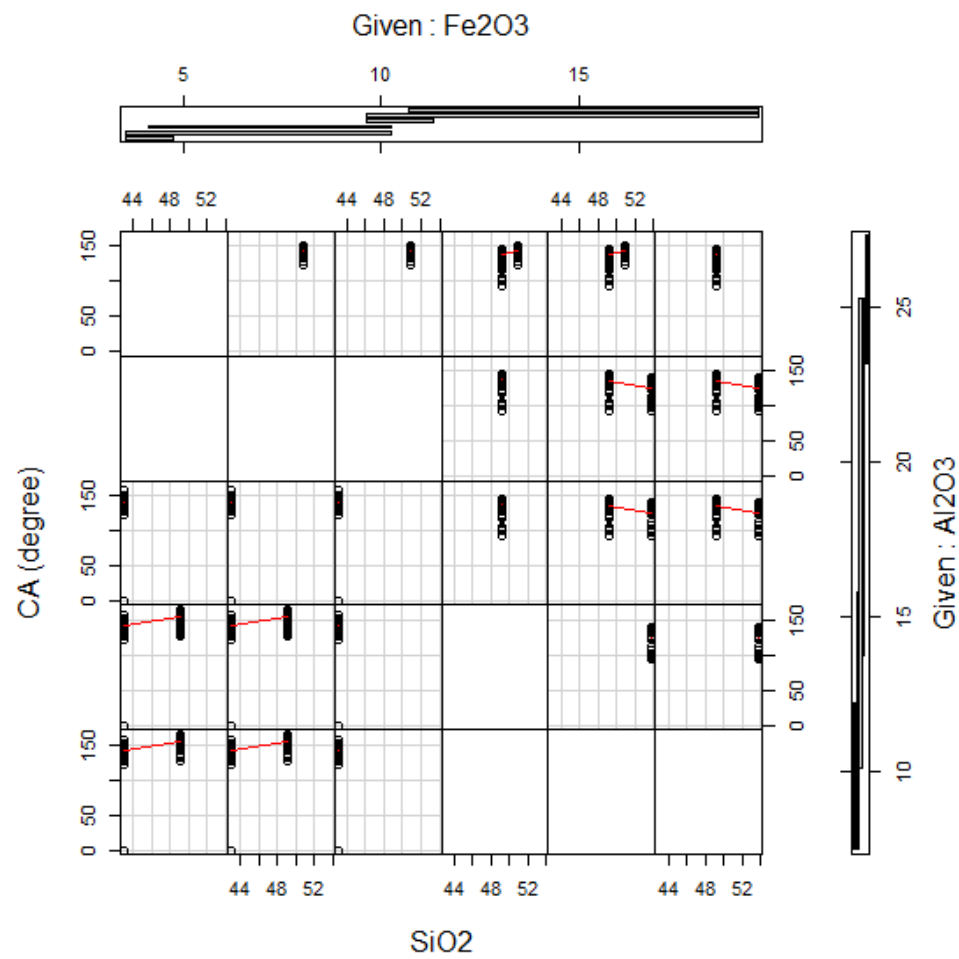


Figure 3. 17. Continued.

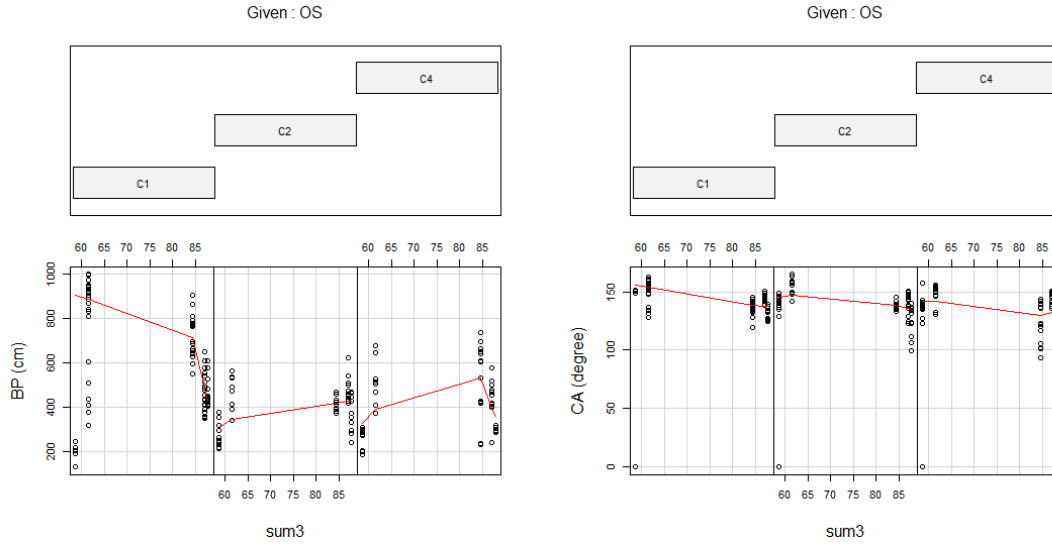


Figure 3.18. The degree of water repellency (BP and CA) as a function of sum3 conditioned by OS.

Hence it can be concluded that there exists a range where sum3 in CFA is effective (61 percent) beyond which the magnitude of water repellency declines. This conclusion can be more elaborated using two examples: the first one is demonstrated in Figure 3. 5. As depicted in the Figure CFA-2 has the highest sum3 percentage, 87.11 but less in BP when compared with similar (Class F) CFA1 and CFA-2. CFA-2 has more than 3 percent sum3 than CFA-1. Yet, CFA-1 able to form higher BP, about 30 percent more than CFA-2. The second is related to the performance of a Class C CFA, CFA-5. Basically, this type of CFA is characterized by high CaO and low sum3 percentage. In both cases the chance to form a larger water repellent surface is low. The percentage of sum3 in CFA-5 is less by more than 37 percent than CFA-1 and 42 percent for CFA-2 and CFA-3. However, the average BP for CFA-5 is more than all the three CFAs. Both insights correspond to Figure 3. 18 such that BP is maximum when sum3 is about 61 percent and slightly declines until it gets to 84 percent. After which a sharp decline in water repellency is observed.

It should be noted that despite other variables the presence of sum3 to the optimal content (61 percent) is one of the reasons for the CFA able to form higher water repellent surface when treated using OS. However; with the highest percent of CaO, the formation of highest BP should be affected to certain degrees. For example CFA-5 has the highest CaO, 27 percent. But after treating using OS CFA-5 is transformed to the highest (average) water repellent surface. This unique behavior of Class C CFA (CFA-5) is analyzed using the effect of oxides.

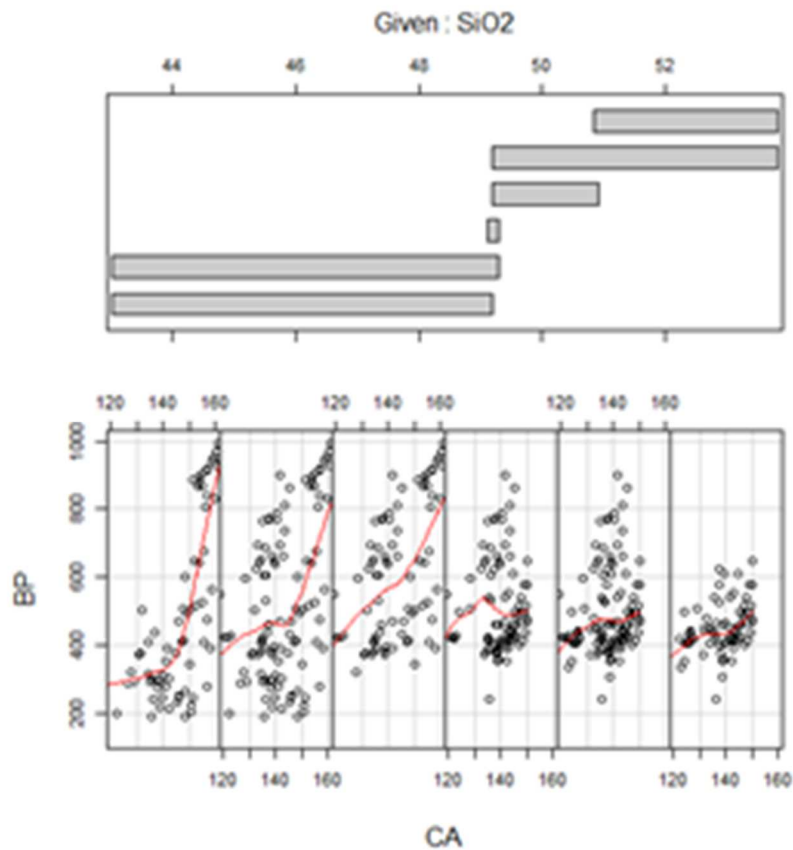


Figure 3.19. Correlation between BP and CA conditioned by SiO2



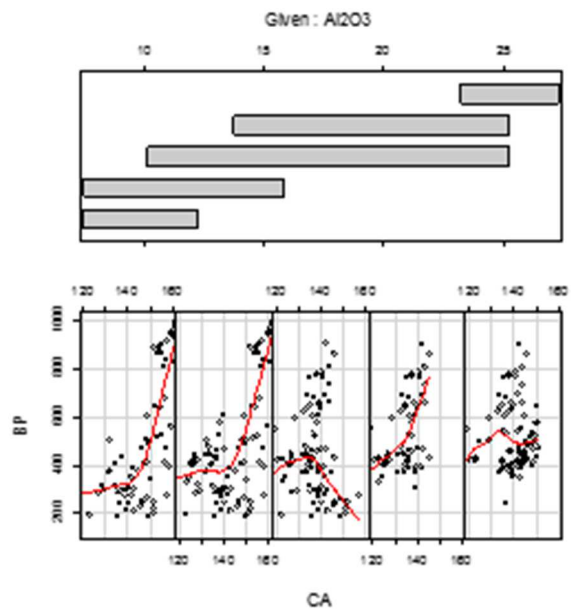


Figure 3.20. Correlation between BP and CA conditioned by  $Al_2O_3$

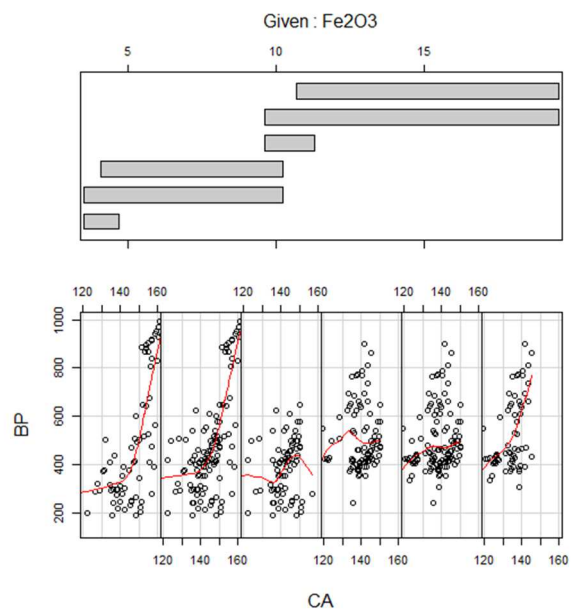


Figure 3.21. Correlation between BP and CA conditioned by  $Fe_2O_3$

Lower percent of CaO in CFA does not alter the formation of water repellent surface in CFA when treated with OS.

#### *3.4.8 Calcium Oxide and a hydrophobic surface formation*

When mixed with water CaO in CFA dissolves and raises the pH of the solution increasing hydroxyl concentration. It is the abundance of this  $\text{OH}^-$  ion that results in transforming CFA to different usable material through the dissociation of metallic ions. Murayama et al. (2002) and Bukhari et al., (2015) in coal fly ash dissolve when the solution has higher  $\text{OH}^-$  in alkali. The abundance of  $\text{OH}^-$  (alkali) due to the dissolution of CaO in the solution not only affects the formation of the bond it can also destroys it once it is formed. Detailed studies regarding the breakdown of a covalent bond between elements in CFA and other materials due to the formation of a larger quantity of alkaline from hydrolysis of CaO were documented in (Bai et al., 2010; Bankowski et al., 2004; Poggemann et al., 2003; Wu et al., 2014). CaO reach CFA (characteristic of Class C CAFA) has shown mixed reaction after the treatment to form water repellent surface. For example, one of Class C CFA (CFA-5) transformed to a highly water repellent surface despite its highest CaO percent content, 27 percent. On the other hand, the treatment of the other Class C CFA (CFA-6) showed the least magnitude to form a water repellent surface but less CaO content, 15 percent. Analysis of various Oxides and minerals in CFA-5 showed that MgO is one of the most abundant oxide in the CFA than any other. The effect and relationship between MgO and CaO with water repellency was conducted using multi variable analysis technique. Figures 3.22 and Figure 3.23 show results of the effect of CaO conditioned by

OS and MgO. As depicted in Figure 3.22 column (a) CaO for all CFAs, column (b) excludes MgO reach CFA (CFA-5) from the evaluation. In column (a) the relationship between both water repellency parameters and CaO is not consistent along the three panels of OS; stronger and weaker up to and beyond 15 percent CaO content, respectively. Whereas; as shown in column (b) the relationship is consistently declining from its highest (at lowest CaO percent) when CFA-5 is excluded. The latter shows the expected relationship between water repellency and CaO. Comparison of CFA (Class C and F) is shown in Figure 3.24. It is believed that a relatively high MgO in CFA-5 plays a significant role to change the relationship between CaO and water repellency through its dissociation property when mixed with water Figure 3.23. However, the existence of CaO up to about 2 percent does not affect the transformation of CFA to a water repellent one when mixed with water Figure 3.22.

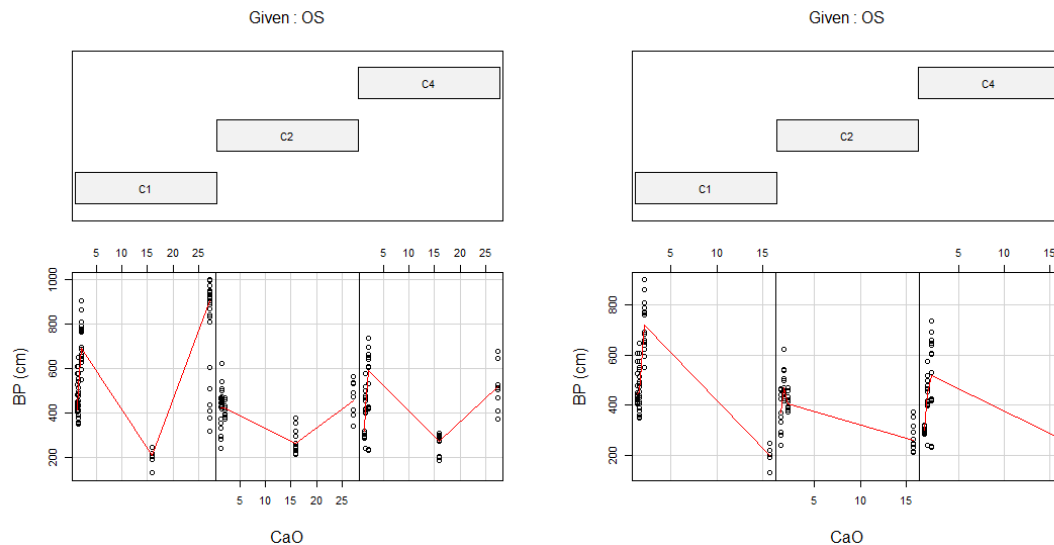


Figure 3.22. The degree of water repellency (BP and CA) as a function of CaO conditioned by OS; column a) all CFA, b) all CFA without high MgO

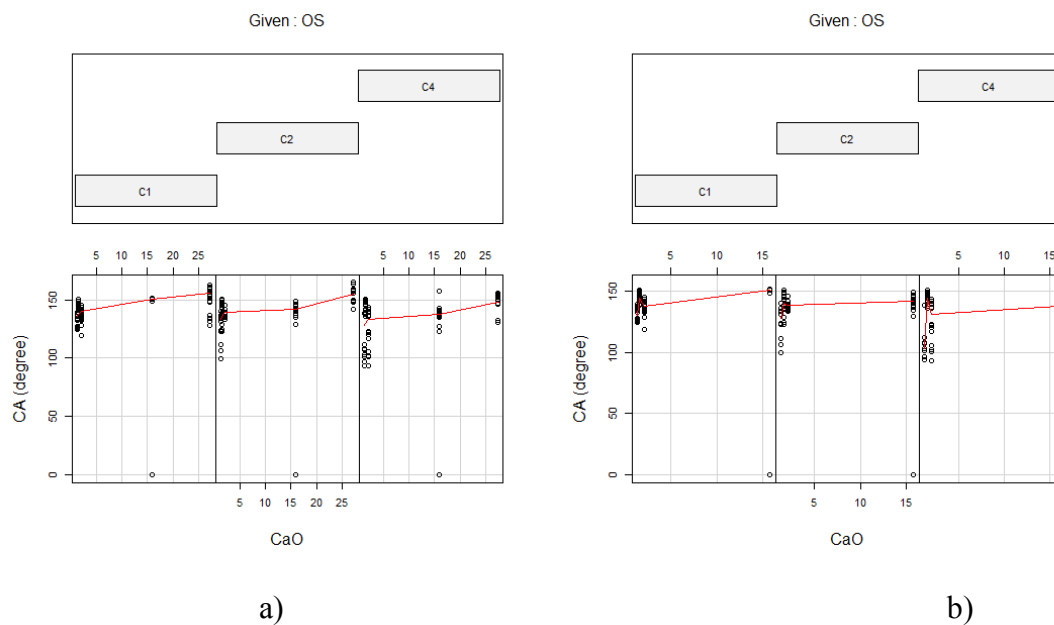


Figure 3.22. continued.

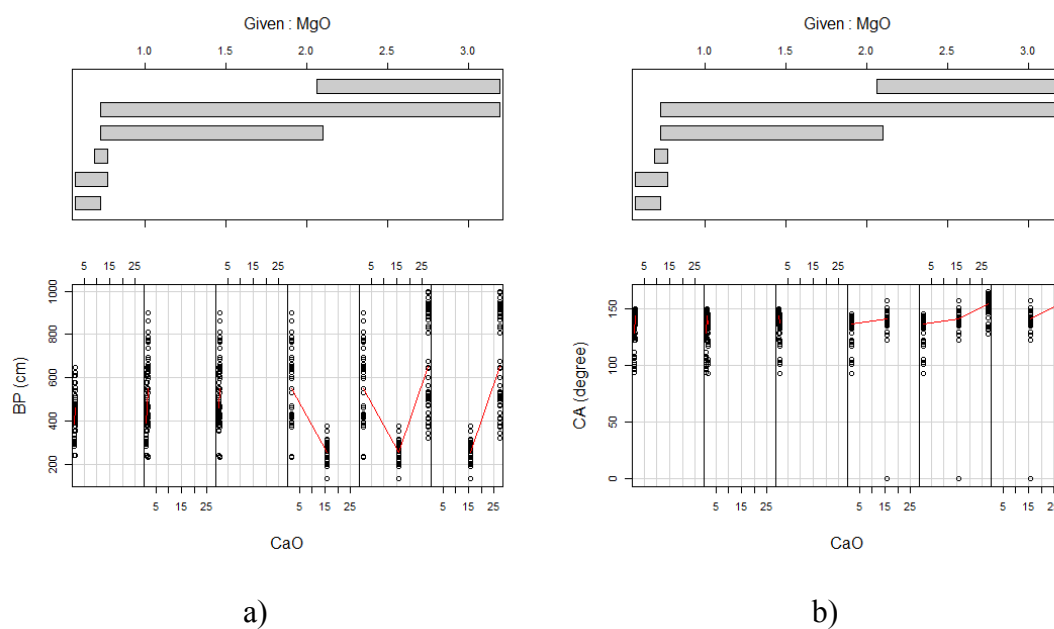


Figure 3.23. The degree of water repellency (BP and CA) as a function of CaO conditioned by MgO.

In another conclusion, if CFA with high CaO is treated with OS its inverse relation with water repellency can be altered through increasing the percent of MgO above 2 percent Figure 3.23. Further study on the chemistry of high MgO in CFA with OS products is important. It is concluded that Class C CFA can be transformed to a water repellent using OS products provided that the percentage content of MgO is beyond 3. Or Class C CFA can be transformed to a water repellent surface through modifying its mineralogical composition using MgO despite its high CaO.

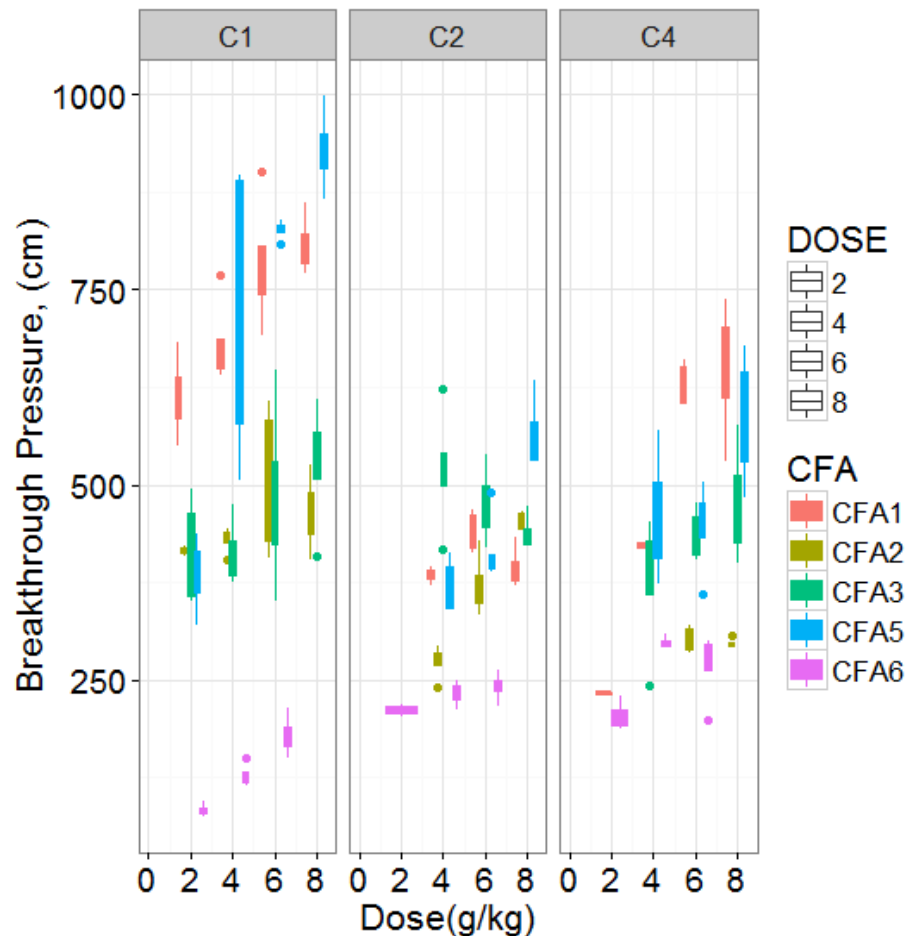


Figure 3. 24. Comparison of water repellency of Class C and F CFA. CFA-6 (Class C) is the least to transform CFA surface to a water repellent one. However, same type, CFA-5 forms a sufficiently high water-resistant surface due to the presence of additional oxides, MgO.

As shown in Table 3.2, Figure 3. 11, and Figure 3. 13 to Figure 3.15, models 1 and 4 are best fit models to the measured BP. In addition; unlike models 2 and 3 that show inconsistency these models are not affected by the type of CFA and/or individual compositions of oxides and minerals, Figure 3. 10 and Figure 3.12, Models 1 and 4 demonstrate universality. Strong relationship between water repellency and quartz is observed along the three panels of OS up to about 55 percent of composition, after which it follows a declining respond Figure 3.25. Figure 3.26 shows gypsum and magnetite declining relationship along the panels.

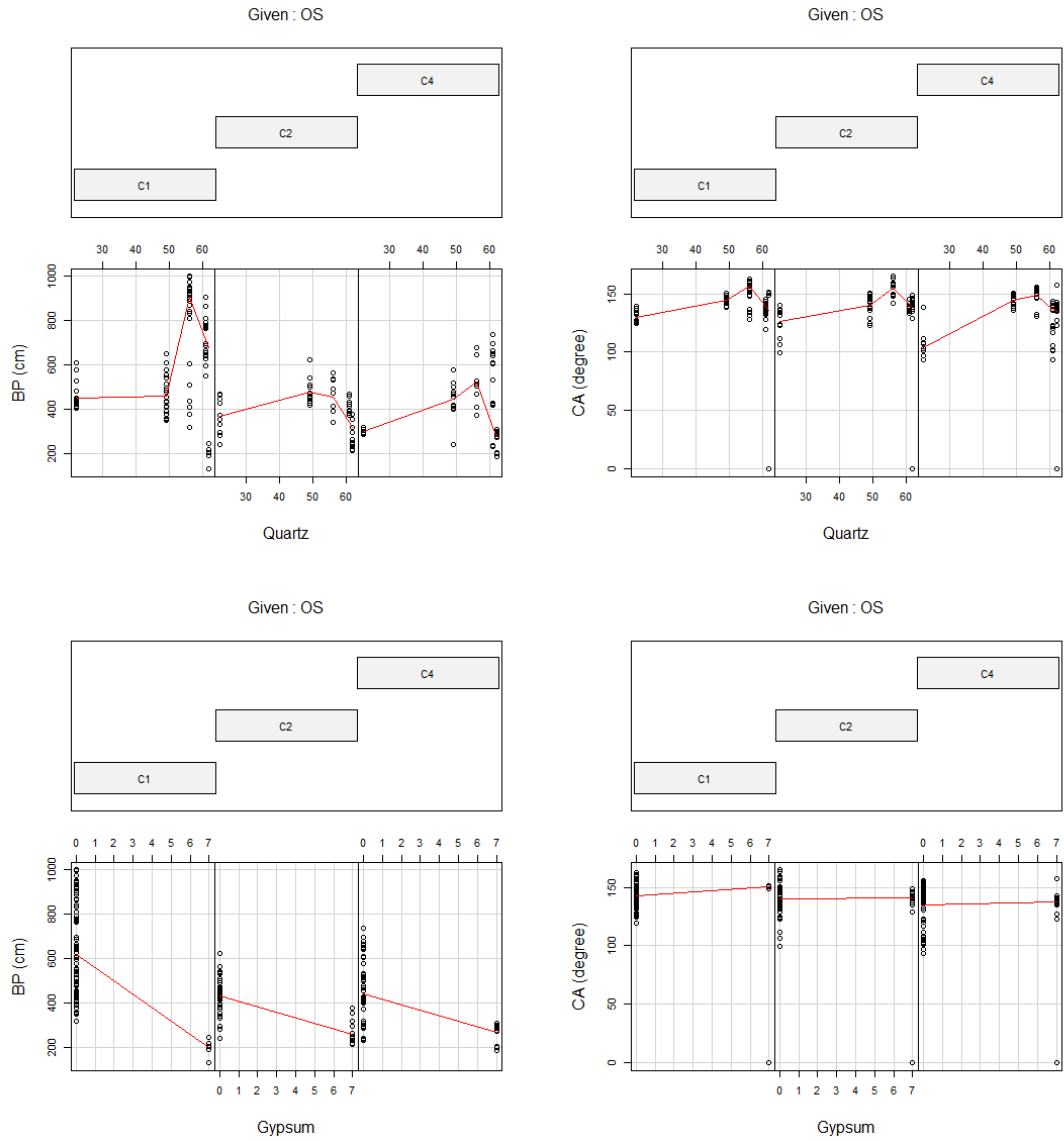


Figure 3.25. The degree of water repellency (BP and CA) as a function of group 1 model (Quartz + Gypsum) conditioned by OS.

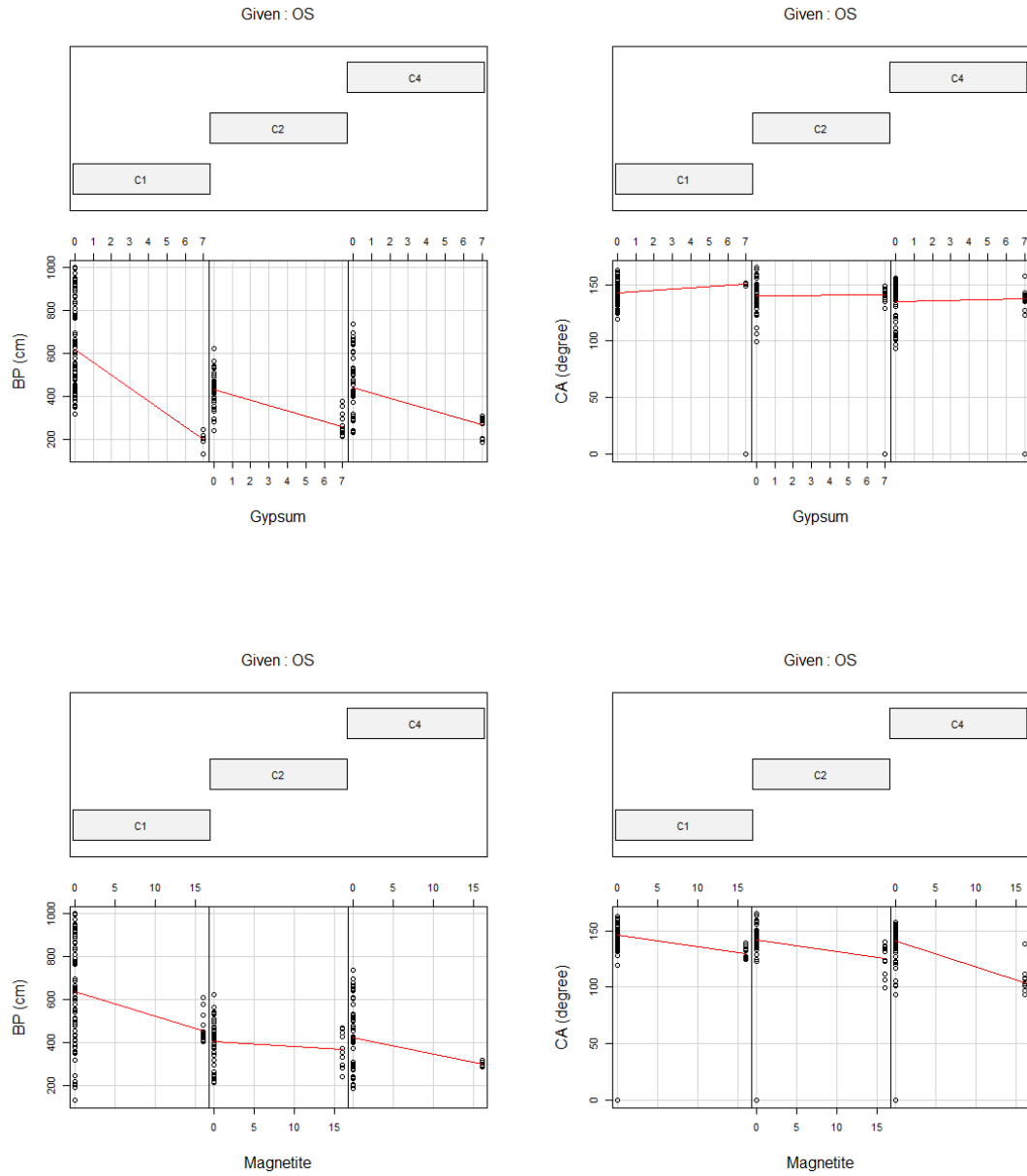


Figure 3.26. The degree of water repency (BP and CA) as a function of group 4 model (Gypsum + Magnetite) conditioned by OS.



## REFERENCES

- Amirfazli, A., and Neumann, A. W. (2004). Status of the three-phase line tension: a review. *Advances in Colloid and Interface Science*, 110(3), 121-141. doi:<http://dx.doi.org/10.1016/j.cis.2004.05.001>
- Arkles, B., Maddox, A., Singh, M., Zazyczny, J., and Matisons, J. (2014). <Silane coupling agents.pdf>. Silane coupling agents. 3. Retrieved from <http://www.gelest.com/wp-content/uploads/Goods-PDF-brochures-couplingagents.pdf>
- Baba, E. M., Cansoy, C. E., and Zayim, E. O. (2015). Optical and wettability properties of polymers with varying surface energies. *Applied Surface Science*, 350, 115-120. doi:<http://dx.doi.org/10.1016/j.apsusc.2015.02.150>
- Bachmann, J., Ellies, A., and Hartge, K. H. (2000). Development and application of a new sessile drop contact angle method to assess soil water repellency. *Journal of Hydrology*, 231–232(0), 66-75. doi:[http://dx.doi.org/10.1016/S0022-1694\(00\)00184-0](http://dx.doi.org/10.1016/S0022-1694(00)00184-0)
- Bai, G.-h., Teng, W., Wang, X.-g., Qin, J.-g., Xu, P., and Li, P.-c. (2010). Alkali desilicated coal fly ash as substitute of bauxite in lime-soda sintering process for aluminum production. *Transactions of Nonferrous Metals Society of China*, 20, s169-s175. doi:[http://dx.doi.org/10.1016/S1003-6326\(10\)60034-9](http://dx.doi.org/10.1016/S1003-6326(10)60034-9)
- Bai, G., Qiao, Y., Shen, B., and Chen, S. (2011). Thermal decomposition of coal fly ash by concentrated sulfuric acid and alumina extraction process based on it. *Fuel Processing Technology*, 92(6), 1213-1219. doi:<http://dx.doi.org/10.1016/j.fuproc.2011.01.017>
- Bankowski, P., Zou, L., and Hodges, R. (2004). Reduction of metal leaching in brown coal fly ash using geopolymers. *Journal of Hazardous Materials*, 114(1), 59-67. doi:<http://dx.doi.org/10.1016/j.jhazmat.2004.06.034>
- Bartell, F. E., Purcell, W. R., and Dodd, C. G. (1948). The measurement of the effective pore size and of the water-repellency of tightly woven textiles. *Discussions of the Faraday Society*, 3(0), 257-264. doi:10.1039/DF9480300257
- Basu, M., Pande, M., Bhadoria, P. B. S., and Mahapatra, S. C. (2009). Potential fly-ash utilization in agriculture: A global review. *Progress in Natural Science*, 19(10), 1173-1186. doi:<http://dx.doi.org/10.1016/j.pnsc.2008.12.006>
- Beatty, S. M., and Smith, J. E. (2010). Fractional wettability and contact angle dynamics in burned water repellent soils. *Journal of Hydrology*, 391(1–2), 97-108. doi:<http://dx.doi.org/10.1016/j.jhydrol.2010.07.007>
- Belibel, R., Avramoglou, T., Garcia, A., Barbaud, C., and Mora, L. (2016). Effect of chemical heterogeneity of biodegradable polymers on surface energy: A static contact angle analysis of polyester model films. *Materials Science and Engineering: C*, 59, 998-1006. doi:<http://dx.doi.org/10.1016/j.msec.2015.10.010>
- Bertola, V., and Wang, M. (2015). Dynamic contact angle of dilute polymer solution drops impacting on a hydrophobic surface. *Colloids and Surfaces A: Physicochemical and Engineering Aspects*, 481, 600-608. doi:<http://dx.doi.org/10.1016/j.colsurfa.2015.05.052>
- Blissett, R. S., and Rowson, N. A. (2012). A review of the multi-component utilisation of coal fly ash. *Fuel*, 97, 1-23. doi:<http://dx.doi.org/10.1016/j.fuel.2012.03.024>

- Böke, N., Birch, G. D., Nyale, S. M., and Petrik, L. F. (2015). New synthesis method for the production of coal fly ash-based foamed geopolymers. *Construction and Building Materials*, 75, 189-199.  
doi:<http://dx.doi.org/10.1016/j.conbuildmat.2014.07.041>
- Boycheva, S., Zgureva, D., and Vassilev, V. (2013). Kinetic and thermodynamic studies on the thermal behaviour of fly ash from lignite coals. *Fuel*, 108, 639-646.  
doi:<http://dx.doi.org/10.1016/j.fuel.2013.02.042>
- Bukhari, S. S., Behin, J., Kazemian, H., and Rohani, S. (2015). Conversion of coal fly ash to zeolite utilizing microwave and ultrasound energies: A review. *Fuel*, 140, 250-266. doi:<http://dx.doi.org/10.1016/j.fuel.2014.09.077>
- Carrillo, M. L. K., Letey, J., and Yates, S. R. (1999). <Measurement of Initial Soil-Water Contact Angle of Water Repellent Soils>. *Soil Science Society of America Proceedings*, 63(3), 433-466.
- Cassie, A. B. D. (1948). Contact angles. *Discussions of the Faraday Society*, 3(0), 11-16.  
doi:10.1039/DF9480300011
- Cheng, P., Li, D., Boruvka, L., Rotenberg, Y., and Neumann, A. W. (1990). Automation of axisymmetric drop shape analysis for measurements of interfacial tensions and contact angles. *Colloids and Surfaces*, 43(2), 151-167.  
doi:[http://dx.doi.org/10.1016/0166-6622\(90\)80286-D](http://dx.doi.org/10.1016/0166-6622(90)80286-D)
- Chi, M., and Huang, R. (2014). Effect of circulating fluidized bed combustion ash on the properties of roller compacted concrete. *Cement and Concrete Composites*, 45, 148-156. doi:<http://dx.doi.org/10.1016/j.cemconcomp.2013.10.001>
- Choo, H., Lim, S., Lee, W., and Lee, C. (2016). Compressive strength of one-part alkali activated fly ash using red mud as alkali supplier. *Construction and Building Materials*, 125, 21-28. doi:<http://dx.doi.org/10.1016/j.conbuildmat.2016.08.015>
- Daniels, J. L., and Hourani, M. (2009). Soil Improvement with Organo-Silane. In *Advances in Ground Improvement* (pp. 217-224): American Society of Civil Engineers.
- Daniels, J. L., Hourani, M. S., and Harper, L. S. (2009). Organo-silane chemistry: A water repellent technology for coal ash and soils. Paper presented at the World of Coal Ash (WOCA), Lexington, KY, USA.
- Daniels, J. L., Mehta, P., Vaden, M., Sweem, D., Mason, D. M., Zavareh, M., and Ogunro, V. (2009). Nano-scale Organo-silane applications in geotechnical and geoenvironmental engineering. *International Journal of Terraspace Science and Engineering*, 1(1), 19-27.
- Daniels, L. J., and Das, P. G. (2006). Leaching Behavior of Lime-Fly Ash Mixtures. *Environmental Engineering Science*, 23.
- de Gennes, P. G. (1985). Wetting: statics and dynamics. *Reviews of Modern Physics*, 57(3), 827-863.
- Dim, P. E., Fletcher, R. S., and Rigby, S. P. (2016). Improving the accuracy of catalyst pore size distributions from mercury porosimetry using mercury thermoporometry. *Chemical Engineering Science*, 140, 291-298.  
doi:<http://dx.doi.org/10.1016/j.ces.2015.10.023>
- Dimitrov, D. I., Milchev, A., and Binder, K. (2007). Capillary Rise in Nanopores: Molecular Dynamics Evidence for the Lucas-Washburn Equation. *Physical Review Letters*, 99(5), 054501.

- Duncan, D., Li, D., Gaydos, J., and Neumann, A. W. (1995). Correlation of Line Tension and Solid-Liquid Interfacial Tension from the Measurement of Drop Size Dependence of Contact Angles. *Journal of Colloid and Interface Science*, 169(2), 256-261. doi:<http://dx.doi.org/10.1006/jcis.1995.1032>
- EPA, U. (2015). <Hazardous and Solid Waste Management System; Disposal of Coal Combustion Residuals From Electric Utilities; Final Rule>. *Federal Register* / Vol. 80,(No. 74).
- EPRI. (2005). Chemical Constituents in Coal Combustion Product Leachate: Boron. Department of Environmental Health Sciences. University of California. Los Angeles, CA 90095-1772.
- EPRI, and Department of Energy, U. S. (2006). Characterization of Field Leachates at Coal Combustion Product Management Sites: Arsenic, Selenium, Chromium, and Mercury Speciation. PA: 2006. 1012578.
- EPRI, and Pacific Northwest Laboratories, R. W. (1988). Leachate chemistry at the Montour Fly Ash test cell. In (pp. 104). Montour: EPRI.
- EPRI (2012). Geotechnical Properties of Fly Ash and Potential for Static Liquefaction: Volume 1 – Summary and Conclusions. EPRI, Palo Alto, CA: 2012. 1023743.
- Erbil, H. Y., Demirel, A. L., Avcı, Y., and Mert, O. (2003). Transformation of a Simple Plastic into a Superhydrophobic Surface. *Science*, 299(5611), 1377-1380. doi:10.1126/science.1078365
- F. de Buyl. (2004). <Organo-Functional Silanes,PDF.pdf>. Silicones in Industrial Applications, in *Inorganic Polymers*, Nova Science Publishers.
- Feyyisa, J. L. (2014). Stochastic approach in groundwater modeling: A case study of the buffalo creek watershed. Available from ProQuest Dissertations & Theses Global. <https://search.proquest.com/docview/1620726678?accountid=14605>
- Feyyisa, J., and Daniels, J. (2016). A Dynamic Contact Angle Measurement Technique for Water-Repellent Coal Fly Ash (CFA). In *Geo-Chicago 2016* (pp. 925-938): American Society of Civil Engineers.
- Feyyisa, J. L., Daniels, J. L., and Pando, M. A. (2017). Contact Angle Measurements for Use in Specifying Organosilane-Modified Coal Combustion Fly Ash. *Journal of Materials in Civil Engineering*, 29(9). doi:10.1061/(ASCE)MT.1943-5533.0001943
- Fink, D. H., and Myers, L. E. (1969). <Synthetic hydrophobic soils for harvesting precipitation >.
- Gao, L., and McCarthy, T. J. (2007). How Wenzel and Cassie Were Wrong. *Langmuir*, 23(7), 3762-3765. doi:10.1021/la062634a
- Gao, L., and McCarthy, T. J. (2007). How Wenzel and Cassie were wrong. *Langmuir*, 23, 3762.
- Gao, S., Wei, N., Li, X., Wang, Y., and Wang, Q. (2014). Cap Rock CO<sub>2</sub> Breakthrough Pressure Measurement Apparatus and Application in Shenhua CCS Project. *Energy Procedia*, 63, 4766-4772. doi:<http://dx.doi.org/10.1016/j.egypro.2014.11.507>
- General Assembly, N. C. (2014). <SENATE BILL 729>. session 2013.
- Geocomp, C. (2017). FlowTrac-II Volume Pressure Controller. Retrieved from [http://www.geocomp.com/Products/Lab\\_Systems\\_FlowTrac2](http://www.geocomp.com/Products/Lab_Systems_FlowTrac2)

- Good, R. E., Good, N. F., and Andresen, J. W. (1979). 16 - The Pine Barren Plains. In R. T. T. Forman (Ed.), *Pine Barrens* (pp. 283-295): Academic Press.
- Heath, J. E., Dewers, T. A., McPherson, B. J. O. L., Nemer, M. B., and Kotula, P. G. (2012). Pore-lining phases and capillary breakthrough pressure of mudstone caprocks: Sealing efficiency of geologic CO<sub>2</sub> storage sites. *International Journal of Greenhouse Gas Control*, 11, 204-220.  
doi:<http://dx.doi.org/10.1016/j.ijggc.2012.08.001>
- Hefer, A. W., Bhasin, A., and Little, D. N. (2006). Bitumen Surface Energy Characterization Using a Contact Angle Approach. *Journal of Materials in Civil Engineering*, 18(6), 759-767. doi:10.1061/(ASCE)0899-1561(2006)18:6(759)
- Heib, F., Hempelmann, R., Munief, W. M., Ingebrandt, S., Fug, F., Possart, W., . . . Schmitt, M. (2015). High-precision drop shape analysis (HPDSA) of quasistatic contact angles on silanized silicon wafers with different surface topographies during inclining-plate measurements: Influence of the surface roughness on the contact line dynamics. *Applied Surface Science*, 342(0), 11-25.  
doi:<http://dx.doi.org/10.1016/j.apsusc.2015.03.032>
- Hildenbrand, A., Schlomer, S., and Krooss, B. M. (2002). Gas breakthrough experiments on fine-grained sedimentary rocks. *Geofluids*, 2, 3-23.
- Imeson, A. C., Verstraten, J. M., van Mulligen, E. J., and Sevink, J. (1992). The effects of fire and water repellency on infiltration and runoff under Mediterranean Class Forest. *CATENA*, 19(3-4), 345-361. doi:[http://dx.doi.org/10.1016/0341-8162\(92\)90008-Y](http://dx.doi.org/10.1016/0341-8162(92)90008-Y)
- Jala, S., and Goyal, D. (2006). Fly ash as a soil ameliorant for improving crop production—a review. *Bioresource Technology*, 97(9), 1136-1147.  
doi:<http://dx.doi.org/10.1016/j.biortech.2004.09.004>
- Jang, J. G., and Lee, H. K. (2016). Effect of fly ash characteristics on delayed high-strength development of geopolymers. *Construction and Building Materials*, 102, Part 1, 260-269. doi:<http://dx.doi.org/10.1016/j.conbuildmat.2015.10.172>
- Johnson, R. E., and Dettre, R. H. (1964). Contact Angle Hysteresis. III. Study of an Idealized Heterogeneous Surface. *The Journal of Physical Chemistry*, 68(7), 1744-1750. doi:10.1021/j100789a012
- Joos, P., Van Remoortere, P., and Bracke, M. (1990). The kinetics of wetting in a capillary. *Journal of Colloid and Interface Science*, 136(1), 189-197.  
doi:[https://doi.org/10.1016/0021-9797\(90\)90089-7](https://doi.org/10.1016/0021-9797(90)90089-7)
- Keatts, M. I. (2014). Geotechnical controls on organo-silane modification of soils and coal combustion fly ash. (1585353 M.S.), The University of North Carolina at Charlotte, Retrieved from <https://librarylink.uncc.edu/login?url=http://search.proquest.com/docview/1665307558?accountid=14605> Dissertations and Theses @ University of North Carolina Charlotte; ProQuest Dissertations and Theses Full Text; ProQuest Dissertations and Theses Global database.
- Kloubek, J. (1981). Hysteresis in porosimetry. *Powder Technology*, 29(1), 63-73.  
doi:[http://dx.doi.org/10.1016/0032-5910\(81\)85005-X](http://dx.doi.org/10.1016/0032-5910(81)85005-X)
- Koc, M., and Bulut, R. (2014). Assessment of a Sessile Drop Device and a New Testing Approach Measuring Contact Angles on Aggregates and Asphalt Binders. *Journal*

- of Materials in Civil Engineering, 26(3), 391-398. doi:10.1061/(ASCE)MT.1943-5533.0000852
- Kwok, D. Y., and Neumann, A. W. (1999). Contact angle measurement and contact angle interpretation. *Advances in Colloid and Interface Science*, 81(3), 167-249. doi:http://dx.doi.org/10.1016/S0001-8686(98)00087-6
- Li, D. (1996). Drop size dependence of contact angles and line tensions of solid-liquid systems. *Colloids and Surfaces A: Physicochemical and Engineering Aspects*, 116(1-2), 1-23. doi:http://dx.doi.org/10.1016/0927-7757(96)03582-0
- Li, H., Hui, J., Wang, C., Bao, W., and Sun, Z. (2014). Extraction of alumina from coal fly ash by mixed-alkaline hydrothermal method. *Hydrometallurgy*, 147, 183-187. doi:http://dx.doi.org/10.1016/j.hydromet.2014.05.012
- Li, S., Dong, M., Li, Z., Huang, S., Qing, H., and Nickel, E. (2005). Gas breakthrough pressure for hydrocarbon reservoir seal rocks: implications for the security of long-term CO<sub>2</sub> storage in the Weyburn field. *Geofluids*, 5(4), 326-334. doi:10.1111/j.1468-8123.2005.00125.x
- Li, X., Fan, X., Askounis, A., Wu, K., Sefiane, K., and Koutsos, V. (2013). An experimental study on dynamic pore wettability. *Chemical Engineering Science*, 104, 988-997. doi:http://dx.doi.org/10.1016/j.ces.2013.10.026
- Li, X., Fan, X., and Brandani, S. (2014). Difference in pore contact angle and the contact angle measured on a flat surface and in an open space. *Chemical Engineering Science*, 117, 137-145. doi:http://dx.doi.org/10.1016/j.ces.2014.06.024
- Liu, J. F., Davy, C. A., Talandier, J., and Skoczylas, F. (2014). Effect of gas pressure on the sealing efficiency of compacted bentonite-sand plugs. *Journal of Contaminant Hydrology*, 170, 10-27. doi:https://doi.org/10.1016/j.jconhyd.2014.09.006
- Lu, N., and Likos, W. (2004). *Unsaturated Soil Mechanics*. Hoboken, New Jersey: John Wiley and Sons, Inc.
- Marmur, A. (1997). Line Tension and the Intrinsic Contact Angle in Solid-Liquid-Fluid Systems. *Journal of Colloid and Interface Science*, 186(2), 462-466. doi:http://dx.doi.org/10.1006/jcis.1996.4666
- Marmur, A. (1998). Line tension effect on contact angles: Axisymmetric and cylindrical systems with rough or heterogeneous solid surfaces. *Colloids and Surfaces A: Physicochemical and Engineering Aspects*, 136(1-2), 81-88. doi:http://dx.doi.org/10.1016/S0927-7757(97)00300-2
- Marmur, A. (2006). Soft contact: measurement and interpretation of contact angles. *Soft Matter*, 2(1), 12-17. doi:10.1039/B514811C
- Martic, G., Gentner, F., Seveno, D., Coulon, D., De Coninck, J., and Blake, T. D. (2002). A Molecular Dynamics Simulation of Capillary Imbibition. *Langmuir*, 18(21), 7971-7976. doi:10.1021/la020068n
- Moon, G. D., Oh, S., and Choi, Y. C. (2016). Effects of the physicochemical properties of fly ash on the compressive strength of high-volume fly ash mortar. *Construction and Building Materials*, 124, 1072-1080. doi:http://dx.doi.org/10.1016/j.conbuildmat.2016.08.148
- Murayama, N., Yamamoto, H., and Shibata, J. (2002). Mechanism of zeolite synthesis from coal fly ash by alkali hydrothermal reaction. *International Journal of Mineral Processing*, 64(1), 1-17. doi:http://dx.doi.org/10.1016/S0301-7516(01)00046-1

- Nickelsen, S., Moghadam, A. D., Ferguson, J. B., and Rohatgi, P. (2015). Modeling and experimental study of oil/water contact angle on biomimetic micro-parallel-patterned self-cleaning surfaces of selected alloys used in water industry. *Applied Surface Science*, 353, 781-787.  
doi:http://dx.doi.org/10.1016/j.apsusc.2015.06.166
- O'Loughlin, M., Wilk, K., Priest, C., Ralston, J., and Popescu, M. N. (2013). Capillary rise dynamics of aqueous glycerol solutions in glass capillaries: A critical examination of the Washburn equation. *Journal of Colloid and Interface Science*, 411, 257-264. doi:http://dx.doi.org/10.1016/j.jcis.2013.05.077
- P. Rigby, S., S. Fletcher, R., and N. Riley, S. (2004). Characterisation of porous solids using integrated nitrogen sorption and mercury porosimetry. *Chemical Engineering Science*, 59(1), 41-51.  
doi:http://dx.doi.org/10.1016/j.ces.2003.09.017
- Park, Y., Abolmaali, A., Kim, Y. H., and Ghahremannejad, M. (2016). Compressive strength of fly ash-based geopolymer concrete with crumb rubber partially replacing sand. *Construction and Building Materials*, 118, 43-51.  
doi:http://dx.doi.org/10.1016/j.conbuildmat.2016.05.001
- Pei, X., Zhang, F., Wu, W., and Liang, S. (2015). Physicochemical and index properties of loess stabilized with lime and fly ash piles. *Applied Clay Science*, 114, 77-84.  
doi:http://dx.doi.org/10.1016/j.clay.2015.05.007
- Poggemann, J. F., Heide, G., and Frischat, G. H. (2003). Direct view of the structure of different glass fracture surfaces by atomic force microscopy. *Journal of Non-Crystalline Solids*, 326, 15-20. doi:http://dx.doi.org/10.1016/S0022-3093(03)00370-3
- Poole, C., Priyatama, H., and Rice, N. M. (2000). Synthesis of zeolite adsorbents by hydrothermal treatment of PFA wastes: A comparative study. *Minerals Engineering*, 13(8), 831-842. doi:http://dx.doi.org/10.1016/S0892-6875(00)00072-8
- Querol, X., Moreno, N., Umaña, J. C., Alastuey, A., Hernández, E., López-Soler, A., and Plana, F. (2002). Synthesis of zeolites from coal fly ash: an overview. *International Journal of Coal Geology*, 50(1), 413-423.  
doi:http://dx.doi.org/10.1016/S0166-5162(02)00124-6
- Rein, M. (1993). Phenomena of liquid drop impact on solid and liquid surfaces. *Fluid Dynamics Research*, 12(2), 61.
- Rezaeyan, A., Tabatabaei-Nejad, S. A., Khodapanah, E., and Kamari, M. (2015). A laboratory study on capillary sealing efficiency of Iranian shale and anhydrite caprocks. *Marine and Petroleum Geology*, 66, Part 4, 817-828.  
doi:http://dx.doi.org/10.1016/j.marpetgeo.2015.07.022
- Rigby, S. P., and Edler, K. J. (2002). The Influence of Mercury Contact Angle, Surface Tension, and Retraction Mechanism on the Interpretation of Mercury Porosimetry Data. *Journal of Colloid and Interface Science*, 250(1), 175-190.  
doi:http://dx.doi.org/10.1006/jcis.2002.8286
- Río, O. I. d., and Neumann, A. W. (1997). Axisymmetric Drop Shape Analysis: Computational Methods for the Measurement of Interfacial Properties from the Shape and Dimensions of Pendant and Sessile Drops. *Journal of Colloid and Interface Science*, 196(2), 136-147. doi:http://dx.doi.org/10.1006/jcis.1997.5214

- Rotenberg, Y., Boruvka, L., and Neumann, A. W. (1983). Determination of surface tension and contact angle from the shapes of axisymmetric fluid interfaces. *Journal of Colloid and Interface Science*, 93(1), 169-183. doi:[http://dx.doi.org/10.1016/0021-9797\(83\)90396-X](http://dx.doi.org/10.1016/0021-9797(83)90396-X)
- Santner, G., Freytag, B., Juhart, J., Baumgartner, E., Schmied, F., and Teichert, C. (2012). Adhesive Power of Ultra High Performance Concrete from a Thermodynamic Point of View. *Journal of Materials in Civil Engineering*, 24(8), 1050-1058. doi:10.1061/(ASCE)MT.1943-5533.0000481
- Schmitt, M., Hempelmann, R., Ingebrandt, S., Munief, W., Durneata, D., Groß, K., and Heib, F. (2014). Statistical approach for contact angle determination on inclining surfaces: “slow-moving” analyses of non-axisymmetric drops on a flat silanized silicon wafer. *International Journal of Adhesion and Adhesives*, 55, 123-131. doi:<http://dx.doi.org/10.1016/j.ijadhadh.2014.08.007>
- Singh, M., and Siddique, R. (2013). Effect of coal bottom ash as partial replacement of sand on properties of concrete. *Resources, Conservation and Recycling*, 72, 20-32. doi:<http://dx.doi.org/10.1016/j.resconrec.2012.12.006>
- Singh, M., and Siddique, R. (2014). Strength properties and micro-structural properties of concrete containing coal bottom ash as partial replacement of fine aggregate. *Construction and Building Materials*, 50, 246-256. doi:<http://dx.doi.org/10.1016/j.conbuildmat.2013.09.026>
- Song, D., Song, B., Hu, H., Du, X., and Ma, Z. (2015). Contact angle and impinging process of droplets on partially grooved hydrophobic surfaces. *Applied Thermal Engineering*, 85, 356-364. doi:<http://dx.doi.org/10.1016/j.applthermaleng.2015.03.071>
- Thierry Materne, F. d. B., Gerald L. Witucki. (2012 ). <Organosilane Technology in Coating Applications: Review and Perspectives >. In (Vol. AGP11933 ). P.O. Box 994, Midland, MI 48640 USA Dow Corning Corporation.
- Thorneloe, A. S., Kosson , S. D., Sanchez , F., Garrabrant , C. A. n. a., and Helms, G. (2010). Evaluating the Fate of Metals in Air Pollution Control Residues from Coal-Fired Power Plants. *Environ. Sci. Technol.*, 44, 7351-7356.
- van der Merwe, E. M., Mathebula, C. L., and Prinsloo, L. C. (2014). Characterization of the surface and physical properties of South African coal fly ash modified by sodium lauryl sulphate (SLS) for applications in PVC composites. *Powder Technology*, 266, 70-78. doi:<http://dx.doi.org/10.1016/j.powtec.2014.06.008>
- Wang, S., Ma, Q., and Zhu, Z. H. (2008). Characteristics of coal fly ash and adsorption application. *Fuel*, 87(15–16), 3469-3473. doi:<http://dx.doi.org/10.1016/j.fuel.2008.05.022>
- Wang, Z., Wu, L., and Wu, Q. J. (2000). Water-entry value as an alternative indicator of soil water-repellency and wettability. *Journal of Hydrology*, 231–232, 76-83. doi:[http://doi.org/10.1016/S0022-1694\(00\)00185-2](http://doi.org/10.1016/S0022-1694(00)00185-2)
- Washburn, E. W. (1921a). The Dynamics of Capillary Flow. *Physical Review*, 17(3), 273-283.
- Washburn, E. W. (1921b). Note on a Method of Determining the Distribution of Pore Sizes in a Porous Material. *Proceedings of the National Academy of Sciences of the United States of America*, 7(4), 115-116.

- Wenzel, R. N. (1936). Reststance of solid surfaces to wetting by water. *Ind. Eng. Chem*, 28(8), 988–994.
- Wu, T., Chi, M., and Huang, R. (2014). Characteristics of CFBC fly ash and properties of cement-based composites with CFBC fly ash and coal-fired fly ash. *Construction and Building Materials*, 66, 172-180.  
doi:<http://dx.doi.org/10.1016/j.conbuildmat.2014.05.057>
- Yuan, Y., and Lee, T. R. (2013). Contact Angle and Wetting Properties. 51, 3-34.  
doi:10.1007/978-3-642-34243-1\_1
- Zhang, Y., Zhang, Z., Liu, Z., Norris, P., and Pan, W.-p. (2017). Study on the mercury captured by mechanochemical and bromide surface modification of coal fly ash. *Fuel*, 200, 427-434. doi:<http://dx.doi.org/10.1016/j.fuel.2017.03.095>



## GENERAL CONCLUSION

### SUMMARY OF NEW KNOWLEDGE GAINED

This research has addressed the problem of leachate generation in coal fly ash through engineered water repellency. The surface of five CFA surfaces were modified using OS products. Water repellency parameters, CA and BP were measured and analyzed. Different statistical and analytical model were used to describe relationship between the two surface energy parameters (CA and BP) and the abundance and type of main components influencing hydrophobic surface formation.

Parameters that influence the formation of water repellency in CFA were analyzed and presented. In response to the current trend to expand the industrial use of CFA and help to protect the environment from leachate, the following findings were addressed through environmentally friendly approach to transform CFA surface from wettable to non wettable one along with surface energy measurement approach.

#### 1. Contact angle measurement

The challenge to measure the surface energy of the MCFA is addressed. For MCFA a dynamic CA measurement technique provides repeatable measurement.

Using a dynamic CA measurement technique in which a drop is made to expand over the sample until it reaches a certain threshold volume was applied to measure CA for five types of MCFA using three OS products. The approach provided not only repeatable measurement it also reduced the disparity of CA measurement using the conventional approach. The technique considers and identified appropriate drop size for different samples at which the three-phase contact line of a drop becomes stable, from which repeatable measurement is possible.

It has been shown that, a dynamic CA measurement is suitable to measure the CA of the modified CFA surface. Results showed that using this approach CA measurement variation was reduced between  $2^{\circ} - 5^{\circ}$ , as opposed to  $15^{\circ} - 20^{\circ}$  in a traditional approach. This threshold volume has been found through a dynamic CA measurement technique in which drop size was made to increase and move over a larger area of a sample while measuring the stability of the three-phase contact line motion. As a result, this study provided the first result on a new approach to measure CA for the modified CFA surface.

## 2. BP measurement and the Washburn equation

Measurement of a water entry resistance in to the pores of the modified CFA showed that, CFA can be modified and made sufficiently water resistant. Results showed that the pore space of the modified surface can resist up to 10 m water entry pressure, as a result infiltration and leachate generation can be avoided. The Washburn (capillary rise) equation was used to model the water entry resistance and estimate parameters that influence imbibition in to the pore space of the modified CFA grains. It was observed that out of the three methods used to estimate pore size, the CFA-WCC and Tetrahedral packing approaches better predicted BP. However, both approaches under-estimate observed BP, according to a certain scale factor. This scaling factor resulted from change in measured CA to pore CA. When an external (positive) pressure is required and applied to drive water in to a pore space of a porous media, the water in pore space is compressed and its radius of curvature changes. This change in the shape of the pore water results in a new CA (pore CA), as opposed to measured CA on flat surface. It was found that, the Washburn equation should be modified for the change of CA as measured on flat surface to pore CA. Further,

the relationship between CA and BP showed that, CA and BP related linearly up to nearly  $140^{\circ}$ , but beyond this range the relationship becomes exponential. The exponential relationship not only predicted BP better, it also proves the absence of pore CA effect near  $90^{\circ}$  (hydrophobic and hydrophilic boundary). The relationship between CA and BP is better described through the type of OS than the type of CFA and dose of OS applied. This attributes to the difference in the performance of OS.

### 3. Wettability and CFA Compositions

The performance of surface modification for CFA using OS product is influenced by the type of OS and CFA. OS performance on the other hand is governed by the percent of reactive elements it possess and the linker length. Regarding performance of CFA, different CFA have different compositions of chemicals and minerals. In general, elements in CFA and OS form a permanent covalent bond to transform CFA surface to a water repellent one. The main chemicals and minerals that form a covalent bond with OS depends on the affinity, quantity, and reactivity of each material. The effect of each chemical, minerals, and their derivatives were evaluated to predict water repellency when treated using OS. It was identified that using two minerals (gypsum and magnetite, out of twenty-eight evaluated) water repellency of an OS modified CFA can be predicted, R-squared about 0.72. In addition, the effectiveness of minerals based on their relative abundance was conducted. Three main chemicals ( $\text{SiO}_2$ ,  $\text{Al}_2\text{O}_3$ , and  $\text{Fe}_2\text{O}_3$ ), pozzolanas state, are known to characterize the type of CFA. These chemicals are also known to form a covalent bond with OS to form water repellent surfaces. However; this study has identified that, OS treated CFA becomes sufficiently higher water repellent surface when the pozzolanas state

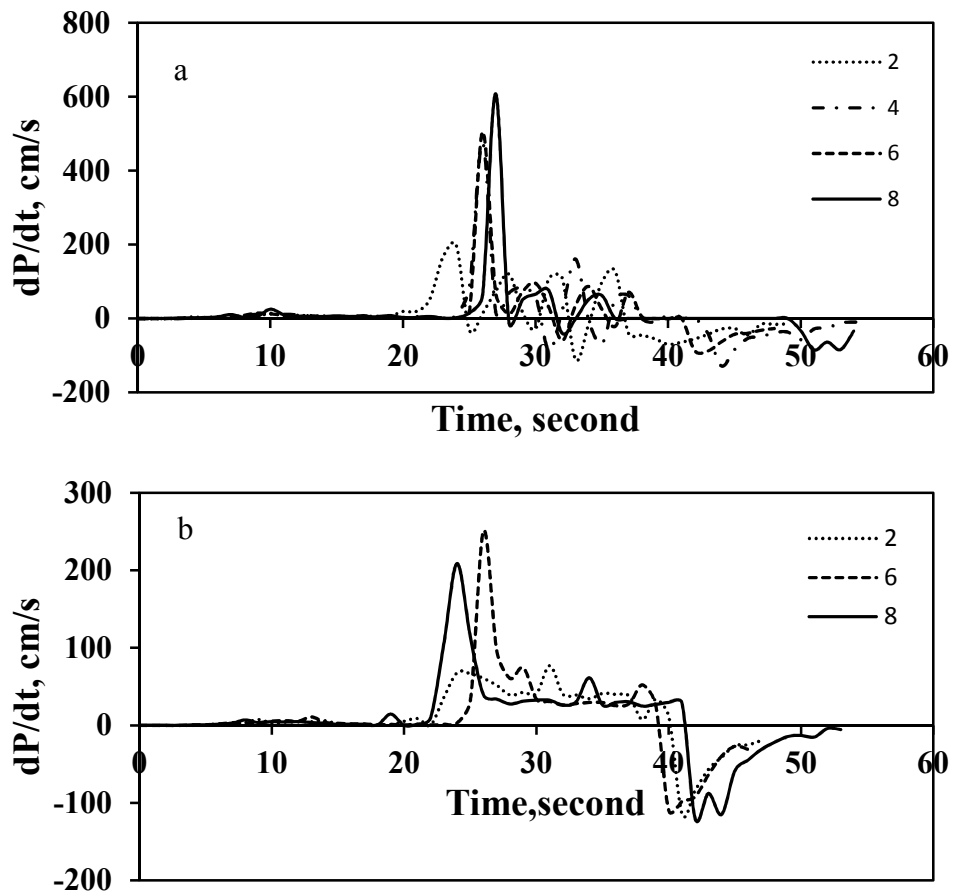
of CFA is between 61 and 84 percent, 61 being the highest in most cases. When this state exceeds 84 percent, water repellency of the modified surface significantly declines. Further analysis on the individual chemicals showed that, the percentage of  $\text{SiO}_2$ ,  $\text{Al}_2\text{O}_3$ , and  $\text{Fe}_2\text{O}_3$  should be less than 48, 15, and 10 to form a higher water repellent surface, respectively.

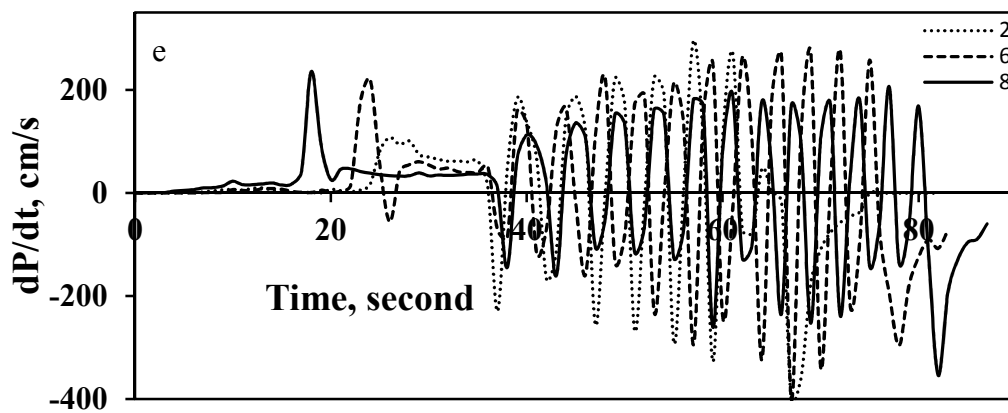
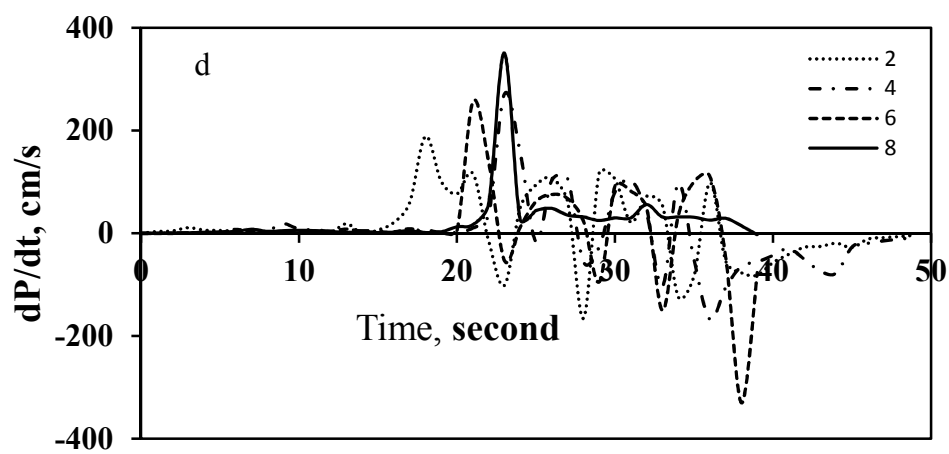
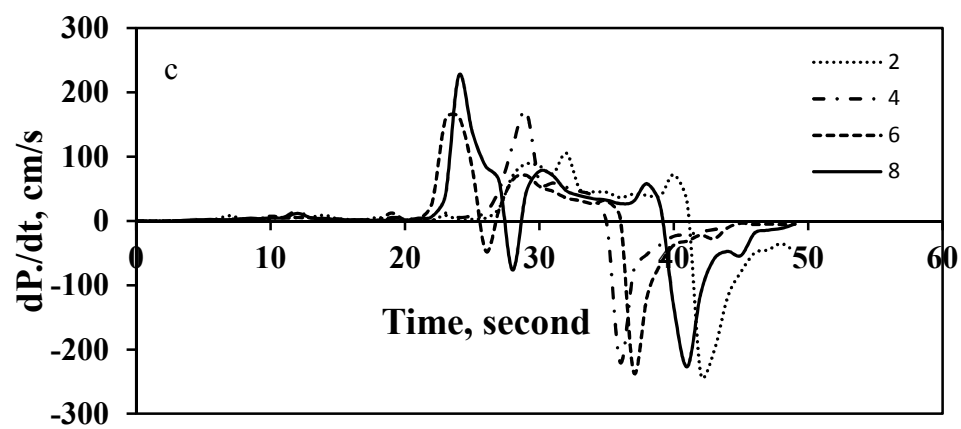
In general, Class C CFA surface cannot be transformed sufficiently to a water repellent character when treated using OS products due to high CaO content. CaO when mixed with water, it rises the concentration of alkali in the solution. This process appears to result in the breakdown of covalent bonds between OS and CFA elements. However, results show that if the amount of MgO in Class C CFA exceeds 2 percent Class C of CFA can also be transformed to a highly water repellent one.

## APPENDIXES

### ADDITIONAL FIGURES

Rate of pressure: pre, during, and post BP corresponding to Figure 2.8 (chapter 2 BP versus time plot).





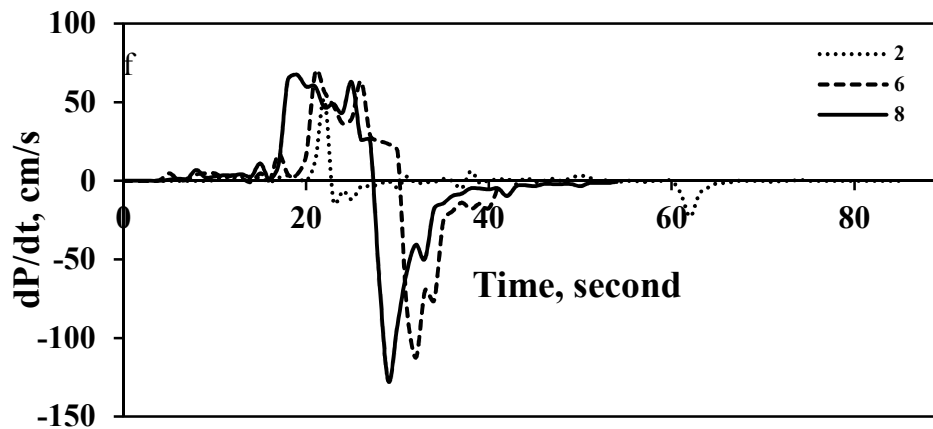


Figure A. 1. Pre-and post-breakthrough sample rate of pressure change for different CFA and OS corresponding to Figure 2.8 at different mix ratio: a, b, c, d, e, and f for CFA1-C1, CFA2-C2, CFA3-C2, CFA3-C4, CFA5-C2, and CFA6-C1, respectively (CFA1-C1 represents sample coal fly ash number 1 treated using organo-silane number1)